Cellular Processing of Infectious Bronchitis Virus Spike, Membrane and Envelope Glycoproteins, Their Role in Virus Biology and as Targets for Antiviral Therapy

Thesis submitted in accordance with the requirements of the University of Liverpool for the degree of Doctor in Philosophy

By

Zana Hameed Mahmood

(BVMS, High Diploma)

December 2018

AUTHOR'S DECLARATION

I declare that the work in this thesis is original; apart from the help and advices acknowledged, this thesis represents the unaided work and it is the author's sole efforts.

.....

Zana Hameed Mahmood

.....

This research was carried out in the Department of Infection Biology, Institute of Infection and Global Health, University of Liverpool

DEDICATION

.....

I dedicate this work to my wife (Nask) for her patience and support during the four-year PhD time and amazing care for our children (Lona, Sena and Ana).

.....

ACKNOWLEDGEMENTS

I would like to express my gratitude and appreciation to my principle supervisor Prof Julian A. Hiscox for the continuous support throughout my PhD study. Julian, Heartfelt thanks for your advices, encouragement and patience. This work would have never been done without your support. Indeed, you helped me on time when I was alone and the work was close to be ended due to the financial difficulties. Very special thanks to my second supervisor Prof James Stuart for his supervision and advises.

My sincere appreciation also goes to Dr Stuart Armstrong for his help on LCMS-proteomic analysis. Special thanks to Dr Isabel, Dr Olivier and Dr Weining for their technical support and the assistance they provided at the lab works for this study. I must acknowledge Mrs. Catherine Hartley, Mrs. Cathy Glover and Mrs. Jenna Lowe for their support in the laboratory as well.

To all of the Hiscox Lab students, Waleed, Sara, Natasha, Elsa and Jordana thank you for the friendships and good times we had. Thanks to the new students specially Abbie, Rebekah and Ghada for being supportive to me during my writing up.

I am also grateful to the people and members of the staff of Department of Infection Biology for the supportive environment they provided. My special thanks to Dr Janine Coombs and Dr Nicholas Evans for their advices and recommendations during advisory panel meetings. Thanks to Ms. Jill Hudson and Miss Hannah Davies for their nice support as well.

I am indebted to both Dr Neil Blake and Dr Robin Flynn for their fantastic support and understandings as student directors in IGH during my hardship times. Many thanks as well to the people in IGH especially Miss Laura Hand and Mrs. Eleanor Tool for their helps in my studentship experience.

Great thanks to the people who provided some laboratory materials from other labs. Dr Erica Bickerton and Dr Helena Maier in the Pirbright Institute for providing the IBV lab strain virus, Vero cells and S antibody for my project. Prof Paul Wigley for providing DF1 and CKC cell lines. Thank you all.

Big special thanks to my parents, brothers and sisters for their love, kindness, encouragement and financial supports. All my successes would not have been possible without the prayers of my mother. Last but not least, unlimited thanks go to my wife for her assistance in statistical analysis and computer works in this thesis. Finally, I would like to thank my daughters and son for their patience throughout this PhD journey, as I couldn’t be with you as you wished.

ABSTRACT

Cellular Processing of Infectious Bronchitis Virus Spike, Membrane and Envelope Glycoproteins, Their Role in Virus Biology and as Targets for Antiviral Therapy

Zana Hameed Mahmood

Avian Infectious Bronchitis Virus (IBV) causes an acute and highly contagious disease of chickens. The virus is a coronavirus and in the same family as SARS and MERS coronaviruses. These viruses have several structural proteins that form integral parts of the viral envelop – a requirement for viral entry. These include the Spike (S), Membrane (M) and Envelope (E) glycoproteins. The addition of glycan groups is essential to their function and is thought to be a non-viral mediated process. Viruses are obligate intracellular parasites and increasingly it has been shown that viral proteins interact with host proteins in order to affect function and manipulate host cell processes. New strategies for anti-viral therapies, which circumvent the emergence of resistance, are to target host proteins that are essential for the virus biology, with repurposed therapeutics. In order to identify cellular proteins that interact with the three IBV structural proteins, to mediate glycosylation, a quantitative label-free proteomic assay was used. This relied on overexpression of GFP-tagged versions of the viral proteins and LC-MS/MS. From the cellular proteins identified a priority list of potential interactions was then assembled. Calnexin, which is an endoplasmic reticulum (ER) chaperon, was identified as potentially a very significant protein for processing and maturation of the targeted IBV proteins. Biological investigation using a combination of siRNA ablation of calnexin and inhibition of enzyme-catalysed function using small molecules in IBV infected cells demonstrated that this protein was involved in N-linked glycosylation of these viral proteins. The work shows how proteomics can be used to inform rapid functional analysis and identify therapeutic targets.

TABLE OF CONTENTS

LIST OF FIGURES

Chapter 1

Chapter 2

Chapter 3

Chapter 4

Chapter 5

LIST OF TABLES

Chapter 2

Chapter 3

Chapter 5

LIST OF ABBREVIATION

AHDB= Agriculture and Horticulture Development Board

APS = ammonium persulphate.

ATP5I = ATP synthase subunit e

BCA= bicinchoninic acid

BCoV = Bovine coronavirus

BSA= Bovine Serum Albumin

BVDV= Bovine viral diarrhoea virus

CANX = Calnexin

CKC = Chicken Kidney Cells

CMV= Cytomegalovirus

COL6A2= Collagen alpha-2 (VI) chain

COL6A3= Collagen alpha-3 (VI) chain

CPE= Cytopathic effect

CPV-2 = Canine parvovirus type 2

CSF= Classical swine fever virus

DCKC =Direct Chicken Kidney cells

ddH2O=Double distilled water

DEFRA= Department for Environment, Food and Rural Affairs

DF-1=Doug-Foster-1 (Chicken Fibroblast)

DMEM =Dulbecco's Modified Eagle Medium

DMJ=Deoxymannojirimycine

DMSO=Dimethylsulfoxide

DNA=Deoxyribonucleic acid

DNJ= Deoxynojirimycine

DTT= Dithiotheritol

E= envelope

ELISA=Enzyme-linked immunosorbent assays

ER= Endoplasmic reticulum

ERAD= Endoplasmic reticulum -Associated protein degradation

ERGIC= Endoplasmic reticulum Golgi intermediate compartment

ERQC= Endoplasmic reticulum quality control

FAO= Food and Agriculture Organization

FBS= Foetal Bovine Serum

FeHV-1= Feline herpesvirus 1

FeLV= Feline Leukaemia virus

FMDV= Foot and mouth disease virus

G19P1= Glucosidase 2 subunit beta

G19P1= Glucosidase 2 subunit beta

Gal= Galactose

GFP= Green Fluorescent Protein

GlcNAc= N-Acetylegalactosamine

gRNA= genomic RNA

GT= Glycosyltransferase

HCoV= Human Coronavirus

HCV= Hepatitis C Virus

HBS= HEPES Buffered Saline

HIV= Human Immunodeficiency Virus

HPACC= Health Protection Agency Culture Collection

IB= Infectious bronchitis

IBV= Infectious Bronchitis Virus

ICTV= International Committee on Taxonomy of Viruses

ILT= Infectious Laryngotracheitis

LB= Luria-Bertani

LC-MS/MS= Liquid Chromatography-Mass Spectrometry/ Mass Spectrometry

Man= Mannose

M= membrane protein

MCS= Multiple cloning site

mg= milligram

ml= millilitre

MHV= Mouse hepatitis virus

MOPS= 3-morpholinopropane-1-sulfonic acid

MS= Mass spectrometry

MYH4= Myosin-4

N =Nucleocapsid protein

N-ANA= N-Acetyleneuraminic acid

NDUFS6= NADH dehydrogenase iron-sulphur protein 6

nsp= Non-structural proteins

NuLS= Nucleolus localization signal

OIE= World Organisation for Animal Health

ORF= Organised according to subsequent open reading frames from 5′ to 3′

UTR= untranslated region

OST= Oligosaccharyltransferase

PPM= Pat per million

PBS= Phosphate buffer saline

PEDV= Porcine epidemic diarrhoea virus

PFA= paraformaldehyde

PNGase F= Peptide-N-Glycosidase F

PT= post treatment

PTM= Post-Translational Modifications

qPCR= Quantitative polymerase chain reaction

RBD= Receptor-binding domain

RIPA= Protein extraction by radioimmunoprecipitation assay

RNA= Ribonucleic acid

RNPs= RNA viruses by having helical ribonucleocapsids

RTC= Replication-transcription complexes

S= Spike glycoprotein

SA= Sialic acid

SDF2L1= Stromal cell derived factor 2-like 1

SDS= Sodium dodecyl-sulphate

SDS-PAGE= Sodium-dodecyl sulphate polyacrylamide gel electrophoresis

SEC61A= Sec61 subunit alpha isoform 1

sgRNA= sub genomic RNA

SILAC= Stable isotope labeling with amino acids in cell culture

SIV= Semian Immunodeficiency Virus

TAE= Tris Acetate EDTA buffer

TCID50 = Median Tissue Culture Infective Dose

TEMED = Tetramethylethylenediamine

TFA= Trifluoroacetic acid

TGEV= Transmissible gastroenteritis virus

TRS= Transcription regulatory sequence

USAD/NASS= United States Department of Agriculture/ National Agricultural Statistics Service

USAD/FAS= United States Department of Agriculture/ Foreign Agricultural Service

ViPR= Virus Pathogen Resource

VLPs= viral-like particles

WB= Western Blot

WR= Working reagent

XML= Extensible Mark-up Language

Amino acids Abbreviations:

1 letter abbreviation	Amino acid name
A	Alanine
R	Arginine
N	Asparagine
D	Aspartic acid
C	Cysteine
Q	Glutamine
E	Glutamic acid
G	Glycine
H	Histidine
I	Isoleucine
L	Leucine
K	Lysine
M	Methionine
F	Phenylalanine
P	Proline
S	Serine
T	Threonine
W	Tryptophan
Y	Tyrosine
V	Valine
X	Any amino acid

Chapter 1

General Introduction and Aims of the Study

1.1 Introduction:

The poultry industry has a considerable involvement in food security and nutrition for humans. In short-term production cycles it changes a wide range of agricultural byproducts and wastes into meat and eggs for human consumptions. This sector is anticipated to grow continuously due to increase in the demand for meat and eggs, which is enhanced by growing populations, increasing incomes and urbanization (Mottet & Tempio 2017). The statistical reports from global (FAOSTAT), continent (Eurostat) and country (UK and USA) perspectives, analyzed the increasing demand for poultry products in general and the meat specifically (AHDB, 2018; DEFRA, 2018; FAO, 2013, 2018; USDA/ FAS, 2018; USDA/ NASS, 2018).

However, generally the poultry disease and especially the viral pathogens are the major risks on the poultry industry causing destructive economic losses and decline in the production efficiency (Trevor, 2013). Some of the viral pathogens are notifiable diseases in avian infections and they cause significant economic losses when outbreaks occur. The World Organization for Animal Health (OIE) created a list of diseases, infections and infestations for avian species, which includes thirteen diseases; eight of them are viral infections (OIE, 2018). A review of high-priority, economically important viral pathogens of poultry in Caribbean region summarized the circulation and impact of the viruses in such a high rate region of poultry consumption in the world (Jordan *et al.,* 2018). Infectious Bronchitis Virus (IBV) was classified as notifiable viral pathogen in both lists mentioned.

1.2 Avian Infectious Bronchitis Virus (IBV):

IBV is a nonsegmented, single-stranded, positive-sense RNA and enveloped virus, which belongs to *Coronaviridae* family. The virus usually infects upper respiratory and also reproductive tract of chickens, however different strains of the virus can also cause renal and digestive diseases (Cavanagh, 2007; Cook *et al.,* 2012). Clinically the infection has been known as Infectious bronchitis (IB), which is an acute, highly contagious and economically important disease of both broiler and layer chickens (Cavanagh & Gelb, 2008).

Coronaviruses including IBV are exceptional among the positive-sense RNA viruses by having helical ribonucleocapsids (RNPs), which is formed by the association between the genome and nucleocapsid (N) protein. The helical RNP complex is also enclosed within a lipid envelope consisting of the spike (S), membrane (M) and envelope (E) proteins, and generating pleomorphic particles of approximately 120nm in diameter with spikes projecting from the surface (Cavanagh, 2005) Figure 1.1.

Morphologically IBV has a round to pleomorphic shape and the mature virions are approximately 120 nm in diameter having drumstick-shaped surface projections known as spikes. The spikes are about 20 nm in length and gives the virus a crown-like appearance, which the name corona (Latin for crown) has come from the shape (Bingham & Almeida, 1977; Masters & Perlman, 2013; Patterson & Bingham, 1976).

A

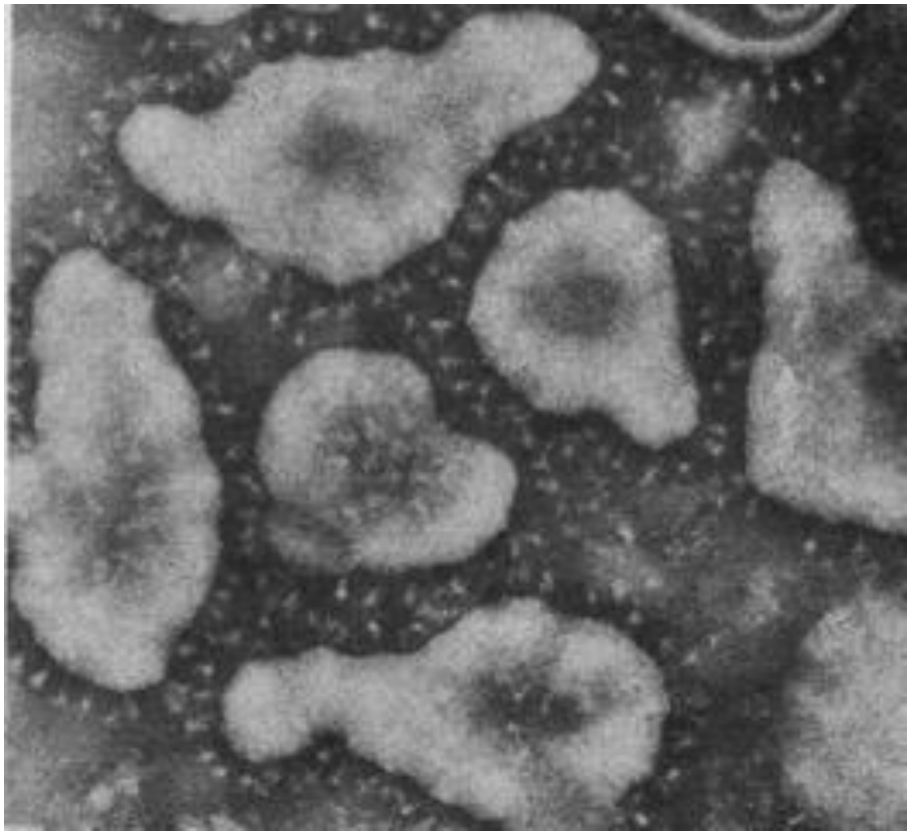

B

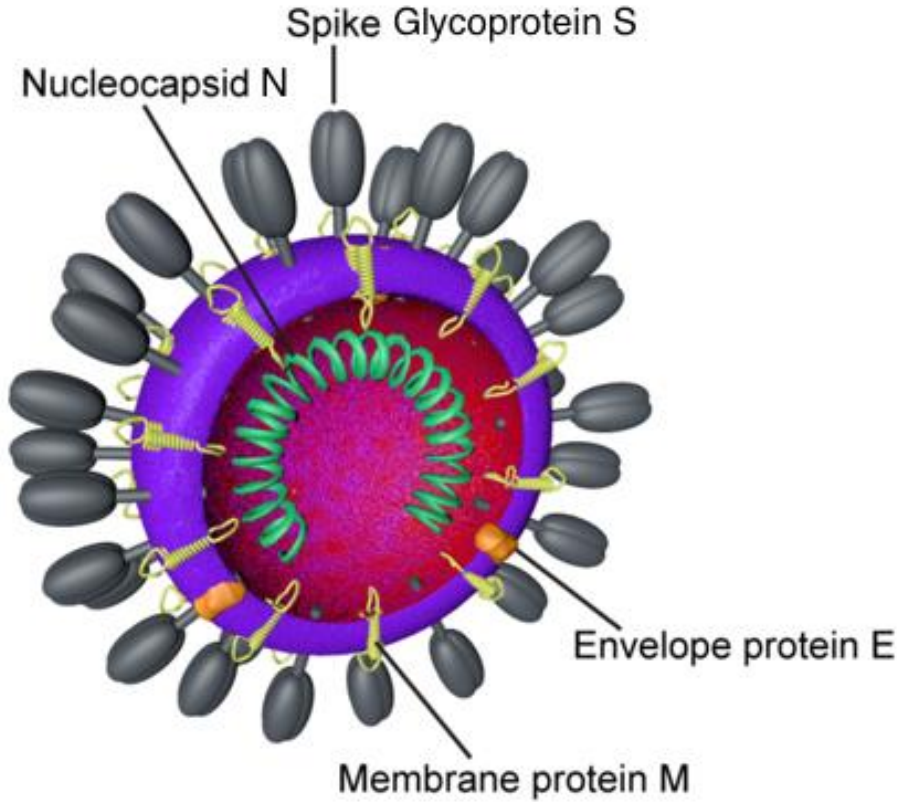

Figure 1.1: The IBV virion. A: Pleomorphic IBV particles showing crown-like projections by Electron Microscopy (Bingham & Almeida, 1977). *B: Schematic representation of a IBV viral particle showing all structural proteins* (Belouzard *et al.,* 2012).

1.2.1 Brief History:

Infectious bronchitis was first described in the United States of America in North Dakota in 1930. A year after, in 1931, the clinical signs and preliminary observation of the cases were recognized by Schalk and Hawn as an apparently new respiratory disease of chicks (Schalk & Hawn, 1931) this was considered as the first report of IB, which described the disease in terms of clinical perceptions. Two years after the clinical description of the disease, the filterable causative agent was established and considered as a mild form of Infectious Laryngotracheitis (ILT) in chicks (Bushnell & Brandly, 1933). However, three years later, after a temporary confusion between ILT and IB, an important early milestone of the aetiology was done by Beach and Schalm in 1936 in which by studying the cross-immunity responses, they proved that the filterable virus was different from that of ILT as the cause of chick respiratory disease (Beach & Schalm, 1936). In the same decade, another significant step was started in 1937, by which Beaudette and Hudson confirmed the first cultivation of the virus in embryonated chicken eggs. In the early 1940s a new era of IBV economical importance, pathogenicity in embryonated eggs and its conversion with the passaging were started in a series of studies by Delaplane and Stuart in 1939-1941 (reviwed in Fabricant 1998) and reached to a first trial of vaccine development from the van Roeckel M-41 strain (van Roekel *et al*. 1941). Later on in each decade the uncountable studies on IBV were conducted in the last seven decades (Cook, *et al*., 2012a; Fabricant, 1998; Hitchner, 2004; Jackwood & de Wit, 2017).

1.2.2 Classification:

IBV is classified in the genus *Gammacoronavirus*, which belongs to subfamily *Coronavirinae* in the family *Coronaviridae* and in the order *Nidovirales*. A complete virion contains a positive-sense, single stranded RNA genome of about 27.6Kb (Lai *et al.,* 2007). So according to Baltimore's virus classification system, IBV belongs to class IV in which the mRNAs are identical to the positive sense RNA genome in terms of base sequences. Poliovirus, Picornavirus and Togavirus were described as the same class as well (Baltimore, 1971).

On the other hand, the International Committee on Taxonomy of Viruses (ICTV), which is a virus classification committee was established in 1966 and has specific virus taxonomy reports over specific times (Davison, 2017). The 10th ICTV report is the most recent one, which was released in July 2018 and available online in (http://ictv.global/report). According to this report, ICTV has classified viruses in to 14 orders, 143 families, 64 subfamilies, 846 genuses and 4958 species. The *Nidovirales* order taxonomy was updated completely and the classified viruses were organised in to seven suborders, however in the previous ICTV 9th report the order just included three families. The *Coronaviridae* family was classified under *Cornidovirineae* suborder and new subfamilies *Letovirinae* and *Orthocoronavirinae* were added to the classification while *Coronavirinae* subfamily was deleted. Consequently, in the new system, Avian Coronavirus species was belonged to *Igacovirus* subgenus, *Gammacoronavirus* genus, *Orthocoronavirinae* subfamily, *Cornidovirineae* suborder and *Nidovirales* order Figure 1.2*.*

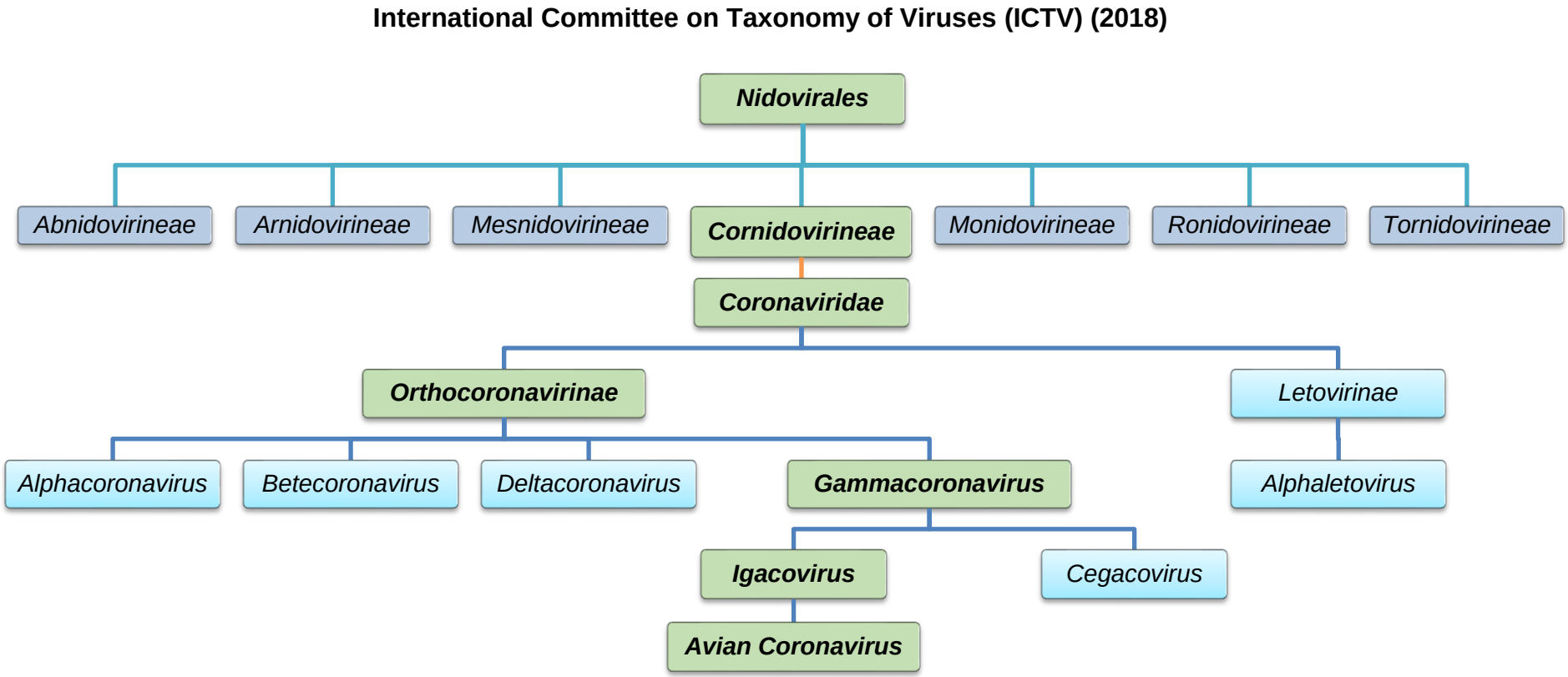

Figure 1.2: IBV taxonomy. The most recent ICTV taxonomy of order Nidovirales in which Avian Coronavirus taxonomy was highlighted in green and showed the virus was belonged to Igacovirus subgenus, Gammacoronavirus genus, Orthocoronavirinae subfamily, Cornidovirineae suborder and Nidovirales order.

1.2.3 Genomic Organization:

IBV genome was completely sequenced in the last two decades of 20th century (Boursnell *et al.,* 1987), which has facilitated genomic research, including the capability of reverse genetics (Casais *et al.*, 2001; Bickerton *et al*., 2017). The genome length is around 27,600 nucleotides, which is transcribed into six major RNAs that encode both structural and non-structural viral proteins. The IBV RNA genome sequence contains nine functional genes and they are organised according to subsequent open reading frames (ORF) from 5′ to 3′ untranslated region (UTR) ends as follow: 5′UTR-Replicase (1a-1b)-S-3a-3b-E-M-5a-5b-N-3′UTR. The transcription system of IBV put all the nine genes into one genomic RNA (gRNA) and five sub genomic mRNAs (sgRNA), which are known as RNA 1-6 successively. The sgRNAs possess a 64-nucleotide leader sequence (L), which derived from the 5′ end of the genome. The L sequences act as signals that are required for replication and packaging of the virion RNA (Dalton *et al.,* 2001). RNA1, which is also the polymerase or replicase gene, comprises about two-thirds of the genome starting from the 5′ end. The gene encodes two ORFs, 1a and 1b. The replicase protein has fundamental role in the virus replication and is also a determinant of the virus pathogenicity (Armesto *et al.,* 2009). RNA2 consists of one encoding ORF of the spike glycoprotein (S), which is further cleaved into the amino terminal S1 and the carboxyl-terminal S2 subunits. RNA3 contains three ORFs for encoding three small proteins 3a, 3b, and 3c. The first two ORFs encode non-structural proteins of unknown function while last one encodes the E protein, which is a structural protein required for virion assembly (Abro *et al.*, 2012).

RNA4 contains one ORF, encoding the M glycoprotein, which is essential for the production of coronavirus-like particles. RNA 5 is present in all group 3 coronaviruses characterized to date. RNA 6 has one ORF and encodes the N protein, which interacts with the genomic RNA and forms the helical nucleocapsid. Finally the 3′UTR located directly downstream to the N gene (Lai & Cavanagh, 1997; Masters, 2006). Approximately all the classical strains have the predicted gene order of 5′-Pol-S-3a-3b-E-M-5a-5b-N-UTR-3. However, an Australian strain has a novel genomic organization of IBV. N1/88 and Q3/88 strains lack the non-structural genes 3a, 3b and 5a and has an additional gene in the gene 3 region, resulting in the genomic organization as 5′-Pol-S-X1-E-M-5b-N UTR- 3′ (Mardani *et al.,* 2008).

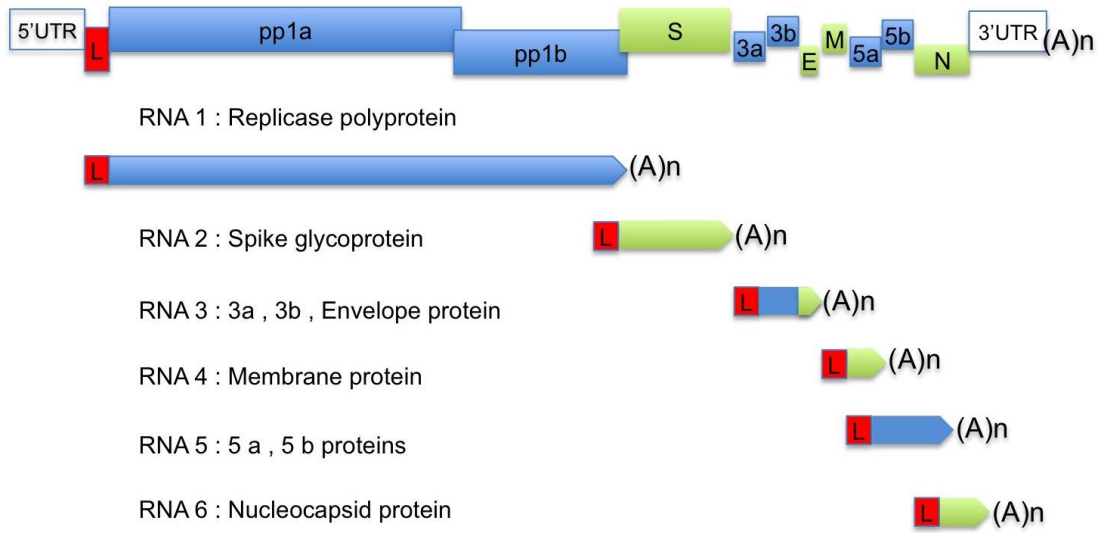

Figure 1.3: Schematic representation of IBV genomic and sub genomic organizations. S: spike glycoprotein gene; M: membrane protein gene; E: envelope protein gene; N: nucleocapsid protein gene. RNA 1 encodes replicase poly protein; RNA 2 encodes S protein; RNA 3 encodes 3a, 3b and the E proteins; RNA 4 encodes the M protein; RNA 5 encodes 5a and 5b and RNA 6 encodes the N protein. The red L box represents leader cap and (A)n represents poly (A) tails.

1.3 Virus Replication Cycle:

As an enveloped RNA coronavirus, IBV has a specific replication cycle in terms of attachment process to the receptor, transcription per sgRNAs, viral protein translation, posttranslational modifications (PTM) and trafficking towards the virion assembly process. A schematic replication cycle is shown in Figure 1.4 page 17.

1.3.1 Attachment, Entry and Uncoating:

The attachment of IBV to the host cells is the crucial step in the virus replication cycle. On the IBV side, the most prominent S glycoprotein on the viral envelope is responsible in the attachment process, while on the host side, sialic acid molecules act as a receptor determinant for the primary binding of the virus (Wickramasinghe *et al.,* 2011; Winter *et al.,* 2006). The first interaction step of the attachment starts by the involving of the receptor-binding domain (RBD) of S glycoprotein, which is located in the N-terminal 253 amino acids, to the host cells by α-2,3-sialic acid dependent manner (Promkuntod *et al.,* 2014). However just recently, lipid rafts were studied as attachment factors during early IBV infections (Guo *et al.,* 2017). Following the attachment, the virus is up taken by viropexis, which is micropinocytosis of the attached virus in to the cytoplasm of the cell and proceed endocytosis into the host cells. This was morphologically studied using the EM (Chasey & Alexander, 1976; Patterson & Bingham, 1976) however the exact mechanism wasn't clear and the accepted method was set on the PH-dependent fusion of the viral and cellular membranes (Chu *et al.,* 2006a).

In addition, the molecular mechanism of the virus endocytosis and intracellular tracking was further studied and the clathrin-mediated endocytosis was confirmed for IBV entry as well. The mechanism indicated that IBV attaches to lipid rafts, induces actin de-polymerization, internalizes into clathrin coated vesicles via dynamin1 snapping, transports along early/late endosome, and lysosome then finally fuses with late endosome-lysosome membrane and releases genome in to the cytoplasm (Chu, *et al*., 2006b; Wang, *et al*., 2018).

1.3.2 Replication and Transcriptions:

Following uncoating of the genomic RNA into cytoplasm, the RNA is recognized by host translation machinery due to the presence of a 5' leader and a 3' poly A tail sequences. Consequently both ORF1a and 1b are directly translated to produce the replicase polyproteins pp1a and pp1ab, which are necessary for transcription and replication processes, the replicase polyproteins are then cleaved by virus-encoded proteinases (Brierley, *et al*., 1987). Then the replication-transcription complexes (RTC) are produce in which the viral genome is copied (Hagemeijer, *et al*., 2010). The negative strand templates are then synthesized from the RNA genome. The full genome-length templates are produced by continuous transcription while sub genomic length templates are produced by discontinuous transcription. The sequences between each gene, termed the intergenic sequences or transcription regulatory sequence (TRS), have a sequence homology of 7 to 18 nucleotides with the 3′ end of the leader sequence, the consensus sequence for IBV is CU(U/G)AACAA (Spaan *et al.*,1988).

During replication process multiple subgenomic mRNAs are generated, which are characteristic features of coronaviruses and even *Nidovirales* order as well. In case of IBV, five subgenomic RNAs are transcribed in infected cells. Each of sgRNAs has a 5′ leader sequence and 3′ poly (A) tail which are identical to the sequence at the 5′ and 3′ ends of the genomic RNA and are not found elsewhere in the genome (Lai & Cavanagh, 1997).

1.3.3 Translations:

Protein synthesis during IBV replication can be divided into two main processes, which are primary or secondary translations. The primary translation is done for the ORF1 in the gRNA and one large polyprotein of 700-800 kDa in size is produced. This synthesis utilizes a ribosomal frame shifting mechanism to produce the entire replicase polyproteins (Boursnell *et al.*, 1987; Lai and Cavanagh, 1997). The secondary protein synthesis is occurred by translations of sgRNAs, which express the structural and accessory viral proteins at the endoplasmic reticulum (ER). The leader and coding sequences are joined by the TRS which and the 5′-proximal ORFs of each sgRNA is translated to produce one of the virus structural proteins, which are spike glycoprotein (S), small membrane protein (E), integral membrane protein (M) and nucleocapsid protein (N). On the other hand another theory describes the process in which the sgRNAs are functionally monocistronic and only the ORF at the 5’ end is translated by a cap-dependent mechanism however bi or tricistronic sgRNAs are translated via an internal ribosome entry or by leaky-scanning mechanism (Dalton *et al*., 2001).

Post-Translational Modifications (PTM):

As an obligate intracellular parasite IBV exploits the protein synthesis machinery of the host cells to facilitate and process the viral proteins to complete the replication cycle. So, the viral proteins are modified by PTMs after being translated. The evidences in other coronavirus proteins, which are modified by various kinds of PTMs and significantly affect viral replication and pathogenesis (reviewed in Fung and Liu, 2018).

Basically, PTMs are the concomitant modifications of proteins following their production by the ribosomes. The addition of new functional groups, such as phosphate and carbohydrates, makes extension in the chemical properties of the amino acids and prepare them for regulating the folding, maturation, trafficking, subcellular localization and interaction with the other proteins (Duan & Walther, 2015).

The PTMs include either structural changes to the polypeptide (for example proteolytic cleavage and disulfide bond formation) or the addition of functional groups such as phosphorylation, glycosylation and lipidation. PTMs are mostly catalyzed by modifying enzymes, in which the functional groups or signals are added and/or removed. For example, asparagine N-linked glycosylation requires the successive activities of enzymes that synthesize the precursor dolichol-linked oligosaccharide group, link the group to the protein and trim the molecules where they are needed. The oligosaccharyltransferase enzyme (OST) transfers the glycan group to a specific consensus amino acid sequence Asparagine-X-Serine/Threonine (N-

X-S/T, where X is any amino acid except proline), then glycosidases trim the glucose molecules from the group to prepare them for folding and glycosyltransferases (GT) aid in accomplishment of the glycoprotein maturation that mediate further processing of the N-linked glycoprotein in the ER (Audagnotto & Dal Peraro, 2017; Breitling & Aebi, 2013).

During the IBV replication cycle, the four structural proteins S, M, E and N proteins undergo PTMs. Glycosylation is one of the important PTMs of S, M and E proteins which facilitate their processing and maturation while phosphorylation is the major PTM for N protein (Lai & Cavanagh, 1997). The localization of S (Winter, *et al*., 2008), M (Wang, *et al*., 2009) and E (Westerbeck & Machamer, 2015) proteins during replication were confirmed inside the ER, Golgi and secretory pathways, however the details of the PTM mechanisms and contribution of cellular pathways for the modification are still unclear.

On the other hand, the PTM and localization of N during the replication cycle of IBV has been well studied. The localization of N in the nucleolus following its translation by ribosome is driven by the nucleolus localization signal (NuLS) in the sequence of N protein (Hiscox, *et al*., 2001) and this lead to the interaction between N and neocleolin protein (Chen, *et al*., 2002) by which the dynamics of the nucleolus is overcome for the virus replication (Hiscox, 2007). The PTM of N, which includes the C-terminal phosphorylation cluster, has a significant influence on RNA binding capability and virus biology (Chen, *et al*., 2005; Spencer, *et al*., 2008; Spencer & Hiscox, 2006).

1.3.4 Virus Assembly and Release:

The membrane-bound S, M and E proteins are firstly introduced into the ER, and then they transit to the site of virion assembly, which is the endoplasmic reticulum Golgi intermediate compartment (ERGIC). ERGIC is a membrane system that is structurally and functionally extended from the ER (Lontok, *et al*., 2004). Following the complementation of protein maturation in ERGIC, the viral particles are assembled through S, M and E interactions, which mainly involve M protein as it is the most abundant protein in the IBV envelope (de Haan *et al.*, 2000). However, despite its central role, the assembly does not occur and complete by expression of M protein alone and it has to interact with at least S or E proteins to become a virion-like structures (Corse & Machamer, 2003; Liu, *et al*., 2013; Neuman, *et al*., 2011).

The interaction of S, M and E proteins to form the envelope of IBV is made through the characteristics per each protein, which is dependent on having specific sequences that render them to be driven to their subcellular localization. For instance S glycoprotein contains two signal sequences; first, a canonical dilysine endoplasmic reticulum retrieval signal (-KKXX-COOH) in its cytoplasmic tail, which can retain a chimeric reporter protein in the ERGIC and when mutated allows transport of the full-length S protein as well as the chimera to the plasma membrane and second a tyrosine-based endocytosis signal in its cytoplasmic tail, in which any S protein that escapes the ERGIC will be rapidly endocytosed when it reaches the plasma membrane (Hogue & Machamer, 2008). The cytoplasmic tail in M and E proteins mediates their

interaction and localization in Golgi as well (Corse & Machamer, 2002, 2003). Simultaneously, the nucleocapsids which are composed from replicated RNA genomes and encapsidated by N protein, which are newly exported from the nucleolus, then interact with the other structural proteins at the budding site ERGIC to form virions particles (Hiscox, 2007).

Finally, following the assembly and budding at ERGIC, progeny virions are exported from infected cells by transport to the plasma membrane in smooth-walled vesicles, which act as putative virion carriers and are driven close to plasma membrane so as to release mature virions by exocytosis (Masters & Perlman, 2013; Ruch & Machamer, 2012b).

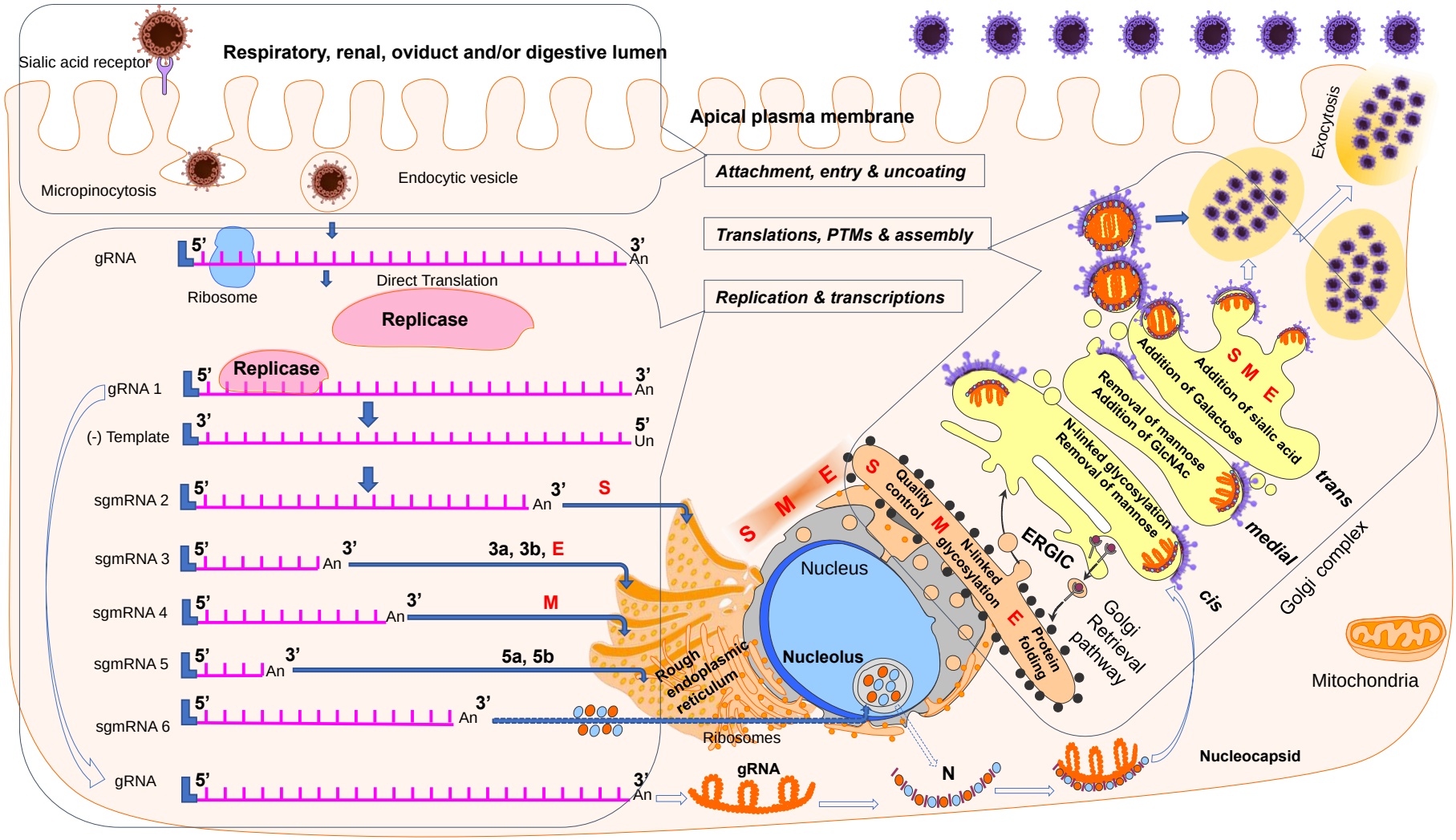

Figure 1.4: Schematic representation of IBV replication cycle. The detail was described in the text of section and subsections of 1.3.

1.4 Viral Proteins:

Generally, the IBV RNA genome encodes nine proteins during the virus replication cycle, four of which are structural proteins. These include spike glycoprotein (S), integral membrane protein (M), small envelope protein (E) and nucleocapsid protein (N). The rest of other five proteins are non-structural proteins, which include replicase and accessory proteins 3a, 3b, 5a and 5b proteins (reviewed in Masters, 2006).

1.4.1 Structural Proteins:

The mature virion of IBV has four structural proteins that carry and protect the RNA genome of the virus. The proteins are spike glycoprotein (S), integral membrane protein (M), small envelope protein (E) and nucleocapsid protein (N).

1.4.1.1 Spike Glycoprotein (S):

The S glycoprotein is the most prominent, multifunctional and largest of IBV structural proteins. Morphologically, the S protein renders the crown-shaped characteristics of the virion by having trimeric drumstick-like projections from the surface of the virus (Masters & Perlman, 2013).

The IBV S is a type I transmembrane glycoprotein, which composed from around 1160 amino acids depending on strains of the virus. The structure of S protein is characterized by having trimeric globular S1 in the upper most protruded part and the liner stalk part in which the S2 sequence of the protein is included (Wickramasinghe, *et al*., 2014). This division is due to a cleavage

that is carried out by a furin-like protease from host cell and cleaves the S into two polypeptides; S1 and S2 domains, which is one of the characteristics of IBV S in the Coronaviridae family (Cavanagh, 1983a). S1 composes N-terminal domain that is responsible for receptor binding and the C-terminal domain is included in S2 and is needed for the fusion process. Consequently the S is considered a class I virus fusion protein (Bosch, *et al*., 2003). The dual role of receptor binding and membrane fusion is sequence-dependent. The RBS in IBV M41 prototype mediates binding to α-2,3-sialic acid and critical amino acid sequence needed for the attachment (Promkuntod, *et al*., 2014). The fusion process is mediated by a putative fusion peptide in S2 domain and following endocytosis, conformational changes of the spike protein are taken place in acidic PH environment (Chu, *et al*., 2006).

The molecular weight of the S per its amino acid sequence and before glycosylation is around 128 kDa, however when it is glycosylated, the mass increases to about 200kDa (Cavanagh, 1983a). Early studies on N-linked glycosylation confirmed that the S protein is highly glycosylated (Cavanagh, 1983b) and S sequence contains 21 to 35 N-glycosylation sites (Binns, *et al*., 1985) in which by using proteomic assay and mutagenesis, 8 and 13 sites were characterized. Furthermore, the glycosylation impact on S mediated cell-cell fusion, virion recovery and infectivity were confirmed as well. The structure of S and its PTM are important in the attachment, antigenicity, epitope neutralization and membrane fusion, however the exact cellular interactive contribution is needed to be further explored (Zheng, *et al*., 2018). This aspect is one of the focuses in this thesis.

1.4.1.2 Membrane Glycoprotein (M):

The M protein is a type III transmembrane glycoprotein and the most abundant protein in the viral envelope, which is estimated as more than one third of the mass of total IBV virion. The M molecular weight is about 25-30 kDa for having 225 amino acids integral protein. The sequence has a short N-terminus exposed to the surface of the virion followed by three membrane-spanning domains and a C-terminus located inside the virion (Boursnell *et al.,* 1984; Masters and Perlman, 2013). The first membrane-spanning domain drives the M protein to the *cis* Golgi and is necessary for membrane binding, retention in the Golgi and protein accumulation (Corse & Machamer, 2002; Machamer, *et al*., 1990; Neuman, *et al*., 2011).

Interaction of the M protein with itself and other viral proteins are important for virus assembly. First M-M interactions constitute the overall frame for the viral envelope, this confirmed for coronavirus MHV (de Haan, *et al*., 2000). Secondly the interaction with S (Liu, *et al*., 2013) and E glycoproteins in the buddying site at ERGIC to form the viral envelope, the latter interaction is mediated through the cytoplasmic tail in each of M and E proteins (Corse & Machamer, 2003). During the buddying process, M is localized primarily in the Golgi and after its interaction with S and E, the M interacts with N protein of the nucleocapsid to assemble to new virions (reviewed in Hogue and Machamer, 2008).

IBV M proteins perform to interact with host proteins as well. For example, using coimmunoprecipitation technique, it has been shown that M interact

with β-actin and results suggest this interaction is important for assembly and budding of virions but not release (Wang, *et al*., 2009). Additional host proteins that interact with M remain to be determined. This is the second focus of this thesis.

1.4.1.3 Envelope Glycoprotein (E):

The IBV small E protein is a minor than other structural proteins, however it is an essential component of the virion. The E protein is composed of 108 amino acids with a predicted molecular mass of approximately 10-12 kDa. It is translated from sub genomic mRNA3, which also contains the ORF for two non-structural proteins (3a and 3b) of unknown functions. The amino acid sequence composed from a short hydrophilic region on the amino terminus, followed by a large hydrophobic region and a large hydrophilic carboxyl terminus (reviewed in Ruch and Machamer, 2012b).

The main function of the E is in the assembly process. As the cytoplasmic tail of the E protein contains Golgi targeting track and concomitantly with M, they bud to form virion envelope (Corse & Machamer, 2003), however the curvature bending during budding and scission of the virion particles following bud completion are other significant roles of the E protein (Ruch & Machamer, 2012b). In addition to the assembly role the E protein also plays a role in modifying the cellular secretory pathway. The process is carried out by the aid of the hydrophobic domain and in turn promotes viral replication and enables efficient trafficking of new virions (Ruch & Machamer, 2011, 2012a; Westerbeck & Machamer, 2015).

Additionally, in terms of PTMs, E is palmitoylated on one or two cysteine residues in the cysteine-rich region adjacent to the transmembrane domain, however the palmitoylation is not required for the Golgi targeting (Corse & Machamer, 2002). The N-linked glycosylation on the IBV E glycoprotein wasn't studied in detail and it thought to be un functional (Corse & Machamer, 2000), however such glycosylation is motif dependent and it is still in debate. This is the third focus in the current study.

1.4.1.4 Nucleocapsid Protein (N):

The fourth structural protein of the IBV is the nucleocapsid protein N. The N is translated from sgRNA 6 and produces 450 amino acid protein around 50 kDa molecular weight phosphoprotein having several functions in both viral replication cycle and cellular response (Emmott, *et al*. 2010a; Emmott *et al*. 2013). The N peptide sequence has three conserved domains including one that interacts with RNA, a cytoplasmic domain that interacts with the M protein and the N-terminal domain that binds RNA in a lure and lock mechanism, which brings the RNA into closer binding to the N protein (Spencer & Hiscox, 2006).

During viral life cycle N protein interacts with genomic RNA forming a nucleocapsid. It also interacts with other structural proteins S, M and E at the budding site for the assembly process and its localization with the replicase, results in genomic RNA replication and mRNA transcriptions (McBride *et al*. 2014). Technically, the N is significant in the reverse genetics systems of IBV as it is essential for the recovery of infectious virions (Casais, *et al*., 2001).

Phosphorylation is the major PTM of IBV N protein by which the limited number of serine and threonine residues. The phosphorylation of N play roles in assembly or maturation of the viral particle (Spencer, *et al*., 2008).

1.4.2 Non-Structural Proteins:

IBV has five non-structural proteins. The major of which is replicase protein and the other four are accessory 3a, 3b, 5a and 5b proteins.

1.4.2.1 Replicase Protein:

The viral gRNA is a single-stranded positive sense RNA that has a messenger-like capacity and once entered into the cell, it is translated into an enormous replicase polyprotein. The IBV replicase protein has two large non-structural precursor polyproteins are produced, pp1a and pp1ab. During the synthesis process, the polyproteins are further cleaved by viral encoded proteinases to 15 non-structural proteins 2-11 (nsp2-nsp16), which are important for viral replication. The other coronaviruses has 16 nsps including nsp1 (Ziebuhr *et al.,* 2000). In addition to its major role in viral replication, replicase has effects on the pathogenesis and it was characterised as a determinant of IBV pathogenicity (Armesto, *et al*., 2009).

1.4.2.2 Accessory Proteins:

IBV has four accessory proteins, which are 3a, 3b, 5a and 5b. They are interspersed between structural proteins and not essential for virus replication (Casais *et al.*, 2005; Hodgson *et al.*, 2006). However, in other coronaviruses the impact of the accessory proteins is different than in case of

IBV. For example, deletion of all accessory proteins of murine hepatitis virus (MHV) produced non-lethal virus in mice as compared to the wild-type (De Haan, *et al*., 2002) reduction in pathogenicity due to the deletion of some of the accessory protein genes of feline coronavirus (Haijema *et al.*, 2004) and knockout of accessory protein from gene 3 of transmissible gastroenteritis TGE has not effective on its enteropathogenicity. More recently in MERS coronavirus accessory proteins 3, 4a, 4b, and 5 were analyzed for their abilities to inhibit the type I interferon response. As a result the 4a protein was found to block interferon induction (Niemeyer, *et al*., 2013).

1.5 Virus-Host Interactions:

As a virus, IBV has a series of interactions with its host and they are dependent on the time and localization of infection, which can be equivalent per the stages of virus replication cycle as well. According to the stages of virus infection, the virus-host cell interactions can be identified as follow:

1.5.1 Virus-Cell Membrane Interactions:

The first site of interaction between the virus and the host is the cell membrane of infected cells. IBV targets ciliated or goblet cells of respiratory epithelium, nephrocytes and/or oviduct lumen cells (Jackwood & de Wit, 2017). The interaction with cell membrane is related to the binding nature between the virus epitope and the host receptor. In the case of IBV, the binding is dependent on S glycoprotein and sialic acid receptor (Winter, *et al*., 2006). This interaction was confirmed for the four major strains of IBV, which are Beaudette, 4/91, QX and Italy 02 (Rahman, *et al*., 2009). The molecular mechanism of this interaction was mentioned in section 1.3.1 in this chapter.

1.5.2 Virus-Cytoplasm Interactions:

The interaction process of IBV in the host cytoplasm is mainly considered in the steps of uncoating, primary translation and RNA genome transcriptions during the viral replication cycle. These interactions may be directly involved in viral replication or result in the modification of some signaling pathways, such as cell stress response and innate immunity, which are required to facilitate viral replication and pathogenesis (Zhong *et al.*,2016). For example

expression of IBV nsp 6 alone, induces autophagic signaling in avian cells which is a suggestion that IBV can inhibit or control autophagy in avian cells (Maier, *et al*., 2013). The cell cycle arrest is another way for IBV to work in which, at both S- and G2/M-phases the cell cycle is manipulated by IBV for the enhancement of viral replication (Dove *et al.*, 2006). This arrest at the S and G2/M phases is catalyzed by viral modification of various cell cyclins/ cyclin-dependent kinases and the accumulation of hypophosphorylated retinoblastoma protein (Li *et al.*, 2007).

1.5.3 Virus-Cellular Organelles Interactions:

The main interactions in relation to the structural proteins of IBV occur in the cellular organelles especially the ER and Golgi complex. Exploiting the cellular translation machinery for the production of structural protein progenies and further maturation of the proteins by using certain enzymatic pathways per each type of PTM, are main interactions in the ER and Golgi. Glycosylation as an example (Breitling & Aebi, 2013; Stanley, 2011).

The interaction, localization and processing of the proteins are mainly sequence and/or motif dependent in the viral proteins. For example the signals inside the S protein act as maturation co-factors, for example due to having a canonical dilysine endoplasmic reticulum retrieval signal (-KKXX-COOH) at the cytoplasmic tail, the immature S proteins can be retained in the ER-Golgi Intermediate Compartment (ERGIC), which is site of virus budding and forming virus particles (Lontok, *et al*., 2004; Winter, *et al*., 2008).

1.5.3.1 Virus-Endoplasmic Reticulum Interactions:

As it is a major site of protein synthesis, folding, modification and sorting in the eukaryotic cells, the ER is intensively involved and during viral infections, the RE stress is accumulated and in response of that a special signalling pathway of unfolded protein response is activated (Fung, *et al*., 2014). The enveloped viruses including IBV, are extensively exploit the ER for processing of glycoproteins by the interaction with enzymes and chaperones that are responsible for adding or trimming glycan to the nascent viral proteins. The N-linked glycosylation PTM is an obvious example in such interaction and it has been characterized for many viruses (Raman, *et al*., 2016). This has not been elucidated for IBV and it is a focus for this study.

1.5.3.2 Virus-Golgi Complex Interactions:

The Golgi is an organelle in which proteins receive various PTMs, including glycosylation. During IBV infections the Golgi is increased in size and fragmented as well. Consequently up taking of large amounts of proteins causes insufficiency of Golgi function such as glycosylation and induces Golgi stress, which in turn leads to increase in the expression of glycosylation enzymes and vesicular transport machinery by the Golgi stress response (Sasaki & Yoshida, 2015). Assembly and budding of IBV virions occur in the ERGIC, in which specific enzyme-aided PTMs are occurred for the preparation of the virions assembly (reviewed in (Fung, *et al*., 2016)). The glycosylation PTM for IBV proteins is focused in the current thesis as well.

1.5.3.3 Virus-Nucleolus Interaction

The nucleolus is an active sub nuclear structure, which involved in biogenesis of ribosome subunit, regulation of cell stress and modulation of the cell cycle and cellular growth. Generally, infection of cells with RNA viruses changes the proteome and structure of the nucleolus (Hiscox, 2007). This interaction and response is to control the nucleolus functions and recruit the proteins to facilitate viral replication (Hiscox, *et al*., 2010). In case of IBV infection, primary studies confirmed localization of N protein in the nucleolus (Hiscox, *et al*., 2001; Wurm, *et al*., 2001), the interaction of N with nucleolar antigens (Chen, *et al*., 2002), change in nucleolar morphology and proteins (Dove *et al.*, 2006) and elucidation of nucleolar proteome by quantitative proteomics (Emmott *et al.*, 2010).

Taken together, in all the cellular sites of the virus interaction there are approaches for further study about the biological mechanism and cellular contributions of the interactions. As per the published data and to the extent of current knowledge there is no study about the direct interaction and cellular proteome for the IBV S, M and E proteins, a label-free proteomics method is introduced in this study for identifying the cellular interactome for these proteins.

1.6 An Overview of Label-Free Proteomics:

Proteomics can be defined as a large-scale study of proteins including their expressions, structures and/or functions. One major aspect of proteomics studies has been used in the quantitative analysis of proteome of a species in relation to expression of a bait protein (Aslam, *et al*., 2017). Since last two decades the advances in molecular biology and bioinformatics have allowed a significant progress of high-throughput techniques to examine protein expression at the cellular level and one example of these technique is mass spectrometry (MS). MS has been extensively used for quantitative proteomics to quantify the absolute or relative protein expression levels from different biological conditions (reviewed in Ankney *et al.*, 2018).

The method of the quantitative proteomics can be categorized into two methods: stable isotope labeling and label-free quantification. In stable isotope labeling the samples are labeled by different isotopes, mixed together and digested into peptides. Due to the mass difference between isotopes, the extracted peptides are recognized by the mass spectrometer and the abundance of them from each sample is quantified. The isotope labeling of the amino acid are either metabolic or chemical. The metabolic method integrates the isotopic labels during cellular metabolism and protein synthesis (Chahrour *et al.*, 2015). An example on metabolic-labeling method is stable isotope labeling with amino acids in cell culture (SILAC) (Ong, *et al*., 2002). The SILAC was used for elucidating cellular proteome during IBV infections (Emmott *et al.*, 2010a; Emmott *et al.*, 2010b; Emmott *et al.*, 2013).

The Label-free quantitative proteomics applies quantification strategies by spectral counting or spectrometric signal intensity (so called Area Under the Curve AUC) to measure the protein abundance in the samples. The samples are analyzed by the mass spectrometer separately using the similar protocol, by which the proteins from each sample are identified, and the abundance is estimated using either the number of MS/MS spectra identifying peptide or the intensity of the corresponding MS spectrum features of the protein (Wong and Cagney, 2010; Otto *et al*., 2014).

Despite the labeling categorization, proteomics studies generate very large amount of raw data, which include several hundred and even thousands of protein peptide sequences. The determination of the abundance of such number of proteins is acquired by computational and statistical analysis of the protein and there are specific software and programs for such data analysis (Välikangas, *et al*., 2017; Yu, *et al*., 2016).

One of the applications of label-free proteomics is to identify the protein-protein interaction of cellular interactome for the protein bait, which purified for injection to Liquid Chromatography-MS/ MS (LC-MS/MS) system (Chelius & Bondarenko, 2002; Wang, *et al*., 2003). Once the data is analyzed, the abundance of samples proteins is compared to the data obtained for controls and the proteins that are statistically significant in the replicates of the bait, are listed as the potential interactome for the bait protein (García-Dorival, *et al*., 2016; Munday, *et al*., 2015). In this thesis, LC-MS/MS is used for cellular interactome of IBV S, M and E proteins.

1.7 Targeting Virus-Host Interactions:

Identification of significant proteins in the samples by MS-based techniques may potentially be a biomarker, signal, chaperone or even a pathway of interest that can be targeted for therapeutics. However, the development pipeline needs to be validated carefully (García-Dorival, *et al*., 2016, 2014). For example, at the protein identification phase, large numbers of proteins are detected in the biological samples. The quantification approaches are then used to compose a short list of candidates for verification. The verification step is an important step to exclude false positive discoveries during the identification phase. Multiple assays are used for verification, such as enzyme-linked immunosorbent assays (ELISA), quantitative polymerase chain reaction (qPCR) and virologic techniques in case of viral protein interactions with the host and any further technique that can provide accurate and consistent comparison of protein levels in the biological samples. The validation of protein biomarkers can be confirmed by testing their performance in large cohorts of samples. Finally, clinical assays by either further in vitro or in vivo trials are developed for testing the biomarker and subjected to approval by regulatory health agencies (reviewed in (Drabovich, *et al*., 2013)). In the current thesis, based on label-free proteomics results, enzyme inhibition systems from the host cells are targeted and validated for potential small molecule therapeutics against IBV S, M and E proteins. This approach might be a supportive way to the classical prevention and control methods in terms of limiting the impact of IBV outbreaks in the vaccinated flocks, which has been challenging for both scientific research and poultry production industry (Bande, *et al*., 2015).

1.8 Aims and objectives of the Study:

The continuous impact of IBV to poultry industry in the world is the considerable economic loss and the control methods are still in challenge. As described before studying the biology of the viral structural S, M and E proteins in the host cells will provide a significant advance on the current literature. Based on that the aim of this PhD study is to determine of host cell proteins in the achieving of IBV S, M and E proteins. This will be obtained using label-free quantitative proteomics to determine the cellular interactome for each of these viral proteins. Experiments include over expression, small molecule inhibition and gene silencing will be used to investigate the functional relevance of the identified cellular proteins in the replication cycle of IBV.

Consequently, the aims of this thesis can be divided in to three work parts:

1- The first aim is the primary investigation for the cellular proteome, which is conducted by applying LC-MS/MS for immunoprecipitated samples from S, M and E over expressions. This part is described in Chapter 3 of this thesis.

2- Validation of the proteome per each of S, M and E protein is the second aim of this study and the results are described in Chapter 4 of this thesis.

3- Finally, targeting of the cellular pathway that is obtained from the validation data is the third aim, which is applied by using small molecule inhibitors and gene silencing assays. The results of this aim are described in Chapter 5 of this thesis.

Chapter 2

Materials and Methods

All the laboratories work in this study were done in **Respiratory and Emerging Viruses group** laboratory (**Hiscox Lab**) **in Infection Biology department,** which belongs to the **Institute of infection and Global Health** in **the University Liverpool.** The LC-MS/MS work was done by Dr. Stuart Armstrong in **Respiratory and Emerging Viruses group** lab.

2.1 General Preparations:

2.1.1 Virus Protein Sequences:

An IBV QX-like isolate (SDIB821/2012) was selected for synthesizing its complete S gene 3498bp (1165 amino acids), M gene 678bp (225 amino acids) and E gene 327bp (108 amino acids) in Life Technologies, Germany. The sequences were obtained from the whole genome sequence of the isolate in the National Center for Biotechnology Information (NCBI) (GenBank Accession Number: KF574761).

The amino acid sequences per each protein are listed bellow in a Fasta format:

>SDIB821/2012 S protein

MLGKSLFLVTILCALCSANLFDPANTYVYYYQSAFRPPNGWHLQGGAYAVVNSTN
YTNNAGSAEHCTVGVIKDVYNQSAASIAMTAPLQGMAWSKSQFCSAHCNFSEITV
FVTHCYSSGSGSCPITGMIARDHIRISAMKNGTLFYNLTVSVSKYPNFKSFQCVNNF
TSVYLNGGLVFTSNKTTDVTSAGVYFKAGGPVNYSIMKEFKVLAYFVNGTAQDVIL
CDNSPKGLLACQYNTGNFSDGFYPFTNSTLVREKFIVYRESSVNTTLALTNFTFTN
VSNAQPNIGGVNTFHLYQTQTAQSGYYNFNLSFLSQFVYKASDFMYGSYHPSCSF
RPETINSGLWFNSLSVSLAYGPLQGGCKQSVFSGRATCCYAYSYNGPIACKGVYA
GELQTNFECGLLIYVTKSDGSRIQTRTEPLVLTQHNYNNITLDKCVDYSIYGRVGQG
FITNVTDSAANFSYLADGGLAILDTSGAIDVFVVQGSYGLNYYKVNPCEDVNQQFV
VSGRNIVGILTSRNETGSEQVENQFYVKLTNSSHRRRRSIGQNVTSCPYVSYGRFC
IEPDGSLKMIVPEELKQFVAPLLNITESVLIPNSFNLTVTDEYIQTRMDKVQINCLQYV
CGNSLECRKLFQQYGPVCDNILSVVNSVGQKEDMELLSFYSSTKPAGYNAPVFSNI
STGDFNISLLLTQPSSPRGRSFIEDLLFTSVETVGLPTDAEYKKCTAGPLGTLKDLIC

AREYNGLLVLPPIITADMQTMYTASLVGAMAFGGITAAGAIPFATQIQARINHLGITQ
SLLLKNQEKIAASFNKAIGHMQEGFRSTSLALQQVQDVVNKQSAILTETMNSLNKN
FGAISSVIQDIYAQLDAIQADAQVDRLITGRLSSLSVLASAKQSEYIRVSQQRELATQ
KINECVKSQSNRYGFCGSGRHVLSIPQNAPNGIVFIHFSYTPESFVNVTAIVGFCVQ
PANASQYAIVPVNGRGIFIQVNGSYYITARDMYMPRDITAGDIVTLTSCQTNYVNVN
KTVITTFVEDDDFDFDDELSKWWNDTKHELPDFDDFNYTVPILNISGEIDHIQGVIQ
GLNDSLINLEELSILKTYIKWPWYVWLAIGFAIIIFILILGWVFFMTGCCGCCCGCFGII
PLMSKCGKKSSYYTTFDNDVVTEQYRPKKSV*

>SDIB821/2012 Membrane protein

MSNETNCTLDSEQAILLFKEYNLFITAFLLFITILLQYGYATRSRFIYILKMIVLWCFWP
LNIAVGVISCIYPPNTGGLVAAIILTVFACFSFIGYWIQSIRLFKRCRSWWSFNPESNA
VGSILLTNGQQCNFAIESVPMVLSPIIKNGALYCEGQWLAKCEPDHLPKDIFVCTPD
RRNIYRMVQKYTGDQSGNKKRFATFVYAKQSVDTGELESVATGGSSLYT*

>SDIB821/2012 E protein

MNFINKSLEENGSFLTALYIFVAFVALYLLGRALQAFVQAADACCLFWYTWVVVPG
AKGTAFVYKHTYGRKLNNPELEHVIVNDFPKNGWNNKSLPNFQDVQRDKLHP*

2.1.2 Gene Synthesis and Vector Preparation:

For tagging the gene by a fluorescent agent, Green Florescent Protein (pEGFP-C1) (BD Biosciences Clonetech, Catalog #6084-1) was selected as the expressing vector for S, M and E genes Figure 2.1. A plasmid Editor (ApE) as bioinformatics tool (ApE-v2.0.47 software) was used to confirm the absence of restriction sites of both *Bgl* II (AGA TCT) and *Sal* I (GTC GAC) restriction enzymes on the S, M and E gene sequences.

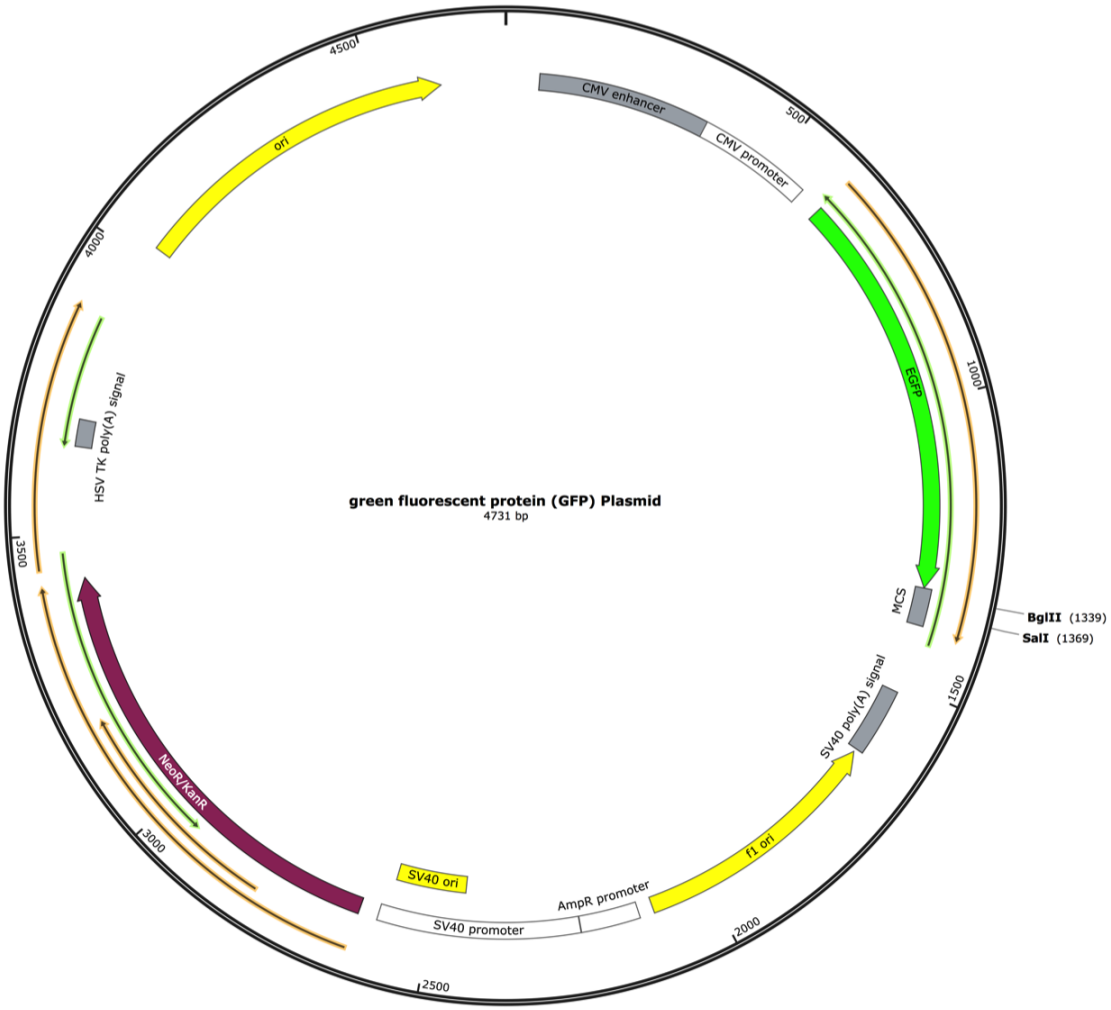

Figure 2.1: pEGFP-C1 restriction map and multiple cloning sites (MCS) (BD Biosciences Clonetech). Bgl II (AGA TCT) and Sal I (GTC GAC) restriction sites were analysed and selected for gene insertions. The MCS are between the EGFP coding sequences and the Simian Virus 40 polyadenylation signals (SV40-PA). Bgl II *and Sal* I *(pointed with lines) are the cloning sites for S, M and E constructs. S, M and E sequences are cloned into plasmid and expressed as fusions to the C-terminus of EGFP. (SV40 ori) is the origin for replication in mammalian cells expressing the SV40 T-antigen (Neor/Kanr) A neomycin/Kanamycin resistance cassette, consisting of the SV40 early promoter, the neomycin/kanamycin resistance gene of Tn5, and polyadenylation signals from the Herpes simplex virus thymidine kinase (HSV TK) gene. (f1 ori) is the origin for single stranded DNA production. The Map was created with SnapGene Viewer software version 4.2.9.*

The synthesized genes were then constructed in to the vector using GeneArt® Gene Synthesis service (Life Technologies). Briefly as described by the manufacturer: plasmid DNA as the synthetic gene (S, M and E genes) was assembled from synthetic oligonucleotides. The fragment was inserted into pEGFP-C1_P596. The plasmid DNA was purified from transformed competent *Escherichia coli* (E.coli) and the concentration was determined by UV spectroscopy. Codon optimization was also done and the following cis-acting sequence motifs were avoided where applicable: Internal TATA-boxes, chi-sites and ribosomal entry sites, AT-rich or GC-rich sequence stretches, RNA instability motifs, repeat sequences and RNA secondary structures and (cryptic) splice donor and acceptor sites in higher eukaryotes. The final construct was verified by sequencing and 5 µg of lyophilized plasmid per each gene was obtained. The plasmid was then dissolved to a final concentration of 5 µg/ml in double distilled water (ddH2O) and divided in to three aliquots for stocking, working and transformation.

2.2 Plasmid Methods:

2.2.1 Plasmid Transformation using Competent Cells:

For obtaining higher concentration of both pEGFP-C1 as positive control and pEGFP-C1-S, M or E as the targets, Subcloning EfficiencyTM DH5αTM Competent Cells (Invitrogen-18265-017), which are E. coli with lacZ∆M15 marker that provides α-complementation of the β-galactosidase gene was used for vectors transformation. According to the manufacturer's protocol, two tubes of 50 µl DH5αTM cell aliquots were thawed on wet ice. 5ng of

vectors were added to the cells and mixed gently without pipetting up and down and directly incubated on ice for 30 minutes. Vector up taking was done by heat shocking of cells for 20 seconds in a 42°C water bath without shaking and tubes were placed on ice for 2 more minutes. Pre-warmed Luria-Bertani (LB) broth medium (950µl) (LB; 1% [w/v] sodium chloride, 1% [w/v] tryptone and 0.5% [w/v] yeast extract) containing 50µg/ml Kanamycin antibiotic was added to each tube and they were incubated at 37°C for 1 hour at 225 rpm shaking incubator. Directly after incubation, two different volumes (20µl and 50µl) from each transformed vector were spread over pre-warmed selective plates LB agar containing Kanamycin antibiotic (50µg/ml) and the remaining transformation reaction were stored at +4°C. The cultured plates then were incubated overnight at 37°C. In the next day a single colony from each plate was picked and inoculated to a starter cultures (1ml LB medium containing Kanamycin antibiotic) and incubated for about 8 hours at 37°C with vigorous shaking (225 rpm). Finally, a large scaled volume (200ml) of selective LB broth medium was inoculated with each starter culture in a 1/500 dilution rate and were grown at 37°C for 12–16 h with vigorous shaking.

2.2.2 Large-scale plasmid DNA preparation (Maxi prep.):

For transfection experiments, high-quality and concentrated plasmid DNA was necessary, so a Plasmid Maxi Kit (10) (QIAGEN, 12162) was used for plasmid extraction and preparation. According to the manufacturer's instructions, following reaching the vector's (pEGFP-C1 and pEGFP-C1-S, M or E) transformed bacteria cultures to a stationary-phase, they were

harvested by centrifugation at 6000 x g for 15 minutes at 4°C and re-suspended in buffer P1 (50mM Tris.Cl [pH 8.0], 10mM EDTA, 100µg/ml RNase A) (stored at 4°C). Buffer P2 (200mM NaOH, 1% SDS [w/v]) was then added and mixed by inverting several times (due to containing Lyse-Blue reagent the mixtures were turned to blue colour). Ice-cold buffer P3 (3M potassium acetate, pH 5.5) was added to the mixtures and incubated on ice for 20 minutes following vigorous mixing by inverting several times until being colourless from blue. The mixtures were then placed in an ultra-fast centrifuge at 20,000 x g at 4°C for 30 minutes. The supernatants were immediately transferred to clean 50ml centrifuge bottles and further clarified by centrifugation at 20,000 x g for 15 minutes at 4°C. Meanwhile, a QIAGEN-tip500 column per each preparation was equilibrated by adding QBT buffer (750mM NaCl, 50mM MOPS [pH 7.0]), 15% isopropanol [v/v], 0.15% Triton® X-100 [v/v]). The clarified supernatants were then applied to the QIAGEN-tips and allowed to enter through the resin by gravity. The columns were washed twice by adding the QC buffer (1M NaCl, 50mM MOPS [pH 7.0], 15% isopropanol [v/v]) in to the columns and moved through the tips by gravity flow. The plasmid DNAs were then eluted using buffer QF (1.25M NaCl, 50mM Tris-Cl [pH 8.5], 15% isopropanol [v/v]) followed by precipitation in isopropanol and centrifugation at 15,000 x g for 10 minutes. The DNA pellet was then washed with 70% (v/v) ethanol and pelleted by centrifugation at 15,000 x g for 10 minutes. Finally, the pellet was air-dried and re-suspended in ddH2O.

2.2.3 Measurement of Plasmid Concentrations:

Concentrations of the plasmids from Maxi prep. were measured by Qubit™dsDNA BR Assay kit (Invitrogen). Briefly, according to the manufacturer's protocol, Working Solution (WS) was prepared from diluting of Qubit™Reagent in Qubit™Buffer in 1/200. The two standards were prepared freshly prepared in 1/200 WS. The samples were diluted in 1/200 in the WS as well. The tubes were then briefly vortexed for 2-3 seconds and incubated in room temperature for 2 minutes. For readings, the Qubit™2.0 Fluorometer was calibrated by freshly prepared standards and then the samples were put in the Qubit™2.0 Fluorometer for readings. The calculation analysis was done on the equipment by entering sample values and the concentrations were obtained in µg/ml.

2.2.4 Agarose Gel Electrophoresis:

The confirmation of plasmid length was confirmed by agarose gel electrophoresis. Briefly, the plasmids were diluted to 10-fold dilution and were run on the prepared agarose gel. In 1% (w/v) 0.5gm from molecular biology grade agarose powder (BIOLINE: BIO-4126) was dissolved in 1X Tris Acetate EDTA buffer (TAE) (Sigma) and boiled by microwave for 3 minutes. Upon cooling down to about 45˚C, SYBR Safe DNA Gel Stain 10,000X concentrate in dimethyl sulfoxide DMSO) (Invitrogen, S33102) was added. The diluted plasmid samples were mixed up with 5X DNA Loading Buffer (BIOLINE). All the samples and HyperLadder™I (BIOLINE) were loaded and run at 100V constant voltage for 40 minutes. The gel was then optimized in ChemiDoc Touch gel documentation system (Bio-Rad).

2.2.5 Plasmid Sequencing:

To check the stability of the sequences after transformation, all three plasmids for S, M and E gens were subjected for sequencing in Eurofins Genomics using either the standard pEGFPC1 forward and reverse primers or gene specific primers, which were designed by Primer-Blast (NCBI) according to the sequence of S gene for IBV SDIB821/2012 isolate as per GenBank Accession Number: KF574761. The list of the primer sequences is shown in Table 2.1.

Table 2.1: *Primers used for plasmids sequencing. pEGFPC1for and pEGFPC1rev primers were used as standard primers by Eurofins Company. The rest of the primers were designed according to the complete S glycoprotein sequence for IBV SDIB821/2012 isolate as per GenBank Accession Number: KF574761.*

Oligo Name	Sequence (5'-3')	Targeting Gene
pEGFPC1for	GATCACTCTCGGCATGGAC	S
SA-rev	GGTTGAAGTTGTAGTAGCCGC	S
SB-for	CAATGTGTCCAACGCCCAGC	S
SB-rev	CTGGTCTGGATGTACTCGTCG	S
SC-for	GCCCGAGGAACTGAAGCAG	S
SC-rev	GCTCTCTCTGCTGGGACAC	S
SD-for	AGACTGAGCAGCCTGTCC	S
pEGFPC1rev	CATTTTATGTTTCAGGTTCAGGG	S
pEGFPC1for	GATCACTCTCGGCATGGAC	M
pEGFPC1rev	CATTTTATGTTTCAGGTTCAGGG	M
pEGFPC1for	GATCACTCTCGGCATGGAC	E
pEGFPC1rev	CATTTTATGTTTCAGGTTCAGGG	E

2.3 Cell Culture Methods:

2.3.1 General Cell Culture Preparations:

In this study, Human Embryonic Kidney containing T antigen (293T) (Health Protection Agency Culture Collection HPACC 12022001) , Green Monkey Kidney (Vero) (ECACC 84113001) (Sheets, 2000), Doug-Foster-1 (Chicken Fibroblast) (DF-1) (Foster & Foster, 1996) and Direct Chicken Kidney (DCKC) (uncharacterized avian origin) cells were used for cell culture based protocols. 293T, Vero and DF-1 cells were cultured in Dulbecco's Modified Eagle Medium (DMEM) containing L-Glutamine (Sigma-Aldrich, D6429) and 10% Foetal Bovine Serum (FBS) (Sigma-Aldrich, F9665) without antibiotics) however DCKC cells were cultured in the same medium with 20% FBS and Penicillin-Streptomycin (Sigma Aldrich, P4333) (10,000 units penicillin and 10 mg streptomycin/mL). General cell culture procedures such as thawing, passaging, counting and freezing of cells were all done in concomitant with the preparation for plasmid transfections, virus infections and small molecules inhibition assays.

2.3.2 Plasmid DNA Transfection:

For expression of the proteins, 293T cell line was pre-seeded and calcium phosphate was used as a transfection-activating chemical. For transfection of a 144mm x 20mm tissue culture big dish (Nunclon™, 168381), 4×10^6 cells were seeded and incubated overnight at 37°C 5% CO_2 for achieving desired confluency of approximately 50%. Previously filtered 2M $CaCl_2$ by Minisart® NML, 0.2µm filters (Sartorius, 16534-K) and 25.6 µg of DNA were mixed and completed up to the specified volume (1280µl) by nuclease-free water. The

mixture was added very slowly in drop wise to an equal volume of 2×HBS HEPES buffered saline (274 mM NaCl, 50 mM HEPES, 1.5 mM Na2HPO4, pH adjusted to 7). They were then incubated for 30 minutes at room temperature before pipetting drop wise onto cells maintained in 25ml of normal growth media DMEM 10% Foetal Bovine Serum (FBS) without antibiotics). A 12 well plate with sterile cover slips in its well bases was also seeded and transfected for purpose of expression, localization imaging and small molecules treatment assays. The procedures were done inside class 2 microbiological safety cabinets.

2.4 Protein Study Methods:

2.4.1 Protein extraction by radioimmunoprecipitation assay (RIPA):

For direct Western Blot (WB) confirmation of proteins, following incubation of the transfected 293T cells (24 hours); they were checked for protein expression. The expressed and whole cellular proteins were then extracted using RIPA buffer (50mM Tris, [pH 7.5], 150mM NaCl, 1% NP40 alternative (v/v), 0.5% sodium deoxycholate (w/v), 0.1% sodium dodecyl-sulphate [SDS]). Briefly, the media were discarded from the dishes and the cells were washed with phosphate buffered saline (PBS) very gently. Sufficient amounts of RIPA buffer containing the protease inhibitor 1X Halt Protease Inhibitor Cocktail (Thermo Scientific, 78420) was then added to cover the cells in the dishes and incubated directly on ice for 15-30 minutes. Using the scraper, cells were taken off and the contents were transferred to microfuge tubes. They were then centrifuged at 14000 g at 4°C for 10 minutes and finally the supernatants were put into a new microfuge for direct quantification and WB.

2.4.2 Protein Extraction using Lysis buffer:

Immunoprecipitation (IP) of expressed proteins depends on non-denatured structures; therefore, after transfection of the plasmids, the proteins were extracted using Lysis buffer (10mM Tris/Cl pH 7.5; 150mM NaCl; 0.5mM EDTA; 0.5% NP-40). Cells in the 145mm^2 dishes were harvested using rubber scrapers and the contents (approximately 25ml) were poured in to a 50ml conical tube (2 dishes per 50ml tube because per an IP, approximately 10^7 of cells were needed which nearly stands for two 145mm^2 dishes). The tubes were then centrifuged at 1000g 4°C for 5 minutes and the supernatants were taken out carefully without disrupting the pellets. They were then washed by ice-cold PBS with disrupting the pellet and centrifuged again at 1000 x g at 4°C for 5 minutes (this step was repeated two more times). After third wash the PBS was discarded without disrupting the pellet and 200µl of the Lysis buffer (containing protease inhibitor) was added per each reaction. The mixtures were incubated on ice for 30 minutes and transferred in to a 1.5 ml microfuge tube before centrifuging 14000 x g at 4C for 10 minutes. Finally the supernatants were taken out and put into another new 1.5ml tube and stored at -80°C.

2.4.3 Protein Quantification by BCA Assay:

The whole cell lysates, which prepared according to the two former protein extraction methods, were subjected to protein concentration quantification by BCA (bicinchoninic acid) protein assay system (Pierce™ BCA Protein Assay Kit, 23225). According to the microplate procedure in the kit, Bovine Serum Albumin (BSA) standards were used to create a standard curve. A working

reagent (WR) was first prepared according to the kits equation (# standards + # unknowns) × (# replicates) × (volume of WR per sample) = total volume WR required). Each standard and unknown sample replicate was pipetted into each microplate well (working range = 100-2000µg/ml). The WR was then added to each well and the plate was mixed thoroughly for 30 seconds before its incubation at 37°C for 30 minutes. The absorbance was then measured at 570nm on TECAN plate reader using Magellan software and an equation for protein concentration calculation.

2.4.4 PEGFP-Trap®_A for Immunoprecipitation of PEGFP-S, M, or E Proteins (Pulldowns):

According to their concentrations, the volume of each lysate-supernatant was adjusted to 500µl – 1000µl by dilution buffer (10mM Tris/Cl pH 7.5; 150mM NaCl; 0.5mM EDTA) (containing 1mM phenyl methane sulfonyl fluoride (PMSF) and protease inhibitors). For direct immunoblot analysis the diluted lysate-supernatant was combined with equal volume of 2x SDS-sample buffer. The PEGFP-Trap®_A beads in the form of bead slurry was then equilibrated by re suspending in ice-cold dilution buffer (It is recommended that during incubation with the beads, the final concentration of detergents does not exceed 0.2% to avoid unspecific binding of the matrix) and spun down at 2500 x g for 2 minutes at 4°C. The supernatant was discarded and the beads were washed 2 more times with ice-cold wash buffer (10mM Tris/Cl pH 7.5; 300mM NaCl; 0.5mM EDTA). The diluted lysate-supernatant was then added to the equilibrated PEGFP-Trap®_A beads and the mixture was incubated for 1 hour at 4°C under constant mixing. The beads-bound

proteins were then eluted by adding 0.2 M glycine pH 2.5 and incubated for 30 seconds under constant mixing followed by 2-minute centrifugation at 4°C. The supernatant was transferred to a clean tube and 1M Tris base pH 10.4 was added for neutralization. The beads were re suspended in 2x SDS-Sample buffer (120mM Tris/Cl pH 6.8; 20% glycerol; 4% SDS, 0.04% bromophenol blue; 10% β-mercaptoethanol) and boiled for 10 minutes at 95°C to dissociate immunocomplexes from them and centrifuged at 2500 x g for 2 minutes at 4°C. The supernatant was then directed to SDS-PAGE.

2.4.5 Sodium-dodecyl sulphate polyacrylamide gel electrophoresis (SDS-PAGE):

Total cellular and/or transfected proteins from either RIPA, Lysis buffer or GFP trapped samples (~5µg) were determined using a Bio-Rad Mini-PROTEAN Tetra electrophoresis system. Resolving and stacking gels were made according to Sambrook & Russell protocol (Sambrook & Russell, 2001). Acrylamide gels were made using 30% acrylamide and due to the predicted high molecular weight of GFP-S proteins (~200 kDa), 12, 10 and 8% resolving gel were prepared according to standard volumes in Table 2.1. The resolving gel solution was gently poured between two clean glass plates that were previously fixed in a stand and a small volume of water was added to provide a smooth gel interface. After hardening of the resolving gel and discarding of the water, the stacking gel solution was prepared and poured on top of the resolving gel and a comb was added. Following stacking gel polymerisation the comb was removed and the wells were washed with 1x SDS-PAGE running buffer (25mM Tris-HCl [pH 8.3], 250mM glycine, 0.1 %

SDS [w/v]). Protein samples were prepared using 5x SDS sample buffer and denatured at 90°C for 10 minutes. Color Prestained Protein Standard, Broad Range (NEB: 11-245 kDa [P7712S]) was loaded as a reference for molecular weight. SDS-PAGE gels were run at 200V in 1x SDS-PAGE running buffer for about 45-55 minutes.

Table 2.2: *SDS-PAGE resolving and stacking gel preparation recipe. Acrylamide stock refers to 30% acrylamide. The green highlighted cells were mostly used in this study. APS = ammonium persulphate. TEMED = Tetramethylethylenediamine.*

Resolving Gel (5 ml)					**Stacking Gel (2.5 ml)**	
% Gel / Materials	**15%**	**12%**	**10%**	**8%**	**% Gel**	**5%**
30% Acrylamide	5 ml	4 ml	3.3 ml	2.7	30 % Acrylamide	830 µl
1.5M Tris-HCl pH8.8	2.5 ml				1M Tris-HCl pH6.8	630 µl
H2O (ml)	2.3	3.3	4	4.6	H2O	3.4 ml
10% (w/v) SDS	100 µl				10% (w/v) SDS	50 µl
10% (w/v) APS	100 µl				10% (w/v) APS	50 µl
TEMED	10 µl				TEMED	5 µl
(kDa)	10-40	20-100	30-100	25-200		

2.4.6 Immunoblotting:

Meanwhile SDS-PAGE reaching its end, transfer membranes (Immobilon®-P transfer, Millipore) were activated in 100% methanol and equilibrated in Towbin buffer (25mM Tris-HCl [pH8.3], 192mM glycine, 20% methanol [v/v]). Two identical thick pieces of filter paper were also soaked in the buffer. One piece of them was then placed on the surface of a Hoefer TE70X semi-dry transfer unit, the soaked membrane was placed on top of this, followed by the complete SDS-PAGE gel. Finally, the second piece of soaked filter paper was placed on top of the SDS-PAGE gel. Due to the large molecular weight of the GFP-S protein over 200 kDa, the transfers were performed for 2 hours at 15 V with soaking the sandwich after first hour to prevent drying. Following transfer, the membranes were blocked in 5% (w/v) non-fat skimmed milk powder prepared in Tris-buffered saline (50mM Tris-HCl [pH 8.3], 150mM NaCl) containing 0.5% (v/v) Tween-20 (TBS-T). Immobilised proteins were detected with primary GFP Rabbit polyclonal IgG antibody 200 µg/ml (Santa Cruz Biotechnology) in 1/2000 dilution rate, which was diluted in 5% milk-TBST (w/v) and applied for either 1 hour at room temperature or overnight at 4°C with gentle rocking. The primary antibodies were then conjugated with the secondary Goat Anti-Rabbit IgG antibodies (Sigma, AG154), which was diluted also 1/2000 in 5% non-fat skimmed milk-TBST (w/v) and incubated for 1 hour at room temperature with rocking. Antibody-bound proteins were determined by Clarity Western ECL substrate (Bio Rad) and visualised using ChemiDoc Touch documentation system (Bio Rad). All antibodies used for immunoblotting are listed in Table 2.5.

2.4.7 Blot Restoring:

For rejuvenation and hydrating dry membranes and to remove antibodies from the first immunoblot, the blotted membranes were washed off with stripping buffers in (Blot Restore kit, Millipore, #2520). Briefly according to the kit's protocol, after dilution of both Blot Restore Solutions A and B from 10X to 1X, the membranes were submerged in the Solution A and incubated for 10 minutes at room temperature with gentle agitation. After discarding Solution A, the Solution B was then added for submerging the membranes and incubation for 15 minutes in room temperature with gentle agitation as well. The membranes were then blocked with blocking buffer (5% milk-TBST (w/v)) for 5 minutes in gentle rocking. After repeating the blocking step with fresh blocking buffer, the membranes were incubated with Rabbit Anti-Calnexin polyclonal primary antibody in a dilution of 1/10000 in the blocking buffer (5% milk-TBST (w/v)) and incubation for 1 hour in room temperature on the rocker. The membranes were then conjugated with the secondary Goat Anti-Rabbit IgG antibody, which was diluted also in the blocking buffer 1/2000 and incubated for 1 hour at room temperature with rocking. Finally, Antibody-bound proteins were then determined by Clarity Western ECL substrate and visualised using ChemiDoc Touch documentation system. All antibodies used for blot restoring are listed in Table 2.5.

2.5 Quantitative Label-Free Mass Spectrometry Method:

2.5.1 Liquid Chromatography-Mass Spectrometry/ Mass Spectrometry (LC-MS/MS):

Three sets of pulldown samples were prepared for LC-MS/MS running and analysis. Set 1 was a sample from each of PEGFP and PEGFP-S were submitted for LC-MS/MS running and optimization analysis, set 2 was five replicates for each of PEGFP and PEGFP-S samples and set 3 was six replicates per each of PEGFP, PEGFP-M and PEGFP-E pulldown samples. The samples were then run and analysed by Dr. Stuart Armstrong in the Department of Infection Biology (University of Liverpool).

Sample preparation for PEGFP, PEGFP-S, PEGFP-M and PEGFP-E started with 80µl from each and diluted by two-fold with 25 mM ammonium bicarbonate. For detergent treatment step, 1% (w/v) Rapigest (Waters MS Technologies) was added to a final concentration of 0.05% (w/v), and the sample was incubated in 80 °C for 10 minutes with intermittent brief vortex and short spin by 5 minutes interval. Proteins were reduced with 10µl of a 9.2 mg/ml dithiothreitol (DTT) (Sigma) to a final concentration of 3mM at 60 °C for 10 minutes. The alkylation step was done by adding of 33mg/ml iodoacetimide solution (Sigma) to a final of approximately 9mM and incubated at room temperature for 30 minutes in the dark. In the digestion step, of proteomic-grade trypsin (Sigma) for a 50:1 protein: trypsin ratio was added (200 µg/ml trypsin in ammonium bicarbonate), and samples were incubated at 37°C 12-16 hours (overnight). To inactivate the detergent, after a quick spin down of the digest, the Rapigest was removed by adding of

trifluoroacetic acid (TFA) to a final concentration of 1% (v/v) and incubated at 37°C for 1-2 hours. Peptide samples were centrifuged twice at 13000 x g for 15 minutes at 4°C to remove all insoluble materials including precipitated Rapigest. The supernatant fraction was then removed carefully and desalted by C_{18} reverse phase stage strips (Thermo Scientific). The samples were then desalted and reduced to dry and re-suspended in 3% (v/v) acetonitrile, 0.1% (v/v) TFA for injection directly to the column in the LC-MS.

Peptides were then analysed by on-line Nanoflow LC and using the Ultimate 3000 nano system (Dionex/Thermo Fisher Scientific) connected with a Q-Exactive mass spectrometer (Thermo Fisher Scientific). Samples were injected in to a Nano-Trap column (Acclaim® PepMap 100, 2 cm × 75µm, C18, 3µm, 100 ˚A) then eluted in line with the analytical column (Easy-Spray PepMap®RSLC, 50cm x 75µm, packed with 2µm C18, 100 ˚A particles) which then fused to a silica nano-electrospray emitter (Dionex). The column was operated at a stable temperature of 35°C. Chromatography was done with a buffer system consisting of 0.1% formic acid (buffer A) and 80% acetonitrile in 0.1% formic acid (buffer B). The peptides were then separated by a linear gradient of 3.8% to 50% buffer B over 90 minutes at a flow rate of 300 nl/min. The Q-Exactive was operated in data-dependent mode with survey scans acquired at a resolution of 70000. Up to the top 10 most abundant isotope patterns with charge states +2, +3, and/or +4 from the survey scan were selected with an isolation window of 2.0Th and fragmented by higher energy collisional dissociation with normalized collision energies of 30. The maximum ion injection times for the survey scan and the MS/MS

scans were 250 and 50 ms, respectively. Finally, the ion target value was set to 1E6 for survey scans and 1E5 for the MS/MS scans.

2.5.2 Data Analysis for Protein Identification and Quantification:

Identification and quantification of the proteins was conducted as practically as described by (Dong, *et al*., 2017). Thermo RAW files were imported into Progenesis QI for proteomics (Nonlinear Dynamics, version 4.1). Runs were time aligned using default settings and using an auto selected run as reference. Peaks were selected by the software on default settings and filtered to include only peaks with a charge state between +2 and +7. Spectral data were then converted into .mgf files with Progenesis QI for proteomics and exported for peptide identification using the Mascot (Matrix Science, version 2.3.02) search engine. Tandem MS data were searched against translated ORFs from UniProt Knowledge Base (UniProtKB) reference entries for S (UniprotKB: T1YWG6), M (UniprotKB: U5U9J5) and E (UniprotKB: U5U766) and a contaminant database (cRAP, GPMDB, 2012). The search parameters were as follows: precursor mass tolerance was set to 10 ppm and fragment mass tolerance was set as 0.05Da. Two missed tryptic cleavages were permitted. Carbamidomethylation (cysteine) was set as a fixed modification and oxidation (methionine) set as variable modification. Mascot search results were further validated using the machine-learning algorithm Percolator embedded within Mascot. The Mascot decoy database function was utilised and the false discovery rate was <1%, while individual percolator ion scores> 13 indicated identities or extensive homology ($p < 0.05$). Mascot search results were imported into Progenesis QI for

proteomics as extensible mark-up language data (XML) files. Peptide intensities were normalised against the GFP reference run by Progenesis QI for proteomics and these intensities were used to highlight relative differences in protein expression between sample groups. Only proteins with 2 or more identified peptides were included in the dataset. Statistical analysis (ANOVA) of the data was performed using Progenesis QI for proteomics to identify significantly ($p<0.05$, $q \leq 0.05$, relative fold change ≥ 2) differentially expressed proteins.

2.6 Proteome Bioinformatics Methods:

2.6.1 Clustering of Proteome lists (Heat maps):

To visualize the analysed data from LC-MS/MS, Morpheus online program was used (https://software.broadinstitute.org/morpheus). In Morpheus program, the core interface is a heat map, in which a matrix of values is mapped to a matrix of colours. The significant protein list from MS data was put in an Excel file and uploaded to the program and the columns in the file were determinant of the annotations on the heat map as well. In analysis of this study, only accession numbers and description of the proteins were left as annotation identities for the columns. Upon analysis of the file, the graphical interface of the program was revealed and in the option window the colour scheme and shapes of the matrix colours were changed up to the desired format. Finally, the heat maps were then exported in to the image files and visualized as results.

2.6.2 Proteome Interaction Network:

The interaction networks among the viral and cellular proteins were further optimized in to the cell. CellWhere1.1 online program (https://www.sys-myo.com/cellwhere) was used (Zhu, *et al*., 2015a). CellWhere is the graphical display of gene or protein association networks organized on subcellular localizations. The UniProt accession number list for the significant proteins were pasted in to the gene or protein's box 1 and the identifier was set on UniProt accession. The localization source in box 2 was set on UniProt and Go as the program recommends it. The interactors from Mentha were added by ticking the box 3 (CellWhere uptakes protein-protein interaction from Mentha browser). The annotation frequency was finally ticked in the box 4 and the protein was submitted for visualization of the interactome and subcellular localizations.

2.6.3 Glycosylation Prediction:

In order to predict the N-linked glycosylation motifs in the amino acid sequences of S, M and E proteins, N-GlycoSite online program (https://www.hiv.lanl.gov/content/sequence/GLYCOSITE/glycosite.html) was used. The program predicts N-linked glycosylations based on NXS/T motifs where the X can be any amino acid except Proline. The amino acid sequences per each protein were put in the Input box of the program. The Options box was selected for exclusion of NPS/T pattern and first asparagine in NN [S/T][S/T], the sequences were submitted and both sequences and graphics were accessed to visualize the results.

2.6.4 Model Design:

In the current study two models were designed for visualizing the process and maturation of the viral proteins inside the ER and Golgi of the host cell. For the design graphics, CellDesigner Version 4.4 software (Funahashi, *et al*., 2003) was used as a modeling tool for a biochemical network between the viral and cellular proteins. The designs were based on the ER and Golgi processes for N-linked glycoproteins involving Calnexin as a cellular chaperone. Technically, the graphical user interface of CellDesigner 4.4 provided illustrative items and transition steps in its toolbar, which were needed for the design process. Basically, for each graph, a specific rectangle with predicted height and width was set for representing the ER and Golgi organelles. In the ER an internal rectangular outline was also put to denote ERQC. The steps and molecules shapes were then put in a subsequent way according to this study's results, proteome databases and literature supports.

2.7 De-glycosylation Methods:

2.7.1 Protein De-glycosylation Assay:

The de-glycosylation study was done for expressed EGFP-tagged proteins using Peptide-N-Glycosidase F (PNGase F) enzyme (Sigma, P7367). PNGase F enzyme was prepared from dissolving lyophilized material by adding 100 µl of high purity water to the 50-unit vial and the final concentration was 0.5 unit/µl. The glycoproteins were denatured by adding about 50 µg of the protein in to 45µl ammonium bicarbonate (PH 8), and then 5 µl of denaturation solution (0.2% SDS and 2-mercaptoethanol) was added

to the mixture. The whole solution mixture was then heated until 100°C for 10 minutes to denature the proteins. After cooling down, 5 units of PNGase F enzyme was added to the mixture and was incubated at 37°C for about 3 hours. The reaction was stopped by reheating the mixture in 100°C for 5 minutes and equal volume from each samples were optimized by WB.

2.7.2 Direct Virus De-Glycosylation Assay:

To investigate the infectivity of IBV virions, direct de-glycosylation of the virions was conducted. A hypothetic protocol was designed for the assay, in which, IBV virions in the centrifuged supernatants with concentration of 10000 PFU/ml were incubated in two different concentrations of 5 and 10 units of the PNGase F enzyme. Each set of enzyme treatment was run with untreated replicates and incubated and in the same buffers for 3 hours in 37°C. The result was optimized by median tissue culture infectious dose (TCID50) quantification of infective virions.

2.8 Fluorescent Microscopy Methods:

2.8.1 Transfected Cell Fixation, Staining and Confocal Imaging:

For localization study of expressed proteins, 2×10^5 or 1×10^5 293T cells were seeded on sterilised cover slips inside 6 or 12 well tissue culture plates with DMEM 10% FBS and incubated overnight at 37°C 5% CO_2. After vectors transfection and another incubation as former one, the media was discarded and the cover slips were washed with 1X PBS (Sigma, D8662). 1 ml of 4% Paraformaldehyde (PFA) PH 7 was then added to each well as a fixation

agent and incubated for 15 minutes in RT. Before remaining in the last wash, the cover slips were washed 3 more time by 1 X PBS. Meanwhile a drop of ProLong® Gold Antifade Reagent with DAPI (Molecular Probes) was put on clean glass slides. The cover slips were then semi dried and placed upside down onto the stain drop on the glass slides. They were then incubated for 24 hours at room temperature in dark and cleaned for imaging under fluorescent microscope (Carl Zeiss, Axio Imager 2) and analysis by ZEN 2 Pro software. An oil emersion lens (63X) was used for studying localization of expressed proteins in side cells. The images were linearized and formatted to automated best fit using blue (DAPI) and green (GFP) imaging filters forming either mono or double colour merge images.

2.8.2 Immunofluorescence Assay:

To detect subcellular localization of protein-protein interactions and validating study of Calnexin with the expressed proteins, the fixed cells, as it was described in section 2.7.1, were permeabilized by the addition of PBS containing 0.1% (v/v) Triton X-100 for 10 min at room temperature. The permeabilization buffer was removed and the monolayer was washed three times with PBS. Rabbit Anti-Calnexin primary antibody was diluted 1:50 in PBS containing 2% (v/v) FBS (Table 2.5) and 50 µl of the primary antibody dilution was pipetted onto each coverslip for 1 hour in room temperature as incubation period. Coverslips were washed three times in PBS-0.5% Tween-20 (PBST) to remove unbound primary antibody. The fluorescently conjugated (Alexa Fluor 546) Donkey anti-Rabbit secondary antibody (Table 2.5) was diluted 1:200 in PBS containing 2% FBS and 50 µl of the secondary

antibody dilution was pipetted onto each coverslip for incubation of 1 hour in room temperature. Coverslips were washed three times in PBST to remove unbound secondary antibody. The cover slips were then semi dried and placed upside down onto the stain drop of ProLong® Gold Antifade Reagent with DAPI (Molecular Probes) on the glass slides and incubated for 24 hours at room temperature in dark. The slides were then cleaned for imaging under fluorescent microscope (Carl Zeiss, Axio Imager 2) and analysis by ZEN 2 Pro software. An oil emersion lens (63X) was used for studying colocalization of Calnexin interaction with expressed proteins in side cells. The images were linearized and formatted to auto best-fit using triple filters of blue 385 nm (DAPI), green 475 nm (GFP) and red 590 nm (Rhodamin) imaging filters and forming both channel specific and merge images.

2.8.3 Image Analysis:

Image analysis by ZEN 2 Pro software on Carl Zeiss, Axio Imager 2 fluorescent microscope was performed for all images obtained from either expression or localization studies. The software parameters were set on the specific Acquisition per the requirements of this study. In the Acquisition Mode, the active camera was set on default; the white balance and saturation were reseted for each channel. In the Mode, the colour mode (RGB) was selected, the live speed was put on slow and the resolution was set on 1388x1040 High Quality. In the post processing options, Black reference was selected and noise filter was enabled. For the Channel usages, two different modes were applied; for the expression only slides, DAPI (Blue) and GFP (Green) were selected while for colocalization study Alexa Fluor 546 (Red)

was added to the previous channel mode. After setting all the parameters and setting exposure of the spots, the images were snapped and they were analysed accordingly. In the Display box, all channels were selected and the Best Fit, which is an automatic correction of the image, was ticked. In the same box the whole image was linearized on 1.0. Finally, the Range Indicator was ticked in the Dimensions box for exposure autocorrecting option. The Scale Bar was then put on the analysed images and before the final export, the images were created from the view using (Create Image from View) icon and saved as analysed images.

2.9 Enzyme and Proteins-Interaction inhibition Methods:

2.9.1 Enzyme Inhibitors:

For validation of protein-protein interaction, enzyme inhibition methods were used by treatment assays with two enzyme-inhibiting small molecules. The approach plan was designed according to the label-free proteomic data and its validations per S, M and E proteins. For inhibiting calnexin interaction and glycosylation of the proteins, 1-Deoxynojirimycin Hydrochloride (DNJ) (D9305, Sigma) and 1-Deoxymanonojirimycin Hydrochloride (DMJ) (D9160, Sigma) were used.

Both DNJ and DMJ have same molecular weight (MW=199.63 g/mol) and the total 5mg of each solute were dissolved in a total volume of exactly 1.002 ml sterile cell culture grade PBS, in which the total final concentration became 25mM. Total volume of the stock referred to the final solution volume, which

was combined volume of solute and solvent. Generally the dilution of the stock was set on diluting 100µl of the 25mM stock solution with PBS to a final volume of exactly 1ml, the concentration of the diluted solution was 2500µM.

2.9.2 siRNA Knockdown:

For abolishing and silencing the effect of Calnexin chaperone, the siRNA for Calnexin was synthesized. The sequence was obtained from a research on Dengue virus envelope protein interaction with ER chaperones (Limjindaporn, *et al*., 2009) Table 2.3. The GAPDH siRNA, which was used as a positive control was designed according to the sequences of GAPDH mRNA for the original species of the cell lines Table 2.3. Briefly, Multiple sequence alignment of the sequences was done, a conserved region was determined and the selected sequence was pasted in to siDirect version 2.0 online program (http://sidirect2.rnai.jp) for siRNA design. However a simple check in the literature realized than the sequence was used by other studies as well (Liu, *et al*., 2010; Wang, *et al*., 2012; Zhu, *et al*., 2015b).

The siRNAs were then synthesized by (Eurofins) and dissolved in 1x siMAX universal buffer, which was diluted from the enclosed stock solution of 5x siMAX universal buffer [30mM HEPES, 100mM KCl, 1mM MgCl 2; pH = 7.3; sterile] (Eurofins). For complete re-suspension of siRNAs, the RNA oligo was heated to a mild treatment of 55-60°C for approximately 5 minutes and stored at -20°C in a freezer. The final stock concentration of the aliquots per each Calnexin and GAPDH siRNAs were set on 100µM for further analysis of cytotoxicity and knockdown concentrations.

Table 2.3: *siRNA oligonucleotides used in this study. CANX stands for Calnexin as the target of knockdown in this study. GAPDH is a positive control knockdown of the housekeeping gene GAPDH. Total µg: is the yielded weight of the oligos after synthesis. Total nmol values are the total concentration after dissolving of the oligos. MW: is the Molecular Weight of the oligos.*

Oligo Name	Sequence (5'-3')	Total µg	Total nmol	MW g/mol
CANX	AUAGAAUGUGGUGGUGCCUAUGUGAdTdT	343	20	17142
Sense 5' - [AUAGAAUGUGGUGGUGCCUAUGUGA] RNA 8688 g/mol Antisense 5' - [UCACAUAGGCACCACCACAUUCUAU] RNA 8454 g/mol				
GAPDH	GUGGAUAUUGUUGCCAUCAdTdT	266	20	13285
Sense 5' - [GUGGAUAUUGUUGCCAUCA] RNA 6648 g/mol Antisense 5' - [UGAUGGCAACAAUAUCCAC] RNA 6637 g/mol				

2.9.3 Cell Viability Assays:

Cell viability or cytotoxicity of DNJ and DMJ small molecules and siRNA was measured using a colorimetric MTT (3-(4,5-Dimethylthiazol-2-yl)-2,5-diphenyltetrazolium bromide) (Sigma, M5655) assay. Vero, 293T and DF1 cells were seeded at density of $1x10^3$ cells/well in clear 96-well micro plates 24 hours prior to DNJ and DMJ treatments Table 2.4. Following the treatment, 1 mg MTT powder was dissolved in 1 ml DMEM (plus 10% [v/v] FBS) at 37°C to make a 10 mM solution, and filtered through a 0.2 µm filter (Minisart® NML, 0.2µm, Sartorius). Media was aspirated and the wells washed with PBS followed by the addition of 100 µl MTT per well. Plates were incubated for 30-40 min at 37°C before 100 µl DMSO per well was added and pipetted thoroughly. MTT (a yellow tetrazole) was reduced to purple formazan in living cells. Absorbance was then measured at between 425 and 570 nm on a Tecan plate reader. A dose-response curve was then produced to assess cell viability. Etoposide (4'-Demethylepipodophyllotoxin9-(4,6-O-Ethylidene-β -D-Glucopyranoside) (Sigma, E1383) was used as a positive control with high cytotoxicity rate. 25 mg of Etoposide (MW = 588.56 g/mol) was dissolved in 850 µl DMSO (Sigma, D8418) and the final concentration of 50 mM as a stock was obtained. The stock was then further diluted until 200 µM was prepared for MTT assay.

Table 2.4: *Cell viability assay plan for drugs and siRNAs. The plan represents calculations of concentrations and volumes of the drugs or siRNAs for 96 well plates in a triplicate well per each either treatments or transfections.*

	<>	1	2	3	4	5	6	7	8	9	10	11	12	
DNJ/ CANX	**A**	PBS	DMSO	5	10	50	100	200	300	400	500	1000	ETOP 200 µM	Conc. µM
	B	PBS	8	0.2	0.4	2	4	8	12	16	20	40	ETOP 200 µM	µl / Well
	C	PBS	24	0.6	1.2	6	12	24	36	48	60	120	ETOP 200 µM	µl / 3 Well
	D													
	E													
DMJ/ GAPDH	**F**	PBS	DMSO	5	10	50	100	200	300	400	500	1000	ETOP 200 µM	Conc. µM
	G	PBS	8	0.2	0.4	2	4	8	12	16	20	40	ETOP 200 µM	µl / Well
	H	PBS	24	0.6	1.2	6	12	24	36	48	60	120	ETOP 200 µM	µl / 3 Well

2.9.4 Treatment Parameters:

Apart from cell viability assay of the small molecule's concentrations, several optimizations and trials were done to detect the best choice of the treatments (data not shown). However, the final concentration of 100 µM was selected as the treatment of choice for both DNJ and DMJ in the time line of 24 hours prophylactic treatment before transfection of the plasmids in 293T cells according to the treatment plan in Figure 2.2.

A: DNJ

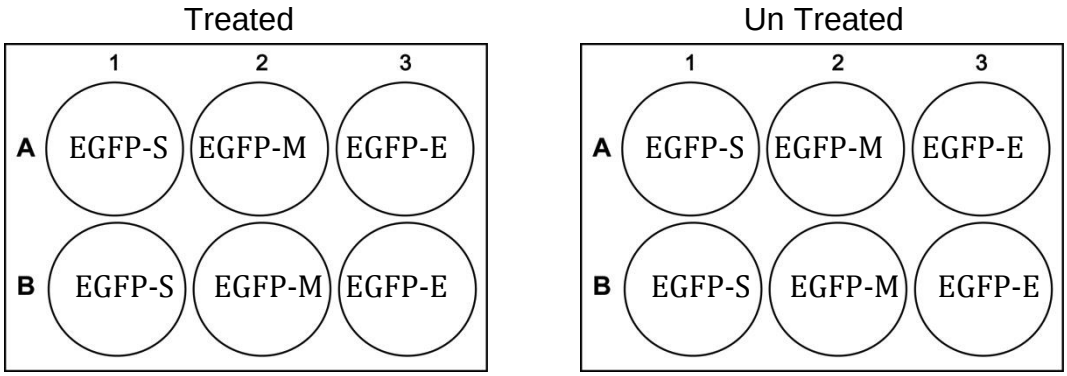

B: DMJ

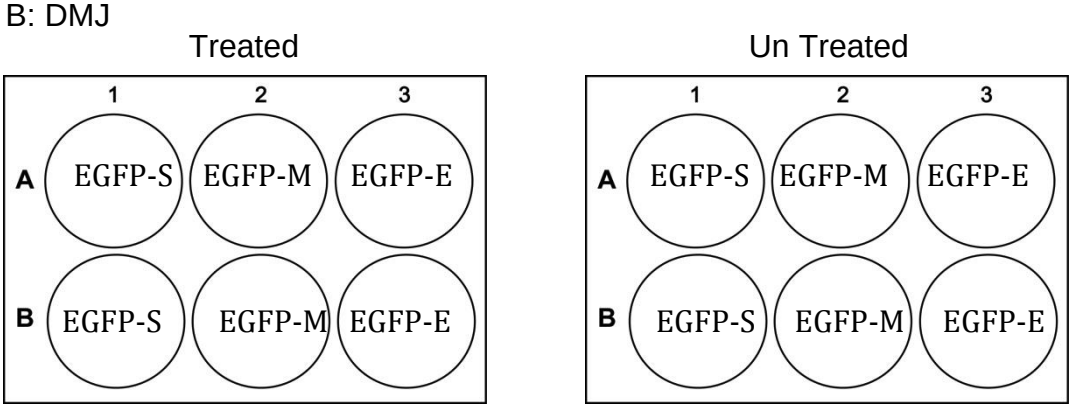

C: Controls

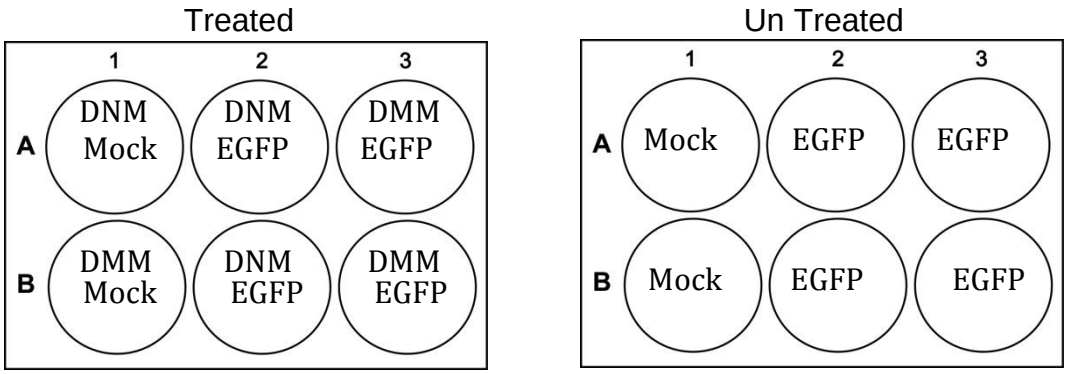

Figure 2.2: Treatment plan of 293T cells by DNJ and DMJ small molecules. A: 6 well plates were prepared as treated and untreated for DNJ 24 hours before plasmid transfection per the written plasmid name inside the wells. B: 6 well plates were prepared as treated and untreated for DMJ 24 hours before plasmid transfection per the written plasmid name inside the wells. C: Controls were prepared per run of WB optimization after expression of proteins under specified conditions. Mock wells were mock transfected for the plasmids and EGFP for the wells transfected with EGFP plasmid only.

The transfection protocol was then applied per the 2 ml media volume of 6 well plates as it was described in section 2.3.2.

2.9.5 Calnexin Knockdown:

As per the cell viability protocol in which most of the concentrations were had high viability ratios, an optimization of Calnexin siRNA transfections were done in both 293T and Vero cells. HiPerFect transfection Reagent (Qiagen) was for transfection and according to the manufacturer's protocol, around 1x 10^5 cells were seeded in 24 well plates 24 hours prior to the siRNA transfections. The transfection was done in a series of concentrations of Calnexin, GAPDH, Scrambled and Mock siRNAs transfections Figure 2.3. The recommended concentrations were diluted in culture medium without FBS serum and mixed with the HiPerFect transfection Reagent. The mixture was then vortexed and incubated for 10 minutes in room temperature before adding as gentle drop-wise over the pre seeded cells. The cells were then left for 48 hours incubation and the optimization was validated by WB.

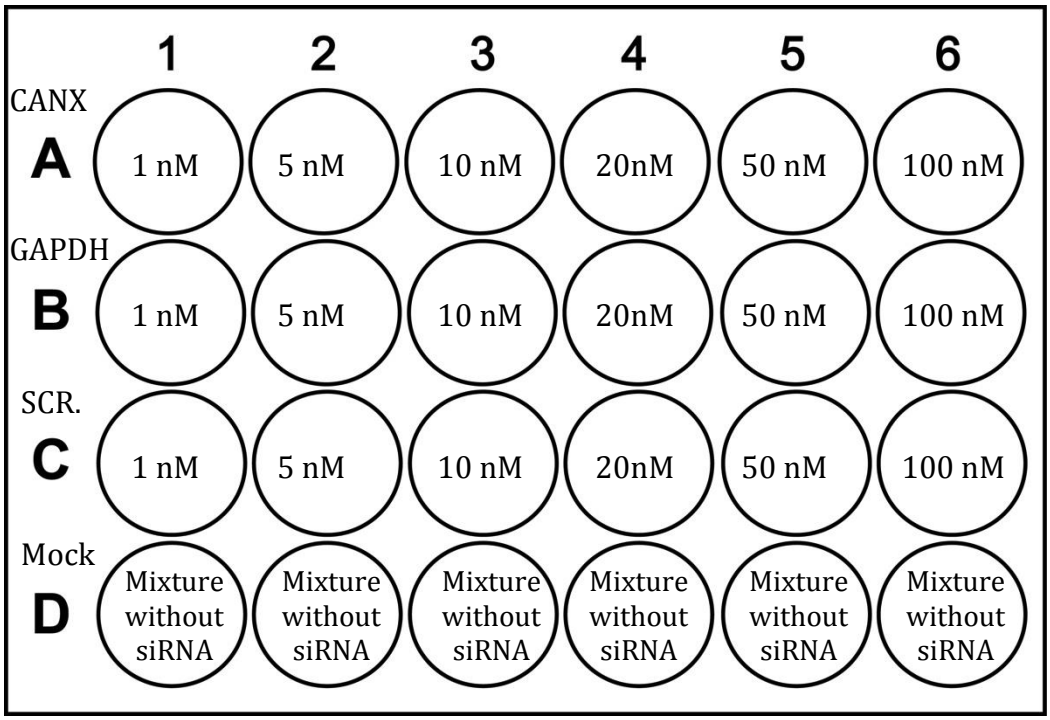

Figure 2.3: siRNA Transfection optimization plan. Row A represents Calnexin siRNA transfection in a serial concentration of the siRNA as per each well. Row B represents GAPDH as a positive control. Row C for Scrambled siRNA transfection as a Negative control. Row D is for mock siRNA transfected wells.

2.10 Virology Methods:

In this study (BeauUS) laboratory adapted IBV strain (kindly provided by Dr. Erica Bickerton from Pirbright Institute) was used for virus infection studies using Vero and DF1 cells.

2.10.1 Virus Propagation in Cells:

The unknown tittered virus was propagated in both Vero and DF1 cells for producing high titer supernatant for further analysis. Briefly, an inoculum was prepared by diluting a part from the virus-containing fluid to 10-fold in the

DMEM medium with Penicillin-Streptomycin antibiotics. The inoculum was then added to the pre washed monolayer Vero and DF1 cells by PBS and incubated for 1 hour in 37°C temperature for virus attachment. Following washing the inoculum, fresh part of DMEM containing 1% FBS was added on the cells and incubated for 72 hours in 37°C Co2 incubator. The supernatant was then filtered by 0.2µm filter (Minisart® NML, 0.2µm, Sartorius) and subjected to titration analysis.

2.10.2 Virus Quantification:

The virus stocks were titrated by quantification assays such as Plaque and TCID50 assays to confirm the titer of the stocks before dilution and further analysis of treatment and siRNA transfections.

2.10.2.1 Plaque Assay:

Viral titration for stock supernatants were determined using plaque assays. Briefly, Vero cells were seeded into 6-well plates 24 hours prior to infection with an inoculum of 10-fold serially diluted virus stock. The inoculum was allowed 1hour of absorption at 37°C, unbound virus particles were washed off twice with PBS and maintained in DMEM 10% Low Glucose, (Sigma, D2429) containing 1% FBS and 1% Carboxymethyl cellulose (CMC) (Sigma) as an overlay agar for 72 hours. The cells were then fixed with 4% paraformaldehyde and stained with 0.1% Crystal Violet. The number of plaques was then counted, and the virus titer was calculated as Plaque Forming Unit per milliliter (PFU/ml) according to the following equation:

$$\text{Titer (PFU/ml)} = \frac{\text{No. of plaques X dilution factor}}{\text{Volume of the inoculum}}$$

2.10.2.2 Median Tissue Culture Infective Dose TCID50:

Viral titers of either stock supernatants or pre treated cells with enzyme inhibitors were also determined using the TCID50/ml in Vero and DF1 seeded cells in 96-well microplates. Cells were seeded in 96-well plates at $1X10^4$ cells/well 24 hours before the titration. Each sample was specified for one plate and serially diluted to tenfold dilution in the titration medium. When the monolayers were nearly confluent, the media were emptied from the 96-well plate and gently tapped the plates to dry on stack of tissues. The wells of column 1 and 12 of the plate were containing only the titration medium and they specified as the negative control wells. Starting with the highest dilution in row H, the wells were dispensed with the descending dilutions till row A. The plates were then incubated at 37 °C for 72 hours and the wells were scored for IBV specific Cytopathic effect (CPE) under the microscope or fixed with 4% PFA and stained by 1% crystal violet for result analysis.

2.10.3 Cytopathic Effect Analysis:

The CPE was characterized by clusters of rounded cells on top of the monolayer and partial or complete slough of the monolayer when fixed and stained. Titers were then calculated using the Spearman and Kaerber method as described by (Hierholzer & Killington, 1996) and quantified in TCID50/ml.

2.11 Antibodies:

Table 2.5: Antibodies used in this study.

Antigen	Type	Product Number	Manufacturer	Species	Dilution
GFP	Primary	SC-8334	Santa Cruz Biotechnology	Rabbit Polyclonal	1/2000
Rabbit	Secondary-HPR	AG154	Sigma	Goat	1/2000
Calnexin	Primary	AB22595	Abcam	Rabbit Polyclonal	1/10000
Rabbit	Secondary-Alexa Fluor 546	A10040	Thermo Scientific	Donkey	1/200
IBV	Primary	-	Charles River	Chicken Polyclonal	1/20000
Chicken	Secondary-HPR	SAB3700199	Sigma-Aldrich	Goat	1/1000
GAPDH	Primary	AB8245	Abcam	Mouse Monoclonal	1/5000
Mouse	Secondary-HRP	A4416	Sigma-Aldrich	Goat	1/2000

Chapter 3

Cellular Interactome of IBV Structural Proteins: Spike (S), Membrane (M) and Envelope (E) Glycoproteins

3.1 Introduction:

The IBV is a globally distributed virus that cause huge economic loss during its outbreaks (Bande, *et al*., 2017). The clinical impact and pathogenesis of IBV are based on the tissue tropism in the host, which is solely mediated through the IBV epitope S proteins. According to that tropism, the IBV infection induces pathogenesis in respiratory, renal, reproductive and digestive system (Jackwood & de Wit, 2017). The outcomes of the virus pathogenesis are either virus induced by replication (Maier, *et al*., 2015) or host responses for example apoptosis and innate immunity (Chhabra, *et al*., 2016). On the other hand, there are differences in the pathogenicity of different strains of IBV such as QX-like and Mass-type strains having tremendous differences even in the tissue tropism (Cheng, *et al*., 2018). However, the impacts are approximately similar and no differences have been noticed in replication cycle of various strains in the infected cells. To sum up, is the importance of cellular proteome for the viral proteins.

During the IBV replication and following an uncoating process inside the infected cells, the virus polymerase complex transcribes sgRNAs that encode four structural proteins, S, M, E and N.

The S protein is the largest structural protein of IBV (1165 amino acids more or less according to specific strains), and is a glycoprotein having a significant role in binding to the host cell receptor and mediating virus-cell and cell-cell fusion (Wickramasinghe *et al*. 2011). The S protein passes posttranscriptional conformational changes including cleavage and

interaction with the cellular proteins, which leads to subsequent maturation of the proteins including their PTM groups, this was characterized in SARS coronavirus but not yet for the IBV (Fukushi, *et al*., 2012).

During the maturation process, the S protein is cleaved to two subunits S1 and S2 and obtains its mature form in such a way that S1 forms the globular part and protrudes towards the outside envelope forming the crown-shape of the virus. The S2 subunit forms the stalk part and part of its domain anchors to the viral envelope (Cavanagh, 2005). Furthermore, the S protein interacts with the host cell receptor in the first step of the virus replication, which is attachment and entry and in this process the S1 subunit is mainly involved in the attachment and S2 in the fusion, consequently the host immune response is induced (Brandão, 2012). Bioinformatics analysis confirmed that the S1 sequence in the virus genome contains 3 hyper variable regions that lead to significant variation in coding sequences. Consequently numerous IBV serotypes have been observed in the outbreaks worldwide, which have poor cross-protection immunity among each other (Cook *et al*. 2012; Khaleil *et al*. 2014; Abro *et al*. 2012; Ma *et al*. 2012; Mo *et al*. 2013; Mahmood *et al*. 2011; Xie *et al*. 2011).

M protein is the most abundant protein in the viral envelope and it plays a major role in virus assembly and budding. During the virus life cycle M protein has several interactions with itself, and also the E and S proteins leading to the formation of viral-like particles (VLPs) (Godeke, *et al*., 2000; Hegde & Keenan, 2011; Liu, *et al*., 2013).

E protein is a small-intercalated membrane protein in the IBV envelope. The function of this protein in Coronaviruses is mainly related to the viral assembly process (Venkatagopalan, *et al*., 2015) and secretory pathway (Westerbeck & Machamer, 2015). Additionally, the E protein appears to have a role in inducing membrane curvature formation of the envelope when interacts with M and S at the virus assembly site and also the scission of the viral particles from cellular membranes (Corse & Machamer, 2002; Ruch & Machamer, 2011). The ion channel activity of E protein has also been confirmed *in vitro* (Ruch & Machamer, 2012b; To, *et al*., 2017).

Overall the pathogenesis of the virus is facilitated through maturation of S, M and E proteins, which are in turn assembled in to the virus envelope. Processing and maturation of the viral proteins are only done using cellular machinery pathways, networks and individual proteins of the host. Making such pathways an ideal target for the anti-viral therapy. Targeting cellular proteins has the potential advantage of overcoming the high rate of virus diversity and potential escape mutants as all strains use the same cellular pathway regardless of their sequences.

To characterize the cellular interactome of the IBV S, M and E proteins, in this chapter, a label-free proteomic study was conducted using LC-MS/MS of immunoprecipitated S, M and E proteins from over expression of their genes in 293T-transfected cells.

The significant impact in economic loss of poultry industry and recurrent outbreaks of IBV QX and QX-like strains in the world has resulted in choosing the (SDIB821/2012) isolate for cloning the S, M and E genes used in this study. The main purpose of such approach is to optimise the interaction of these viral proteins with intracellular proteins using GFP-tagged gene transfection, GFP-trapped protein pulldown and LC-MA/MS analysis techniques. Despite the fact that IBV infects chickens and chicken cells are preferred to be used for transfections, however due to the availability of advanced human protein lists, interactome in human proteins and better transfection efficiency, 293T cells were used for vector transfections in this study.

This kinds of approaches have been used successfully to define and investigate cellular interactomes in a diverse array of viral proteins including the RNA dependent RNA polymerase (Munday, *et al*., 2015), the NS1 and NS2 protein (Wu, *et al*., 2012) from human respiratory syncytial virus (HRSV), the IBV (Emmott, *et al*., 2013) and porcine respiratory and reproductive virus (PRRSV) (Trinkle-Mulcahy, 2012) N proteins and the Ebola virus VP24 protein (García-Dorival, *et al*., 2016, 2014).

3.2 Results:

The results in this chapter was to confirm the first aim of this study, which was technically based on over expression of IBV structural S, M and E proteins which were tagged into Green Fluorescent Protein (GFP) vector separately.

3.2.1 Construction of Plasmids and Sub Cloning Analysis:

The whole sequence of the S gene (3498bp, 1165 amino acids), M gene (678bp, 225 amino acids) and E gene (327bp, 108 amino acids) (annotated with red arrows in Figure 3.1), were synthesized and sub cloned in to the C terminus of the EGFP-C1 vector (Figure 3.2).

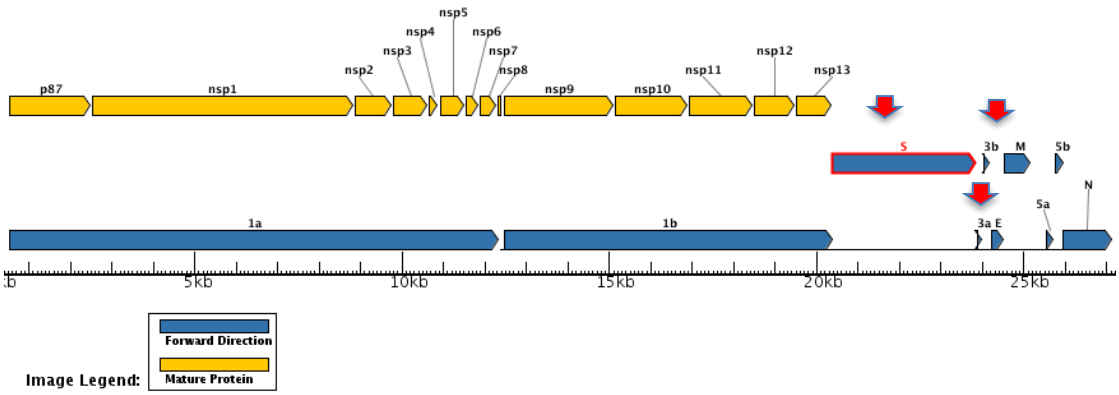

Figure 3.1: Genomic organization and proteins of SDIB821/2012 IBV isolate. S, E, M (marked with red arrows) and N are structural proteins.1a, 1b, 3a, 3b, 5a and 5b are non-structural proteins (nsp). The graphs were generated from the Virus Pathogen Resource (ViPR) for the relevant SDIB821/2012 IBV isolate available in the database (https://www.viprbrc.org/brc/home.spg?decorator=corona).

The bioinformatics preparation analysis, which include sequence confirmation per each of the genes, showed whole genome availability of SDIB821/2012 isolate in the GenBank, as it is a recent and virulent nephropathogenic IBV strain of Asia and the Middle East. Using a plasmid editor (ApE) software, the S, M and E gene sequences indicated that both *Bgl* II (AGATCT) and *Sal* I (GTCGAC) restriction enzyme cloning sites could be used as cloning sites for the genes into the pEGFP-C1 vector.

Due to its significant transfection efficiency and functional annotation of the human genome, the 293T human cell line was used as the final expression host for the constructs. Consequently, the optimization process of codon usage for the IBV proteins has been adapted to *Homo sapiens*. The S, M and E gene constructs were cloned to pEGFP-C1 vector forming the final vector-construct formula of 8205, 5385 and 5034 bp length plasmids containing (pUC) origin, cytomegalovirus (CMV) promoter and SV40-PA terminator for both GFP and the cloned genes. Moreover, for rendering a specific selective media growth, the plasmid contains the antibiotic resistance loci for both neomycin-kanamycin and ampicillin antibiotics.

The final results of the plasmid constructs in which each of the S, M and genes included, were analysed and visualised using SnapGene viewer software (Figure 3.2).

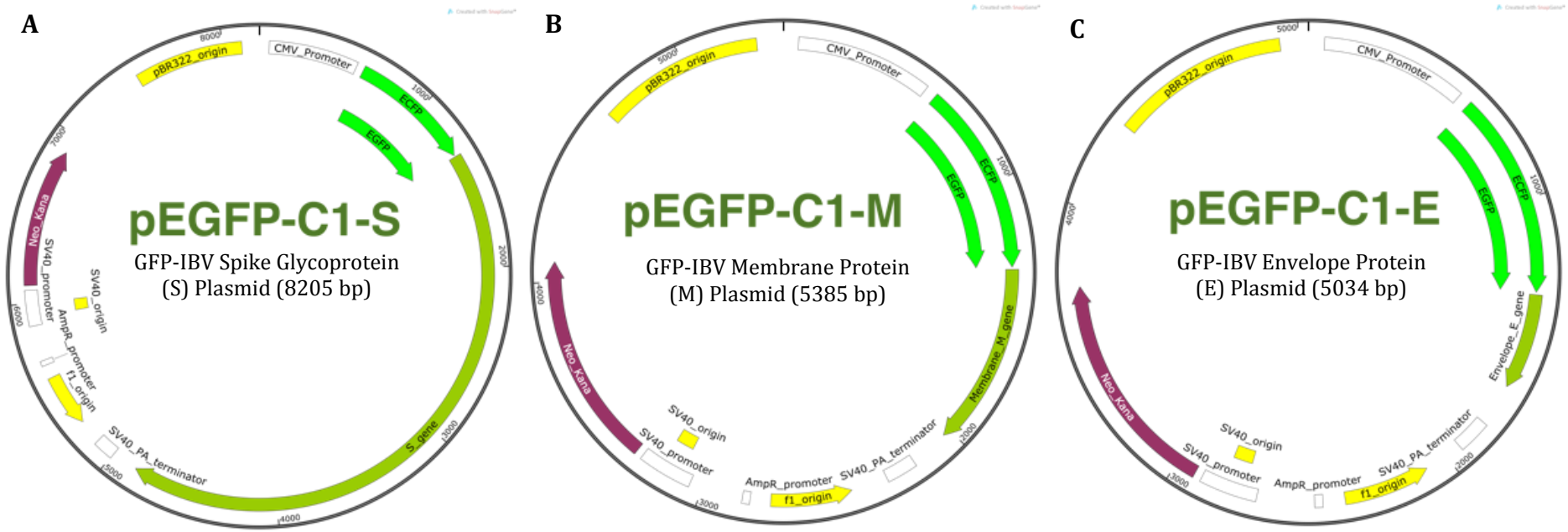

Figure 3.2 A-C: Maps show final version of GFP- S, GFP-M and GFP-E construct plasmids. A: The S construct is cloned directly at the C-terminus of GFP gene. B: M gene cloned to GFP plasmid. C: E gene cloned to GFP plasmid. Maps were created with SnapGene Viewer software version 2.8.2. The detail of the ORFs and genes was described in the Figure 3.2.

To obtain sufficient DNA for transfection, all plasmids (pEGFP-C1, pEGFP-S, pEGFP-M and pEGFP-E) were amplified in competent cell transformation by bacterial culture technique (Chapter 2, Section 2.2.1). Sub cloning confirmation by transformation was also determined the efficiency of take up of a relatively large plasmid in case of pEGFP-S plasmid (Figure 3.3 A) in to the bacterial cells and surviving in selective media containing the kanamycin antibiotic.

The outcome of high concentration plasmid DNA (>1.5 µg/ µl) after maxi preparation was confirmed by Quibit™ Assay and the molecular weight of the circular plasmids were also obtained by running on agarose gel (Figure 3.3).

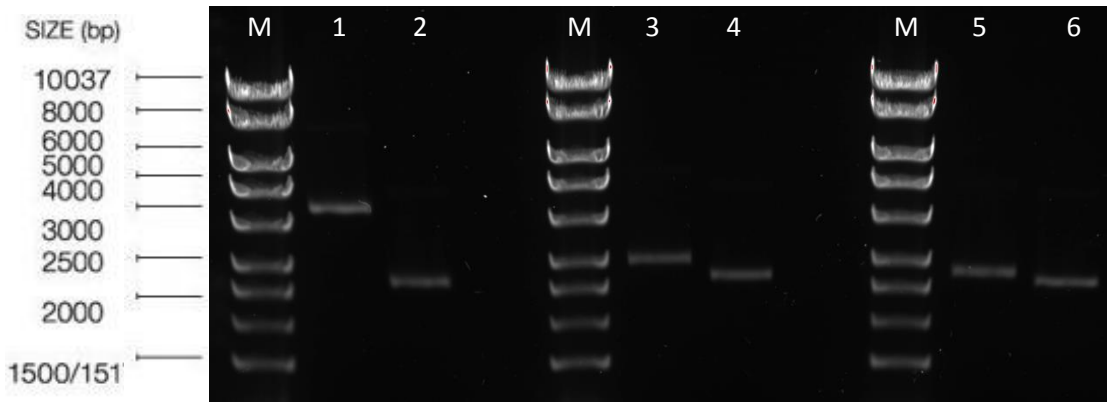

Figure 3.3: Agarose gel electrophoresis of EGFP-C1, EGFP-C1-S, EGFP-C1-M and EGFP-C1-E plasmids. M: 1kb DNA ladder. Lane 1 indicates GFP-S plasmid. Lane 3 indicates 5385 bp GFP-M plasmid. Lane 5 indicates 5034 bp GFP-E plasmid. Lane 2, 4 and 6 indicate 4731 bp of GFP plasmid only.

3.2.2 Confirmation of Plasmids by Sequencing:

For confirmation of plasmids and the stability of the insert genes, all three amplified plasmids from competent cells were sequenced by Eurofins. Universal forward and reverse primers for pEGFP-C1 only, were used for sequencing the genes in pEGFP-M and pEGFP-E plasmids, however for the GFP-S six more gene specific primers in addition to universal primers were used to cover whole S gene sequence in the plasmid (Table 2:1). The analysis confirmed the stability of all sequences in the plasmids by which the assembled sequences were compared to the gene sequences that were previously sent for gene synthesis service (Gene Art, Thermo Scientific).

3.2.3 Expressions and Localizations of GFP-S, GFP-M and GFP-E Proteins:

To conduct an interactome analysis between the viral S, M and E and host cytoplasmic intracellular proteins, the GFP-tagged S, M and E plasmids were expressed in 293T cells. These cells were transformed with the large T antigen and it is important for replicating plasmids to contain the SV40 origin of replication (such as pEGFP-C1 vector) to produce a high copy number during transfection) following its calcium phosphate-induced transfection. The routine optimisation of expression following vector transfection was performed using the fluorescent microscope. The green light emission from all GFP, GFP-S, GFP-M and GFP-E, confirmed the successful expression of these proteins (Figure 3.4 A-D). Moreover, the detailed expression strategy and/or localization of proteins were illustrated by DAPI nuclear staining in

cells fixed with 4% paraformaldehyde (PFA) under 63X magnification of the fluorescent microscope (Figure 3.4).

The GFP, which was used as a control for transfection, was expressed in the cytoplasm and diffuses into the nucleus as well (Figure 3.4 A), however the expression of the S, M and E genes were localised only in the cytoplasm (Figure 3.4 B-D). This confirms the usual site of expression and processing for IBV S, M and E proteins in host cells as previously published in (Klumperman, *et al*., 1994; Lontok, *et al*., 2004; Venkatagopalan, *et al*., 2015).

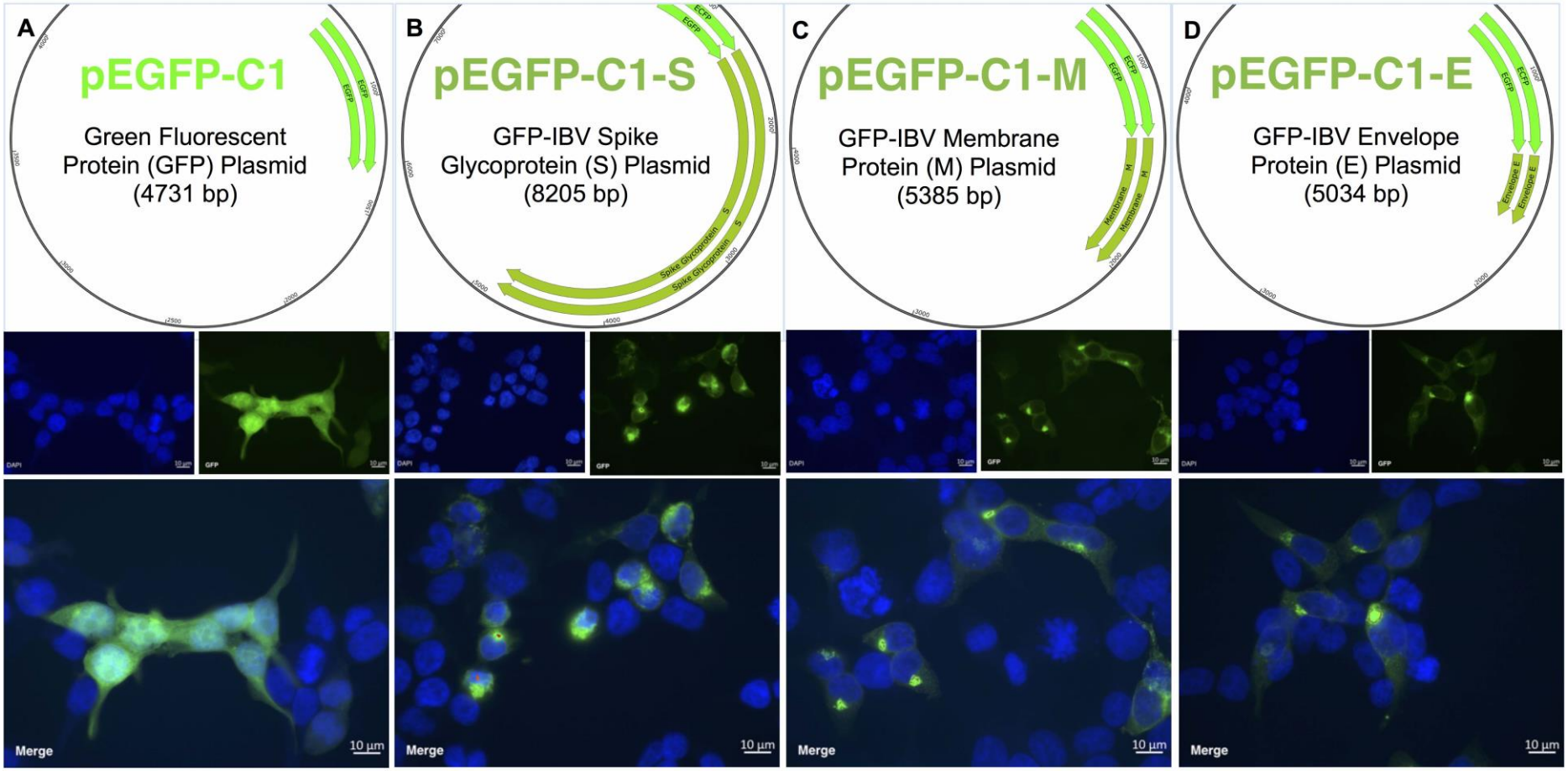

Figure 3.4: A-D 293T cell transfection with vectors. A: GFP expression in 293T cells. B: GFP-S expression in 293T cells. C: GFP-M expression. D: GFP-E expressions. Fluorescent imaging of GFP shows general distribution in the cells while for all of GFP-S, GFP-M and GFP-E show cytoplasmic accumulation of the proteins.

3.2.4 Pulldown Analysis for S, M and E Glycoproteins:

To trap and purify the expressed proteins with their potential cellular interactome, specific agarose beads that have high affinity antibodies to GFP, were used to immunologically precipitate both the GFP and GFP-tagged proteins. A small volume from the pulldown samples, which were prepared from GFP as control and GFP-S, M and E transfected 293T cells as the targets, were aliquoted apart for direct immunoblotting (Figure 3.5 S, M and E). However, the remaining samples were held for LC-MS/MS analysis.

The molecular weight of GFP is 27kDa, which was detected in its right size and even it was cleaved from tagged proteins and remained in the same size. However, the GFP tagged S protein migrated at about 240 kDa (Figure 3.5 S), which was higher than its theoretical (predicted) molecular weight (~130kDa+27 kDa of GFP= ~158kDa). A question arose itself here about the reason of such mass difference? For answering this question, a hypothesis was predicted that glycosylation led to this difference, which is a well characterised (PTM) of the proteins and this was confirmed by enzymatic analysis. Consequently a label free proteome analysis by MS was conducted for obtaining details of proteins and/or chaperons that needed for protein processing including PTM.

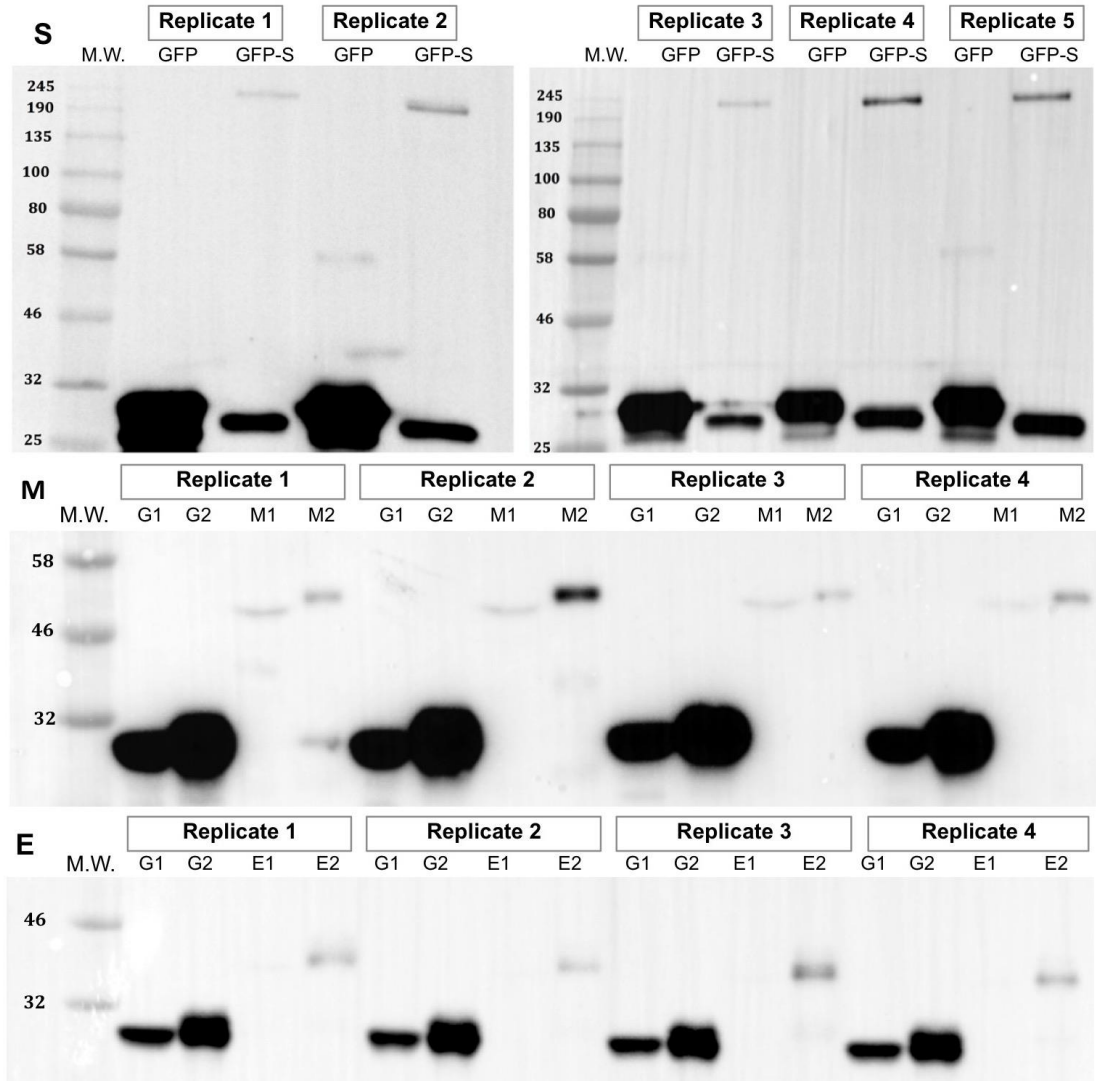

Figure 3.5: Immunoblot visualization of immunoprecipitated proteins from GFP-tagged S, M and E proteins. ***S****: Pulled down samples of GFP (control) and GFP-S proteins in 5 replicates and immunoblotted by GFP anti body incubation. M.W. lanes are protein markers. GFP lanes are GFP pulldown samples. GFP-S lanes are GFP-S pulldown samples. M: Cell lysates and pulled down samples of GFP (control) and GFP-M proteins in 4 replicates and immunoblotted by GFP anti body incubation. G1 lanes are GFP whole cell lysates. G2 lanes are GFP pulldown samples. M1 lanes are GFP-M whole cell lysates. M2 lanes are GFP-M pulldown samples. E: similar arrangement as for M lanes. All pulldown samples in this figure were subjected to LC/MS-MS analysis.*

3.2.5 Potential Cellular Interactome Identification Analysis:

For optimization of the GFP-tagged proteins and their interaction with cellular proteins, immunoprecipitated samples (Figure 3.5 S: GFP-S lanes), (Figure 3.5 M: M2 lanes) and (Figure 3.5 E: E2 lanes) were analysed by LC-MS/MS. The data outcome was analysed by Progenesis QI software package, which is designed for analysing large mass-spectrometry data sets. The software is specifically used at high-resolution MS data and label-free quantification is also supported. The analysis was resulted in identifying list of potential cellular interactomes for each protein.

To obtain statistical significance for the potential cellular proteins that interact with the bait, five replicates of 293T cell transfection with GFP, GFP-S and six replicates with GFP-M and GFP-E were prepared. Approximately 7-8x10^6 cells were used for each pulldown and transfected with the GFP control and GFP-tagged proteins as targets and similar amount retained as mock transfected negative control for WB. The whole cell lysates from each replicate were subjected to the immunoprecipitation protocol by the GFP antibody pulldown and all samples were visualized by WB. The analysis of five replicates for the S and six replicates for each of the M and E proteins, showed significant increase in the abundance of some cellular proteins in GFP-S, M and E transfected cells as compared to the GFP only as the control.

3.2.5.1 Identification of Potential Interactome with the S Protein:

In support of bioinformatics analysis for the MS data regarding S interaction with intracellular proteins, 70 proteins were detected. However, these were not likely to all interact with the S protein and were further triaged depending on their statistical significance by Anova (p) values. This resulted in 9 proteins being selected with less than 0.05 in Anova (p) values and can be regarded as potentially having a high chance of interacting with the S protein (Table 3.1). Consequently, a heat map was created for the most abundant proteins in GFP-S transfected cells versus GFP control pulldown samples (Figure 3.6). After the high-resolution analysis and selection of the most abundant proteins as potential interactome for S, a few proteins were downselected for further validation. Calnexin (CANX) (a molecular chaperon in the endoplasmic reticulum) is one of the most significant proteins and appeared to have high affinity of interaction with S protein. This interaction was shown in all replicates. Stromal cell derived factor 2-like 1 (SDF2L1) protein is another protein that showed significant abundance of max fold changes with GFP-S. Tubulin proteins have also shown their abundant availablity with the bait expression including both alpha and beta chains.

Table 3.1: Cellular protein list of GFP-S interactome in 293T cells. Anova (p) values and Max Fold change were obtained from label-free proteomics data set of immunoprecipitated samples analysed by LC/MS-MS and Progenesis QI software. The highlighted rows in the table are mutual interactome for both S and E proteins Table 3.3. Calnexin and Stromal cell-derived factor 2-like protein 1 are the most significant proteins in the list, which they are involved in PTM glycosylation of glycoproteins.

	Accession	Description	Anova (p)	Max fold change	Gene Name	Peptide count	Unique peptides	Confidence score	Highest mean	Lowest mean
1	P42212	Green fluorescent protein	0.000041	145.189	GFP	19	19	4392.64	GFP	S
2	P11223	Spike glycoprotein	0.001944	85.785	S	3	3	613.56	S	GFP
3	Q9HCN8	Stromal cell-derived factor 2-like protein 1	0.002629	600.938	SDF2L1	3	3	534.96	S	GFP
4	O14950	Myosin regulatory light chain 12B	0.005212	87.333	ML12B	3	3	613.56	GFP	S
5	P27824	Calnexin	0.006489	131.877	CANX	3	3	263.32	S	GFP
6	P07437	Tubulin beta chain	0.021139	33.696	TUBB	6	2	731	S	GFP
7	P05023	Sodium/potassium-transporting ATPase subunit alpha-1	0.023651	93.672	ATP1A1	4	4	644.09	S	GFP
8	O95816	BAG family molecular chaperone regulator 2	0.027405	51.443	BAG2	2	2	172.92	S	GFP
9	O43175	D-3-ph phoglycerate dehydrogenase	0.028874	11.575	PHGDH	5	5	723.37	S	GFP
10	Q9BQE3	Tubulin alpha-1C chain	0.032036	22.552	TUBA1C	7	7	1217.31	S	GFP
11	P68371	Tubulin beta-4B chain	0.040151	17.352	TUBB4B	6	3	668.92	S	GFP
12	P0CG47	Polyubiquitin-B	0.048604	18.092	UBB	3	3	447.85	S	GFP

The most significant interactome candidates with S versus the GFP control were also analysed using the Morpheus online program and illustrated as a heat map (Figure 3.6). This visualize that all significant proteins interacted with S (5 replicate values in red circles) and represents increase in abundance for normalized log^2 data set. The high abundant values were calculated as higher than the universal mean for control and sample replicates and visualized as red circles.

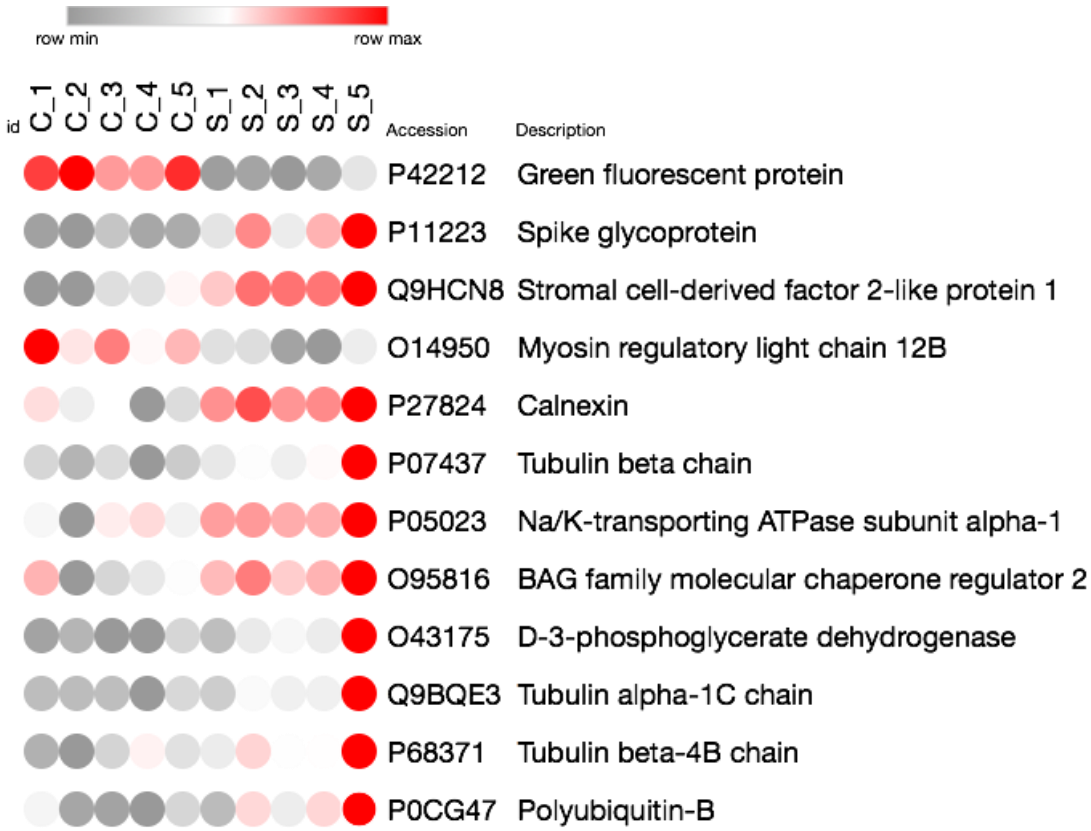

Figure 3.6: A Heat map for Label-free quantification of GFP-S versus GFP as a control. Significant increase in abundance of some cellular proteins occurred in the immunoprecipitated samples in 5 replicates. Calnexin and Stromal cell-derived factor 2-like protein 1 are the most interested proteins in the list, which they are involved in PTM glycosylation of glycoproteins (Fabregat, et al., 2018).

3.2.5.2 Identification of Potential Interactome with M Protein:

To obtain the potential interactome of M protein, 6 replicates of immunoprecipitated samples were analysed by LC-MS/MS and Progenesis QI combination platform. The data outcome from statistical and computational analysis showed significant hits for potential protein-protein interactions for the M protein. The initial priority list of 62 potential proteins was generated, however the significant proteins, which were significant by their Anova p values less than 0.05, were 14 cellular proteins as listed in Table 3.2. Seven proteins (Cytochrome b-c1 complex subunit 6, ATP synthase subunit e, NADH dehydrogenase iron-sulphur protein 6, Collagen alpha-2 (VI) chain, Stress-70 protein, Collagen alpha-3 (VI) chain and Myosin-4) were significantly increased in abundance in M proteome lists Table 3.2. The cellular proteins in the list belong to mitochondrial and cytosolic localization activities.

Table 3.2: Cellular protein list of GFP-M interactome in 293T cells. Anova (p) values and Max Fold change were obtained from label-free proteomics data set of immunoprecipitated samples analysed by LC/MS-MS and Progenesis QI software. The highlighted rows in the table are mutual interactome for both M and E proteins Table 3.3.

	Accession	Description	Anova (p)	Max fold change	Gene Name	Peptide count	Unique peptides	Confidence score	Highest mean	Lowest mean
1	P42212	Green fluorescent protein	0.0000001	130.585	GFP	20	20	4910.67	GFP	M
2	Q9BRQ6	MICOS complex subunit MIC25	0.000360	7.749	CHCHD6	2	2	175.25	M	GFP
3	P06753	Tropomy in alpha-3 chain	0.000610	95.164	TPM3	4	2	340.53	M	GFP
4	P07919	Cytochrome b-c1 complex subunit 6	0.000684	16.933	UQCRH	6	6	1015.9	M	GFP
5	P49006	MARCKS-related protein	0.001842	4.897	MARCKSL1	2	2	307.56	M	GFP
6	P56385	ATP synthase subunit e	0.002886	16.747	ATP5I	2	2	461.34	M	GFP
7	U5U9J5	Membrane protein	0.003195	154.450	M	2	2	175.25	M	GFP
8	O75380	NADH dehydrogenase iron-sulphur protein 6	0.005230	18.868	NDUFS6	3	3	452.6	M	GFP
9	O43678	NADH dehydrogenase 1 alpha subunit 2	0.006360	55.128	NDUFA2	2	2	307.56	M	GFP
10	Q9UFG5	UPF0449 protein C19orf25	0.013645	203.524	C19orf25	2	2	35.55	M	GFP
11	P25705	ATP synthase subunit alpha, mitochondrial	0.014718	3.033	ATPA	4	4	346.43	GFP	M
12	P12110	Collagen alpha-2 (VI) chain	0.016021	3.503	COL6A2	2	2	186.03	M	GFP
13	P38646	Stress-70 protein	0.017499	8.820	HSPA9	2	2	307.56	M	GFP
14	P12111	Collagen alpha-3 (VI) chain	0.017659	3.605	COL6A3	2	2	232.81	M	GFP
15	Q9Y623	Myosin-4	0.017785	5.068	MYH4	3	3	194.45	M	GFP
16	P02545	Prelamin-A/C	0.022548	4.334	LMNA	2	2	42.94	M	GFP
17	P10606	Cytochrome c oxidase subunit 5B	0.030409	21.070	COX5B	5	5	575.58	M	GFP

The significant interaction with M protein were also analysed using the Morpheus online program and illustrated as a heat map (Figure 3.7). This indicates that all significant proteins interacted with M (6 replicate values in red circles) and represents increase in abundance for normalized log^2 data set. The highest abundant values were obtained as higher than the universal mean for control and sample replicates.

Figure 3.7: A Heat map for Label-free quantification of GFP-M versus GFP as a control. Significant increase in abundance of some cellular proteins occurred in the immunoprecipitated samples in 6 replicates. Anova (p) and Max fold change values were described in Table 3.2.

3.2.5.3 : Identification of Potential Interactome with E Protein:

To produce the proteome list for E protein, similar method was done exactly as M protein and 23 cellular proteins were significantly increased in abundance in which 6 and 7 of them were shared with S and M protein respectively Table 3.3.

The most significant interactome candidates with E versus the GFP control were analysed by the Morpheus online program as well. The outcome was illustrated as a heat map (Figure 3.8). This visualize the significant proteins interacted with the E protein (6 replicate values in red circles) and represents increase in the abundance for normalized $\log^2$ data set. The high abundant values were calculated as higher than the universal mean for control and sample replicates and visualized as red circles.

Table 3.3: Cellular protein list of GFP-M interactome in 293T cells. Anova (p) values and Max Fold change were obtained from label-free proteomics data set of immunoprecipitated samples analysed by LC/MS-MS and Progenesis QI software. The highlighted rows in the table are mutual interactome with both S and M proteins Table 3.1 and 3.2.

	Accession	Description	Anova (p)	Max fold change	Gene Name	Peptide count	Unique peptides	Confidence score	Highest mean	Lowest mean
1	P42212	Green fluorescent protein	0.000002	41.108	GFP	21	21	4438.52	GFP	E
2	U5U766	E protein	0.000008	175.121	E	2	2	321.19	E	GFP
3	P19338	Nucleolin	0.000024	15.186	NCL	3	3	120.59	E	GFP
4	Q9BSJ8	Extended synaptotagmin-1	0.000128	9.623	ESYT1	2	2	55.74	E	GFP
5	O43175	D-3-ph phoglycerate dehydrogenase	0.001613	8.419	PHGDH	4	4	387.71	E	GFP
6	P10809	60 kDa heat shock protein	0.004631	22.578	HSPD1	11	11	1282.27	E	GFP
7	P05023	Sodium/potassium-transporting ATPase subunit α1	0.005350	49.267	ATP1A1	8	8	628.03	E	GFP
8	P07919	Cytochrome b-c1 complex subunit 6	0.005382	9.502	UQCRH	6	6	462.25	E	GFP
9	P60709	Actin, cytoplasmic 1	0.006302	3.054	ACTB	5	5	445.16	E	GFP
10	O75380	NADH dehydrogenase iron-sulfur protein 6	0.007467	6.332	NDUFS6	4	4	469.73	E	GFP
11	P56385	ATP synthase subunit e	0.009790	6.159	ATP5I	2	2	296.14	E	GFP
12	P27824	Calnexin	0.011546	9.718	CANX	2	2	94.6	E	GFP

13	P11142	Heat shock cognate 71 kDa protein	0.011822	2.947	HSPA8	7	4	530.54	E	GFP
14	P07437	Tubulin beta chain	0.015125	13.800	TUBB	6	3	664.08	E	GFP
15	P67809	Nuclease-sensitive element-binding protein 1	0.016554	2.682	YBX1	2	2	232.47	E	GFP
16	P14314	Glucosidase 2 subunit beta	0.018382	14.267	PRKCSH	2	2	167.96	E	GFP
17	Q9BQE3	Tubulin alpha-1C chain	0.020056	15.595	TUBA1C	3	3	490.73	E	GFP
18	P12111	Collagen alpha-3 (VI) chain	0.021474	3.560	COL6A3	4	4	312.7	E	GFP
19	P38646	Stress-70 protein	0.024651	6.553	HSPA9	3	3	284.42	E	GFP
20	P10321	HLA class I histocompatibility antigen Cw-7 α-chain	0.026375	93.565	HLA-C	2	2	252.11	E	GFP
21	P68371	Tubulin beta-4B chain	0.027210	6.186	TUBB4B	5	3	497.53	E	GFP
22	Q9Y623	Myosin-4	0.027578	5.555	MYH4	4	4	276.14	E	GFP
23	P02751	Fibronectin	0.028937	4.073	FN1	2	2	175.65	E	GFP
24	P12110	Collagen alpha-2 (VI) chain	0.040399	3.183	COL6A2	2	2	137.11	E	GFP
25	P11021	78 kDa glucose-regulated protein	0.047992	2.930	HSPA5	8	6	607.78	E	GFP

Figure 3.8: A Heat map for Label-free quantification of GFP-E versus GFP as a control. Significant increase in abundance of some cellular proteins occurred in the immunoprecipitated samples in 6 replicates. Anova (p) and Max fold change values were described in Table 3.3.

3.2.6 Protein-Protein Interaction and Network Analysis:

To visualize the interaction localization in side the cytoplasm and to identify which cellular organelles are included for such interactions, a bioinformatcally predicted network analysis of the proteome data was conducted. For this purpose the significant proteome data sets per each of viral proteins were applied for network analysis using CellWhere V1.1 online program. The CellWhere presents a graphical display of protein association networks which are organised on subcellular localizations. The network was created according to the significant cellular proteins involved in the interaction with the baits. The significant proteins in the proteome data sets were also showed according to their interaction and localization in the cytoplasm and cellular organelles. This analysis created the whole image for interesting candidates for further validations (Figure 3.8 A-C).

Based on this analysis the interactome in the ER was confirmed for CANX interaction with The S and E proteins. CANX is an ER chaperon involved in glycoprotein maturation. In the S network, a network interaction with Protein transport protein Sec61 subunit alpha isoform 1 (SEC61A), ER degradation-enhancing alpha-mannosidase-like protein 1 (EDEM) and Translocon-associated protein subunit alpha (PSEC0262) are all involved in protein processing in ER. In the E network as well, three important proteins, (CANX), Endoplasmic reticulum chaperone BiP (HSPA5) and Glucosidase 2 subunit beta (G19P1) are involved in protein folding and N-linked glycosylation processes. Cosequently the involvement of CANX and N-linked glycosylation is subjected to be validated in the subsequent chapters.

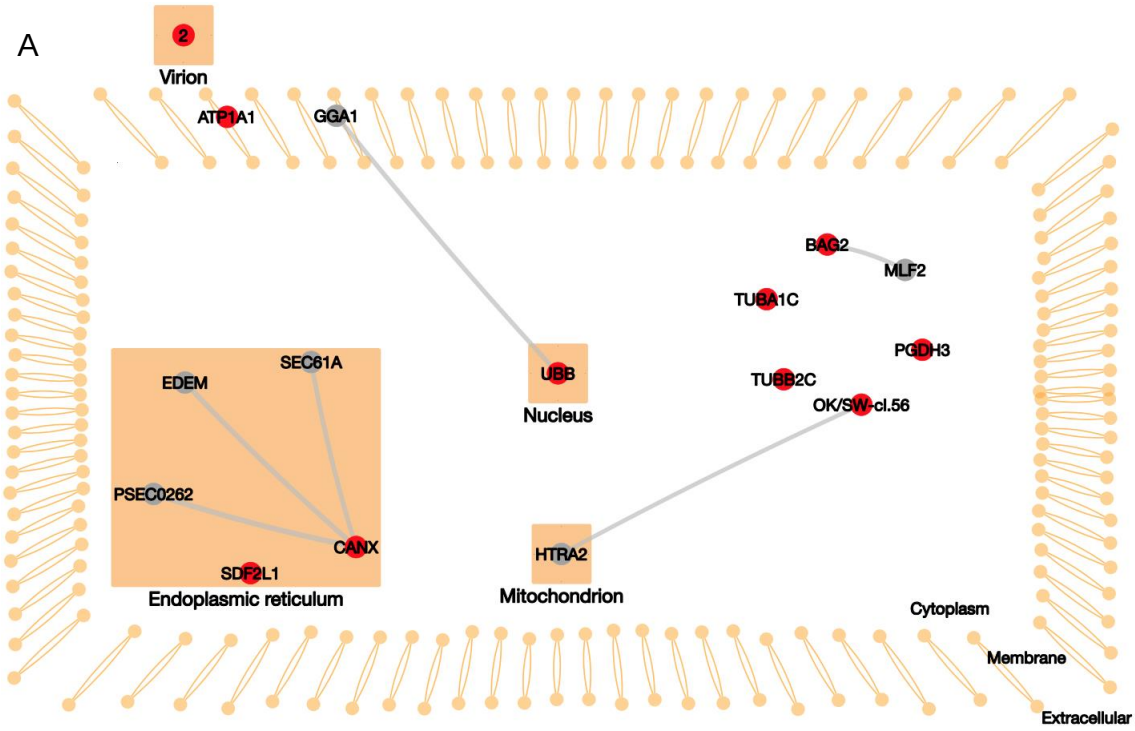

Figure 3.9 A-C: Network and localization of S, M and E interactomes. Graphical presentation of S, M and E proteomes using CellWhere1.1 online program. The UniProt accessions of significant protein lists (Anova (p) value <0.05) were put in to the program under default parameters of identifier type: UniProt, Species: Homo sapiens, localization sources: UniProt and Go and display localization based on annotation frequency.

A: The interactome networks and their localization for S proteome. Basically, ER and cytosol are included and the most significant interaction is in Calnexin cycle in ER. Calnexin is an ER chaperon involved in glycoprotein maturation. It has network interaction with Protein transport protein Sec61 subunit alpha isoform 1 (SEC61A), ER degradation-enhancing alpha-mannosidase-like protein 1 (EDEM) and Translocon-associated protein subunit alpha (PSEC0262) which are all involved in protein processing in ER. Six significant proteins are mutually significant in the E proteome.

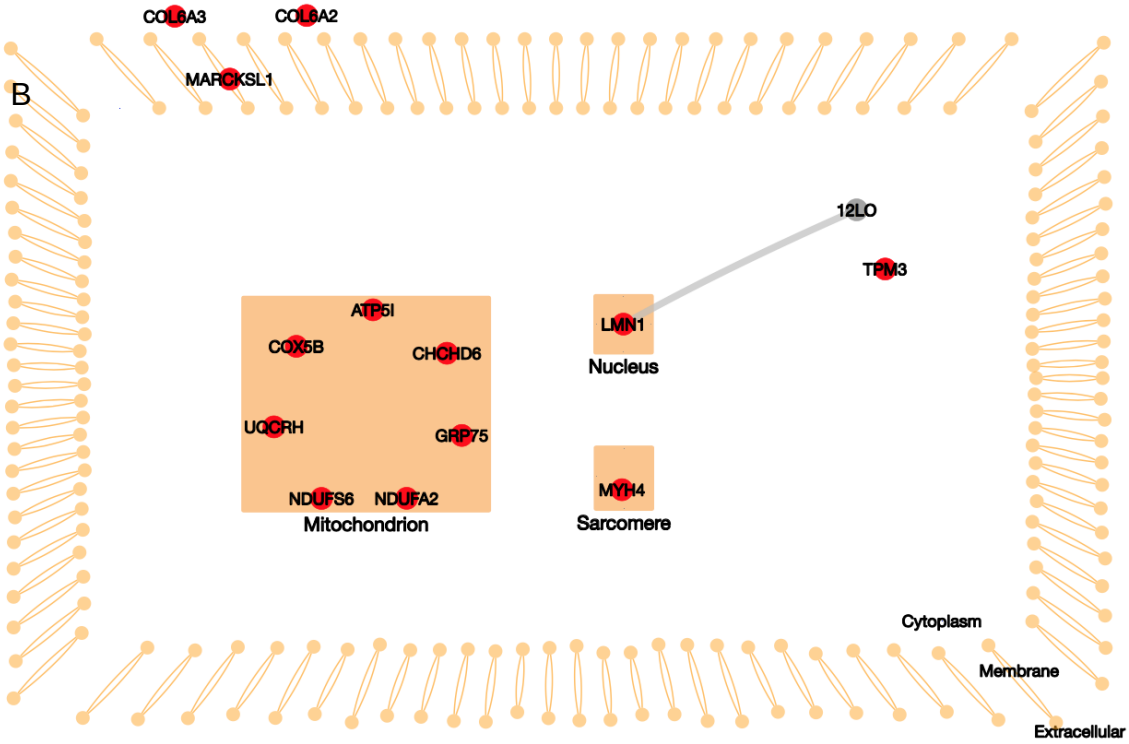

B: The interactome networks and their localization for M proteome. Seven cellular proteins (Cytochrome b-c1 complex subunit 6 (UQCRH), ATP synthase subunit e (ATP5I), NADH dehydrogenase iron-sulphur protein 6 (NDUFS6), Collagen alpha-2 (VI) chain (COL6A2), Stress-70 protein, Collagen alpha-3 (VI) chain (COL6A3) and Myosin-4 (MYH4)) are significant in the M proteome and they are significant in E proteome as well. Overall proteins are related to protein transportation activities.

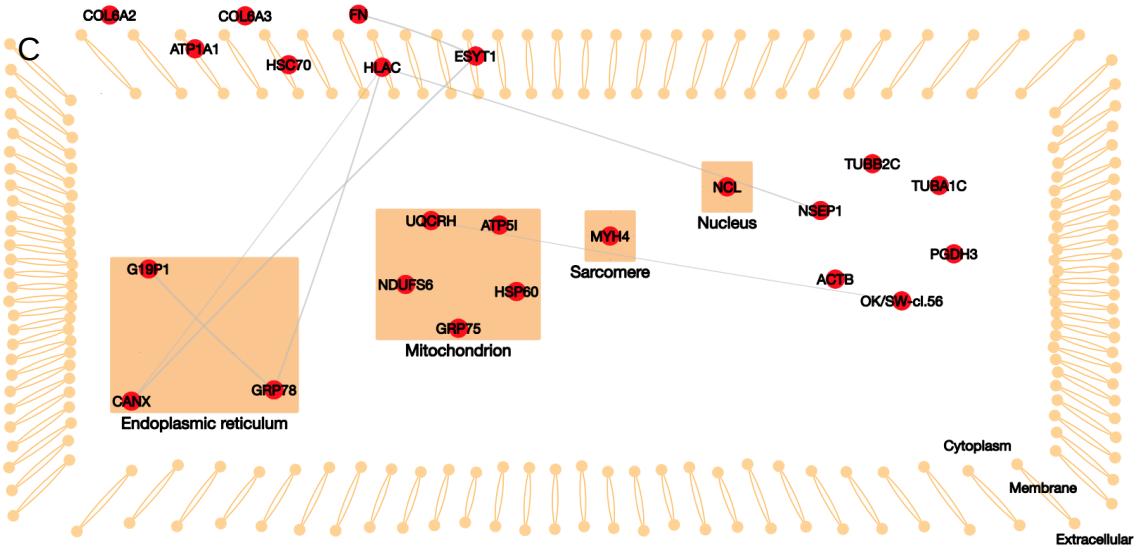

C: The interactome networks and their localization for E proteome. The 23 cellular proteins in E proteome list are significant in several protein pathways in cytosol. Thirteen proteins were shared in S and M proteome. In ER, three important proteins, Calnexin (CANX), Endoplasmic reticulum chaperone BiP (HSPA5) and Glucosidase 2 subunit beta (G19P1) are involved in protein folding and N-linked glycosylation processes. The rest of cytosolic and mitochondrial proteins are involved in cellular protein trafficking.

3.3 Discussion

In the current study, the first main objective was to investigate the interaction of S, M and E proteins with host cell proteins. Consequently, constructs were designed to allow the individual expression of the S, M and E genes for a QX-like SDIB821/2012 isolate due to its morbidity and mortality rates (Xue, *et al*., 2012). The S gene was tagged to carboxylic (C) terminal end of GFP in the form of EGFP-C1 vector to overcome its split to 2 halves by posttranslational cleavage during cellular expression (Jackwood, *et al*., 2014). Similar tagging system was used for both M and E proteins as well. Targeting the S protein to optimize its intracellular proteins interaction and localization has been tried by many researchers for laboratory adapted and classical strains such as Massachusetts IBV (classical and common serotype of the virus in North America) (Ghani, *et al*., 2012; Promkuntod, *et al*., 2014).

The expression of complete S, M and E genes were optimized by fluorescence microscope from transfected cells with the construct vector (Figure 3.4), which is an early optimization capability of the vector and it is a reason for using such GFP tagging of the target. Another reason is protein localization study inside cells in which the tagged genes have noticeable expression profiles in the cytoplasm of PFA fixed cells and in most of them formed greenish granules, however in GFP-transfected cells the expression was identified through out the cells including nucleus diffusion as well. The cytoplasmic localization per each protein was confirmed previously and it seems to be due to post translational configuration and maturation in the ERGIC (Fukushi, *et al*., 2012; Lontok, *et al*., 2004).

The interactome proteins were chosen according to their abundance and significance in the analysis. The LC-MS/MS data analysis indicated the significant interaction of calnexin protein to S, which was also confirmed by the previous proteome work of SARS coronavirus S protein (Fukushi, *et al*., 2012; Schrag, *et al*., 2001).

The significant interactome proteins for M protein are mostly related to protein trafficking and mitochondrial activities in cells. Cytochrome b-c1 complex subunit 6, ATP synthase subunit e, NADH dehydrogenase iron-sulphur protein 6, Collagen alpha-2 (VI) chain, Stress-70 protein, Collagen alpha-3 (VI) chain and Myosin-4 were the potential interactome for the M protein mutually significant with the E proteome in the current study.

There are poor availability in the literature for such label-free proteomic study for M protein, however Tropomyosin alpha-3 chain protein binds to actin filaments in cells and implicated in stabilizing cytoskeleton actin filaments. Beta Actin was previously studied for its interaction with M and has role in virion assembly and buddying (Wang, *et al*., 2009).

The E interactome protein list was included more significant proteins (23 cellular proteins). The significant list was larger than both S and M proteomes and the potential E interactome list contained a shared list per each of the S and M proteins. According to UniProt characterization of the proteins, the main feature for cellular protein specifications are three major group of processing. First and the most important is PTM of N-linked glycosylation

and chaperon activities per related proteins as linked to CANX, Endoplasmic reticulum chaperone BiP (HSPA5) and Glucosidase 2 subunit beta (G19P1) proteins. Secondly, protein transportation and trafficking in cytoplasm and organelles, which are inclusive in Tubulins and Actin proteins. Finally, mitochondrial and transmembrane transporter activities which include the mutual protein list with M protein especially ATP synthase subunit e protein.

To sum up this chapter, the potential interactome was characterised for IBV S, M and E proteins. Calnexin was selected for further validation and biological studies. The functional importance of selected examples of these cellular proteins, focusing on the chaperone and PTM activities of calnexin were investigated and the data presented in the subsequent chapters.

Chapter 4

Analysis of IBV S, M and E Proteomes Indicates that the Calnexin Pathway is Essential for IBV biology

4.1 Introduction:

One of the current fields of virology is a comprehensive understanding of the biology in the virus-host interactions. The change in the status of a cell from uninfected to infected, alters numerous pathways and have been main targets of molecular investigation. The concerns about the biology of the viruses are regulated paths, alteration of defences, pathogenesis and transmission in host which are related to a relatively small viral genomes overcoming dynamic machinery of the hosts (Masters & Perlman, 2013).

Pathogenesis of the IBV depends on several extracellular and intracellular processes, which are included in the relationship between the virus interactions with its host. The virus-host interactions are established during IBV infections and they have direct effects on the viral replication (Cao, *et al*., 2012). Additionally, the interactions lead to the modification of numerous cellular pathways as well, such as cellular stress and/or host antiviral innate immune response (Zhong, *et al*., 2016). Apoptosis is another impact of the virus pathogenesis and greater levels of apoptosis is correlated with the elevated expression of some cellular proteins including interferon beta, which are in turn associated with increased pathogenicity of the IBV in kidney and respiratory tissues (Chhabra, *et al*., 2016). However, more detailed interaction processes are involved in the regulation control of cellular protein synthesis machineries so as to prepare the best condition for viral replication and virion assembly (Cao, *et al*., 2011; Emmott, *et al*., 2013; Fung, *et al*., 2014; Kong, *et al*., 2010; Vogels, *et al*., 2011; Wang, *et al*., 2009).

The posttranslational modification (PTM) of proteins is one of the major processes that occur in almost all types of the proteins and have significant role in the cellular biology. The process includes conversions in both structure and dynamics of the proteins in which the modifications take place at multiple sites of proteins (Audagnotto & Dal Peraro, 2017). Over 400 forms of PTMs have been characterized in proteins; phosphorylation, glycosylation, sulfation, nitration, glycation, acetylation, prenylation, methylation, proteolytic cleavage and various forms of oxidation are the most common types of PTMs (Rotilio, *et al*., 2012).

The PTM of IBV proteins after cellular and viral protein translations inside host cells has been poorly understood and few studies described IBV S (Zheng, *et al*., 2018), M and E (Ruch & Machamer, 2012a) proteins; however, more details were obtained from the cellular interactome of N protein (Jayaram, *et al*., 2005) (Spencer, *et al*., 2008) (Emmott, *et al*., 2013). On the other hand, the PTMs for other Coronavirus proteins has been in focus and different types of PTM were studied (Corse & Machamer, 2000).

Glycosylation of viral glycoproteins is one of the major areas of virology. The modification includes mainly N-linked glycosylation, which occurs in the ERGIC and supports maturations of the glycoproteins during virus replication and assembly (Vigerust & Shepherd, 2007). The Processed and matured viral glycoproteins are one of the major components of pathogenic viruses. They have been determined to have essential roles in infection, pathogenesis and immunity (Banerjee & Mukhopadhyay, 2016).

Coronaviruses have main structural glycoproteins in their envelope, which are determinant of tissue tropism and pathogenicity (Wickramasinghe, *et al*., 2011). The glycoproteins are very sensitive proteins to conformational changes for example in the IBV S glycoprotein, a single amino acid mutation affects the biology of the virus by hampering the S maturation and incorporation in to virions (Shen, *et al*., 2004). In addition to that, earlier in this year (Zheng, *et al*., 2018) study identified functional impact of N-linked glycosylation of IBV S protein on the replication and infectivity of the virus using bioinformatics prediction tool and proteomic assays. The study characterised 13 mutated asparagine to aspartic acid (N-D) and asparagine to glutamine (N-Q) sites from total 29 predicted N sites. However, the study didn't show the effect of cellular interactome on the maturation, folding and assembly processes.

In the ER and Golgi, the cellular machinery for regulating proteins including folding and quality control is a complicated process. Newly translated proteins are processed in the ER and when they are fully folded and assembled conformation, they are transported to the Golgi complex (Hammond, 1994). Molecular chaperons in the ER are the major protein folding machineries and they have principal effects in maturation and retrieving of unfolded proteins (Horwich, 2014).

Calnexin is a 90-kDa protein and one of the major membrane-bound chaperones in the ER, which interact with newly synthesized glycoproteins (Bergeron *et al*. 1994; Helenius *et al*. 1997; Hammond & Helenius 1994). The

first report of interaction and chaperoning effects of calnexin in virus biology was done for Influenza A and vesicular stomatitis viruses and the report identified the relation of the interaction due to the composition of N-linked oligosaccharide side chains in the viral glycoproteins (Hammond, *et al*., 1994).

Coronavirus structural proteins S, M and E of *Alphacoronavirus*, *Betacoronavirus* and *Gammacoronavirus* are mainly dependant on the N-linked glycosylation for processing and maturation. The validation of the process was reviewed by (Corse & Machamer, 2000) for each of the proteins. S protein of mouse hepatitis virus (MHV), transmissible gastroenteritis virus (TGEV), bovine coronavirus (BCoV), SARS-CoV and the IBV viruses, E protein of SARS-CoV and IBV viruses and M protein of TGEV, Porcine epidemic diarrhoea virus (PEDV), IBV and turkey enteric coronavirus are all modified by N-linked glycosylation (Fung & Liu, 2018). In addition to the glycosylation in these viruses, calnexin interaction with S protein of SARS-CoV and its functional impact was studied in detail (Fukushi, *et al*., 2012).

In this chapter, as a validation of quantitative label-free proteomics using LC-MS/MS in the previous chapter, the interaction of calnexin with IBV S, M and E proteins was characterised and confirmed. Moreover, deglycosylation of immunoprecipitated samples confirmed the heavily N-linked glycosylation of S glycoprotein.

4.2 Results:

To characterise the significance of calnexin interaction with the viral proteins, several validation techniques were conducted according to two major aspects of the protein-protein interactions and the glycosylation properties of the proteins. Direct immunoblot and immunofluorescent assays were applied for the interaction and colocalizations of calnexin with the viral proteins. In addition, the N-linked glycosylation for each protein were characterized by bioinformatics prediction and enzymatic removal of the glycogroups. Finally, as a result of the subsequent optimization outcomes and a support from the literature, a model was built for the processing and maturation of S, M and E proteins in the ER and Golgi complex.

4.2.1 Optimization of Calnexin Interaction by Immunoblotting:

In chapter 3 of this thesis, the label-free quantitative proteomics using LC-MS/MS for S, M and E, detected a number of proteins with various affinities of interactions. The significant proteins were short listed according to the significance of Anova (p) values <0.05. Calnexin as a molecular chaperone was significant in both S and E proteome and was selected for validations. To confirm positive interactions between the GFP-tagged proteins and calnexin, nitrocellulose membrane from all sample replicates were washed off using stripping buffers and were re-incubated with calnexin polyclonal antibody. The result showed potent interaction between GFP-S immunoprecipitated samples and negative interaction for GFP protein as a control. An illustrated result of GFP-S showed 90 kDa, which clearly interact with immunoprecipitated GFP-S sample only (Figure 4.1).

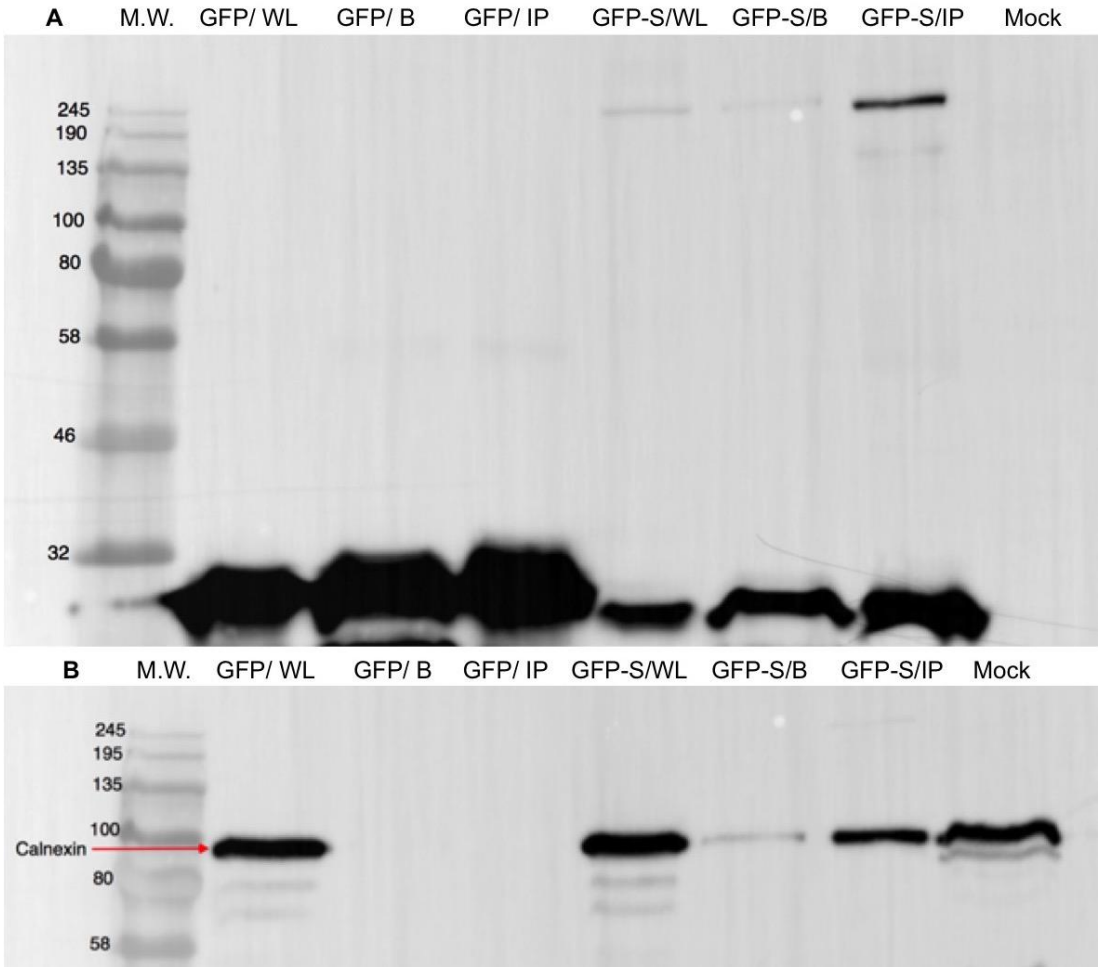

Figure 4.1: Illustrated optimization for calnexin interaction with S protein but not the GFP control. M.W. lanes are protein markers. A: membrane was incubated with anti-GFP antibody. Lane GFP/WL: GFP whole cell lysate. Lane GFP/B: GFP beads. Lane GFP/IP: GFP pulldown sample. Lane GFP-S/WL: GFP-S whole cell lysate. Lane GFP-S/B: GFP-S beads. Lane GFP-S/IP: GFP-S pulldown sample. Lane Mock: cell lysate only. B: membrane A was incubated with anti-calnexin antibody.

4.2.1.1 Interaction of IBV S, M and E with Calnexin:

To exclude any possibilities of false positive interaction between the bait and calnexin, the results were confirmed with all five replicates of S protein and six replicates for each of M and E proteins (the same samples which were applied for LC-MS/MS analysis) and confirmed the interaction with the baits

but not GFP. Immunoprecipitated samples from GFP control and GFP-tagged proteins were run on the same WBs and validated under similar incubation time and concentration of anti-calnexin antibody (Figure 4.2 A-D).

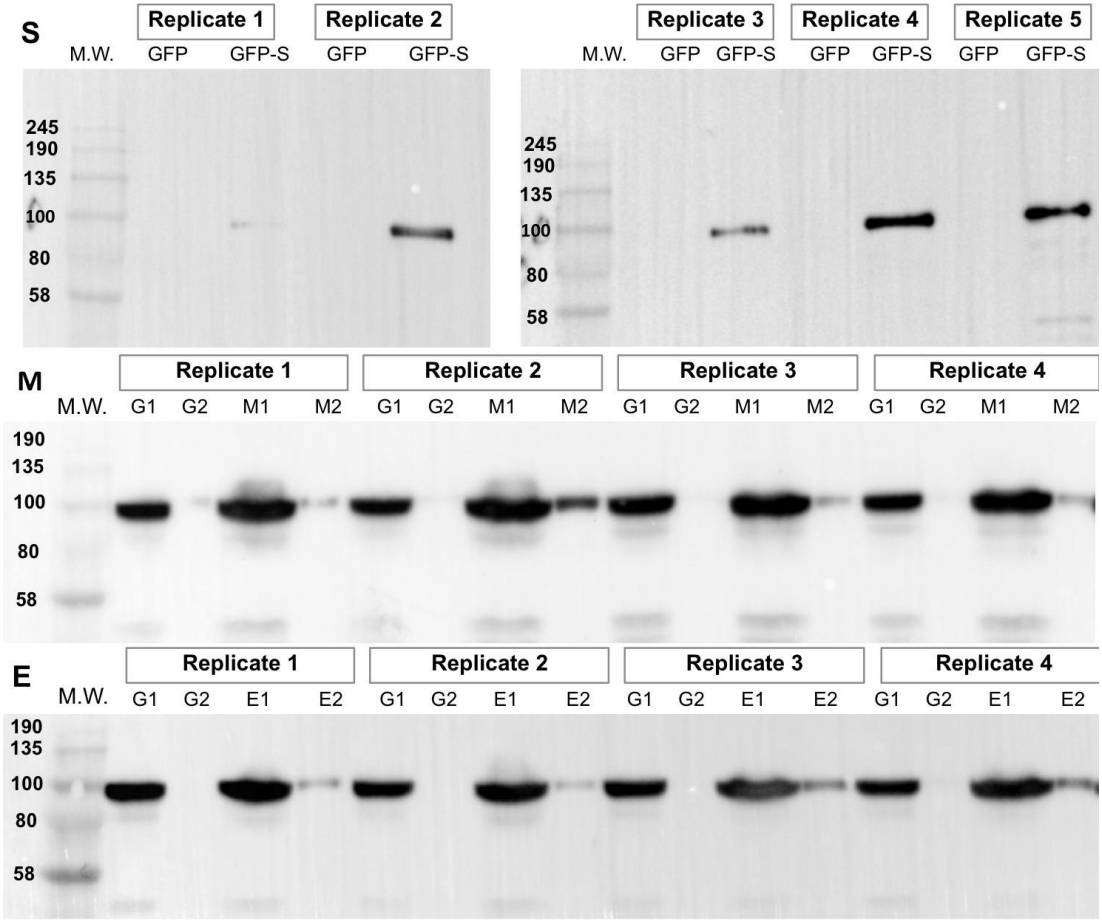

Figure 4.2: A-D: Immunoblot validation of calnexin interaction to GFP-tagged S, M and E proteins. Same membranes from Figure 3.5 were incubated with anti-calnexin antibody. ***S****: Pulled down samples of GFP (control) and GFP-S proteins in 5 replicates. M.W. lanes are protein markers. GFP lanes are GFP pulldown samples. GFP-S lanes are GFP-S pulldown samples. M: Cell lysates and pulled down samples of GFP (control) and GFP-M proteins in 4 replicates. G1 lanes are GFP whole cell lysates. G2 lanes are GFP pulldown samples. M1 lanes are GFP-M whole cell lysates. M2 lanes are GFP-M pulldown samples. E: similar arrangement as for M lanes.*

4.2.1.2 Calnexin did not interact with the HRSV M and EBOLA N Proteins:

Calnexin predominantly localizes in the ER and react to the ER stress and cellular responses. To confirm the specificity of its interaction with S, M and E proteins, both HRSV M and EBOLA N proteins as GFP tagged viral proteins were subjected under the same immunoblot and blot restore protocols with the GFP-S triplicate Figure 4.3 A and B.

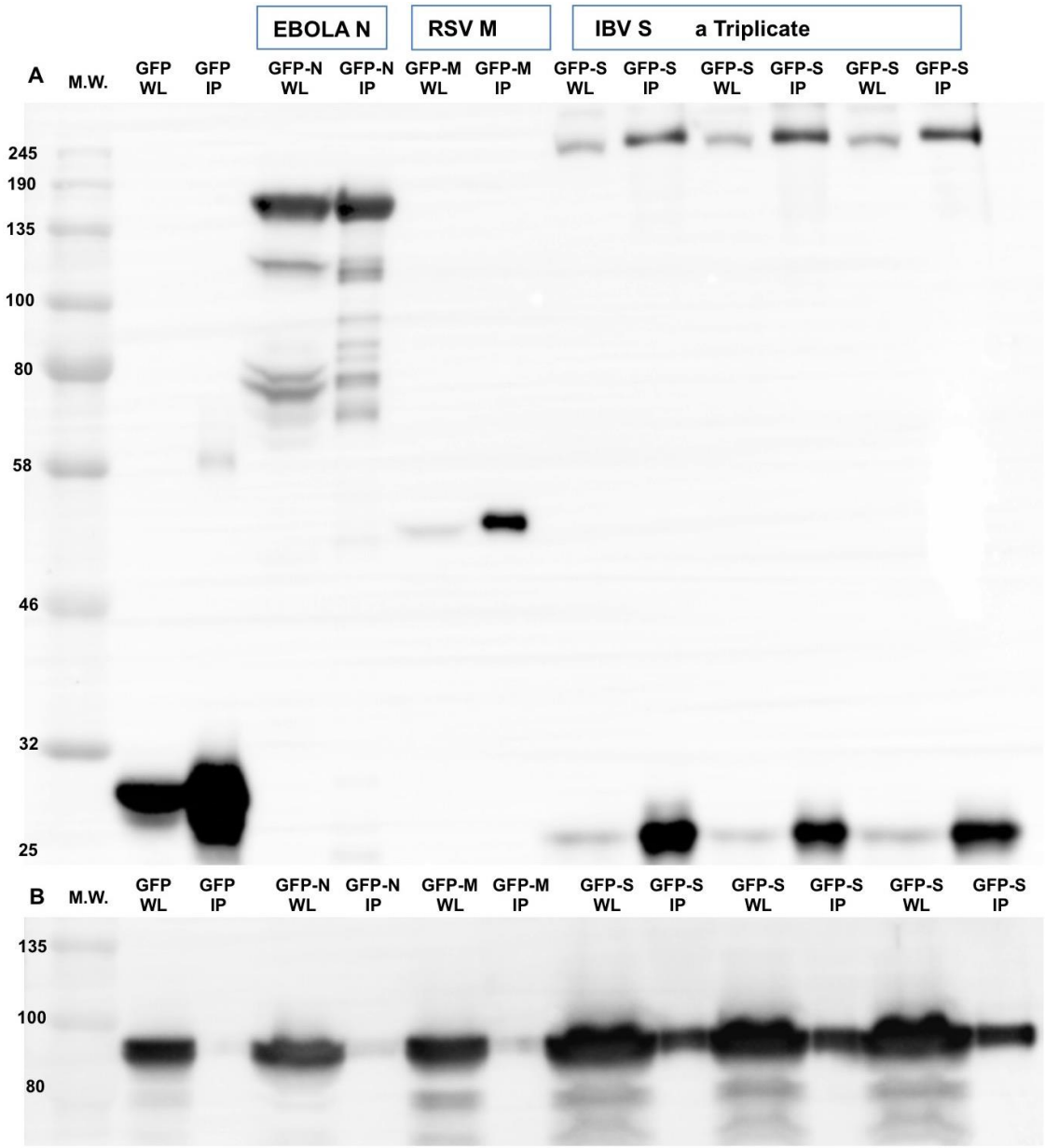

Figure 4.3 A and B: Optimization of calnexin interaction with other viral proteins. A: an immunoblot for expression and Immunoprecipitation of GFP, GFP-RSV M, GFP-EBOLA N and a triplicate of GFP-IBV-S proteins. A: Lane M.W.: Protein marker, Lane GFP-WL: GFP whole lysate, Lane GFP-IP: GFP pulldown, Lane GFP-N-WL: GFP-EBOLA-N whole lysate. Lane GFP-N-IP: GFP-EBOLA-N pulldown. Lane GFP-M-WL: GFP-RSV-M whole lysate. Lane GFP-M-IP: GFP-RSV-M pulldown. Lane GFP-S-WL: GFP-IBV-S whole lysates. Lane GFP-S-IP: GFP-IBV-S pulldown samples. B: Same membrane in A was incubated with anti-calnexin antibody. Calnexin showed significant interaction with IBV S, however the interaction is absent with GFP, RSV-M and EBOLA N proteins.

4.2.2 Optimization of Calnexin Interaction by Immunofluorescent Assay:

In order to confirm the interaction of calnexin with S, M and E proteins and observe the localization in the site of interaction, an immunofluorescent assay was conducted. The expressed GFP-tagged S, M and E proteins were processed in 293T cells and were then fixed and permeabilized for incubation with primary anti-calnexin and secondary AlexaFluor-labeled fluorescent antibodies subsequently. The incubated cells were held in the final staining with nucleus-targeted DAPI staining. Following microscopic analysis of the stained cells, the results showed significant interaction and identified the localization of the interaction between the expressed GFP-tagged viral proteins and calnexin Figure 4.4.

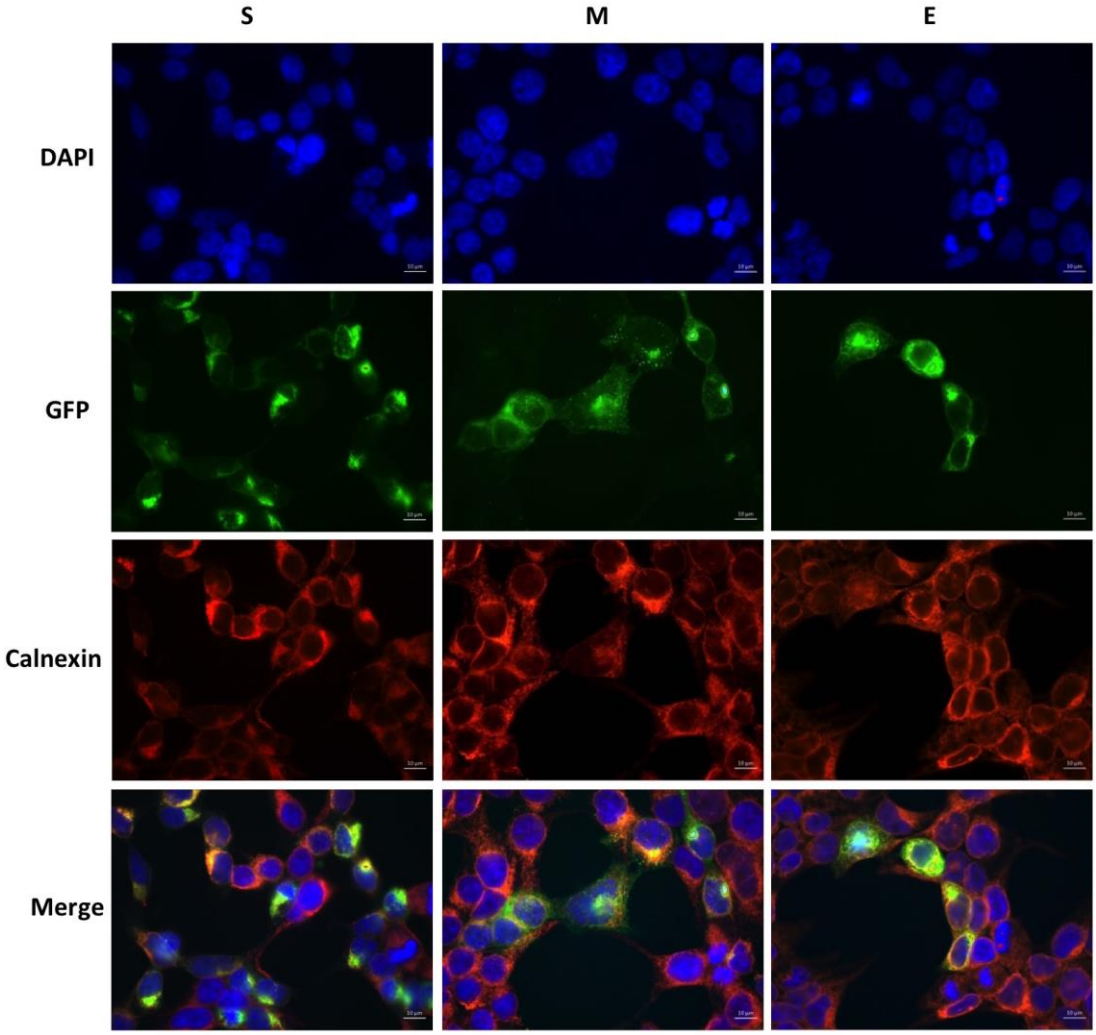

Figure 4.4: Immunoflourescent validation of Calnexin interaction to GFP-tagged S, M and E proteins. Columns S, M and E represent expressions and staining per each protein in 293T cells. Nuclei are colored blue (DAPI), GFP signals expressed in green; AlexaF stands for AlexaFluor 546nm red signals from Calnexin staining and MERGE images per each protein. Scale bars represent 10 µm.

For closer investigation about the interaction details, the images from S proteins were analyzed with Cytosketch software and the best-expressed cell was zoomed in for interaction and localization details Figure 4.5.

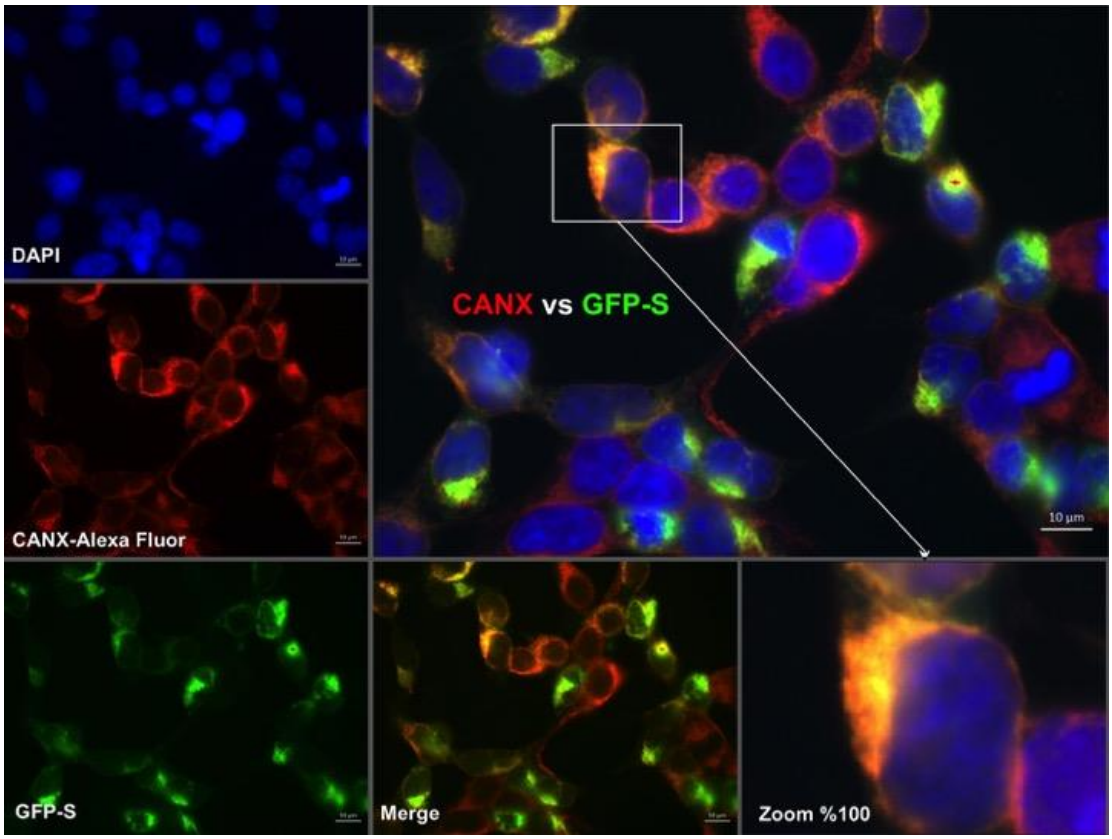

Figure 4.5: Image analysis of calnexin interaction to GFP-tagged S protein. Similar images from column S of Figure 4.4 were analyzed by Cytosketch software. Nuclei are colored blue (DAPI), GFP signals expressed in green; AlexaF stands for AlexaFluor 546nm red signals from calnexin staining and MERGE images per each protein. Scale bars represented 10 µm.

As the expressed proteins are usually processed in chicken cells and the construct gene sequences were derived from a nephropathogenic isolate of the IBV (SDIB821/2012), the expression, interaction and localization with calnexin was validated in Chicken Kidney Cells (CKC) as well. The cells were hardly grown; however the result showed bright interaction in the merge image as well Figure 4.6.

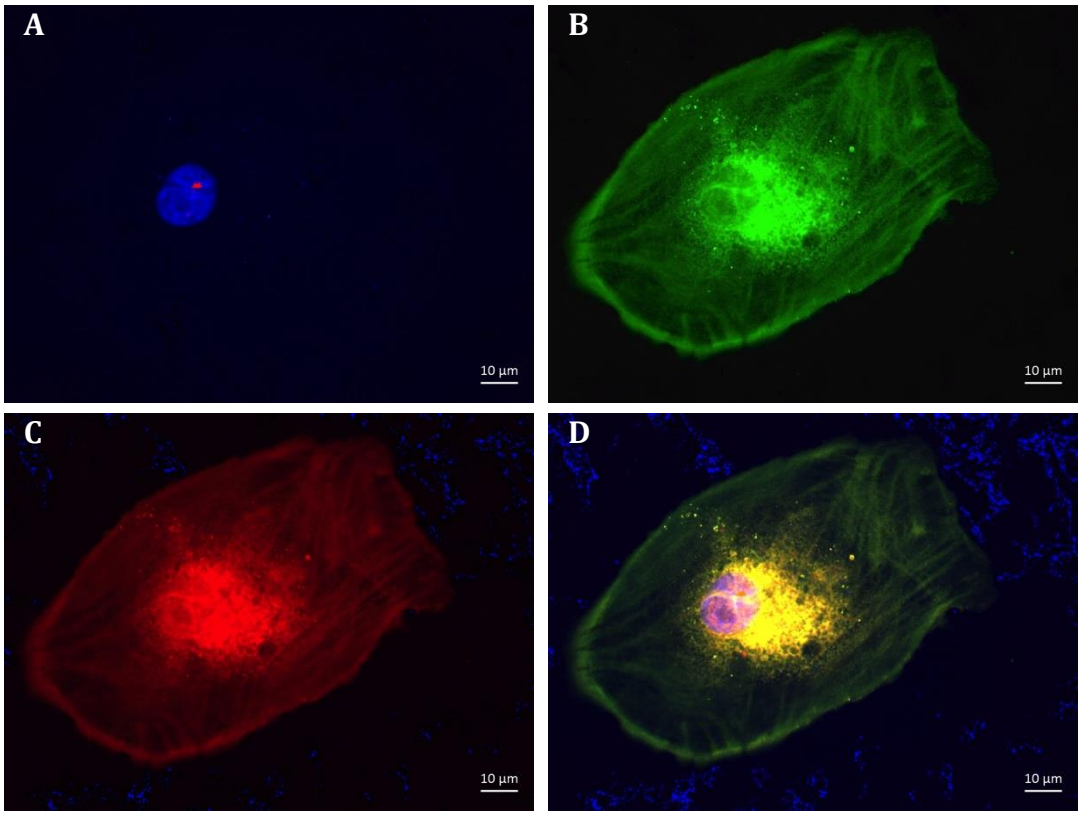

Figure 4.6: Immunoflourescent validation of calnexin interaction to GFP-S protein in CKC cells. A: Nucleus is colored blue (DAPI). B: GFP signals expressed in green. C: AlexaFluor 546nm red signals from Calnexin staining. D: Merge of A, B and C. Scale bars represented 10 µm.

4.2.3 Study of S, M and E N-linked Glycosylations:

Based on results in Chapter 3 and the previous sections in this chapter, calnexin was validated as a cellular interactome partner for IBV S, M and E proteins. As a membrane-bounded molecular chaperon; it was confirmed that calnexin interacts with nascent glycoproteins in the ER and it has specific affinity for N-linked glycoprotein folding and maturation processes (Fukushi, *et al*., 2012). To characterize the N-linked properties of S, M and E proteins, bioinformatics prediction and enzymatic deglycosylation analysis were conducted.

4.2.3.1 Glycosylation Prediction for S, M and E Proteins:

To predict the number of N-linked glycosylations for each protein, the original amino acid sequences for S, M and E genes, which were used for constructs, were applied to N-GlycoSite online program (Zhang, *et al*., 2004). N-GlycoSite is N-linked glycosylation prediction program for viruses based on NXS/T motif in which the X can be any amino acid other than proline. The program was originally designed for the viral analysis of glycoproteins and included Human Immunodeficiency Virus (HIV), Semian Immunodeficiency Virus (SIV), Hepatitis C Virus (HCV) and Influenza viruses and available online in the HIV Sequence Database https://www.hiv.lanl.gov/content/sequence/GLYCOSITE/glycosite.html.

The results showed 34 N- linked glycosylation sites for S, 2 sites for M and 3 sites for E proteins (Figure 4.7 A-C) for the selected SDIB821/2012 IBV isolate. The S glycoprotein is heavily glycosylated to N-linked motifs especially in the first 300 amino acids of the S1 domain. S and E proteins possessed about 2.92% and 2.78% N-linked glycosylation motifs respectively, however M has only about 0.89% N-linked motifs.

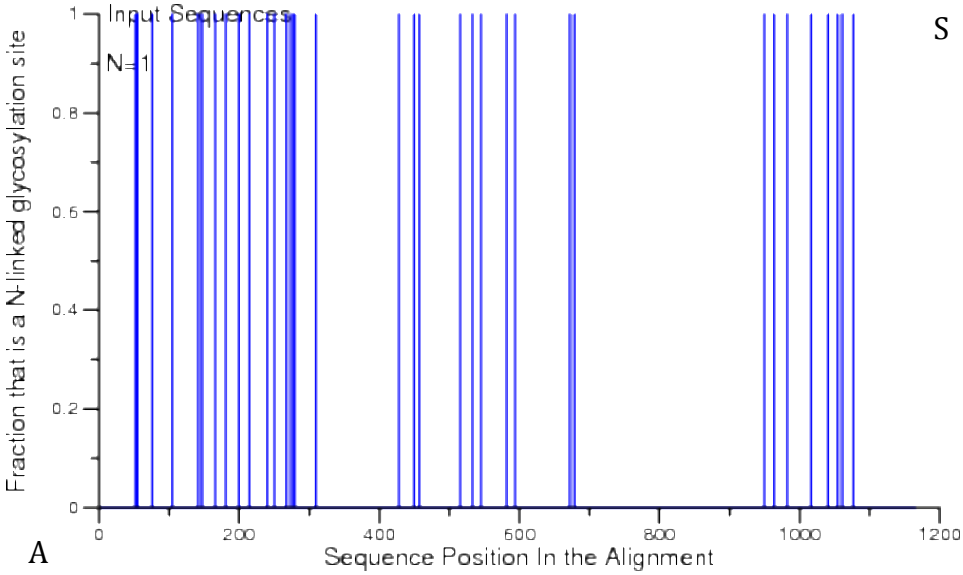
Input Sequences
N=1
Fraction that is a N-linked glycosylation site
Sequence Position In the Alignment
S
A

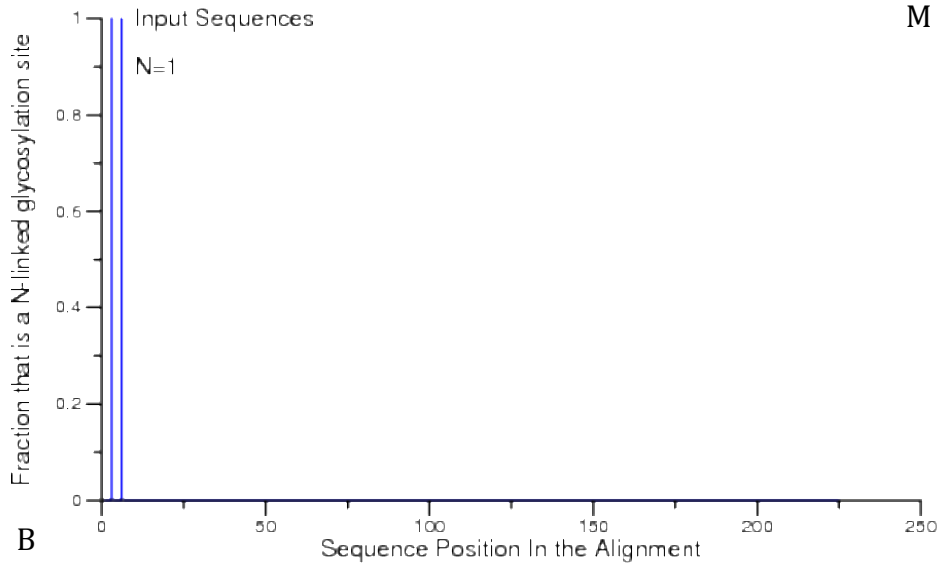
Input Sequences
N=1
Fraction that is a N-linked glycosylation site
Sequence Position In the Alignment
M
B

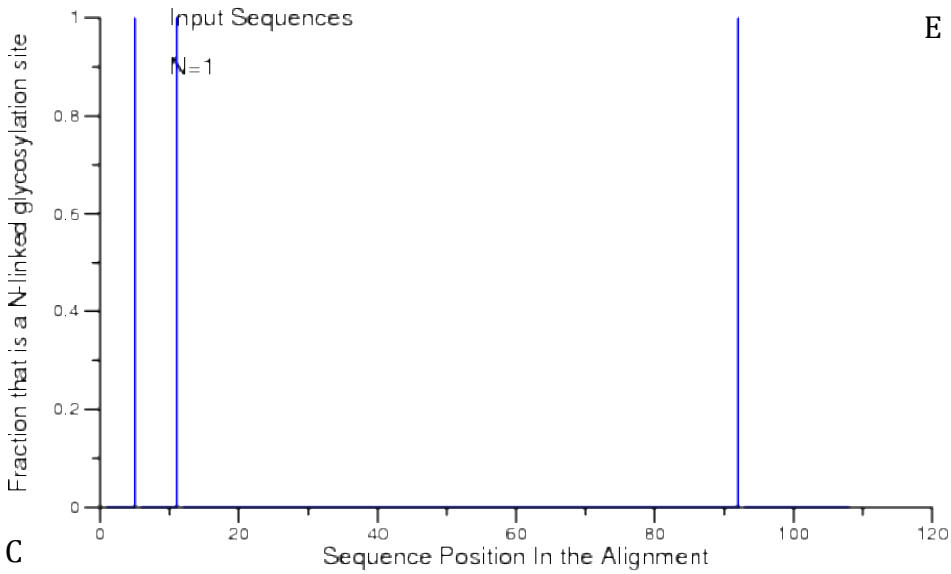
Input Sequences
N=1
Fraction that is a N-linked glycosylation site
Sequence Position In the Alignment
E
C

Figure 4.7 A-C: N-linked glycosylation prediction for S, M and E proteins using N-GlycoSite online program. A: Spike glycoprotein has 34 NXS/T ex. P motifs. The motifs were clustered according to their positions and the N amino acids, which have NXS/T arrangements, were annotated as red in the N-GlycoSite. B: M proteins has only has 2 NXS/T ex. P motifs. C: E protein has 3 NXS/T ex. P motifs.

4.2.3.2 Enzymatic Deglycosylation Study:

As known in the literature, the average molecular weight of the IBV S glycoprotein is about 130 kDa (Masters, 2006). The molecular weight calculation for the S protein of (SDIB821/2012) isolate using sequence manipulation software online on www.bioinformatics.org, predicted exactly 128.28 kDa. However, in all the immunoblots, the expressed GFP-S protein were about 240 kDa, so excluding the 27 kDa of the GFP, it was hypothesized that this surplus molecular weight (50 kDa) might be due to having 34 N-linked glycan groups on glycosylation chains of the S protein (Figure 4.7 A).

The deglycosylation study was done for a triplicate of GFP trapped S proteins using Peptide-N-Glycosidase F (PNGase F) enzyme. S glycoprotein was denatured by heating in denaturation solution and incubated with PNGase F enzyme, before result confirmation by WB. The deglycosylated GFP-S protein were optimized on WB using anti-GFP antibody and the outcome was a significant reduction in the molecular weight by 50 kDa as compared to normal glycosylated GFP-S glycoprotein (Figure 4.8).

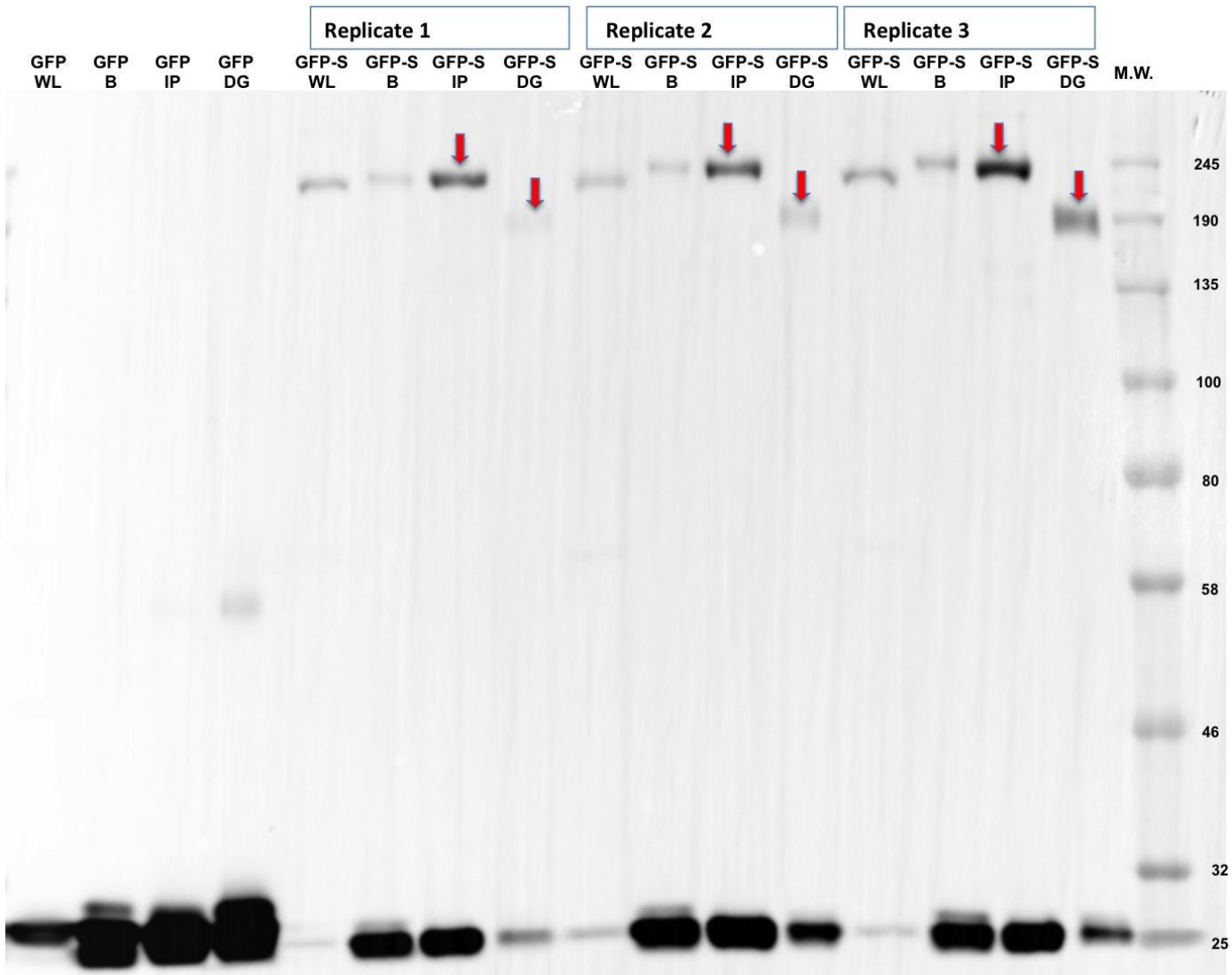

Figure 4.8: Deglycosylation of GFP-S glycoprotein. Lane M.W.: Protein marker. Lane GFP: whole cell lysate, bead-bounded, immunoprecipitated and deglycosylated of GFP control samples. Lane GFP-S: cell lysate, bead-bounded, trapped and deglycosylated GFP-S proteins in triplicate. GFP: Green Fluorescent Protein. WL: Whole Cell Lysate. B: Beads-bounded. IP: immunoprecipitated. S: Spike glycoprotein. A significant mass shift of deglycosylated proteins were detected in the triplicate.

4.3 Discussion:

In support of the interactome results from chapter 3, the validation data results in this chapter represent the first confirmation of calnexin interactions with IBV glycoproteins using label-free proteomic assay by LC-MS/MS of immunoprecipitated proteins. The results are compatible with the previous findings for SARS Coronavirus S protein, which binds to calnexin in the ER (Fukushi, *et al*., 2012). There are two studies which used calnexin as a localization marker in the ER for studying localization of IBV S (Lontok, *et al*., 2004) and hydrophobic domain of E protein (Ruch & Machamer, 2011). However they did not study the interaction of calnexin with the IBV S and E proteins. On the other hand, for negative sense single stranded RNA viruses, calnexin interaction with the viral glycoproteins are well studied especially as the case for Influenza virus Hemagglutinin (HA) and VSV glycoprotein (G) (Hammond, *et al*., 1994) (Hebert, *et al*., 1995, 1996; Tatu & Helenius, 1997). Other than Helenius group works, there are further studies in calnexin interaction with the viral glycoproteins such as Rabies virus (Gaudin, 1997), Dengue virus (Idris, *et al*., 2016; Limjindaporn, *et al*., 2009), Hepatitis B virus (HBV) (Werr & Prange, 1998), Hepatitis C virus (HCV) (Choukhi, *et al*., 1998), rotavirus (Mirazimi, *et al*., 1998) and HIV (Hunegnaw, *et al*., 2016).

Calnexin is a membrane bound chaperon of the ER that interacts with recently translated glycoproteins having mono glucose molecule at the up most arm of the N- linked glycogroup (Bergeron, *et al*., 1994). The viral glycoproteins are obligatorily dependant on the cellular machinery translation

and post translation processes that are mainly induce the ER stress during viral infections especially in the case of Coronaviruses (Fung, *et al*., 2014).

In the current study all three structural proteins of the IBV envelope S, M and E, were showed high affinity of interaction with Calnexin in the immunoprecipitated samples of GFP-tagged proteins. The detection of interaction was confirmed by stripping and reprobing method, which is basically used in case of having precise comparison of specific bands when they are needed within the same membrane (Kurien & Scofield, 2006). In the illustrated immunoblot Figure 4.1 the interaction between S and Calnexin proteins is very clear in the pulldown and bead sample lanes only and it can be relatively obvious between beads and pulldown samples. However, in the whole lysate wells the calnexin band was detected even in the GFP as a control, this is mainly because calnexin is one of the major resident proteins in the ER and it is highly expressed either in cross-link to other chaperons (Tatu & Helenius, 1997) or individually in response to cellular stress, which is induced by the accumulation of misfolded protein (Hammond, 1994).

The interaction affinity was obvious in S, M and E proteins; although in the M interactome protein list, calnexin wasn't detected as a significant candidate, however M showed affinity to interact with calnexin by immunoprecipitation and localization immunofluorescence assays. The reason for the M proteome, might be the ratio of NXS/T motifs in M protein, which was only 0.89%, however for S and E proteins the ratios were 2.92% and 2.78%

respectively. Consequently, it can be hypothesized that the higher the ratio of N-linked glycosylation, the higher the affinity for interaction with calnexin.

The S glycoprotein has been well characterized both for IBV and other coronaviruses in terms of structure (Shang, *et al*., 2018), PTMs especially N-linked glycosylation (Zheng, *et al*., 2018) and trafficking in side host cell (Ujike & Taguchi, 2015; Youn, *et al*., 2005). However, the cellular contribution and direct interaction with the host proteins were held in hypothesis and they were poorly understood. A reason for that might be the case of focus on IBV S-host receptor interaction (Belouzard, *et al*., 2012). In an exceptional study for SARS Coronavirus S protein, the physical interaction was confirmed between the S and calnexin proteins (Fukushi, *et al*., 2012). The validation results for IBV S protein in this chapter, was completely compatible with the results in for the SARS S protein, except for the original data that was based on label-free proteomic assay by LC-MS/MS from chapter 3 this thesis.

On the other hand, the interaction study of IBV M protein was mostly localized in the Golgi, which is either homotypic interaction between M proteins (de Haan, *et al*., 2000) or heterotypic with the other structural viral proteins such as S (Ujike & Taguchi, 2015), E (Ruch & Machamer, 2012b) and N (Narayanan, *et al*., 2000) proteins. However the interaction of the M and cellular proteins was studied to interact with actin protein (Wang, *et al*., 2009). The interaction of IBV M with calnexin was neither described in any studies nor obtained in the proteome study of the current work, however the N-linked glycosylation prosperity in its ectodomain as characterized

previously (Stern & Sefton, 1982) and in the N-linked glycosylation prediction analysis which confirmed the third and sixth N amino acids, confirmed the susceptibility of M for the specific PTM glycosylation.

In the current study, E protein interaction with calnexin is very significant in the proteome data (chapter 3) and validated by immunoblotting and immunoprecipitation assays. The E protein was also well studied for its molecular structure (Ruch & Machamer, 2011, 2012a) and trafficking to assembly site (Corse & Machamer, 2000, 2002), however the interactions with cellular proteins has been poorly studied and no direct interaction was clearly identified. Consequently the results for IBV E proteomics based on label-free LC-MS/MS data and validations, confirm the interaction of E with calnexin in the ER.

The interaction localization study for S, M and E with calnexin by immunofluorescent assays are another evidences for confirming the virus-host interactions in perinuclear regions mainly supports the localization of the interaction in the ER and Golgi complexes. Calnexin as a resident protein marker was previously used for localization studies (Lontok, *et al*., 2004),

Other than Coronaviruses, calnexin interacts with some other viral glycoproteins such Influenza virus (HA) (Hebert, *et al*., 1997), VSV (G) (Hebert, *et al*., 1995, 1996; Tatu & Helenius, 1997), Rabies virus G protein (Gaudin, 1997) and Dengue virus Envelope E (Idris, *et al*., 2016; Limjindaporn, *et al*., 2009). Due to such a relatively high affinity of calnexin

interaction, two other different proteins from different viruses from the previous studies of our lab, EBOLA N (García-Dorival, *et al*., 2016) and RSV M (Aljabr, 2016) were analysed in a similar condition with a triplicate of IBV S glycoprotein. As a result both EBOLA N and RSV M didn't interact with calnexin as well as the GFP alone, which was used as the tag in all vectors.

N-linked Glycosylation plays major role in the interaction between viral glycoproteins and calnexin. Newly translated glycoprotein in side the ER lumen undergoes glucose molecule reduction and interacts with calnexin to proceed proper folding and maturation of the glycoprotein (Hammond, *et al*., 1994; Hebert, *et al*., 1995; Helenius, *et al*., 1997). The N-linked glycosylation for the proteins in this study showed different ratios according to the prediction method (Zhang, *et al*., 2004) 2.92% and for the S, 2.78% for the E and 0.89% for the M protein. Additionally, the enzymatic deglycosylation by PNGase F confirmed the predicted heavy glycosylation of the S protein. Taken together, the cellular machinery of glycoprotein maturation was identified in the model of the ER and Golgi complex trafficking. Overall, the interaction of the IBV glycoproteins with calnexin was validated and a model was built for detailed pathway showing how viral glycoproteins are processed in the molecular level and what enzymes are included per each step.

4.3.1 Model of IBV Glycoprotein Processing and Maturation:

To characterize the whole process of calnexin interaction and glycosylation mechanism of the viral glycoproteins in the ER and Golgi, two models were built for each the ER and Golgi complex's process and maturation of the

glycoproteins. Using CellDesigner4.4 software (Funahashi, *et al*., 2003) as a modeling tool for biochemical networks and in support of the Reactome database, the process of specific PTMs of the viral glycoproteins in both the ER and Golgi were designed Figures 4.9 A and B.

4.3.1.1 The Model In the ER:

As a result of the model, viral glycoproteins are trafficked in to the ER lumen in which on translocation site, glycogroups are added to NXS/T motifs by Oligosaccharyltransferase (OST). The Glucosidases then trim two molecules from the glycogroup and one is left on the group, which acts as a signal for interaction with calnexin so as to enter the folding and maturation process in calnexin pathway. The glycoprotein is then matured by adding N-Acetylegalactosamine (GlcNAc) and Mannose (M) molecules, which are in turn translocated in to the Golgi for further process, however all misfolded proteins are retrieved in to the ER quality control for either reprocessing or degradation processes Figure 4.9 A.

4.3.1.2 The Model In the Golgi:

In the Golgi complex more PTMs are occurred in the presence of Mannosidases. Four mannose molecules are then trimmed and GlcNAc and Galactose (Gal) molecules are added to the N-linked groups. Finally either N-Acetyleneuraminic acid (N-ANA) or Sialic acid (SA) molecules are added to the Gal on the group by which the viral glycoproteins become mature and translocated to the assembly site in the aid of cytosolic movement and cellular protein interactions Figure 4.9 B.

Figure 4.9: Proposed model for the PTMs, processes and maturation of the viral glycoproteins from the ER to Golgi complex.

A: Proteins enter the ER are N-glycosylated by oligosaccharyltransferase (OST) enzyme once they transit n to the lumen. Two glucoses are trimmed by the successive action of Glucosidase I and II to produce monoglucosylated proteins, which are recognized by CANX/CRT complex. The complex between the chaperones and folding intermediates bifurcate to two processes, either removal of the last glucose by glucosidase II causes folded substrate release from CNX/CRT complex or misfolded glycoproteins retains the glucose and is reformed by GT activity. If the protein reached its innate structure, it will be released from the ER through the protein secretory pathway. However, if the protein is not perfectly folded, it will be recognized by glycosyltransferase (GT). The completed proteins are not recognized by GT and are transported to the Golgi. However improperly folded proteins will be targeted to the ERQC for degradation.

A

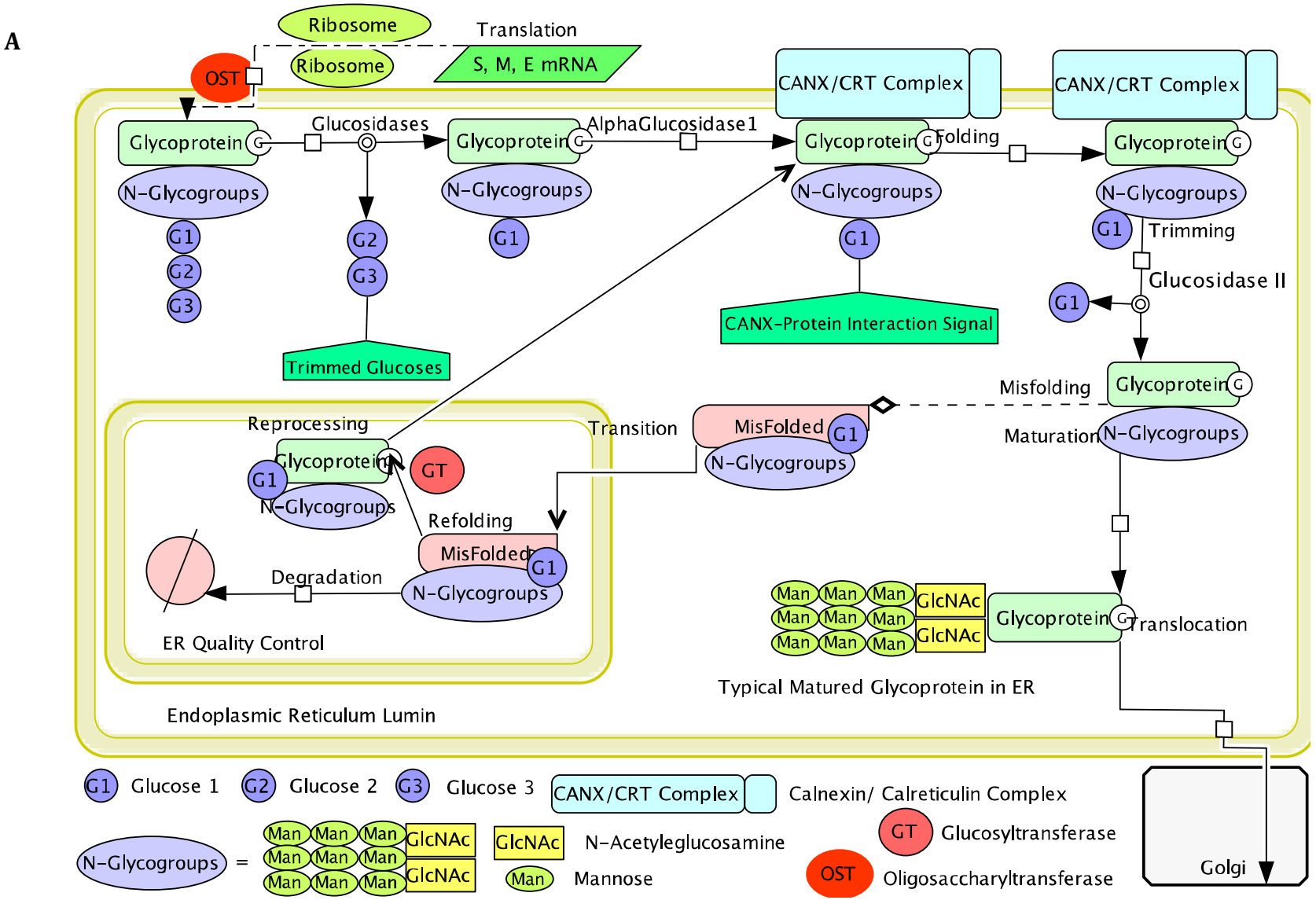
Ribosome
Translation
Ribosome
S, M, E mRNA
OST
CANX/CRT Complex
CANX/CRT Complex
Glycoprotein
Glucosidases
Glycoprotein
AlphaGlucosidase1
Glycoprotein
Folding
Glycoprotein
N-Glycogroups
G1
G2
G3
N-Glycogroups
G1
N-Glycogroups
G1
N-Glycogroups
G1
Trimming
Glucosidase II
G1
G2
G3
Trimmed Glucoses
CANX-Protein Interaction Signal
Misfolding
Glycoprotein
Reprocessing
Transition
MisFolded
G1
N-Glycogroups
Maturation
N-Glycogroups
Glycoprotein
G1
N-Glycogroups
GT
Refolding
MisFolded
G1
Degradation
N-Glycogroups
ER Quality Control
Man
GlcNAc
Glycoprotein
Translocation
Typical Matured Glycoprotein in ER
Endoplasmic Reticulum Lumin
G1 Glucose 1
G2 Glucose 2
G3 Glucose 3
CANX/CRT Complex
Calnexin/ Calreticulin Complex
N-Glycogroups =
GlcNAc
N-Acetyleglucosamine
Man
Mannose
GT
Glucosyltransferase
OST
Oligosaccharyltransferase
Golgi

B: Proteins having N-glycans are translocated from the ER and processed in the Golgi. In the cis- Golgi mannosidases remove Mannose (Man) residues to produce the Man5GlcNAc2Asn intermediate, which acts as the substrate of the medial Golgi Glucosyltransferases (GT). The GT transfers GlcNAc to Man5GlcNAc2Asn and synthesises hybrid and complex N-glycans. Hybrid N-glycans has five Man molecules and extend the arm that obtained GlcNAc by adding Gal and Salic acid. In trans Golgi conversion from hybrid to complex needs the N-glycans to lose the terminal two of the five Man molecules and obtain a second GlcNAc on to the complex N-glycan. The latter complex intermediate is then elongated by the addition of different molecules such as Gal, N-ANA and SA.

B

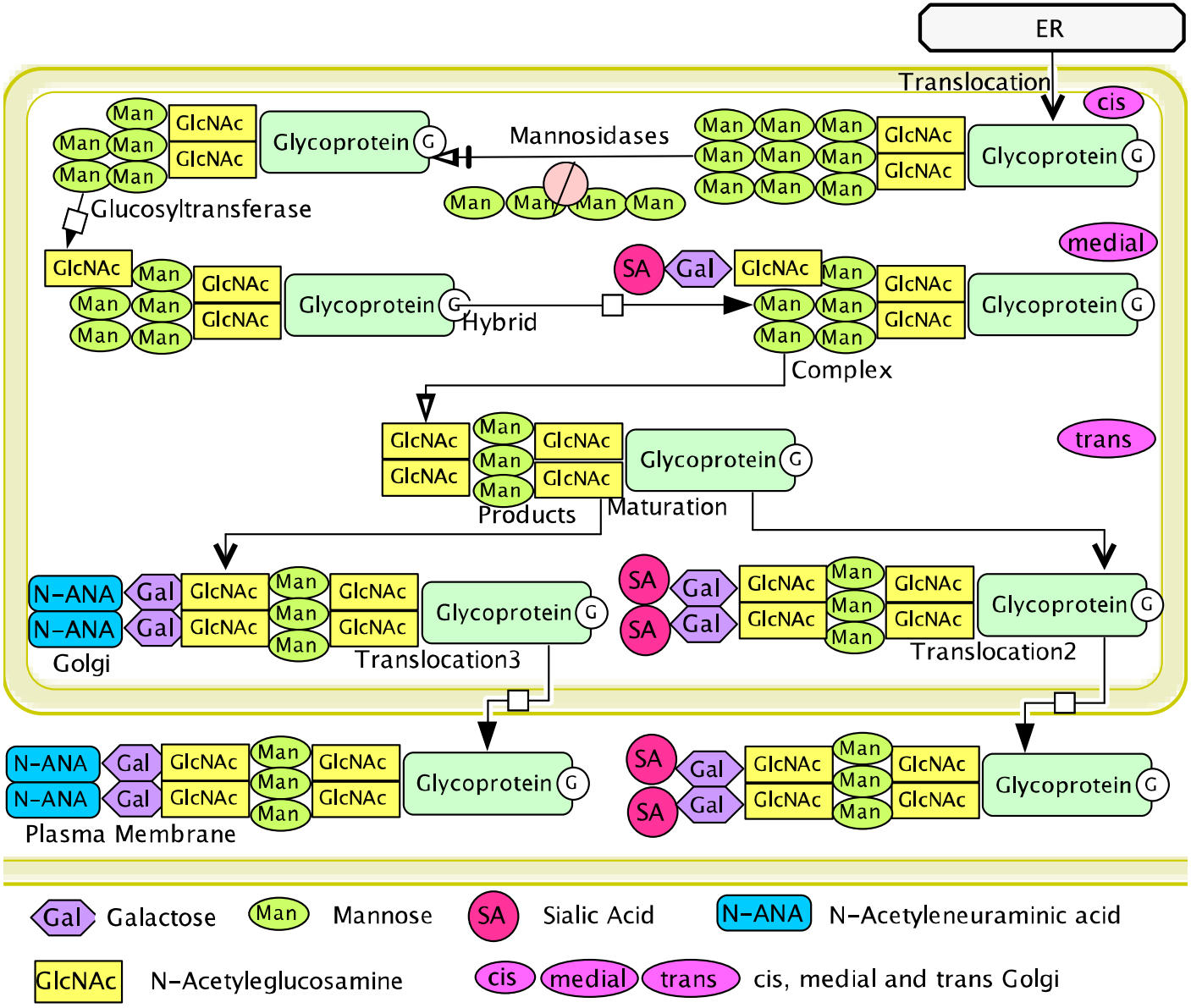
ER
Translocation
cis
Mannosidases
Glucosyltransferase
Glycoprotein
Hybrid
medial
Complex
trans
Products
Maturation
Golgi
Translocation3
Translocation2
Plasma Membrane
Man
GlcNAc
Gal
SA
N-ANA
Galactose
Mannose
Sialic Acid
N-Acetyleneuraminic acid
N-Acetyleglucosamine
cis, medial and trans Golgi

In conclusion of this chapter, there are transition steps for processing and maturation of the viral glycoproteins and these processes are depended on signals and enzymatic activities. Consequently, it can be hypothesized that inhibition of one or some of the transition steps, affects the virus biology in general. The hypothesis was optimized and validated in the next chapter using enzyme inhibitors and siRNA knockdown of calnexin.

Chapter 5

N-Linked Glycosylation of IBV S, M and E Proteins Plays a Role in Determining Virus Infectivity

5.1 Introduction:

IBV has exceptional challenges regarding its control especially in commercial broiler and layer chickens. As a result of error prone replication (Holmes, 2003; Ulferts & Ziebuhr, 2011), and recombination (Kottier *et al*. 1995), the genome of IBV is constantly modified. This has resulted in greater genomic diversity and resulted in the availability of diverse serotypes of the virus. Many studies have shown that the cross protection between vaccine strains and the circulatory isolates is approximately close to zero especially in terms of clinical preventions (Bande, *et al*., 2017; Khaleil, *et al*., 2014; Ma, *et al*., 2012). Consequently, the attenuated live vaccines, which are supposed to control the disease, have to match closely to the serotype of IBV, which is responsible for the particular outbreak in an endemic area. This is very similar to the situation with the selection of the appropriate vaccine components to influenza virus each year. Influenza virus RNA genome also undergoes mutation (antigenic drift) and recombination (antigenic shift) (Shao, *et al*., 2017). The existence of serologically different variant strains, for which no specific vaccines are available, have made the control and prevention of the IBV outbreaks more challenging (de Wit, *et al*., 2011; Jackwood, 2012; Mahmood, *et al*., 2011). Apart from the virus genome diversity, there are the additional complications of the slow development of novel vaccine technology and a deficiency in the knowledge of IBV proteins and host cell interactions. These currently make targeted vaccine strategies close to impossible (Jordan, 2017).

On the other hand, meanwhile the trials for vaccine development has been in challenge, the attempts for IBV antiviral research and intervention of new chemotherapies and/or new treatment methods have been limited as well. There have been a few trials on some natural plants and botanic extracts as potential antiviral inhibitors for treatment of the IBV (Chen, *et al*., 2014; Jackwood, *et al*., 2010; Mohajer Shojai, *et al*., 2016; Yang, *et al*., 2011). However, the trials were insufficient compared to human antiviral drug trials in the past five decades, in which the antiviral drugs were expanding in discovery, approval and clinical use. Following the first antiviral drug (Idoxuridine) which was approved in 1963, a further 90 antiviral drugs were licenced to treat some human infectious viruses such as HIV, HBV, HCV, Influenza virus, CMV, Varicella-zoster virus, RSV and HPV (reviwed in De Clercq & Li, 2016).

Moreover, the antiviral drugs have been developed in veterinary medicine as well. The use of animal models for the development of human therapies suggested that such therapies may also be relevant for infections of livestock and companion animals. The viral infections for livestock including foot and mouth disease virus (FMDV), classical swine fever virus (CSF), bovine viral diarrhoea virus (BVDV), bluetongue virus and orf virus were part of trials for anti-viral therapies. In companion animals, other viruses were targeted including feline herpesvirus 1 (FeHV-1), feline Leukaemia virus (FeLV), canine parvovirus type 2 (CPV-2) and equine herpesvirus 1 (reviewed in (Dal Pozzo & Thiry, 2014). However, in the poultry industry, the focus was significantly on AIV antiviral trials (Abdelwhab & Hafez, 2015).

Almost all the enveloped viruses including the coronaviruses require the host ER glycoprotein-folding machinery in order to properly fold their glycoproteins and in such cellular machinery, several enzymes such as glucosidases and mannosidases are essential (Ujike & Taguchi, 2015; Zhang, *et al*., 2004). Intervention with the activity of the enzymes leads to PTM impairment of N-linked glycosylation and results in unfolded glycoproteins, which in turn leads to non-infective and deactivated viruses. The glucosidase inhibitors have been studied extensively and are known as iminosugars (Chang, *et al*., 2013; Tyrrell, *et al*., 2017; Zhao, *et al*., 2015).

Iminosugars are broad-spectrum antivirals, which target the glucosidases and inhibit the sequential glucose trimming processes in the ERGIC. The main examples of these molecules are DNJs and castanospermine. Consequently, the use of these molecules in virus infected cells prevents viral glycoproteins interacting with the protein-folding machinery, which leads to viral protein misfolding and degradation by ER-Associated Protein Degradation (ERAD) in ERQC pathway. This results in the production of an antiviral effect against the virus's structural assembly and infectivity (Alonzi, *et al*., 2017). As the iminosugars target host cell enzymes, they are refractive to mutations in the virus genome to generate resistance; therefore they have promising potential for obtaining broad- spectrum antiviral treatments (Tyrrell, *et al*., 2017).

Coronaviruses are sensitive to iminosugars and there are some studies, which investigated the effect of these compounds on a few coronavirus

species mainly SARS coronavirus (Fukushi, *et al*., 2012; Zhao, *et al*., 2015), mouse hepatitis virus (Repp, *et al*., 1985) and human coronavirus (HCoV) (Zhao, *et al*., 2015).

In the previous two chapters of this thesis, (Chapter 3 and Chapter 4), based on the label-free proteomics and its validations, a model for N-linked glycoprotein processing was proposed. According to this model, IBV S, M and E glycoproteins were processed in the ER and their N-linked glycosylation PTM was driven by calnexin interaction. Enzymatically, the glucosidases also provided an essential function in the such PTM. In the Golgi, the mannosidases were also involved in the completion of viral glycoprotein processing and maturation. Accordingly, in support of the model and the previous usage of iminosugars, a new approach for targeting glucosidases in the ER and mannosidases in the Golgi was designed. In this chapter, various treatment inhibitors (DNJ and DMJ) were used either alone or in combination to disrupt N-linked glycosylation of viral glycoproteins. As calnexin was involved in the interaction with the viral glycoproteins, the protein was also depleted using siRNA.

5.2 Results:

To make further analysis for the virus-host interactions, especially processing of viral proteins in the host cells, small molecule-induced enzyme inhibition of N-linked glycosylation of the viral glycoproteins was conducted to test the model presented in the previous chapter. The approach involved impairment of N-linked glycosylation per either single proteins of S, M or E using GFP-tagged plasmid transfections or the whole viral glycoproteins during virus infections *in vitro*.

The identification of enzymatic inhibition effect on N-linked glycosylation of S, M and E proteins was carried out using 293T and Vero cells which were subjected to treatment with both DNJ and DMJ iminosugars. Optimization trials were conducted in the first instance with different drug concentrations and treatment timelines.

5.2.1 Cell Viability (MTT) Assays:

For determining small molecule treatment and the siRNA transfections concentrations, cell viability using MTT assay was conducted. Investigation of cytotoxicity of the iminosugars and siRNAs were determined by a series of final concentrations from 5-1000 µM iminosugars or 5-1000 nM siRNA in the MTT assay for 293T and Vero cells (Figure 5.1 A-H). According to the results and concentration obtained from optimization trials, the final concentration of 100 µM for both DNJ and DMJ and 200 nM of siRNAs were selected for treatment and transfection studies.

A

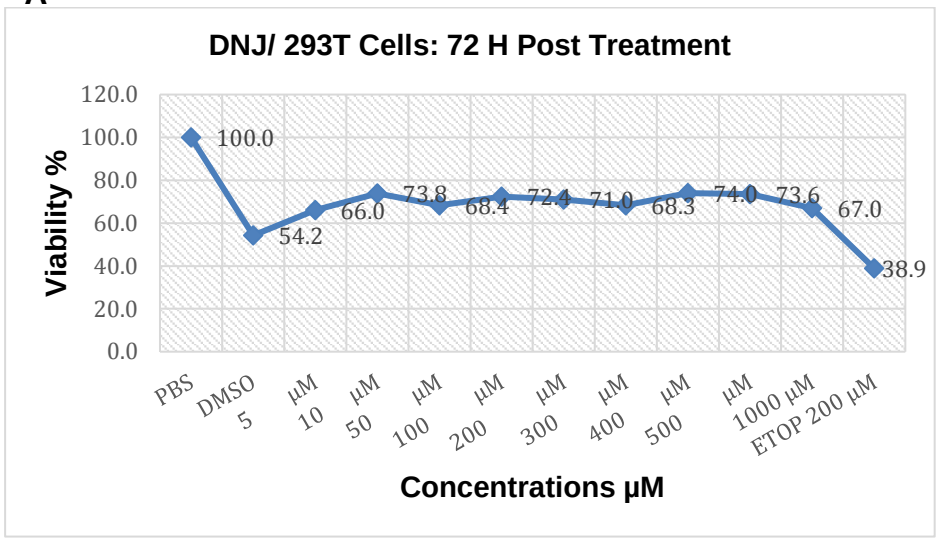
DNJ/ 293T Cells: 72 H Post Treatment
Viability %
120.0
100.0
80.0
60.0
40.0
20.0
0.0
100.0
54.2
66.0
73.8
68.4
72.4
71.0
68.3
74.0
73.6
67.0
38.9
PBS
DMSO 5
μM 10
μM 50
μM 100
μM 200
μM 300
μM 400
μM 500
μM 1000 μM
ETOP 200 μM
Concentrations μM

C

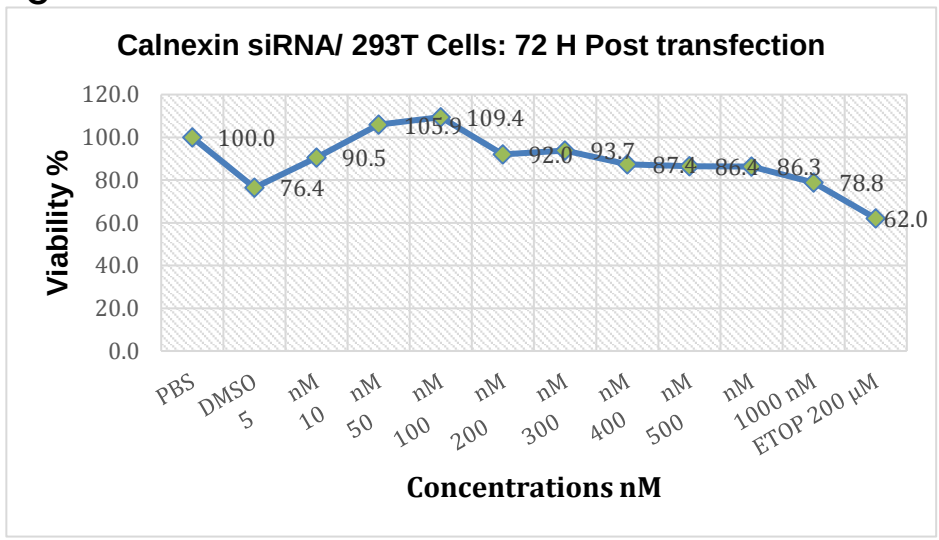
Calnexin siRNA/ 293T Cells: 72 H Post transfection
Viability %
120.0
100.0
80.0
60.0
40.0
20.0
0.0
100.0
76.4
90.5
105.9
109.4
92.0
93.7
87.4
86.4
86.3
78.8
62.0
PBS
DMSO 5
nM 10
nM 50
nM 100
nM 200
nM 300
nM 400
nM 500
nM 1000 nM
ETOP 200 μM
Concentrations nM

B

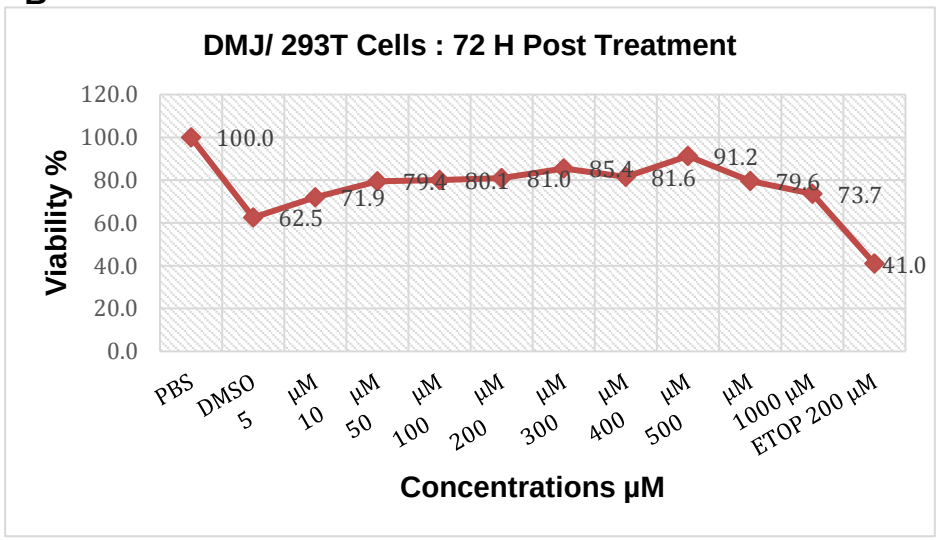
DMJ/ 293T Cells : 72 H Post Treatment
Viability %
120.0
100.0
80.0
60.0
40.0
20.0
0.0
100.0
62.5
71.9
79.4
80.1
81.0
85.4
81.6
91.2
79.6
73.7
41.0
PBS
DMSO 5
μM 10
μM 50
μM 100
μM 200
μM 300
μM 400
μM 500
μM 1000 μM
ETOP 200 μM
Concentrations μM

D

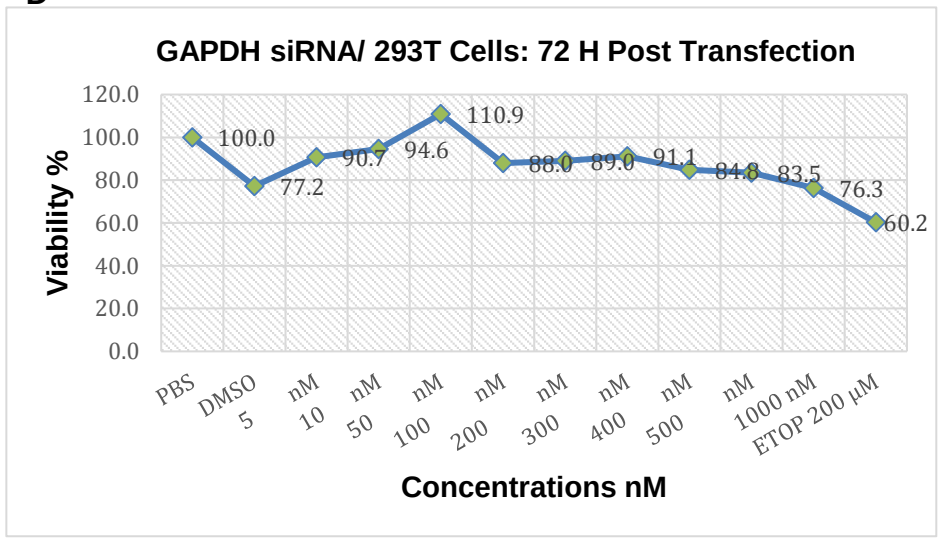
GAPDH siRNA/ 293T Cells: 72 H Post Transfection
Viability %
120.0
100.0
80.0
60.0
40.0
20.0
0.0
100.0
77.2
90.7
94.6
110.9
88.0
89.0
91.1
84.8
83.5
76.3
60.2
PBS
DMSO 5
nM 10
nM 50
nM 100
nM 200
nM 300
nM 400
nM 500
nM 1000 nM
ETOP 200 μM
Concentrations nM

E

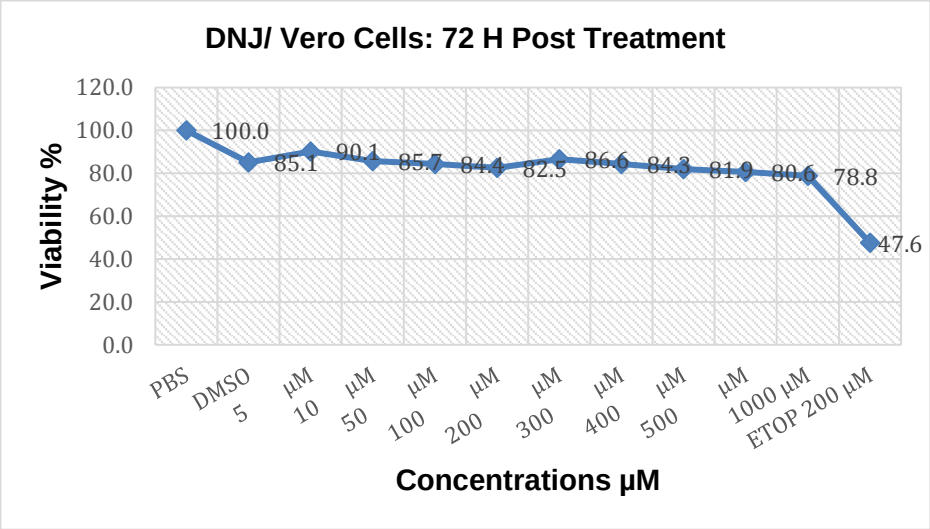
DNJ/ Vero Cells: 72 H Post Treatment
Viability %
120.0
100.0
80.0
60.0
40.0
20.0
0.0
100.0
85.1
90.1
85.7
84.4
82.5
86.6
84.3
81.9
80.6
78.8
47.6
PBS
DMSO 5
μM 10
μM 50
μM 100
μM 200
μM 300
μM 400
μM 500
μM 1000 μM
ETOP 200 μM
Concentrations μM

G

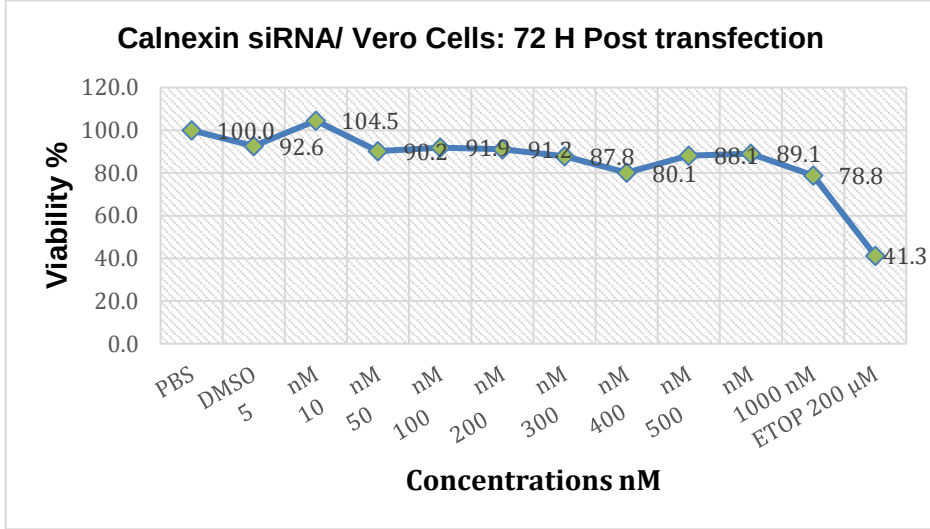
Calnexin siRNA/ Vero Cells: 72 H Post transfection
Viability %
120.0
100.0
80.0
60.0
40.0
20.0
0.0
100.0
92.6
104.5
90.2
91.9
91.2
87.8
80.1
88.1
89.1
78.8
41.3
PBS
DMSO 5
nM 10
nM 50
nM 100
nM 200
nM 300
nM 400
nM 500
nM 1000 nM
ETOP 200 μM
Concentrations nM

F

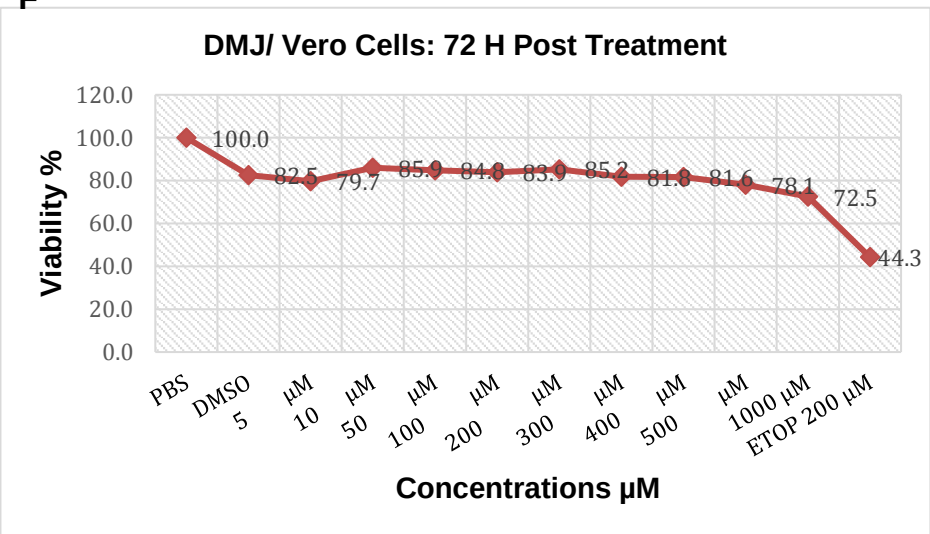
DMJ/ Vero Cells: 72 H Post Treatment
Viability %
120.0
100.0
80.0
60.0
40.0
20.0
0.0
100.0
82.5
79.7
85.9
84.8
83.9
85.2
81.8
81.6
78.1
72.5
44.3
PBS
DMSO 5
μM 10
μM 50
μM 100
μM 200
μM 300
μM 400
μM 500
μM 1000 μM
ETOP 200 μM
Concentrations μM

H

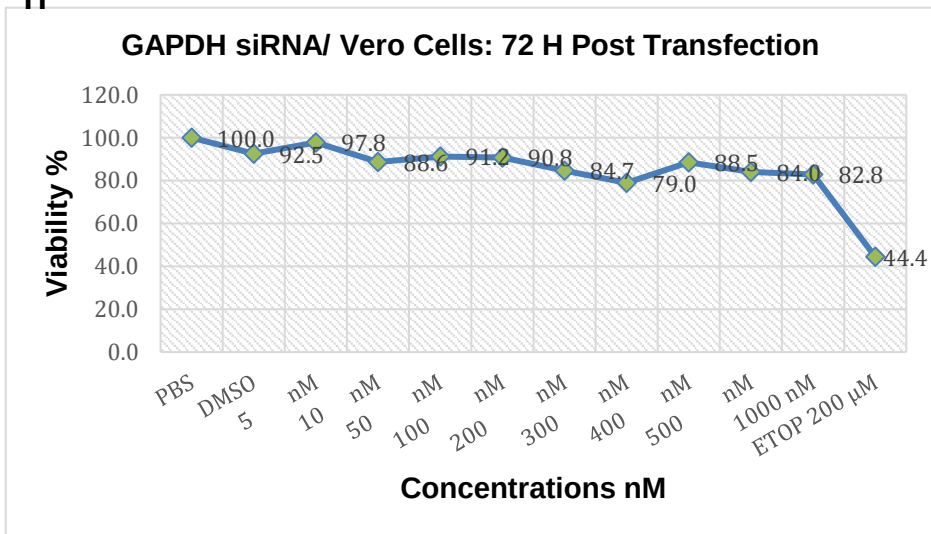
GAPDH siRNA/ Vero Cells: 72 H Post Transfection
Viability %
120.0
100.0
80.0
60.0
40.0
20.0
0.0
100.0
92.5
97.8
88.6
91.2
90.8
84.7
79.0
88.5
84.0
82.8
44.4
PBS
DMSO 5
nM 10
nM 50
nM 100
nM 200
nM 300
nM 400
nM 500
nM 1000 nM
ETOP 200 μM
Concentrations nM

Figure 5.1: Cell Viability (MTT) assay for iminosugars DNJ/DMJ small molecules treatments and siRNA transfections.

A-D: Viability assays for 293T cells, which were subjected to iminosugars treatments and siRNA transfections.

A and B: Viability percentage of 293T cells, which had prophylactic treatment of 24 hours by a series of concentrations of DNJ and DMJ (5-1000 μM) before MTT assay. C and D: Viability percentage of 293T cells, which had siRNA transfections by a series of concentrations of calnexin and GAPDH siRNAs (5-1000 nM) 24 hours before MTT assay. PBS, DMSO were put as negative controls and Etoposide was put as a high cytotoxic agent control.

E-H: Viability assays for Vero cells, which were subjected to iminosugars treatments and siRNA transfections.

E and F: Viability percentage of Vero cells, which had prophylactic treatment of 24 hours by a series of concentrations of DNJ and DMJ (5-1000 μM) before MTT assay. G and H: Viability percentage of 293T cells, which had siRNA transfections by a series of concentrations of calnexin and GAPDH siRNAs (5-1000 nM) 24 hours before MTT assay. PBS, DMSO were put as negative controls and Etoposide was put as a high cytotoxic agent control.

5.2.2 Impairment of N-linked Glycosylation modified the electrophoretic nature of S and M proteins but not the E Protein:

5.2.2.1 DNJ Treatment:

DNJ has α-glucosidase I and II inhibition activities and leads to impairment of an interaction between calnexin and nascent glycoproteins in the ER (Borges de Melo, *et al*., 2006; Zhao, *et al*., 2015). The final concentration of 100 µM DNJ was used for treatment of 293T cells 24 hours prior to transfection by each of EGFP-S, EGFP-M and EGFP-E plasmids separately. The outcomes were visualized by WB and different sized molecular weights of the targeted viral proteins were identified. The reason for these different molecular weight species is the increase in production of immature, fully glycosylated or unfolded glycoproteins as explained in (Chapter 4 Section 4.2.3.3). A duplicate of each of treated and untreated cells were transfected for the production of each of EGFP-S, EGFP-M and EGFP-E proteins and all the samples including EGFP control and mock transfected samples were visualized by WB for comparison analysis Figure 5.2 A-C. The results were analyzed by Image Lab version 5.2.1 build 11 software (Bio-Rad). Image Lab analyzed the band profiles for each of the lanes, then the profiles were compared to the controls. For EGFP-S and EGFP-M, the difference between treated and untreated proteins were significant by having obvious extra protein bands, which indicated the mass shift due to impairment in deglycosylation and generation of incomplete glycoproteins. However, for EGFP-E the mass shift was absent which might be due to the small size of the protein or no glycosylation Figure 5.3.

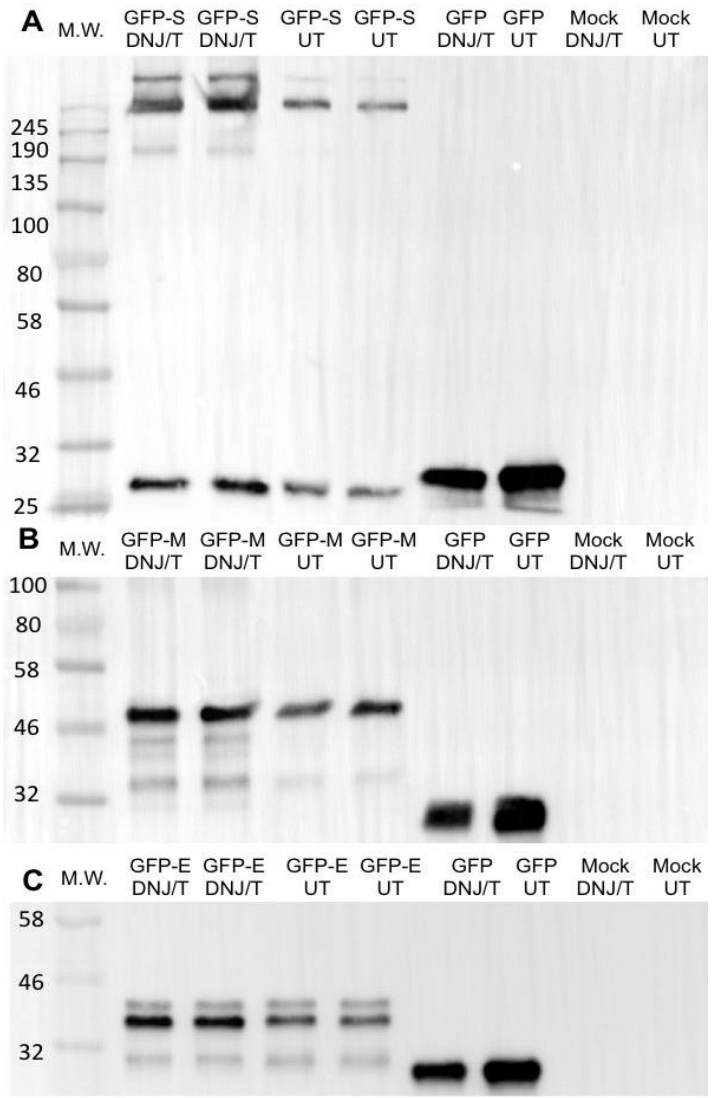

Figure 5.2 A-C: DNJ effects on EGFP-S, EGFP-M and EGFP-E proteins. Two duplicate samples of 293T cells were prepared; a duplicate was treated with DNJ and the other was left as a treatment control. Two more duplicates were used as EGFP and Mock transfection controls. M.W. lanes: Protein markers. A: DNJ treatment for EGFP-S transfected cells. Lanes GFP-S DNJ/T: A duplicate of DNJ-treated cells and transfected with EGFP-S plasmids. Lanes GFP-S UT: A duplicate of untreated cells and transfected with EGFP-S plasmids. Lane GFP DNJ/T: DNJ-treated cells which was transfected with EGFP plasmid (Vector Control). Lane GFP UT: Untreated cells, which was transfected with EGFP plasmid (Vector Control). Lane Mock DNJ/T: DNJ-treated and mock transfected for either EGFP-S or EGFP plasmids. Lane Mock UT: Untreated and mock-transfected control. B: DNJ treatment for EGFP-M transfected cells. Lanes are similar arrangements as for A but the transfection was by EGFP-M plasmid. C: DNJ treatment for EGFP-E transfected cells. Lanes are similar arrangements as for A but the transfection was by EGFP-E plasmid.

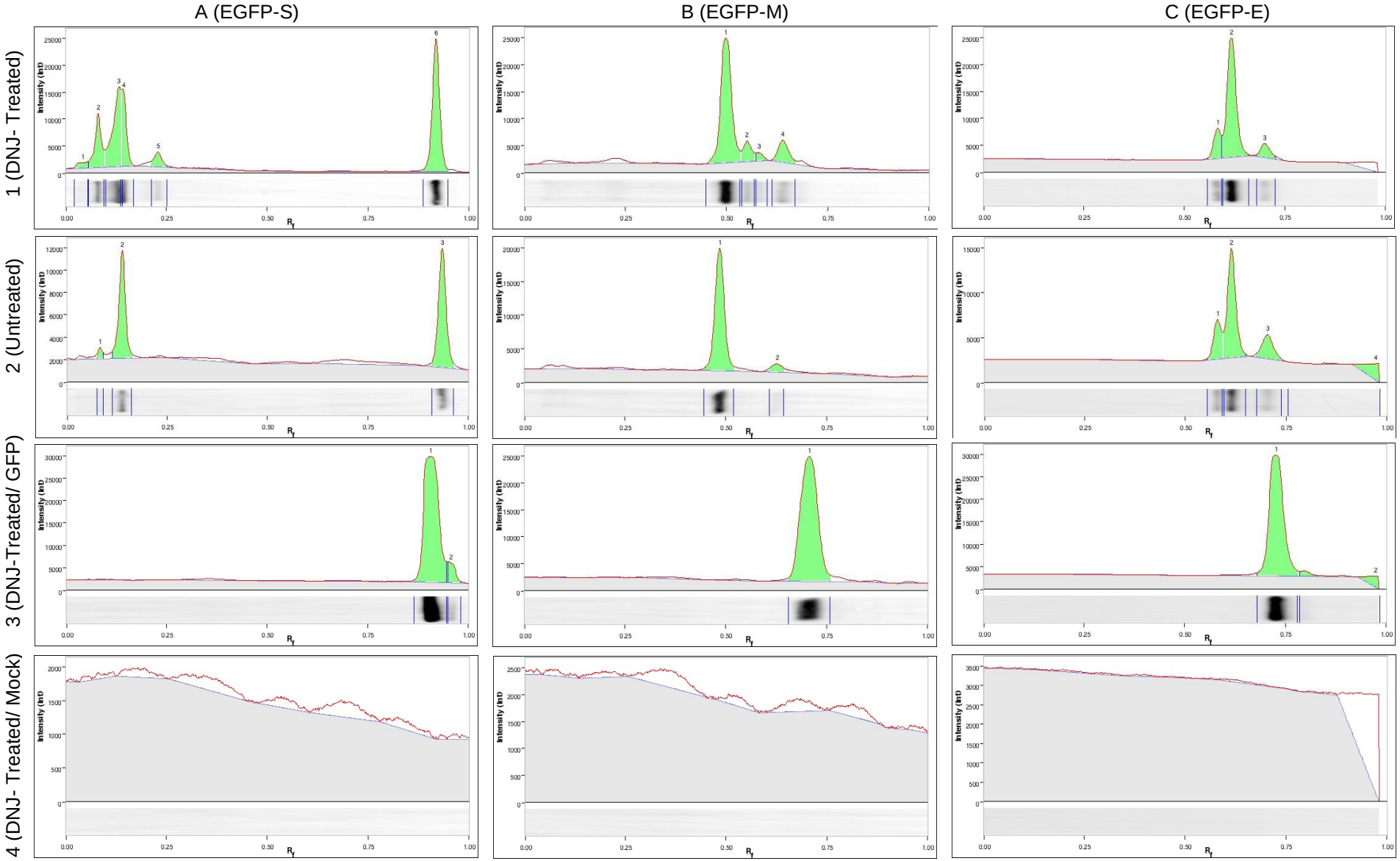
A (EGFP-S)
B (EGFP-M)
C (EGFP-E)
1 (DNJ- Treated)
2 (Untreated)
3 (DNJ-Treated/ GFP)
4 (DNJ- Treated/ Mock)
Intensity (Int)
Rf

Figure 5.3 A-C: Comparative analysis for DNJ effects on EGFP-S, EGFP-M and EGFP-E proteins. The WB images from Figure 5.2 A-C were analysed by Image Lab program for lane and band profiles per DNJ-treated, untreated, EGFP plasmid and mock-transfected controls. The columns A, B and C in the figure represent analysis of the samples per EGFP- tagged proteins and the rows 1-4 are treatment parameters. The main results of the DNJ-treated cells was having extra bands in the lane profile, which indicated the immature or unprocessed proteins due to glycosylation impairments in the ER.

A1: DNJ treatment for EGFP-S transfected cells. A2: Untreated cells were transfected with EGFP-S. A3: DNJ treatment for EGFP transfected cells as a control of the plasmid. A4: DNJ treatment for Mock transfected cells as a negative control.

B1: DNJ treatment for EGFP-M transfected cells. B2: Untreated cells were transfected with EGFP-M. B3: DNJ treatment for EGFP transfected cells as a control of the plasmid. B4: DNJ treatment for Mock transfected cells as a negative control.

C1: DNJ treatment for EGFP-M transfected cells (the lane profile didn't show any extra band, which may be due to the size of the protein). C2: Untreated cells were transfected with EGFP-M. C3: DNJ treatment for EGFP transfected cells as a control of the plasmid. C4: DNJ treatment for Mock transfected cells as a negative control.

Note: A sample profile report and more details of this figure are available in the Appendix 1.

5.2.2.2 DMJ Treatment:

Studies of the activity of DMJ as an α-mannosidase I and II inhibitor were understood for some viral glycoproteins especially influenza HA glycoprotein which lead to block the removal of the mannose residues, consequently the glycan group remained as $Man_8GlcNAc_2$, which cannot be further processed for complete maturation (Stanley, *et al*., 2015; Tyrrell, *et al*., 2017). As both DNJ and DMJ have the same molecular weight, the similar final concentration of 100 µM DMJ was used for treatment of 293T cells 24 hours prior to transfection by each of EGFP-S, EGFP-M and EGFP-E plasmids separately. The predicted effect of DMJ which was generation of different sized molecular weight of the targeted proteins was approached. This was based upon the inhibition of mannose trimming in the *cis* Golgi which facilitate the addition of other molecules such as galactose and sialic acid (Stanley, *et al*., 2015). A duplicate of each of the treated and untreated cells were transfected for the production of EGFP-S, EGFP-M and EGFP-E proteins and all the samples including EGFP control and mock transfected samples were optimized by WB for comparison analysis Figure 5.4 A-C. The results were analyzed by Image Lab version 5.2.1 build 11 software (Bio-Rad). Image Lab analyzed the band profiles for each of the lanes then the profiles were compared to the controls. For each of the three viral proteins, the results were as the case of DNJ in section 5.2.1.2, however the profiles of the bands were less significant than in DNJ treatment, which might be due the molecular weight of the glycan groups in the ER versus to Golgi Figure 5.5.

A sample profile report is available in the Appendix 2.

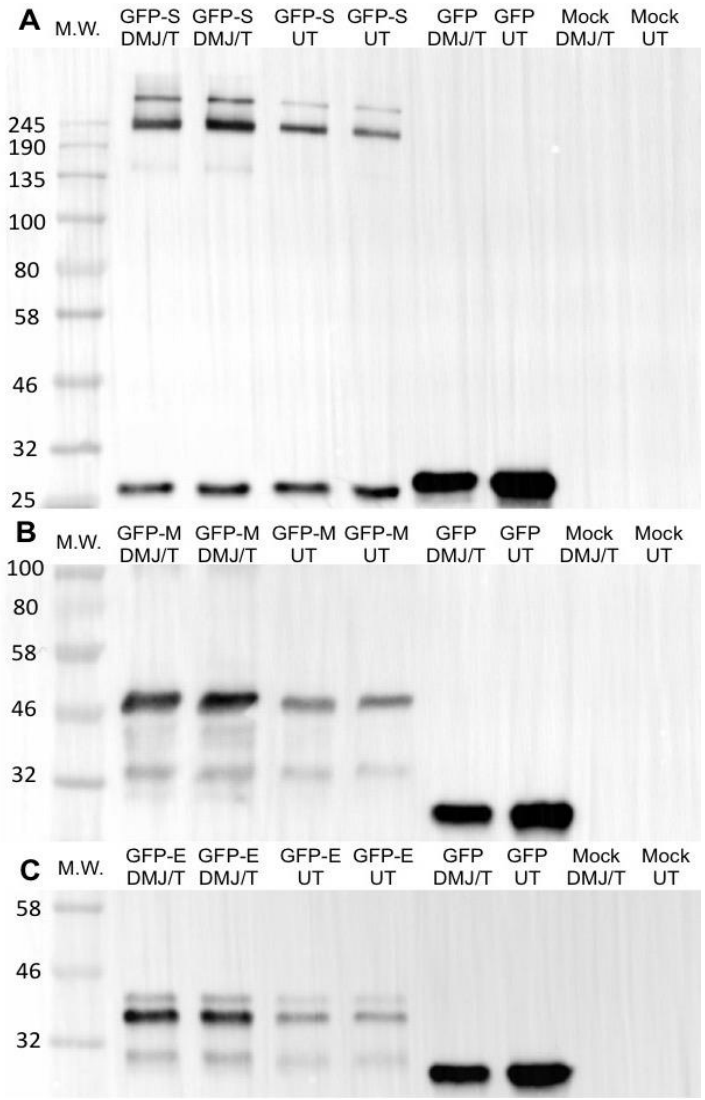

Figure 5.4: A-C: DMJ effects on EGFP-S, EGFP-M and EGFP-E proteins. Two duplicate samples of 293T cells were prepared; a duplicate was treated with DNJ and the other was left as a treatment control. Two more duplicates were used as EGFP and Mock transfection controls M.W. lanes: Protein markers. A: DMJ treatment for EGFP-S transfected cells. Lanes GFP-S DMJ/T: A duplicate of DMJ-treated cells and transfected with EGFP-S plasmids. Lanes GFP-S UT: A duplicate of untreated cells and transfected with EGFP-S plasmids. Lane GFP DMJ/T: DMJ-treated cells which was transfected with EGFP plasmid (Vector Control). Lane GFP UT: Untreated cells, which was transfected with EGFP plasmid (Vector Control). Lane Mock DMJ/T: DMJ-treated and mock transfected for either EGFP-S or EGFP plasmids. Lane Mock UT: Untreated and mock-transfected control. B: DMJ treatment for EGFP-M transfected cells. Lanes are similar arrangements as for A but the transfection was by EGFP-M plasmid. C: DMJ treatment for EGFP-E transfected cells. Lanes are similar arrangements as for A but the transfection was by EGFP-E plasmid.

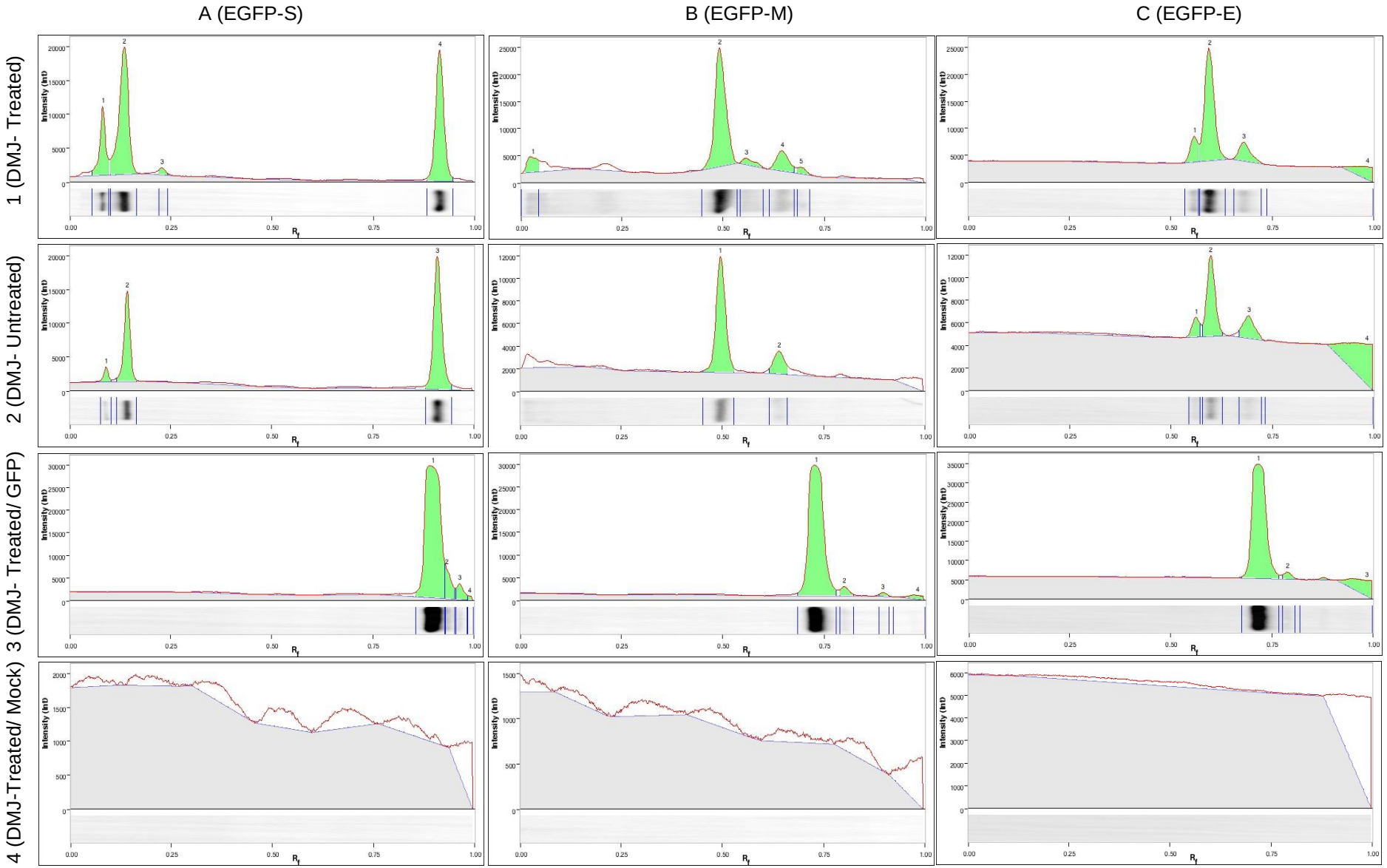
A (EGFP-S)
B (EGFP-M)
C (EGFP-E)
1 (DMJ- Treated)
2 (DMJ- Untreated)
3 (DMJ- Treated/ GFP)
4 (DMJ-Treated/ Mock)
Intensity (Int)
Rf

Figure 5.5 A-C: Comparative analysis for DMJ effects on EGFP-S, EGFP-M and EGFP-E proteins. The WB images from Figure 5.4 A-C were analysed by Image Lab program for lane and band profiles per DMJ-treated, untreated, EGFP plasmid and mock-transfected controls. The columns A, B and C in the figure represent analysis of the samples per EGFP- tagged proteins and the rows 1-4 are treatment parameters. The main results of the DMJ-treated cells was having extra bands in the lane profile, which indicated the immature or unprocessed proteins due to glycosylation impairments in the ER. However the bands were fainter than in the case of DNJ treatment Figure 5.3.

A1: DMJ treatment for EGFP-S transfected cells. A2: Untreated cells were transfected with EGFP-S. A3: DMJ treatment for EGFP transfected cells as a control of the plasmid. A4: DMJ treatment for Mock transfected cells as a negative control.

B1: DMJ treatment for EGFP-M transfected cells. B2: Untreated cells were transfected with EGFP-M. B3: DMJ treatment for EGFP transfected cells as a control of the plasmid. B4: DMJ treatment for Mock transfected cells as a negative control.

C1: DMJ treatment for EGFP-M transfected cells (the lane profile didn't show any extra band, which may be due to the size of the protein). C2: Untreated cells were transfected with EGFP-M. C3: DMJ treatment for EGFP transfected cells as a control of the plasmid. C4: DMJ treatment for Mock transfected cells as a negative control.

Note: A sample profile report and more details of this figure are available in the Appendix 2.

5.2.3 Impairment of N-linked Glycosylation decline the virus Infectivity:

IBV BeauUS strain was propagated in Vero cells and the supernatants from 90% CPE cells were filtered for titration by plaque assays. The final titration of ($2.5x10^6$ PFU/ml) from the filtered virus supernatant was obtained for the study of small molecules responses and inhibition analysis.

5.2.3.1 Iminosugars and Calnexin siRNA Transfection Treatments:

As the effects of the small molecule iminosugars and calnexin siRNA was confirmed for the S, M and E proteins in the previous sections, for identifying such effects in the virus infection an antiviral approach in cell culture was conducted. Vero cells were seeded in 24 well plates and a duplicate per each of treatment were specified Figure 5.6. A duplicate of rows (A and B) were treated prophylactically with iminosugars and siRNA combination 24 hours prior to the virus infection at MOI 0.1. The other duplicate rows (C and D) in the 24 well plate was used for the iminosugars only in the similar 24 hours prophylactic treatment before viral infection at MOI 0.1 as well. The treatment parameters were used per each column from 1-6 as represented in the Figure 5.6. The reason for the treatment parameters and combinations was approached according to the model of glycosylation inhibition in chapter four. After adsorption of the virus, which was held for 1 hour, the plates were incubated up to 48 and 72 hours post treatment (PT) timelines. The virus supernatants were collected and the results were optimized both in quantitative and qualitative methods using TCID50 and WB of the virus supernatants respectively.

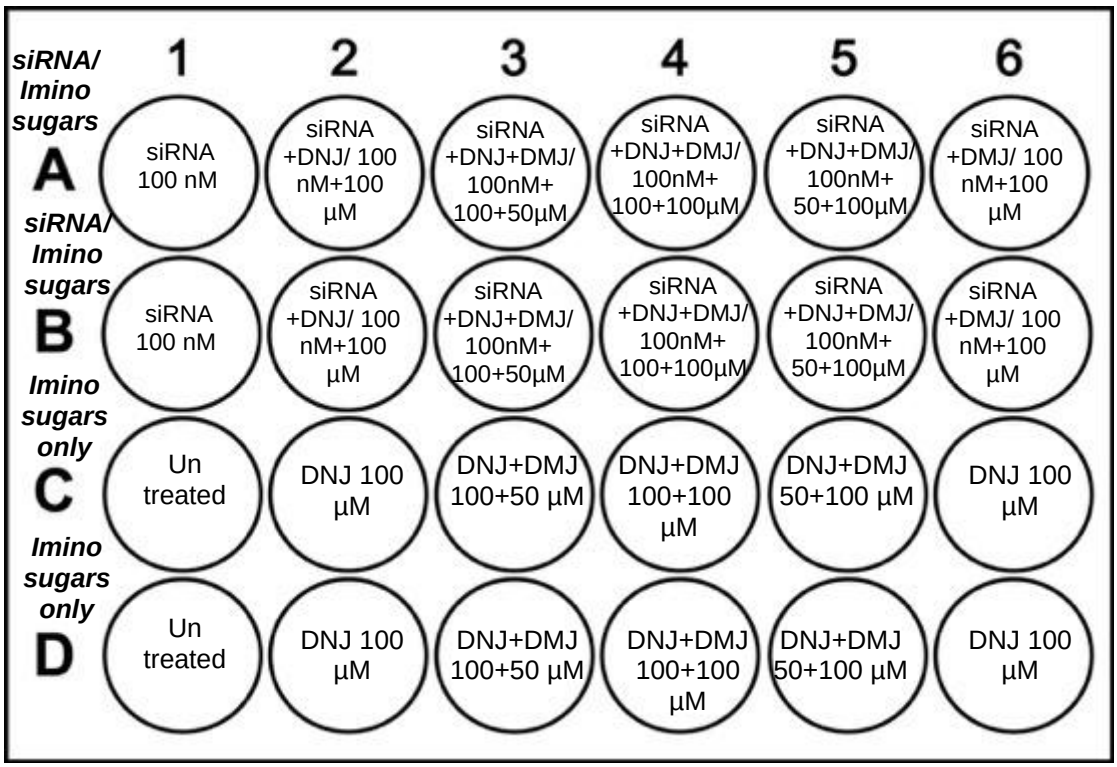

Figure 5.6: Iminosugars and siRNA Transfection treatment plan for IBV in Vero cells.

Row A and B: Calnexin siRNA transfection and iminosugars combination treatment in various concentrations of the molecules as shown per each well. Well 1: siRNA 100 nM. Well 2: siRNA 100 nM+ DNJ 100 µM. Well 3: siRNA 100 nM+ DNJ 100 µM+ DMJ 50 µM. Well 4: siRNA 100 nM+ DNJ 100 µM+ DMJ 100 µM. Well 5: siRNA 100 nM+ DNJ 50 µM+ DMJ 50 µM. Well 6: siRNA 100 nM+ DMJ 100 µM.

Row C and D: iminosugars only treatment in various concentrations of the molecules as shown per each well. Well 1: Untreated. Well 2: DNJ 100 µM. Well 3: DNJ 100 µM+ DMJ 50 µM. Well 4: DNJ 100 µM+ DMJ 100 µM. Well 5DNJ 50 µM+ DMJ 50 µM. Well 6: DMJ 100 µM.

5.2.3.2 Quantitative Treatment Response Analysis:

To study the infectivity of the treated virus supernatants and compare it with that from untreated cells, the CPE of the virus from treated and untreated cells were quantified in TCID50/ml. The calculation for both combination treatments was carried out according to the Spearman and Kaerber algorithm as described by (Hierholzer & Killington, 1996) and the Mean values per each parameter were obtained for statistical analysis (Table 5.1).

Table 5.1: *Virus quantification (TCID50/ml) for iminosugars and calnexin siRNA treatments 24 hours prior to IBV infection at MOI 0.1. The value represent calculation of Mean of a duplicate wells per each of treated and untreated cells according to the treatment parameters of iminosugars and/or calnexin siRNA combinations. Virus titers were collected at 48 and 72 hours PT.*

Treatment Parameters	TCID50/ml 48 H PT	TCID50/ml 72 H PT
Un Treated	1,260,000	3,160,000,000
DNJ 100 µM	66,970	39,800,000
DNJ 100 µM+DMJ 50 µM	31,350	37,900,000
DNJ 100 µM+DMJ 100 µM	23,055	30,100,000
DNJ 50 µM+DMJ 100 µM	330,050	89,000,000
DMJ 100 µM	897,000	324,500,000
CANX siRNA 200nM	514,500	2,580,000,000
CANX siRNA 200nM+DNJ 100 µM	42,855	3,980,000
CANX siRNA 200nM+DNJ 100µM+DMJ 50µM	19,770	1,420,000
CANX siRNA 200nM+DNJ 100µM+DMJ 100 µM	6,930	1,290,000
CANX siRNA 200nM+DNJ 50 µM+DMJ 100 µM	68,000	238,700,000
CANX siRNA 200nM+DMJ 100 µM	47,350	251,000,000

The TCID50 results, which were obtained from untreated (control) and treated cells showed variable values in both 48 and 72 hours PT timelines. To visualize the difference between all parameters per each timeline, the data values were summarized in plotted bars by GraphPad Prism 7. Obviously the treatment response showed differences between untreated controls and treated cells and the difference occurred between various treatment parameters as well Figure 5.7 A and B.

To characterise the significance of the treatment response, the datasets for both 48 and 72 hours PT were analysed by Ordinary One-way ANOVA as a built-in analysis method in GraphPad Prism 7. In brief, the data table for all 12 parameters (a duplex per each), which was built for data plots, was designed as non-matched values for ANOVA analysis. The Dunnett's test, which is multiple comparison procedure to compare each of a number of treatments with a single control (Dunnett, 1955), was then selected for comparing the control Mean of untreated sample with each of treated sample Means to compute confidence intervals and multiplicity adjusted *P* values.

The ANOVA summary outcome for both 48 and 72 H PT were obtained as significant difference among the Means by *P* value <0.0001 and <0.0005 subsequently. The F ratio, which is the ratio of two mean square values and as far as the null hypothesis is true, the F ratio is closer to 1, however in both datasets the F ratios for 48 H PT was 16.13 and 72 H PT, was 8.347, which confirmed that the null hypothesis for the treated sample Means was false and the treatment combinations were effective statistically.

A

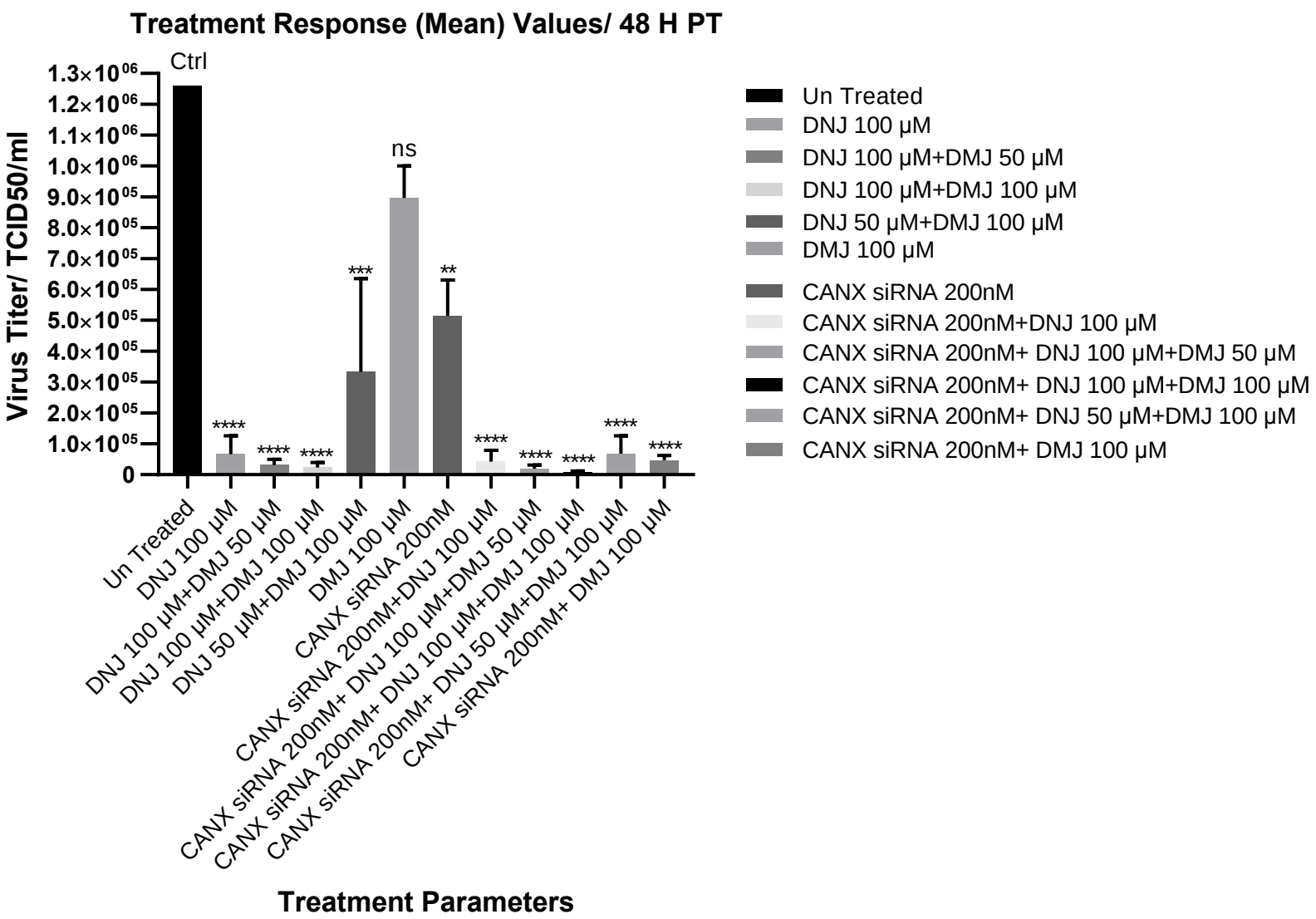
Treatment Response (Mean) Values/ 48 H PT
Virus Titer/ TCID50/ml
1.3×10^06
1.2×10^06
1.1×10^06
1.0×10^06
9.0×10^05
8.0×10^05
7.0×10^05
6.0×10^05
5.0×10^05
4.0×10^05
3.0×10^05
2.0×10^05
1.0×10^05
0
Ctrl
ns
***
**
****
Un Treated
DNJ 100 µM
DNJ 100 µM+DMJ 50 µM
DNJ 100 µM+DMJ 100 µM
DNJ 50 µM+DMJ 100 µM
DMJ 100 µM
CANX siRNA 200nM
CANX siRNA 200nM+DNJ 100 µM
CANX siRNA 200nM+ DNJ 100 µM+DMJ 50 µM
CANX siRNA 200nM+ DNJ 100 µM+DMJ 100 µM
CANX siRNA 200nM+ DNJ 50 µM+DMJ 100 µM
CANX siRNA 200nM+ DMJ 100 µM
Treatment Parameters

B

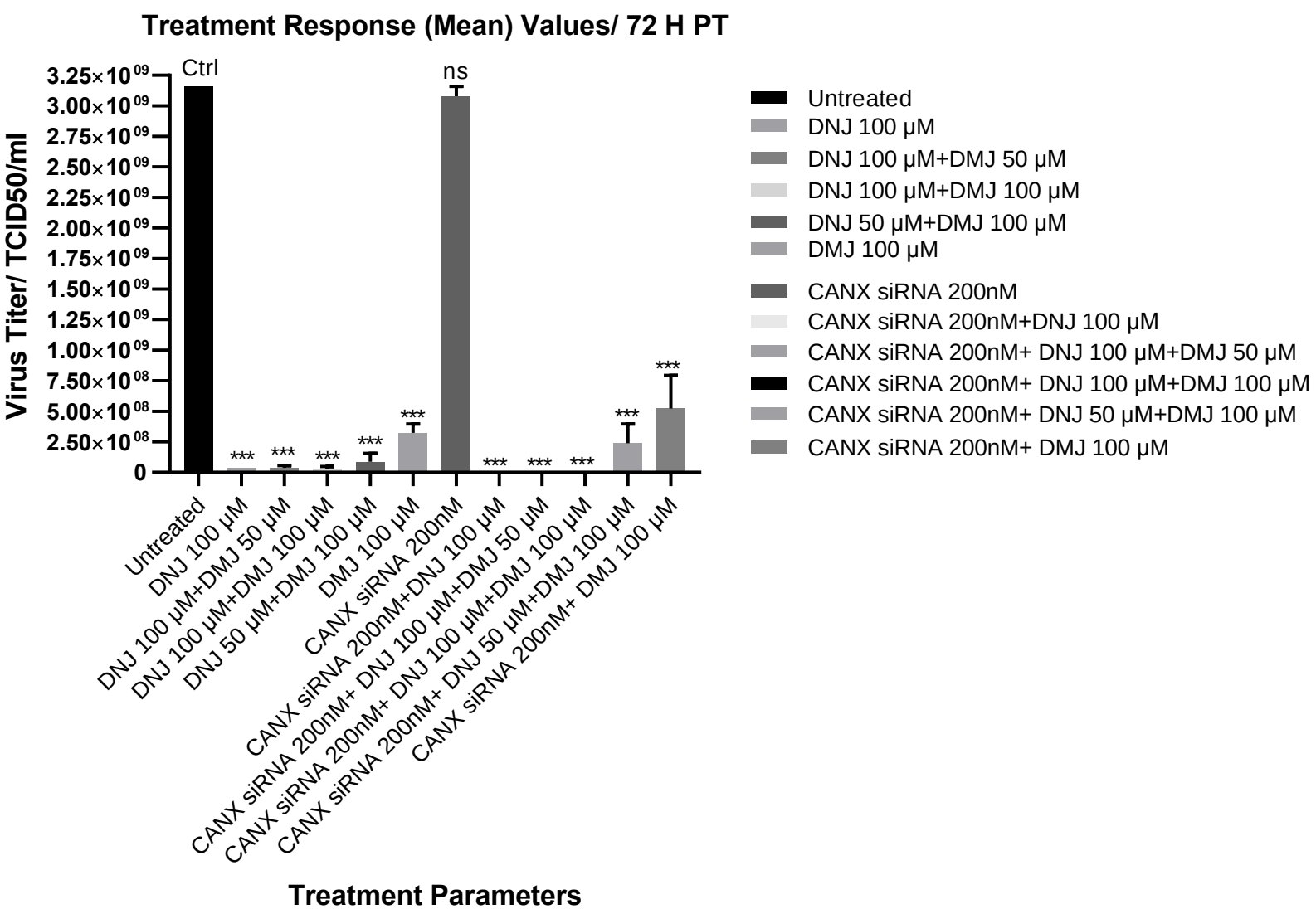
Treatment Response (Mean) Values/ 72 H PT
Virus Titer/ TCID50/ml
3.25×10 09
3.00×10 09
2.75×10 09
2.50×10 09
2.25×10 09
2.00×10 09
1.75×10 09
1.50×10 09
1.25×10 09
1.00×10 09
7.50×10 08
5.00×10 08
2.50×10 08
0
Ctrl
ns
***
Untreated
DNJ 100 µM
DNJ 100 µM+DMJ 50 µM
DNJ 100 µM+DMJ 100 µM
DNJ 50 µM+DMJ 100 µM
DMJ 100 µM
CANX siRNA 200nM
CANX siRNA 200nM+DNJ 100 µM
CANX siRNA 200nM+ DNJ 100 µM+DMJ 50 µM
CANX siRNA 200nM+ DNJ 100 µM+DMJ 100 µM
CANX siRNA 200nM+ DNJ 50 µM+DMJ 100 µM
CANX siRNA 200nM+ DMJ 100 µM
Treatment Parameters

Figure 5.7: Virus quantifications (TCID50/ml) in response to DNJ, DMJ and/or calnexin siRNA transfection treatment combinations 24 H prior to IBV infection (MOI 0.1) in Vero cell.

Basically untreated control response was plotted against the final concentration treatment of DNJ 100 µM, DNJ 100 µM+ DMJ 50 µM, DNJ 100 µM+ DMJ 100 µM, DNJ 50 µM+ DMJ 50 µM, DMJ 100 µM, calnexin siRNA 100 nM, calnexin siRNA 100 nM+ DNJ 100 µM, calnexin siRNA 100 nM+ DNJ 100 µM+ DMJ 50 µM, calnexin siRNA 100 nM+ DNJ 100 µM+ DMJ 100 µM, calnexin siRNA 100 nM+ DNJ 50 µM+ DMJ 50 µM and calnexin siRNA 100 nM+ DMJ 100 µM.

A: Quantified TCID50/ml plots for 48 H PT. It is obvious that all the treatment parameters that contain DNJ were more effective in declining the infectivity of the virus, however the DMJ and calnexin siRNA knockdown alone, were less effective as compared to DNJ.

B: Quantified TCID50/ml plots for 72 H PT. It is similar to A that all the treatment parameters that contain DNJ were more effective in declining the infectivity of the virus.

As the significance of each treatment parameter was necessary for analysing its effect on the virus, the comparison of the untreated (control) mean to each of other single treatment parameters was implemented for the same data table in One-way ANOVA analysis. The Dunnett's test was selected in One-way ANOVA for multiple comparison of untreated TCID50/ml value as the control to the values per each of the other treatment parameters. As a result the significant differences between the treated means and the control were obtained both in numeric values as a mean Difference and the *P* values as well Table 5.2.

Clearly, all the treated parameters, which contain DNJ in both 48 and 72 H PT timelines, showed highly significant mean difference and lowest *P* values in the analysis. Both DMJ and calnexin siRNA transfection treatment showed either non-significance or unconfident results per timelines; so overall they are less effective than DNJ alone. However the highest mean differences were obtained for combination treatments of DNJ and DMJ with higher drug concentrations. In addition and top of all, the (CANX siRNA 200nM + DNJ 100µM + DMJ 100µM) showed maximum mean difference as compared to untreated control and this result was compatible with the model which was designed for N-linked glycosylation pathway starting in the ER and ending in the Golgi for completely processed and mature glycoproteins.

Table 5.2: *Multiple comparison of untreated mean versus each mean of treated parameters using Dunnett's test.*

Dunnett's Multiple Comparisons Test	48 H PT				72 H PT			
Untreated Control versus to:	**Mean Diff.**	**Significance**	**Summary**	***P* Value**	**Mean Diff.**	**Significance**	**Summary**	***P* Value**
DNJ 100 µM	1193030	Yes	****	0.0001	3120200000	Yes	***	0.0003
DNJ 100 µM+DMJ 50 µM	1228650	Yes	****	0.0001	3122100000	Yes	***	0.0003
DNJ 100 µM+DMJ 100 µM	1236945	Yes	****	0.0001	3129950000	Yes	***	0.0003
DNJ 50 µM+DMJ 100 µM	929950	Yes	***	0.0003	3071000000	Yes	***	0.0003
DMJ 100 µM	363000	No	ns	0.165	2835500000	Yes	***	0.0007
CANX siRNA 200Nm	745500	Yes	**	0.002	1182500000	No	ns	0.1879
CANX siRNA 200nM+ DNJ 100 µM	1217145	Yes	****	0.0001	3156020000	Yes	***	0.0003
CANX siRNA 200nM+ DNJ 100 µM+ DMJ 50 µM	1240230	Yes	****	0.0001	3158580000	Yes	***	0.0003
CANX siRNA 200nM+ DNJ 100 µM+ DMJ 100 µM	1253070	Yes	****	0.0001	3158710000	Yes	***	0.0003
CANX siRNA 200nM+ DNJ 50 µM+ DMJ100 µM	1192000	Yes	****	0.0001	2921300000	Yes	***	0.0005
CANX siRNA 200nM+ DMJ 100 µM	1212650	Yes	****	0.0001	2909000000	Yes	***	0.0006

5.2.3.3 Qualitative Treatment Response Analysis:

For visualizing the effects of the iminosugars and calnexin siRNA transfection responses either alone or in the specific combinations, equal volumes from the treated and untreated virus supernatants were analysed by WB using polyclonal anti-IBV antibodies Figure 5.8. The results for both 48 and 72 H PT were comparable to the quantitative TCID50 assays in which the treatment combinations included DNJ showed less virus titer in the treated supernatants as compared to untreated sample.

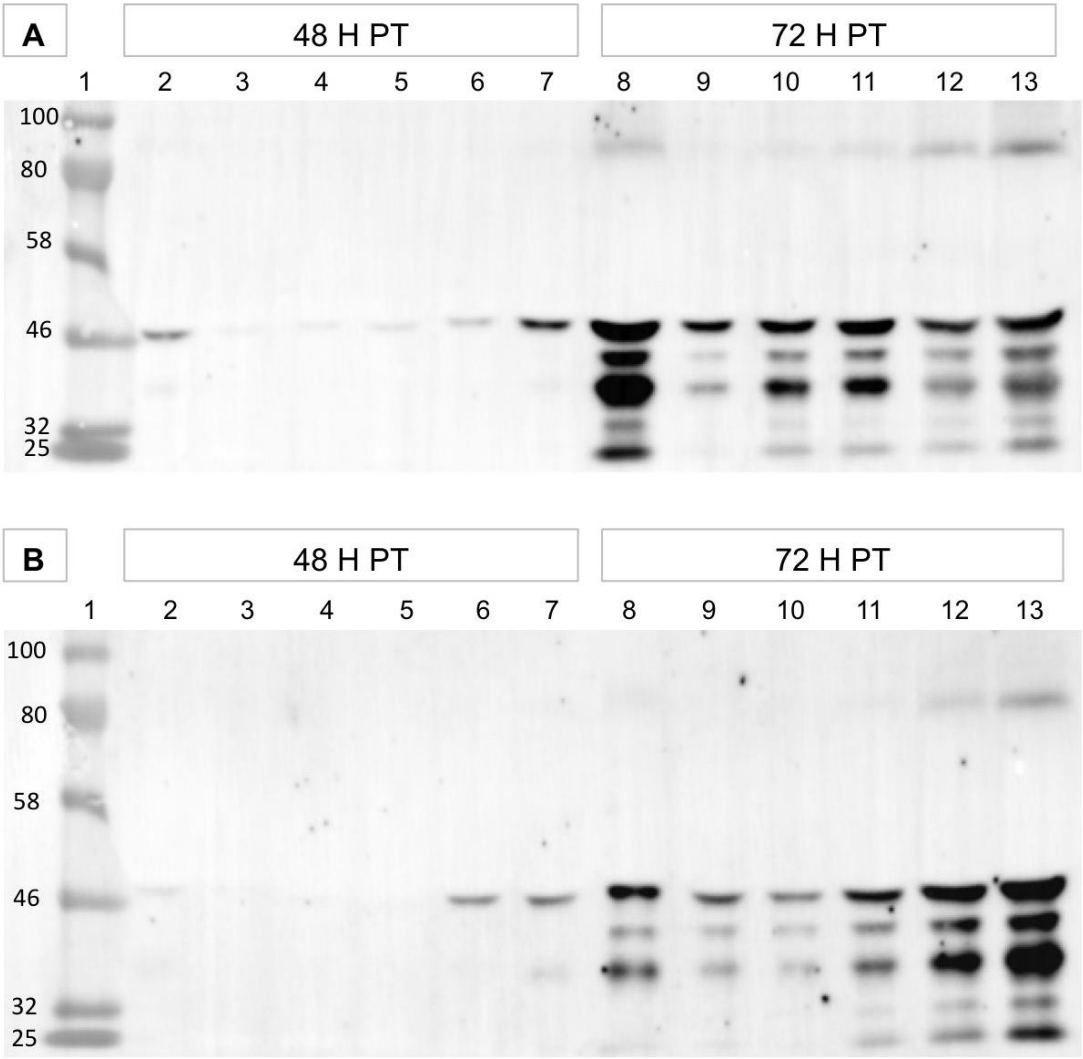

Figure 5.8. Virus detection in response to DNJ, DMJ and/or calnexin siRNA transfection treatment combinations 24 H prior to IBV infection (MOI 0.1) in Vero cell. A: Anti-IBV antibody incubation for the 48 and 72 H PT drug treatment parameters. Lane 1: Protein marker. Lane 2-7: Untreated, DNJ 100 µM, DNJ 100 µM+ DMJ 50 µM, DNJ 100 µM+ DMJ 100 µM, DNJ 50 µM+ DMJ 50 µM and DMJ 100 µM for 48 H PT. Lane 8-13: similar loading as Lane 2-7 but for 72 H PT. B: Anti-IBV antibody incubation for the 48 and 72 H PT drug and calnexin siRNA treatment parameters. Lane 1: Protein marker. Lane 2-7: calnexin siRNA 100 nM, calnexin siRNA 100 nM+ DNJ 100 µM, calnexin siRNA 100 nM+ DNJ 100 µM+ DMJ 50 µM, calnexin siRNA 100 nM+ DNJ 100 µM+ DMJ 100 µM, calnexin siRNA 100 nM+ DNJ 50 µM+ DMJ 50 µM and calnexin siRNA 100 nM+ DMJ 100 µM for 48 H PT. Lane 8-13: similar loading as Lane 2-7 but for 72 H PT.

5.2.4 Direct Virus De-glycosylation Assay:

Due to the results in response to N-linked glycosylation inhibition both per singular proteins in 293T cell transfections and virus infections in Vero cells, the hypothesis of direct deglycosylation for the virions was generated. Basically the enzymatic deglycosylation of S protein by PNGase F enzyme produced a mass shift of the protein for about 45-50 kDa in the previous chapter, so technically the globular part of the S protein, which exposes outward from the envelope of mature IBV virion, was more susceptible to enzymatic removal of the glycan group from the virion. Equal amounts of the virus supernatants were incubated in buffers containing final concentrations of 5U, 10U and Mock PNGase F enzyme for 3 hours at 37°C and the virus infectivity was then tested by TCID50 assay. The TCID50/ml was quantified according to Spearman and Kaerber method. The results showed significant

difference between the mock treated viruses with PNGase F treated viruses in two different concentrations 10U and 5U of the enzyme. In 10U concentration the virus became 100% non-infective as no well in the TCID50 plate had CPE of the virus and in 5U treatment only one well over five had CPE, which resulted. However, the mock treated viruses had CPE in 8 wells over three rows in the plate. The results were in the high variance so they were plotted in to log10 values Figure 5.9. The sample number was small, however the results were analysed by One-way ANOVA and Brown-Forsythe test in which the *P* value <0.0001 was obtained indicating the significant difference between PNGase F treated and PNGase F mock treated viruses.

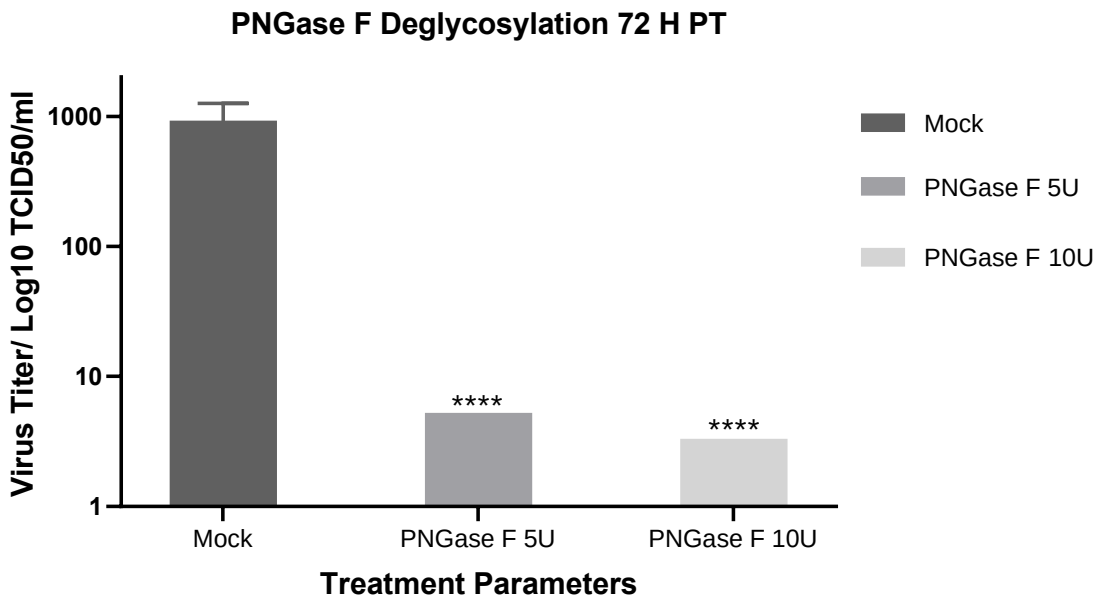

Figure 5.9: Virus quantifications (TCID50/ml) in response to 5U, 10U and Mock PNGase F treatment for IBV in Vero cell. The Mock PNGase F treated virus (control) response was plotted against the final concentration treatment of 5U and 10U respectively. The main result was the significant difference in TCID50/ml between PNGase F treated and untreated samples.

5.3 Discussion:

In this chapter, the N-glycosylation impairment approaches using iminosugars treatments, confirmed the results of IBV glycoproteins processing in the host cells, which were obtained in the previous chapters. The treatment responses were achieved from either the processing of single protein per each of S, M and E glycoproteins or the whole virus infections. The approach of using the iminosugars was based on the enzyme targeting mechanisms of N-linked glycosylation in the ER and Golgi complexes and more specifically focusing on the inhibition of calnexin interaction with the viral glycoproteins. This interaction was studied well in SARS coronavirus (Fukushi, *et al*., 2012), AIV (Tatu & Helenius, 1997), Dengue virus (Limjindaporn, *et al*., 2009), VSV (Hammond & Helenius, 1994) and Rabies virus (Gaudin, 1997). Meanwhile, the iminosugars small molecules were mainly used as an antiviral approach in such studies. However, for IBV, neither the direct interaction between calnexin and the glycoproteins nor the usage of iminosugars as an antiviral treatment was approached.

In this study, the approach of using the iminosugars against IBV was specifically designed according to the characteristics of the virus infection and targeting the assembled progeny of the virions from infected cells. DNJ targeted and inhibited α-glucosidase I and II, which are involved in pre and post calnexin interaction with the viral glycoprotein in the ER (McLaughlin & Vandenbroeck, 2011) and furthermore, the calnexin itself was targeted by siRNA knockdown to shutdown the complete system of calnexin pathway in the ER. DMJ targeted α-mannosidase I and II, which are involved in

mannose trimming process for preparing the upcoming glycoprotein from the ER to produce the hybrid intermediate molecule in *cis* Golgi (Balzarini, 2007). Consequently, both cellular machinery organelles for N-linked glycoprotein processing were targeted and the infectivity of the virus was defeated.

The molecular mechanism of impairing the glycosylation pathway by DNJ, DMJ and calnexin knockdown, led to the sequential impact on processing of the viral proteins. Starting from the ER, after the introduction of the nascent viral glycoproteins from the translocon and adding of the glycan group ($Glc_3Man_9GlcNAc_2$-N) by OST, the subsequent removal of glucose molecules by α-glucosidase I and II were inhibited. Consequently, the mono glucose signals in the glycan group ($Glc_1Man_9GlcNAc_2$-N) did not appear to interact with calnexin for folding process and as a result, molecules with different molecular weight were generated, hence, the detection of various sized molecules was confirmed by WB when the 293T cells were treated with small molecules 24 hours before vector transfections. Additionally, in the small molecules and siRNA combination treatment, the calnexin became silent and in turn the glycoprotein folding process was impaired as well. However, in case of any escape from the previous steps, the last glucose molecule removal in the (calnexin-$Glc_1Man_9GlcNAc_2$-N) intermediate by α-glucosidase II was impaired as well and the viral glycoproteins were retained in the interactive intermediate, which were not completely folded. On the other hand, if for any reason, the viral glycoproteins passed their N-linked glycosylation and maturely-folded $Man_9GlcNAc_2$-N were translocated from the ER to the *cis* Golgi, the α-mannosidase I and II were inhibited by DMJ

and the mannose trimming process was inhibited as well. This resulted in subsequent lack of hybrid and complex intermediates of the viral glycoproteins, on which the sialic acid molecules were not added as a final step before the virions assembly.

In IBV, the major biological impact of glycosylation impairment model is dependant upon S glycoprotein. The results in this study for recombinant S glycoprotein showed more susceptibility of S to either PNGase F enzyme or iminosugars DNJ and DMJ as compared to M and E proteins. The S glycoprotein is the most prominent epitope on the envelope and it is main determinant of IBV tropism to the host tissues (Wickramasinghe, *et al*., 2011). More importantly, the sequence of S gene contain the receptor binding domain (RBD) in its N terminal 253 amino acids, which is required for binding to α-2, 3-sialic acid receptors on the host cells, especially the residues from 19-69 that overlap the hypervariable region on S1, which have critical role in the attachment process (Promkuntod, *et al*., 2014). Moreover, Sialic acid molecules bound to glycan groups on S glycoproteins have important role on the affinity of attachment with the sialic acid receptors on the host cells. Studying the histochemistry of IBV M41 S1 glycoprotein using novel avian tissue microarrays (TMAs) confirmed the preference of S1 glycoprotein to sialic acids type I lactosamine ($Gal_{1-3}GlcNAc$) over type II ($Gal_{1-4}GlcNAc$), however the fine glycan specificities of pigeon and partridge CoVs were different, as chicken CoV S1-specific sialylglycopolymers could not block their binding to tissues (Wickramasinghe, *et al*., 2015). This indicated the sensitivity of tissue and host tropism according to the

histochemistry of sialic acid molecules. Taken together, the infectivity of the virus is significantly affected by the change in the chemistry of the molecules attached to the glycan groups during N-linked glycosylation in the ERGIC complex, which finally affect the receptors recognitions and attachment mechanism by sialic acids when assembled inappropriately.

Iminosugar small molecules are naturally occurring carbohydrate mimics that inhibit carbohydrate catalytic enzymes. Structurally, they are low molecular weight sugar analogues, where an oxygen atom has been replaced by nitrogen atom (Horne, *et al*., 2011). DNJ and DMJ are monocyclic iminosugars and they are 1-deoxy analogues of nojirimycin. Nojirimycin which was initially found as a bio product of Streptomyces fermentation (Ishida, *et al*., 1967) however it was naturally unstable in neutral and acidic status and its biopotency was rapidly declined at room temperature, so several synthetic forms were designed as well (Iida, *et al*., 1987; Inouye, *et al*., 1968). 1-deoxynojirimycin (DNJ), is one of the stable forms that naturally occurring iminosugars found in mulberry plants, Streptomyces, Bacillus spp. Interestingly, the DNJ biosynthetic genes were identified in *Bacillus subtilis* MORI 3K-85 strain and even the genes were subcloned in to *Escherichia coli* (Kang, *et al*., 2011). Strikingly, the production was improved by metabolic engineering, which used a recombinant *E. coli* and in the combination of using fructose-6-phosphate as a precursor and specific media condition, the highest production of 1-DNJ was obtained (Rayamajhi, *et al*., 2018). DMJ as well, either naturally occurred and isolated from *Lonchcarpus spp*. plant or even synthesized chemically (Fleet, *et al*., 1987, 1989). In this study, the cell

viability assays showed a high survival rate of the cells under low to high concentrations of DNJ and DMJ, which indicated the possibility to use such small molecules in the treatment approach. The most recent fact about the safety of 1-DNJ in vivo use, was studied as well and the evaluation of oral administration suggested safety of DNJ (Takasu, *et al*., 2018). Consequently, the availability and safety of iminosugars are supportive in their practical implications. Decline of the virus infectivity in most of the treatment parameters that were used in this study, confirmed the importance of N-linked glycosylation by cellular machinery during virus replication cycle and even hypothesizing the possibility of solitary role of the N-linked glycan groups in the attachment and infection as well. Direct deglycosylation trial for the mature virions in the filtered supernatant was confirmed the unique involvement of the glycan molecules on the epitopes of the viral envelope, which were mainly presented on the globular part of S glycoprotein. In regards to the results in this chapter, a glycosylation impairment model was proposed as a significant method for declining the infectivity of the IBV. The mechanism of the model was proposed as follow:

5.3.1 Glycosylation impairment model:

The enzymatic processing of glycan molecules were targeted for impairing the glycosylation pathway in both the ER and Golgi. In the ER, α-Glucosidase I and II were targeted and inhibited by DNJ and in Golgi, α-Mannosidase I and II were targeted and inhibited by DMJ. The approach of using DNJ and DMJ combination was to overcome the cellular processing of the virus and in turn produce non-infective virus release.

5.3.2 The Model In the ER:

In the translocon of the ER and after the S, M and E mRNAs were translated to the peptides, the N-linked glycogroups, which has three glucose molecules, were added by OST. DNJ treatments inhibited α-Glucosidase I from trimming the far most two glucose molecules in the end of the glycogroup. The trimming inhibition resulted in the absence of single glucose, which acts as the signal for introduction in to the calnexin pathway, and as a result, the folding of the glycoproteins were inhibited as well. However any molecules passed the inhibition and became folded had to trim the last glucose molecule so as to release from the calnexin/calreticulin complex. This process usually aids by α-Glucosidase II, which can be inhibited by DNJ as well. Consequently, all the unfolded and incomplete glycoproteins were transitioned in to the ERQC by GT enzyme and the mature one were significantly declined to translocate to *cis* Golgi Figure 5.10 A.

5.3.3 The Model In the Golgi:

In the Golgi, the completed glycoproteins from the ER have nine mannose molecules and need to trim four of them by the aid of α-Mannosidase I and produce the $Man_5GlcNAc_2N$ intermediate so as to become hybrid and complex by the addition of N-acetyl glucosamine, galactose and sialic acid subsequently. DMJ inhibited the α-Mannosidase I from trimming the four-mannose molecules and in turn all the subsequent intermediates were declined. The major importance of this inhibition in IBV is production of glycoproteins lacking sialic acid molecules, which act as receptor recognition molecules for the adjacent and/or next cell infection Figure 5.10 B.

Figure 5.10 A and B: Proposed model for N-linked glycosylation of the viral glycoproteins trafficking from the ER to Golgi complex.

A: Proteins enter the ER are N-glycosylated by oligosaccharyltransferase (OST) enzyme once they transit in to the lumen. The process of glucose trimming was inhabited by the effect of DNJ, which inhibited Glucosidase I and as a result monoglucosylated proteins were not produced, which in turn the signals were absent to be recognized by CANX/CRT complex. The complex between the chaperones and folding intermediates either became absent due to inhibition of Glucosidase I or misfolded glycoproteins produced due to retaining the last glucose by inhibition of Glucosidase II. The release of glycoprotein from CNX/CRT complex was defected and reformed by GT activity. Consequently, the protein was not perfectly folded and recognized by glycosyltransferase (GT) and became transmitted to the ERQC for degradation. The rest of completed proteins, which are not recognized by GT, were transported to the Golgi.

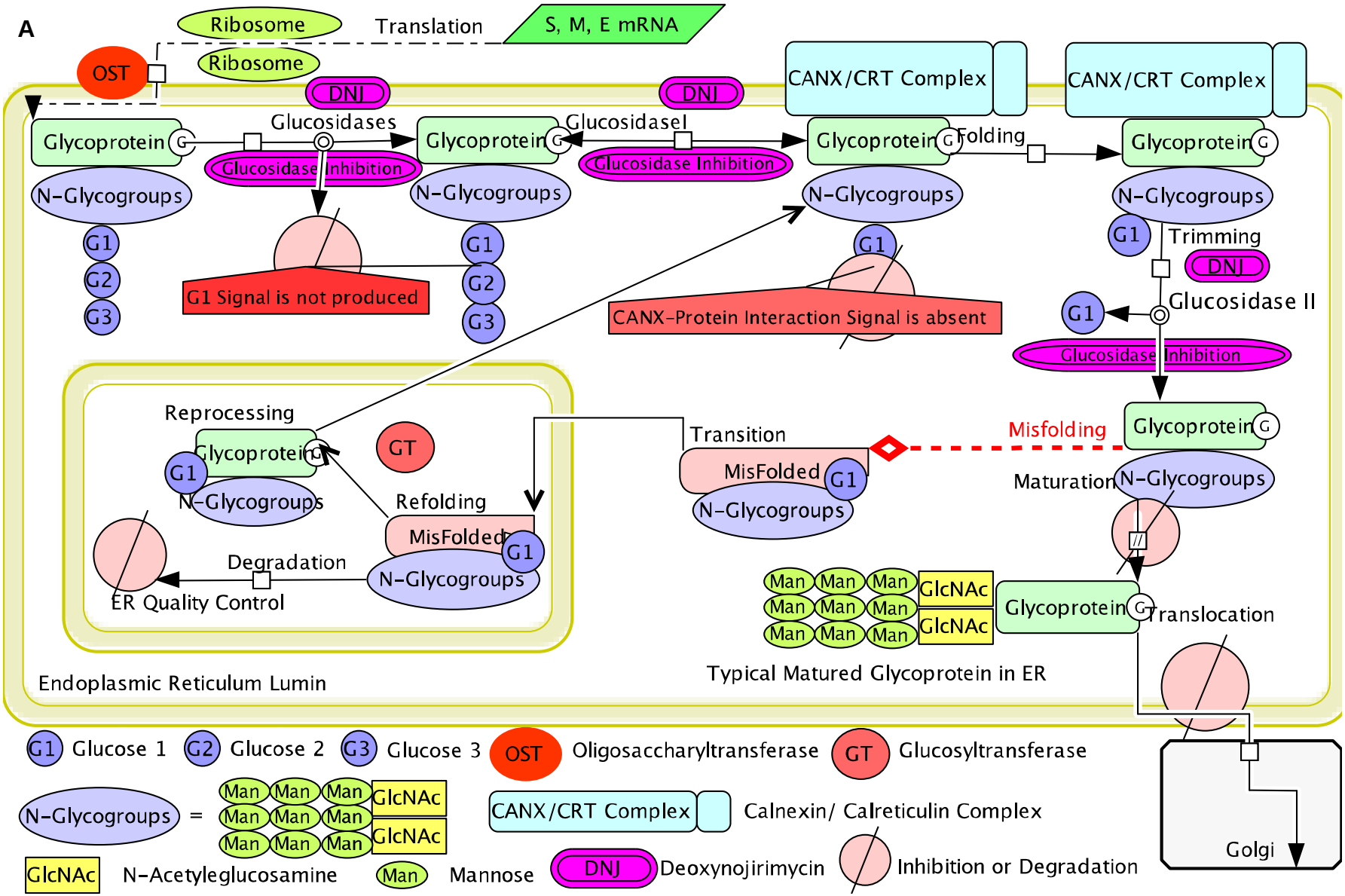
A
Ribosome
Translation
S, M, E mRNA
Ribosome
OST
DNJ
DNJ
CANX/CRT Complex
CANX/CRT Complex
Glycoprotein
Glucosidases
Glycoprotein
GlucosidaseI
Glycoprotein
Folding
Glycoprotein
Glucosidase Inhibition
Glucosidase Inhibition
N-Glycogroups
N-Glycogroups
N-Glycogroups
N-Glycogroups
G1
G2
G3
G1
G2
G3
G1
G1
G1
Trimming
DNJ
Glucosidase II
G1 Signal is not produced
CANX-Protein Interaction Signal is absent
Glucosidase Inhibition
Reprocessing
Glycoprotein
GT
G1
N-Glycogroups
Refolding
MisFolded
G1
N-Glycogroups
Degradation
ER Quality Control
Transition
MisFolded
G1
N-Glycogroups
Misfolding
Glycoprotein
Maturation
N-Glycogroups
Man
GlcNAc
Glycoprotein
Translocation
Endoplasmic Reticulum Lumin
Typical Matured Glycoprotein in ER
G1 Glucose 1
G2 Glucose 2
G3 Glucose 3
OST Oligosaccharyltransferase
GT Glucosyltransferase
N-Glycogroups =
CANX/CRT Complex
Calnexin/ Calreticulin Complex
GlcNAc N-Acetyleglucosamine
Man Mannose
DNJ Deoxynojirimycin
Inhibition or Degradation
Golgi

Figure 5.10 A and B: Proposed model for N-linked glycosylation of the viral glycoproteins trafficking from the ER to Golgi complex.

B: Mature proteins having N-glycans were translocated from the ER and processed in the Golgi. In the cis- Golgi mannosidases remove four Mannose (Man) residues to produce the Man5GlcNAc2Asn intermediate, which acts as the substrate of the medial Golgi Glucosyltransferases (GT). However DMJ inhibit the Mannosidases to trim the Mannose molecules and consequently the Man5GlcNAc2Asn became reduced. The main next step which is the Hybrid N-glycans is inhibited to convert to complex one by adding Gal and Salic acid. In trans Golgi conversion from hybrid to complex needs the N-glycans to lose the terminal two of the five Man molecules and obtain a second GlcNAc on to the complex N-glycan. The latter complex intermediate is then elongated by the addition of different molecules such as Gal, N-ANA and SA

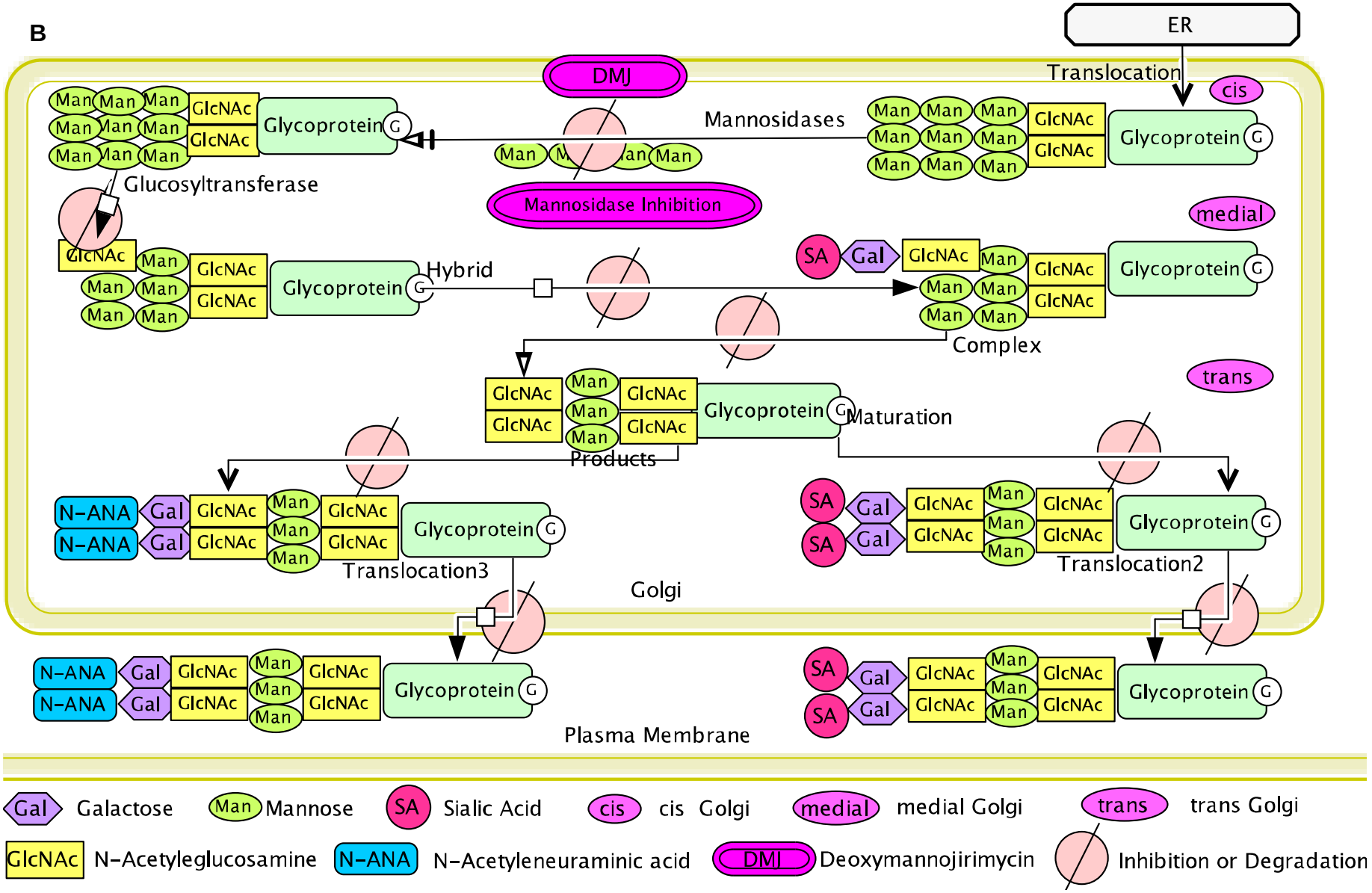
B
ER
Translocation
cis
DMJ
Mannosidases
Glycoprotein
Glucosyltransferase
Mannosidase Inhibition
medial
Hybrid
Complex
trans
Maturation
Products
Translocation3
Translocation2
Golgi
Plasma Membrane
Gal Galactose
Man Mannose
SA Sialic Acid
cis cis Golgi
medial medial Golgi
trans trans Golgi
GlcNAc N-Acetyleglucosamine
N-ANA N-Acetyleneuraminic acid
DMJ Deoxymannojirimycin
Inhibition or Degradation

Taken all together, the results of this chapter, which were concluded in the sub sequential N-linked glycosylation impairment model in both the ER and Golgi, that showed promising impact for the approach of combination treatment parameters by using DNJ and DMJ iminosugar small molecules. Finally the clinical implication and perspective impact of the whole story of glycosylation impairment and its comparison to the classical prevention methods in the world will be discussed in the next chapter.

Chapter 6

General Discussion, Conclusions and Future Work

Since 1930s and almost nine consecutive decades, the IBV is still one of the threats on poultry industry, which causes enormous economic losses in both broiler and layer chickens worldwide. It has been believed that, almost all losses were triggered due to the outbreaks of various serotypes of the virus. This was resulted from the highly contagious efficiency and rapid spread of the virus after a relatively short incubation period (as short as 18 hours) following an airborne inhalation by the host (Jackwood & de Wit, 2017). Regardless of tissue tropism (respiratory, renal and reproductive organs) of the virus strains the infection is mainly introduced through the respiratory tract and then diffuse to other organ systems of the host (Raj & Jones, 1997). This indicates the significant role of the virus contagiousness and its airborne-facilitated incidence in the outbreaks. On the other hand the intervention and control strategies to overcome the IBV outbreaks are challenging as well. The major important challenge is in the vaccines of the IBV, which continuously prone to potential failure due to the continuous emergence of the new IBV genotypes and lack of cross protection among different IBV genotypes (Bande, *et al*., 2015; Jordan, 2017). There are several evidences of the IBV outbreak incidence in the vaccinated flocks in different countries around the world for example in China (Liu & Kong, 2004), Egypt (Abdel-Moneim, *et al*., 2002), Turkey (Kahya, *et al*., 2013), Iraq (Mahmood, *et al*., 2011), Taiwan (Huang, *et al*., 2004), Russia (Bochkov, *et al*., 2006) and the most recent detection of a Middle-East GI-23 lineage (Var2-like) of infectious bronchitis virus in Poland, Europe (Lisowska, *et al*., 2017). The alternative strategies to overcome or lessen down the IBV outbreaks are limited as well.

On the other hand, the specific treatment by anti-viral drugs still unavailable for the IBV and only the supporting treatment for secondary infection and nutrition management can be done during IBV infection (Jackwood & de Wit, 2017). Additionally the intracellular virus-host interaction knowledge especially the cellular proteome during IBV infection has been appeared to be limited as well, which could identify the mechanism of interventions in the virus replication cycle. Therefore, the story of this study was started due to such limitation and continuous problem of the IBV.

Basically, the aims of this study were to characterise different approaches in the research of the IBV biology. So that the interactome of three structural proteins S, M and E were targeted to determine the cellular pathways related to the proteins processing in the cell (Aim 1) and the pathways were then validated (Aim 2) and targeted for inhibition studies (Aim 3).

In Chapter 3, the cellular interactome for each of S, M and E proteins were identified (Aim 1). The selection of the proteins was based on some reasons. First, all three proteins are incorporated in to the viral envelope, which has important role in the viral attachment to the host receptor (Masters, 2006). Secondly at the time of the approach there wasn't similar approaches except for the IBV N protein, which was done by our lab as well (Emmott, *et al*., 2013), however the study used labelled proteomics as SILAC technique. The approach for S, M and E was based on the overexpression of individual proteins in the GFP-tagged vectors and purified by immunoprecipitation before a label-free proteomic analysis by LC-MS/MS was done for the

proteins. This technique was previously worked for some other viruses in the lab in which this study was done (García-Dorival, *et al*., 2016, 2014; Munday, *et al*., 2015; Wu, *et al*., 2012). The proteins were down listed to a statistically significant ones, which were categorized to 9, 14 and 23 proteins per each of S, M and E proteomes subsequently (Chapter 3, Section 3.2.5). The post statistics analysis indicated the importance of the proteome per the viral proteins as localization of the interactions were identified bioinformatically by CellWhere program, which categorized the interactions according to subcellular compartments including the organelles. One reason for such analysis was to be more specific in terms of selection criteria of the proteins and pathways for further validations. The other factor was to identify the possibility of supportive information from other viruses and was not to be off-targeted in the validation approach later on.

The statistical significance in the proteome of S and E, the active interactions in subcellular localization analysis and the optimization of its effect in other viruses were all the main factors for choosing calnexin for further validation analysis of the proteome results. Calnexin is the membrane-bounded chaperon, which interacts with newly synthesized glycoproteins in side the ER lumen. The interaction between calnexin and the glycoproteins is based on the availability of a mono glucose signal on the glycan groups, which are linked to asparagine amino acids and lead to proper folding and maturation of the glycoproteins (Hammond, *et al*., 1994; Tatu & Helenius, 1997). The viruses that were described to interact with calnexin involved SARS coronavirus (Fukushi, *et al*., 2012), influenza virus (Hebert, *et al*., 1997), VSV

(Hammond & Helenius, 1994), rabies virus (Gaudin, 1997), HCV (Choukhi, *et al*., 1998), HBV (Werr & Prange, 1998), rotavirus (Mirazimi, *et al*., 1998), dengue virus (Limjindaporn, *et al*., 2009), and HIV (Hunegnaw, *et al*., 2016).

In Chapter 4, the S, M and E proteome outcomes were analysed and calnexin chaperone was validated as an essential pathway in the biology of the IBV (Aim 2). The validation results in Chapter 4 focused on physical interaction between calnexin and the targeted proteins and identified the localization of the interaction inside the cells as well. Furthermore the N-linked glycosylation nature of the S, M and E proteins, which is a primary and essential factor for calnexin interaction, was characterized too. The immunoblots showed significant interactions between calnexin and the proteins in such a way that the two different proteins from different viruses were analysed as controls to exclude the false positivity of the results. HRSV M and EBOV N proteins were obtained as GFP tagged viral proteins from previous studies in the lab (García-Dorival, *et al*., 2016; Munday, *et al*., 2015) were subjected to the analysis under similar immunoblot and blot restore protocols as for the IBV S triplicate. The results were significantly different and none of HRSV M and EBOV N interacted with calnexin as it was obtained for the IBV S. The interaction localization study showed the exact localization as per the predicted analysis obtained in Chapter 4, which was the ER and usually appeared as perinuclear regions in the cells and the normal resident for calnexin as well (Pollard, *et al*., 2017). For species specificity, chicken cells were stained for the localization a part from the 293T cells, which were used for overexpression and localization studies as well.

Another important outcome of Chapter 4 was the study of N-linked glycosylation of the proteins. The N-linked glycosylation is based on NXS/T motif in which the X can be any amino acid other than proline (Zhang, *et al*., 2004). For the selected IBV protein's deduced amino acid sequences, 34, 2 and 3 N-linked glycosylation sites were predicted for S, M and E proteins subsequently, which can be calculated as 2.92%, 0.89% and 2.78% N-linked glycosylation motifs for S, M and E proteins respectively. On the enzymatic deglycosylation approach, the outcome was significant as well, as the significant mass decline shift was obtained for S, which was about 50 kDa less that its obtained molecular weight on the immunoblotts. However, the M and E mass shift couldn't be seen on the immunoblotts, which might be due to their overall small sizes or the few NXS/T motifs.

Generally the outcomes of the Chapter 4 were concluded in the model for the IBV glycoprotein processing and maturations. The model was approached according the outcomes and the confirmed pathways in the Reactome database (Fabregat, *et al*., 2018). Based on the model the IBV glycoproteins processing are proteomically divided in to two steps; the ER and Golgi, which are the usual sequential compartments of the IBV during the replication cycle (Masters & Perlman, 2013). Briefly in the ER, when proteins enter the lumen, they are N-glycosylated by oligosaccharyltransferase (OST) enzyme. The N-linked glycans have three glucose molecules and two glucoses are trimmed by the successive action of Glucosidase I and II enzymes to produce monoglucosylated proteins, which are recognized by CANX/CRT complex. The complex between the chaperones and folding intermediates bifurcate to

two processes, either removal of the last glucose by glucosidase II, which causes folded substrate release from CNX/CRT complex or misfolded glycoproteins retains the glucose and is reformed by glycosyltrnaferase (GT) activity. If the protein reached its innate structure, it will be released from the ER through the protein secretory pathway. However, if the protein is not perfectly folded, it will be recognized by the GT. The completed proteins that are not recognized by GT are transported to the Golgi. However improper folded proteins will be targeted to the ERQC for degradation. In the Golgi, basically proteins having N-glycans are translocated from the ER and processed in the cis- Golgi, in which mannosidases remove mannose residues to produce the intermediate, which acts as the substrate of the medial Golgi Glucosyltransferases (GT). The GT synthesizes hybrid and complex N-glycans. In the trans Golgi conversion from hybrid to complex needs the N-glycans to lose the terminal mannose molecules and obtain a second glucosaminoglycan on to the complex N-glycan. The latter complex intermediate is then elongated by the addition of different molecules such as galactose and sialic acid reviewed in (Fabregat, *et al*., 2018).

In Chapter 5, the interference strategy of the IBV glycoproteins processing was approached (Aim 3). In the model of the glycoprotein processing, calnexin has fundamental role in the folding and maturation of the viral glycoproteins in the ER (Hammond, *et al*., 1994; Ruddock & Molinari, 2006). For facilitation of such process, calnexin needs an essential signal on the glycan group, which is a single glucose molecule and it is solely catalysed by α-glucosidase I enzyme by trimming two glucose molecules in a sequential

catalysis (Hebert, *et al*., 1995). As a result of such effect, the anti-viral approach of the α-glucosidase inhibitors was started. On the bases of the approach, the inhibition of glucose trimming inhibit the interaction between calnexin and the viral glycoproteins, which in turn leads to impairment of the glycoprotein folding (Borges de Melo, *et al*., 2006). Furthermore the glucosidase inhibitors are usually inhibit both α-glucosidase I and II, by which even following folding of glycoprotein at some point, the process prevented to be continue due to the lack of α-glucosidase II activity (Ruddock & Molinari, 2006). Meanwhile the inhibition strategy of the viral glycoprotein in the ER is approached, the maturation process in the Golgi can be targeted as well. The α-mannosidase I and II inhibitors can inhibit the Golgi processing of the glycoproteins, which in turn affect the either the assembly process or lead to improper viral particles (Balzarini, 2007; Rose, 2012).

The results of Chapter 5 were obtained from two inhibition methods, which were used either for the individual proteins or during the viral infections. For this purpose, DNJ and DMJ were selected. The DNJ and DMJ are small molecule iminosugars having glucosidase and mannosidase inhibition effects respectively (Howe, 2014). The small molecules were applied for the prophylactic treatment of the cells 24 hours before transfection of the vectors or infection by the IBV Beaudette strain. Consequently, the expression of the S and M proteins showed generation of different masses of the extra protein bands on the immunoblot membrane, which were absent in untreated controls. This might be due to untrimmed and/or deglycosylated versions of the proteins under the effect of the small molecules (section 5.2.2).

Strikingly the more significant and practical effects of the small molecules were obtained from the virus infection of the treated cells under various treatment parameters Figure 5.6. The results in this approach (section 5.2.3) were presented a promising outcome of the impairment effect in N-linked glycosylation on the infectivity of the IBV. Quantitative and qualitative analysis confirmed the significant decline in the virus titers from DNJ/DMJ treatment in combination with calnexin siRNA transfection. This was exactly as hypothesized for the glycosylation impairment approach.

The direct deglycosylation of the IBV was another approach for confirming the direct relation of the viral epitope N-linked glycosylation, which is mainly represented by the S protein (Promkuntod, *et al*., 2014).

The concluding interpretation of N-linked glycosylation impairments effect on the IBV infectivity can be categorized in the following points:

1- The viral glycoproteins are failed to completely fold in the ER and in turn lead to decline in sufficient proteins for viral replication.

2- The viral glycoproteins are unable to assemble in the Golgi due to incomplete maturation.

3- The virus are become non infective when bear incomplete glycoproteins in their envelope.

Taken all together, the results in this thesis showed a complete strategy of identifying the interactome of the IBV S, M and E structural proteins using label-free proteomics, validating the most significant pathway in the interactome (calnexin) and implying the impairment approach using small molecules that have potential impact as anti-viral therapeutics.

Although the outcomes were obtained completely form an *in vitro* research using cell culture methods, however this work might has clinical implication *in vivo* as well. The major potential impact of this work can be hypothesized as one of the solutions during the IBV outbreaks. So when an outbreak happens, the virus is rapidly replicate in the first few hosts and then in few days can infect the whole flock. However if there is a prophylactic treatment by iminosugar molecules, the virus's effect can be declined both in replication and infectivity. This approach can be a future work for further progress in the control and prevention of the IBV using *in ovo* and *in vivo* studies.

In the final conclusion, it can be summarized that the results in this thesis complied all the objectives of the study and as far as to the knowledge available currently, it is the first work in identifying the interactome for the IBV S, M and E structural proteins.

Chapter 7

References

Abdel-Moneim, A S, H M Madbouly, J Gelb, B S Ladman, J Gelb, and B S Ladman. 2002. 'Isolation and Identification of Egypt/Beni-Seuf /O1 a Novel Genotype of Infectious Bronchitis Virus'. *Vet.Med.J., Giza* 50 (4): 1065–78.

Abdelwhab, El-Sayed M, and Hafez M Hafez. 2015. 'Control of Avian Influenza in Poultry with Antivirals and Molecular Manipulation'. In *Epidemiology II Theory, Research and Practice*. ISBN:978-1-922227-76-8. iConcept Press.

Abro, Shahid Hussain, Lena H M Renström, Karin Ullman, Sándor Belák, and Claudia Baule. 2012. 'Characterization and Analysis of the Full-Length Genome of a Strain of the European QX-like Genotype of Infectious Bronchitis Virus'. *Archives of Virology* 157 (6): 1211–15.

Abro, Shahid Hussain, Karin Ullman, Sándor Belák, and Claudia Baule. 2012. 'Bioinformatics and Evolutionary Insight on the Spike Glycoprotein Gene of QX-like and Massachusetts Strains of Infectious Bronchitis Virus'. *Virology Journal* 9 (1): 211.

AHDB. 2018. 'Poultry Pocketbook-2018'.

Aljabr, Waleed A. 2016. 'Using Label Free Proteomics and RNA Sequencing to Investigate the Human Respiratory Syncytial Virus and the Effects of the Antiviral Ribavirin'. PhD Thesis. University of Liverpool, UK.

Alonzi, Dominic S, Kathryn A Scott, Raymond A Dwek, and Nicole Zitzmann. 2017. 'Iminosugar Antivirals: The Therapeutic Sweet Spot.' *Biochemical Society Transactions* 45 (2): 571–82.

Ankney, J Astor, Adil Muneer, and Xian Chen. 2018. 'Relative and Absolute Quantitation in Mass Spectrometry–Based Proteomics'. *Annual Review of Analytical Chemistry* 11 (1): 49–77.

Armesto, M, D Cavanagh, and P Britton. 2009. 'The Replicase Gene of Avian Coronavirus Infectious Bronchitis Virus Is a Determinant of Pathogenicity'. *PLoS ONE* 4 (10).

Aslam, Bilal, Madiha Basit, Muhammad Atif Nisar, Mohsin Khurshid, and Muhammad Hidayat Rasool. 2017. 'Proteomics: Technologies and Their Applications'. *Journal of Chromatographic Science* 55 (2): 182–96.

Audagnotto, Martina, and Matteo Dal Peraro. 2017. 'Protein Post-Translational Modifications: In Silico Prediction Tools and Molecular Modeling'. *Computational and Structural Biotechnology Journal* 15: 307–19.

Baltimore, David. 1971. 'Expression of Animal Virus Genomes.' *Bacteriological Reviews* 35 (3): 235–41.

Balzarini, Jan. 2007. 'The Alpha(1,2)-Mannosidase I Inhibitor 1-Deoxymannojirimycin Potentiates the Antiviral Activity of Carbohydrate-Binding Agents against Wild-Type and Mutant HIV-1 Strains Containing Glycan Deletions in Gp120.' *FEBS Letters* 581 (10): 2060–64.

Bande, Faruku, Siti Suri Arshad, Mohd Hair Bejo, Hassan Moeini, and Abdul Rahman Omar. 2015. 'Progress and Challenges toward the Development of Vaccines against Avian Infectious Bronchitis'. *Journal of Immunology Research* 2015: 1–12.

Bande, Faruku, Siti Suri Arshad, Abdul Rahman Omar, Mohd Hair-Bejo, Aliyu Mahmuda, and Venugopal Nair. 2017. 'Global Distributions and Strain Diversity of Avian Infectious Bronchitis Virus: A Review'. *Animal Health Research Reviews* 18 (1): 70–83.

Banerjee, Nilotpal, and Sumi Mukhopadhyay. 2016. 'Viral Glycoproteins: Biological Role and Application in Diagnosis'. *VirusDisease* 27 (1): 1–11.

Beach, J. R., and O. W. Schalm. 1936. 'A Filterable Virus, Distinct from That of Laryngotracheitis, the Cause of a Respiratory Disease of Chicks'. *Poultry Science* 15 (3): 199–206.

Belouzard, Sandrine, Jean K. Millet, Beth N. Licitra, and Gary R. Whittaker. 2012. 'Mechanisms of Coronavirus Cell Entry Mediated by the Viral Spike Protein.' *Viruses* 4 (6): 1011–33.

Bergeron, John J.M., Michael B. Brenner, David Y. Thomas, and David B. Williams. 1994. 'Calnexin: A Membrane-Bound Chaperone of the Endoplasmic Reticulum'. *Trends in Biochemical Sciences* 19 (3): 124–28.

Bickerton, Erica, Sarah M. Keep, and Paul Britton. 2017. 'Reverse Genetics System for the Avian Coronavirus Infectious Bronchitis Virus'. In *Methods in Molecular Biology*.

Bingham, R W, and J D Almeida. 1977. 'Studies on the Structure of a Coronavirus-Avian Infectious Bronchitis Virus.' *The Journal of General Virology* 36 (3): 495–502.

Binns, M. M., M. E. G. Boursnell, D. Cavanagh, D. J. C. Pappin, and T. D. K. Brown. 1985. 'Cloning and Sequencing of the Gene Encoding the Spike Protein of the Coronavirus IBV'. *Journal of General Virology* 66 (4): 719–26.

Bochkov, Yury A., Galina V. Batchenko, Lidiya O. Shcherbakova, Alexander V. Borisov, and Vladimir V. Drygin. 2006. 'Molecular Epizootiology of Avian Infectious Bronchitis in Russia'. *Avian Pathology* 35 (5): 37–41.

Borges de Melo, Eduardo, Adriane da Silveira Gomes, and Ivone Carvalho. 2006. 'α- and β-Glucosidase Inhibitors: Chemical Structure and Biological Activity'. *Tetrahedron* 62 (44): 10277–302.

Bosch, B. J., R. van der Zee, C. A. M. de Haan, and P. J. M. Rottier. 2003. 'The Coronavirus Spike Protein Is a Class I Virus Fusion Protein: Structural and Functional Characterization of the Fusion Core Complex'. *Journal of Virology* 77 (16): 8801–11.

Boursnell, M. E. G., T. D. K. Brown, I. J. Foulds, P. F. Green, F. M. Tomley, and M. M. Binns. 1987. 'Completion of the Sequence of the Genome of the Coronavirus Avian Infections Bronchitis Virus'. *Journal of General Virology* 68 (Pt 1): 57–77.

Boursnell, M. E G, T. D.K Brown, and M. M Binns. 1984. 'Sequence of the Membrane Protein Gene from Avian Coronavirus IBV'. *Virus Research* 1 (4): 303–13.

Boursnell, M E, T D Brown, I J Foulds, P F Green, F M Tomley, and M M Binns. 1987. 'Completion of the Sequence of the Genome of the Coronavirus Avian Infectious Bronchitis Virus'. *Journal of General Virology* 68 (1): 57–77.

Brandão, Paulo E. 2012. 'Avian Coronavirus Spike Glycoprotein Ectodomain Shows a Low Codon Adaptation to Gallus Gallus with Virus-Exclusive Codons in Strategic Amino Acids Positions'. *Journal of Molecular Evolution* 75 (1–2): 19–24.

Breitling, Jörg, and Markus Aebi. 2013. 'N-Linked Protein Glycosylation in the Endoplasmic Reticulum'. *Cold Spring Harbor Perspectives in Biology* 5 (8): a013359–a013359.

Brierley, I, M E G Boursnell', M M Binns', B Bilimoria, V C Blok, T D K Brown, S C Inglis, and J E Walker. 1987. 'An Efficient Ribosomal Frame-Shifting Signal in the Polymerase-Encoding Region of the Coronavirus EBV The Polymerase-Encoding Region of the Genomic RNA of The'. *The EMBO Journal*. Vol. 6.

Brown Jordan, Arianne, Victor Gongora, Dane Hartley, and Christopher Oura. 2018. 'A Review of Eight High-Priority, Economically Important Viral Pathogens of Poultry within the Caribbean Region.' *Veterinary Sciences* 5 (1).

Bushnell, L. D., and C. A. Brandly. 1933. 'Laryngotracheitis in Chicks'. *Poultry Science* 12 (1): 55–60.

Cao, Zhongzan, Zongxi Han, Yuhao Shao, Heyuan Geng, Xiangang Kong, and Shengwang Liu. 2011. 'Proteomic Analysis of Chicken Embryonic Trachea and Kidney Tissues after Infection in Ovo by Avian Infectious Bronchitis Coronavirus.' *Proteome Science* 9 (1): 11.

Cao, Zhongzan, Zongxi Han, Yuhao Shao, Xiaoli Liu, Junfeng Sun, Demin Yu, Xiangang Kong, and Shengwang Liu. 2012. 'Proteomics Analysis of Differentially Expressed Proteins in Chicken Trachea and Kidney after Infection with the Highly Virulent and Attenuated Coronavirus Infectious Bronchitis Virus in Vivo'. *Proteome Science* 10 (1).

Casais, R, V Thiel, S G Siddell, D Cavanagh, and Paul Britton. 2001. 'Reverse Genetics System for the Avian Coronavirus Infectious Bronchitis Virus.' *Journal of Virology* 75 (24): 12359–69.

Casais, Rosa, Marc Davies, David Cavanagh, and Paul Britton. 2005. 'Gene 5 of the Avian Coronavirus Infectious Bronchitis Virus Is Not Essential for Replication'. *J. Virol.* 79 (13): 8065–78.

Cavanagh, Dave. 2005. 'Coronaviridae: A Review of Coronaviruses and Toroviruses'. *Coronaviruses with Special Emphasis on First Insights …*, 1–54.

Cavanagh, Dave. 2007. 'Coronavirus Avian Infectious Bronchitis Virus.' *Veterinary Research* 38 (2): 281–97.

Cavanagh, David. 1983a. ‘Coronavirus IBV Glycopolypeptides: Size of Their Polypeptide Moieties and Nature of Their Oligosaccharides’. *Journal of General Virology* 64 (5): 1187–91.

Cavanagh, David. 1983b. ‘Coronavirus IBV: Structural Characterization of the Spike Protein’. *Journal of General Virology* 64 (12): 2577–83.

Cavanagh, David, and Jack Jr Gelb. 2008. ‘Infectious Bronchitis’. In *Diseases of Poultry*, edited by A. M. Fadly, J. R. Glisson, L. R. McDougald, L. K. Nolan, and D. E. Swayne, 12th ed. Blachwell.

Chahrour, Osama, Diego Cobice, and John Malone. 2015. ‘Stable Isotope Labelling Methods in Mass Spectrometry-Based Quantitative Proteomics’. *Journal of Pharmaceutical and Biomedical Analysis* 113 (September): 2–20.

Chang, Jinhong, Ju-Tao Guo, Yanming Du, and Timothy Block. 2013. ‘Imino Sugar Glucosidase Inhibitors as Broadly Active Anti-Filovirus Agents’. *Emerging Microbes & Infections* 2 (11): e77.

Chasey, D., and D. J. Alexander. 1976. ‘Morphogenesis of Avian Infectious Bronchitis Virus in Primary Chick Kidney Cells’. *Archives of Virology* 52 (1–2): 101–11.

Chelius, Dirk, and Pavel V Bondarenko. 2002. ‘Quantitative Profiling of Proteins in Complex Mixtures Using Liquid Chromatography and Mass Spectrometry’. *Journal of Proteome Research* 1 (4): 317–23.

Chen, Christie, David M Zuckerman, Susanna Brantley, Michka Sharpe, Kevin Childress, Egbert Hoiczyk, and Amanda R Pendleton. 2014. ‘Sambucus Nigra Extracts Inhibit Infectious Bronchitis Virus at an Early Point during Replication’.

Chen, Hongying, Andrew Gill, Brian K Dove, Stevan R Emmett, C Fred Kemp, Mark A Ritchie, Michael Dee, and Julian A Hiscox. 2005. 'Mass Spectroscopic Characterization of the Coronavirus Infectious Bronchitis Virus Nucleoprotein and Elucidation of the Role of Phosphorylation in RNA Binding by Using Surface Plasmon Resonance'. *Journal of Virology* 79 (2): 1164–79.

Chen, Hongying, Torsten Wurm, Paul Britton, Gavin Brooks, and Julian A Hiscox. 2002. 'Interaction of the Coronavirus Nucleoprotein with Nucleolar Antigens and the Host Cell.' *Journal of Virology* 76 (10): 5233–50.

Cheng, Jinlong, Caiyun Huo, Jing Zhao, Tong Liu, Xiao Li, Shihong Yan, Zhujun Wang, Yanxin Hu, and Guozhong Zhang. 2018. 'Pathogenicity Differences between QX-like and Mass-Type Infectious Bronchitis Viruses'. *Veterinary Microbiology* 213 (January): 129–35.

Chhabra, Rajesh, Suresh V Kuchipudi, Julian Chantrey, and Kannan Ganapathy. 2016. 'Pathogenicity and Tissue Tropism of Infectious Bronchitis Virus Is Associated with Elevated Apoptosis and Innate Immune Responses'. *Virology* 488: 232–41.

Choukhi, a, Sophana Ung, Czeslaw Wychowski, Jean Dubuisson, and L I E Choukhi. 1998. 'Involvement of Endoplasmic Reticulum Chaperones in the Folding of Hepatitis C Virus Glycoproteins.' *Journal of Virology* 72 (5): 3851–58.

Chu V.C., McElroy L.J., Ferguson A.D., Bauman B.E., Whittaker G.R. . 2006 Avian Infectious Bronchitis Virus Enters Cells Via the Endocytic Pathway. In: Perlman S., Holmes K.V. (eds) The Nidoviruses. Advances in Experimental Medicine and Biology, vol 581. Springer, Boston, MA

Chu, Vicky C, Lisa J McElroy, Vicky C Chu, Beverley E Bauman, and Gary R Whittaker. 2006. 'The Avian Coronavirus Infectious Bronchitis Virus

Undergoes Direct Low-PH-Dependent Fusion Activation during Entry into Host Cells'. *J.Virol.* (80): 3180–88.

Clercq, Erik De, and Guangdi Li. 2016. 'Approved Antiviral Drugs over the Past 50 Years.' *Clinical Microbiology Reviews* 29 (3): 695–747.

Cook, Jane, Mark Jackwood, and R. C. Jones. 2012. 'The Long View: 40 Years of Infectious Bronchitis Research'. *Avian Pathology* 41 (3): 239–250.

Cook, Jane, Mark Jackwood, R. C. Jones, F. Awad, R. Chhabra, M. Baylis, K. Ganapathy, *et al*. 2012. 'Review of Infectious Bronchitis Virus Around the World Review of Infectious Bronchitis Virus Around the World'. *Current Opinion in Virology* 7 (3): 281–97.

Corse, Emily, and Carolyn E. Machamer. 2003. 'The Cytoplasmic Tails of Infectious Bronchitis Virus E and M Proteins Mediate Their Interaction.' *Virology* 312 (1): 25–34.

Corse, Emily, and Carolyn E Machamer. 2000. 'Infectious Bronchitis Virus E Protein Is Targeted to the Golgi Complex and Directs Release of Virus-like Particles.' *Journal of Virology* 74 (9): 4319–26.

Corse, Emily, and Carolyn E Machamer. 2002. 'The Cytoplasmic Tail of Infectious Bronchitis Virus E Protein Directs Golgi Targeting.' *Journal of Virology* 76 (3): 1273–84.

Dal Pozzo, F, and E Thiry. 2014. 'Antiviral Chemotherapy in Veterinary Medicine: Current Applications and Perspectives.' *Revue Scientifique et Technique (International Office of Epizootics)* 33 (3): 791–801.

Dalton, Kevin, R Casais, Kathy Shaw, Kathleen Stirrups, S Evans, Paul Britton, T D Brown, and Dave Cavanagh. 2001. 'Cis-Acting Sequences Required for Coronavirus Infectious Bronchitis Virus Defective-RNA

Replication and Packaging.' *Journal of Virology* 75 (1): 125–33.

Davison, Andrew J. 2017. 'Journal of General Virology - Introduction to "ICTV Virus Taxonomy Profiles".' *The Journal of General Virology* 98 (1): 1.

DEFRA. 2018. 'United Kingdom Poultry and Poultry Meat Statistics – September 2018'. Vol. 44.

Dong, Xiaofeng, Stuart D. Armstrong, Dong Xia, Benjamin L. Makepeace, Alistair C. Darby, and Tatsuhiko Kadowaki. 2017. 'Draft Genome of the Honey Bee Ectoparasitic Mite, Tropilaelaps Mercedesae, Is Shaped by the Parasitic Life History.' *GigaScience* 6 (3): 1–17.

Dove, Brian, Gavin Brooks, Katrina Bicknell, Torsten Wurm, and Julian a Hiscox. 2006. 'Cell Cycle Perturbations Induced by Infection with the Coronavirus Infectious Bronchitis Virus and Their Effect on Virus Replication Cell Cycle Perturbations Induced by Infection with the Coronavirus Infectious Bronchitis Virus and Their Effect on Virus R'. *Society* 80 (8): 4147–56.

Dove, Brian K, Jae-Hwan You, Mark L Reed, Stevan R Emmett, Gavin Brooks, and Julian A Hiscox. 2006. 'Changes in Nucleolar Morphology and Proteins during Infection with the Coronavirus Infectious Bronchitis Virus'. *Cellular Microbiology* 8 (7): 1147–57.

Drabovich, Andrei P., Maria P. Pavlou, Ihor Batruch, and Eleftherios P. Diamandis. 2013. 'Proteomic and Mass Spectrometry Technologies for Biomarker Discovery'. In *Proteomic and Metabolomic Approaches to Biomarker Discovery*, 17–37. Elsevier.

Duan, Guangyou, and Dirk Walther. 2015. 'The Roles of Post-Translational Modifications in the Context of Protein Interaction Networks.' *PLoS Computational Biology* 11 (2): e1004049.

Dunnett, Charles W. 1955. ‘A Multiple Comparison Procedure for Comparing Several Treatments with a Control’. *Journal of the American Statistical Association* 50 (272): 1096–1121.

Emmott, Edward, Diane Munday, Erica Bickerton, Paul Britton, Mark a Rodgers, Adrian Whitehouse, En-Min Zhou, and Julian A Hiscox. 2013. ‘The Cellular Interactome of the Coronavirus Infectious Bronchitis Virus Nucleocapsid Protein and Functional Implications for Virus Biology.’ *Journal of Virology* 87 (17): 9486–9500.

Emmott, Edward, Catriona Smith, Stevan R Emmett, Brian K Dove, and Julian A Hiscox. 2010. ‘Elucidation of the Avian Nucleolar Proteome by Quantitative Proteomics Using SILAC and Changes in Cells Infected with the Coronavirus Infectious Bronchitis Virus’. *PROTEOMICS* 10 (19): 3558–62.

Emmott, Edward, Helen Wise, Eva M Loucaides, David A Matthews, Paul Digard, and Julian A Hiscox. 2010. ‘Quantitative Proteomics Using SILAC Coupled to LC−MS/MS Reveals Changes in the Nucleolar Proteome in Influenza A Virus-Infected Cells’. *Journal of Proteome Research* 9 (10): 5335–45.

Fabregat, Antonio, Steven Jupe, Lisa Matthews, Konstantinos Sidiropoulos, Marc Gillespie, Phani Garapati, Robin Haw, *et al*. 2018. ‘The Reactome Pathway Knowledgebase’. *Nucleic Acids Research* 46 (D1): D649–55.

Fabricant, Julius. 1998. ‘The Early History of Infectious Bronchitis’. *Source: Avian Diseases*. Vol. 42. https://doi.org/Doi 10.2307/1592697.

FAO. 2013. *Poultry Development Review*. *Poultry Welfare in Developing Countries*.

FAO. 2018. ‘MEAT MARKET REVIEW’. Rome.

Fleet, G W J, L E Fellows, and P W Smith. 1987. 'Synthesis of Deoxymannojirimycin, Fagomine, and Deoxynojirimycin, 2-Acetamido-1,5-Imino-1,2,5-Trideoxy-D-Mannitol, 2- Acetamido-1,5-Imino-1,2,5-Trideoxy-D-Glucitol, 2S, 3R, 4R, 5R-Trihydroxypipecolic Acid and 2S, 3R, 4R, 5S-Trihydroxypipecolic Acid from M'. *Synthesis*, no. 5: 979–90.

Fleet, George W J, Nigel G Ramsden, and David R Witty. 1989. 'Practical Synthesis Op Deoxymannojirimycin And Mannonolactam Prom L-Gulonolactone. Synthesis Of L-Deoxymannojirimycin And L-Mannonolactam Prom D-Gulonolactone'. *Tetrahedron* 45 (1): 319–26.

Foster, Douglas N, and Linda K Foster. 1996. IMMORTALIZED CELL LINES FOR VIRUS GROWTH, issued 30 September 1996.

Fukushi, Masaya, Yoshiyuki Yoshinaka, Yusuke Matsuoka, Seisuke Hatakeyama, Yukihito Ishizaka, Teruo Kirikae, Takehiko Sasazuki, and Tohru Miyoshi-Akiyama. 2012. 'Monitoring of S Protein Maturation in the Endoplasmic Reticulum by Calnexin Is Important for the Infectivity of Severe Acute Respiratory Syndrome Coronavirus.' *Journal of Virology* 86 (21): 11745–53.

Funahashi, Akira, Naoki Tanimura, Yukiko Matsuoka, Naritosi Yosinaga, and Hiroaki Kitano. 2003. 'CellDesigner2.0: A Process Diagram Editor for Gene-Regulatory and Biochemical Networks'.

Fung, To Sing, Mei Huang, and Ding Xiang Liu. 2014. 'Coronavirus-Induced ER Stress Response and Its Involvement in Regulation of Coronavirus–Host Interactions'. *Virus Research* 194 (December): 110–23.

Fung, To Sing, Ying Liao, and Ding Xiang Liu. 2016. 'Regulation of Stress Responses and Translational Control by Coronavirus.' *Viruses* 8 (7): 184. https://doi.org/10.3390/v8070184.

Fung, To Sing, and Ding Xiang Liu. 2018. 'Post-Translational Modifications of Coronavirus Proteins: Roles and Function'. *Future Virology* 13 (6): 405–30.

García-Dorival, Isabel, Weining Wu, Stuart D Armstrong, John N Barr, Miles W Carroll, Roger Hewson, and Julian A Hiscox. 2016. 'Elucidation of the Cellular Interactome of Ebola Virus Nucleoprotein and Identification of Therapeutic Targets'. *Journal of Proteome Research* 15 (12): 4290–4303.

García-Dorival, Isabel, Weining Wu, Stuart Dowall, Stuart Armstrong, Olivier Touzelet, Jonathan Wastling, John N. Barr, *et al*. 2014. 'Elucidation of the Ebola Virus VP24 Cellular Interactome and Disruption of Virus Biology through Targeted Inhibition of Host-Cell Protein Function'. *Journal of Proteome Research* 13 (11): 5120–35.

Gaudin, Y. 1997. 'Folding of Rabies Virus Glycoprotein: Epitope Acquisition and Interaction with Endoplasmic Reticulum Chaperones.' *Journal of Virology* 71 (5): 3742–50.

Ghani, Sepideh, Seyed Davood Hosseni, Mohammad Reza Zolfaghari, and Shahin Masoodi. 2012. 'Expression of S1 Glycoprotein Gene of Infectious Bronchitis Virus (IBV) in Escherichia Coli' 6 (13): 3139–43.

Godeke, G J, C a de Haan, J W Rossen, H Vennema, and P J Rottier. 2000. 'Assembly of Spikes into Coronavirus Particles Is Mediated by the Carboxy-Terminal Domain of the Spike Protein.' *Journal of Virology* 74 (3): 1566–71.

Guo, Huichen, Mei Huang, Quan Yuan, Yanquan Wei, Yuan Gao, Lejiao Mao, Lingjun Gu, *et al*. 2017. 'The Important Role of Lipid Raft-Mediated Attachment in the Infection of Cultured Cells by Coronavirus Infectious Bronchitis Virus Beaudette Strain'. Edited by Yongchang Cao. *PLOS ONE* 12 (1): e0170123.

Haan, C A de, Harry Vennema, and P J Rottier. 2000. 'Assembly of the Coronavirus Envelope: Homotypic Interactions between the M Proteins.' *Journal of Virology* 74 (11): 4967–78.

Haan, Cornelis A.M. De, Paul S. Masters, Xiaolan Shen, Susan Weiss, and Peter J.M. Rottier. 2002. 'The Group-Specific Murine Coronavirus Genes Are Not Essential, but Their Deletion, by Reverse Genetics, Is Attenuating in the Natural Host'. *Virology* 296 (1): 177–89.

Hagemeijer, Marne C, Monique H Verheije, Mustafa Ulasli, I. A. Shaltiel, L. A. de Vries, Fulvio Reggiori, Peter J M Rottier, and C. A. M. de Haan. 2010. 'Dynamics of Coronavirus Replication-Transcription Complexes'. *Journal of Virology* 84 (4): 2134–49.

Haijema, Bert Jan, Haukeline Volders, and Peter J M Rottier. 2004. 'Live, Attenuated Coronavirus Vaccines through the Directed Deletion of Group-Specific Genes Provide Protection against Feline Infectious Peritonitis'. *Journal of Virology* 78 (8): 3863–71.

Hammond, Craig. 1994. 'Quality Control in the Secretory Pathway: Retention of a Misfolded Viral Membrane Glycoprotein Involves Cycling between the ER, Intermediate Compartment, and Golgi Apparatus'. *The Journal of Cell Biology* 126 (1): 41–52.

Hammond, Craig, Ineke Braakman, and Ami Helenius. 1994. 'Role of N-Linked Oligosaccharide Recognition, Glucose Trimming, and Calnexin in Glycoprotein Folding and Quality Control.' *Proceedings of the National Academy of Sciences* 91 (3): 913–17.

Hammond, Craig, and Ari Helenius. 1994. 'Folding of VSV G Protein: Sequential Interaction with BiP and Calnexin'. *Science* 266 (5184): 456–58.

Hebert, D N, B Foellmer, and a Helenius. 1995. 'Glucose Trimming and Reglucosylation Determine Glycoprotein Association with Calnexin in the Endoplasmic Reticulum.' *Cell* 81 (3): 425–33.

Hebert, D N, B Foellmer, and a Helenius. 1996. 'Calnexin and Calreticulin Promote Folding, Delay Oligomerization and Suppress Degradation of Influenza Hemagglutinin in Microsomes.' The EMBO Journal 15(12): 2961–2968.

Hebert, Daniel N., Jian-Xin Zhang, Wei Chen, Brigitte Foellmer, and Ari Helenius. 1997. 'The Number and Location of Glycans on Influenza Hemagglutinin Determine Folding and Association with Calnexin and Calreticulin'. *The Journal of Cell Biology* 139 (3): 613–23.

Hegde, Ramanujan S, and Robert J Keenan. 2011. 'Tail-Anchored Membrane Protein Insertion into the Endoplasmic Reticulum.' *Nature Reviews. Molecular Cell Biology* 12 (12): 787–98.

Helenius, A., E. S. Trombetta, D. N. Hebert, and J. F. Simons. 1997. 'Calnexin, Calreticulin and the Folding of Glycoproteins'. *Trends in Cell Biology* 7 (5): 193–200.

Hierholzer, J.C., and R.A. Killington. 1996. 'Virus Isolation and Quantitation'. In *Virology Methods Manual*, 25–46. Elsevier.

Hiscox, J. A., T. Wurm, L. Wilson, P. Britton, D. Cavanagh, and G. Brooks. 2001. 'The Coronavirus Infectious Bronchitis Virus Nucleoprotein Localizes to the Nucleolus'. *Journal of Virology* 75 (1): 506–12.

Hiscox, J A, Adrian Whitehouse, and David A Matthews. 2010. 'Nucleolar Proteomics and Viral Infection.' *Proteomics* 10 (22): 4077–86.

Hiscox, Julian A. 2007. 'RNA Viruses: Hijacking the Dynamic Nucleolus.' *Nature Reviews. Microbiology* 5 (2): 119–27.

Hitchner, Stephen B. 2004. 'History of Biological Control of Poultry Diseases in the U.S.A'. *Avian Diseases* 48 (1): 1–8.

Hodgson, Teri, Paul Britton, and Dave Cavanagh. 2005. 'Neither the RNA nor the Proteins of Open Reading Frames 3a and 3b of the Coronavirus Infectious Bronchitis Virus Are Essential for Replication'. *Journal of Virology* 80 (1): 296–305.

Hogue, Brenda G., and Carolyn E. Machamer. 2008. 'Coronavirus Structural Proteins and Virus Assembly'. In *Nidoviruses*, 179–200. American Society of Microbiology.

Holmes, Edward C. 2003. 'Error Thresholds and the Constraints to RNA Virus Evolution'. *Trends in Microbiology* 11 (12): 543–46.

Horne, Graeme, Francis X Wilson, Jon Tinsley, David H Williams, and Richard Storer. 2011. 'Iminosugars Past, Present and Future: Medicines for Tomorrow'. *Drug Discovery Today* 16 (3–4): 107–18.

Horwich, Arthur L. 2014. 'Molecular Chaperones in Cellular Protein Folding: The Birth of a Field.' *Cell* 157 (2): 285–88.

Howe, Jonathon D. 2014. 'Antiviral Mechanisms Of Small Molecules Targeting The Endoplasmic Reticulum And Golgi Apparatus' (PhD Thesis). Oxford University, UK.

Huang, YP, HC Lee, MC Cheng, CH Wang - Avian diseases, and undefined 2004. 2004. 'S1 and N Gene Analysis of Avian Infectious Bronchitis Viruses in Taiwan'. *Aaapjournals.Info*, no. 10: 581–89.

Hunegnaw, Ruth, Marina Vassylyeva, Larisa Dubrovsky, Tatiana Pushkarsky, Dmitri Sviridov, Anastasia A Anashkina, Aykut Üren, *et al*. 2016. 'Interaction between HIV-1 Nef and Calnexin: From Modeling to Small Molecule Inhibitors Reversing HIV-Induced Lipid Accumulation

HHS Public Access Author Manuscript'. *Arterioscler Thromb Vasc Biol* 36 (9): 1758–71.

Idris, Fakhriedzwan, Siti Hanna Muharram, and Suwarni Diah. 2016. 'Glycosylation of Dengue Virus Glycoproteins and Their Interactions with Carbohydrate Receptors: Possible Targets for Antiviral Therapy'. *Archives of Virology* 161 (7): 1751–60.

Iida, Hideo, Naoki Yamazaki, and Chihiro Kibayashi. 1987. 'Total Synthesis of (+)-Nojirimycin and (+)-1-Deoxynojirimycin'. *The Journal of Organic Chemistry* 52 (15): 3337–42.

Inouye, S, T Tsuruoka, T. Ito, and T Niida. 1968. 'STRUCTURE AND SYNTHESIS OF NOJIRIMYCIN'. *Tetrahdron* 23: 2125–44.

Ishida, Nakao, Katsuo Kumagai, Taro Niida, Takashi Tsuruoka, and Hiroshi Yumoto. 1967. 'Nojirimycin, a New Antibiotic. II. Isolation, Characterization, and Biological Activity'. *Journal of Antibiotics*.

Jackwood, M.W., R Rosenbloom, M Petteruti, D.A. Hilt, A.W. McCall, and S.M. Williams. 2010. 'Avian Coronavirus Infectious Bronchitis Virus Susceptibility to Botanical Oleoresins and Essential Oils in Vitro and in Vivo'. *Virus Research* 149 (1): 86–94.

Jackwood, M W, D a Hilt, S a Callison, C W Lee, H Plaza, and E Wade. 2014. 'Spike Glycoprotein Cleavage Recognition Site Analysis of Infectious Bronchitis Virus.' *Avian Diseases* 45 (2): 366–72.

Jackwood, Mark W. 2012. 'Review of Infectious Bronchitis Virus Around the World'. *Avian Diseases* 56 (4): 634–41.

Jackwood, Mark W., and Sjaak de Wit. 2017. 'Infectious Bronchitis'. In *Diseases of Poultry*, edited by David E. Swayne, 13th ed., 139–59. Chichester, UK: John Wiley & Sons, Ltd.

Jayaram, Jyothi, Soonjeon Youn, and Ellen W. Collisson. 2005. 'The Virion N Protein of Infectious Bronchitis Virus Is More Phosphorylated than the N Protein from Infected Cell Lysates'. *Virology* 339 (1): 127–35.

Jordan, Brian. 2017. 'Vaccination against Infectious Bronchitis Virus: A Continuous Challenge'. *Veterinary Microbiology* 206 (July): 137–43.

Kahya, Serpil, Fethiye Coven, Seran Temelli, Aysegul Eyigor, and Kamil Tayfun Carli. 2013. 'Presence of IS/1494/06 Genotype-Related Infectious Bronchitis Virus in Breeder and Broiler Flocks in Turkey'. *Ankara Üniv Vet Fak Derg* 60 (2): 27–31.

Kang, Kyung-Don, Yong Seok Cho, Ji Hye Song, Young Shik Park, Jae Yeon Lee, Kyo Yeol Hwang, Sang Ki Rhee, Ji Hyung Chung, Ohsuk Kwon, and Su-Il Seong. 2011. 'Identification of the Genes Involved in 1-Deoxynojirimycin Synthesis in Bacillus Subtilis MORI 3K-85.' *Journal of Microbiology (Seoul, Korea)* 49 (3): 431–40.

Khaleil, Samy, Naglaa Hagag, Abd-elhafeez Samir, and Mohamed Hasan. 2014. 'Molecular Diversity Between Field Isolates and Vaccinal Strains of Avian Infectious Bronchitis Virus in Egypt Reference Laboratory for Veterinary Quality Control on Poultry Production ', 13 (5): 820–27.

Klumperman, J, J K Locker, A Meijer, M C Horzinek, H J Geuze, and P J Rottier. 1994. 'Coronavirus M Proteins Accumulate in the Golgi Complex beyond the Site of Virion Budding.' *Journal of Virology* 68 (10): 6523–34.

Kong, Qingming M, Chunyi Y Xue, Xiangpeng P Ren, Chengwen W Zhang, Linlin L Li, Dingming M Shu, Yingzuo Z Bi, and Yongchang C Cao. 2010. 'Proteomic Analysis of Purified Coronavirus Infectious Bronchitis Virus Particles.' *Proteome Science* 8: 29.

Kottier, Sanneke A., David Cavanagh, And Paul Britton. 1995. 'Experimental Evidence of Recombination in Coronavirus Infectious Bronchitis Virus'.

Virology 213 (2): 569–80.

Kurien, Biji T, and R Hal Scofield. 2006. 'Western Blotting.' *Methods (San Diego, Calif.)* 38 (4): 283–93.

Lai, Stanley Perlman and Anderson, Larry J. 2007. 'Coronaviridae'. In *Fields Virology*, edited by Peter M. Knipe, David M.; Howley, 5th ed., 1306–36. Lippincott Williams & Wilkins.

Lai, Michael M.C., and David Cavanagh. 1997. 'The Molecular Biology of Coronaviruses'. In *Advances in Virus Research*, 48:1–100.

Li, Frank Q., James P. Tam, and Ding Xiang Liu. 2007. 'Cell Cycle Arrest and Apoptosis Induced by the Coronavirus Infectious Bronchitis Virus in the Absence of P53'. *Virology* 365 (2): 435–45.

Limjindaporn, Thawornchai, Wiyada Wongwiwat, Sansanee Noisakran, Chatchawan Srisawat, Janjuree Netsawang, Chunya Puttikhunt, Watchara Kasinrerk, *et al*. 2009. 'Interaction of Dengue Virus Envelope Protein with Endoplasmic Reticulum-Resident Chaperones Facilitates Dengue Virus Production'. *Biochemical and Biophysical Research Communications* 379 (2): 196–200.

Lisowska, Anna, Joanna Sajewicz-Krukowska, Alice Fusaro, Anna Pikula, and Katarzyna Domanska-Blicharz. 2017. 'First Characterization of a Middle-East GI-23 Lineage (Var2-like) of Infectious Bronchitis Virus in Europe'. *Virus Research* 242 (October): 43–48.

Liu, C., Yang Xiang, Huijun Liu, Y. Li, Yurong Tan, Xiaolin Zhu, Dan Zeng, Menglan Li, Liwen Zhang, and Xiaoqun Qin. 2010. 'Integrin 4 Was Downregulated on the Airway Epithelia of Asthma Patients'. *Acta Biochimica et Biophysica Sinica* 42 (8): 538–47.

Liu, Genmei, Lishan Lv, Lijuan Yin, Xiaoming Li, Dongu Luo, Kang Liu, Chunyi Xue, and Yongchang Cao. 2013. 'Assembly and Immunogenicity of Coronavirus-like Particles Carrying Infectious Bronchitis Virus M and S Proteins'. *Vaccine* 31 (47): 5524–30.

Liu, Shengwang, and Xiangang Kong. 2004. 'A New Genotype of Nephropathogenic Infectious Bronchitis Virus Circulating in Vaccinated and Non-Vaccinated Flocks in China'. *Avian Pathology* 33 (3): 321–27.

Lontok, Erik, Emily Corse, and Carolyn E Machamer. 2004. 'Intracellular Targeting Signals Contribute to Localization of Coronavirus Spike Proteins near the Virus Assembly Site'. *Journal of Virology* 78 (11): 5913–22.

Ma, Huijie, Yuhao Shao, Chuyang Sun, Zongxi Han, Xiaoli Liu, Hongbo Guo, Xiaozhen Liu, Xiangang Kong, and Shengwang Liu. 2012. 'Genetic Diversity of Avian Infectious Bronchitis Coronavirus in Recent Years in China'. *Avian Diseases* 56 (1): 15–28.

Machamer, Carolyn E, S A Mentone, John K Rose, and M G Farquhar. 1990. 'The E1 Glycoprotein of an Avian Coronavirus Is Targeted to the Cis Golgi Complex.' *Proceedings of the National Academy of Sciences of the United States of America* 87 (18): 6944–48.

Mahmood, Zana H., Rizgar R. Sleman, and Aumaid U. Uthman. 2011. 'Isolation and Molecular Characterization of Sul/01/09 Avian Infectious Bronchitis Virus, Indicates the Emergence of a New Genotype in the Middle East'. *Veterinary Microbiology* 150 (1–2): 21–27.

Maier, Helena J., Eleanor M. Cottam, Phoebe Stevenson-Leggett, Jessica A. Wilkinson, Christopher J. Harte, Tom Wileman, and Paul Britton. 2013. 'Visualizing the Autophagy Pathway in Avian Cells and Its Application to Studying Infectious Bronchitis Virus'. *Autophagy* 9 (4): 496–509.

Maier, Helena Jane, Erica Bickerton, and Paul Britton. 2015. *Coronaviruses*. Edited by Helena Jane Maier, Erica Bickerton, and Paul Britton. *Methods in Molecular Biology (Clifton, N.J.)*. Vol. 1282. Methods in Molecular Biology. New York, NY: Springer New York.

Mardani, K., A. H. Noormohammadi, P. Hooper, J. Ignjatovic, and G. F. Browning. 2008. 'Infectious Bronchitis Viruses with a Novel Genomic Organization'. *Journal of Virology* 82 (4): 2013–24.

Masters, Paul S. 2006. 'The Molecular Biology of Coronaviruses'. *Advances in Virus Research*. https://doi.org/10.1016/S0065-3527(06)66005-3.

Masters, Paul S., and Stanley Perlman. 2013. 'Fields Virology-Coronaviridae'. In *Fields Virology*, 825–58.

McBride, Ruth, Marjorie van Zyl, and Burtram C Fielding. 2014. 'The Coronavirus Nucleocapsid Is a Multifunctional Protein.' *Viruses* 6 (8): 2991–3018.

McLaughlin, Martin, and Koen Vandenbroeck. 2011. 'The Endoplasmic Reticulum Protein Folding Factory and Its Chaperones: New Targets for Drug Discovery?' *British Journal of Pharmacology* 162 (2): 328–45.

Mirazimi, Ali, Mikael Nilsson, and Lennart Svensson. 1998. 'The Molecular Chaperone Calnexin Interacts with the NSP4 Enterotoxin of Rotavirus in Vivo and in Vitro.' *Journal of Virology* 72 (11): 8705–9.

Mo, Mei-Lan, Meng Li, Bai-Cheng Huang, Wen-Sheng Fan, Ping Wei, Tian-Chao Wei, Qiu-Ying Cheng, Zheng-Ji Wei, and Ya-Hui Lang. 2013. 'Molecular Characterization of Major Structural Protein Genes of Avian Coronavirus Infectious Bronchitis Virus Isolates in Southern China.' *Viruses* 5 (12): 3007–20.

Mohajer Shojai, Tabassom, Arash Ghalyanchi Langeroudi, Vahid Karimi, Abbas Barin, and Naser Sadri. 2016. 'The Effect of Allium Sativum (Garlic) Extract on Infectious Bronchitis Virus in Specific Pathogen Free Embryonic Egg.' *Avicenna Journal of Phytomedicine* 6 (4): 458–267.

Mottet, A., And G. Tempio. 2017. 'Global Poultry Production: Current State and Future Outlook and Challenges'. *World's Poultry Science Journal* 73 (02): 245–56.

Munday, Diane C., Weining Wu, Nikki Smith, Jenna Fix, Sarah Louise Noton, Marie Galloux, Olivier Touzelet, *et al*. 2015. 'Interactome Analysis of the Human Respiratory Syncytial Virus RNA Polymerase Complex Identifies Protein Chaperones as Important Cofactors That Promote L-Protein Stability and RNA Synthesis'. Edited by D. S. Lyles. *Journal of Virology* 89 (2): 917–30.

Narayanan, K., A. Maeda, J. Maeda, and S. Makino. 2000. 'Characterization of the Coronavirus M Protein and Nucleocapsid Interaction in Infected Cells'. *Journal of Virology* 74 (17): 8127–34.

Neuman, Benjamin W., Gabriella Kiss, Andreas H. Kunding, David Bhella, M Fazil Baksh, Stephen Connelly, Ben Droese, *et al*. 2011. 'A Structural Analysis of M Protein in Coronavirus Assembly and Morphology'. *Journal of Structural Biology* 174 (1): 11–22.

Niemeyer, Daniela, Thomas Zillinger, Doreen Muth, Florian Zielecki, Gabor Horvath, Tasnim Suliman, Winfried Barchet, Friedemann Weber, Christian Drosten, and M. A. Muller. 2013. 'Middle East Respiratory Syndrome Coronavirus Accessory Protein 4a Is a Type I Interferon Antagonist'. *Journal of Virology* 87 (22): 12489–95.

OIE. 2018. 'Diseases, Infections And Infestations Listed By The OIE'.

Ong, Shao-En, Blagoy Blagoev, Irina Kratchmarova, Dan Bach Kristensen, Hanno Steen, Akhilesh Pandey, and Matthias Mann. 2002. 'Stable Isotope Labeling by Amino Acids in Cell Culture, SILAC, as a Simple and Accurate Approach to Expression Proteomics'. *Molecular & Cellular Proteomics* 1 (5): 376–86.

Otto, Andreas, Dörte Becher, and Frank Schmidt. 2014. 'Quantitative Proteomics in the Field of Microbiology'. *PROTEOMICS* 14 (4–5): 547–65.

Patterson, S., and R. W. Bingham. 1976. 'Electron Microscope Observations on the Entry of Avian Infectious Bronchitis Virus into Susceptible Cells'. *Arch Virol* 52 (3): 191–200.

Pollard, Thomas D., William C. Earnshaw, Jennifer Lippincott-Schwartz, and Graham T. Johnson. 2017. 'Cell Biology'. In *Cell Biology*, Third, 331–50. Elsevier.

Promkuntod, N., R. E W van Eijndhoven, G. de Vrieze, a. Gröne, and M. H. Verheije. 2014. 'Mapping of the Receptor-Binding Domain and Amino Acids Critical for Attachment in the Spike Protein of Avian Coronavirus Infectious Bronchitis Virus'. *Virology* 448: 26–32.

Rahman, S. Abd El, A. A. El-Kenawy, U. Neumann, G. Herrler, C. Winter. 2009. 'Comparative Analysis of the Sialic Acid Binding Activity and the Tropism for the Respiratory Epithelium of Four Different Strains of Avian Infectious Bronchitis Virus'. *Avian Pathology* 38 (1): 41–45.

Raj, G. Dhinakar, and R. C. Jones. 1997. 'Infectious Bronchitis Virus: Immunopathogenesis of Infection in the Chicken'. *Avian Pathology* 26 (4): 677–706.

Raman, Rahul, Kannan Tharakaraman, V Sasisekharan, and Ram Sasisekharan. 2016. 'Glycan–Protein Interactions in Viral Pathogenesis'.

Current Opinion in Structural Biology 40 (October): 153–62.

Rayamajhi, Vijay, Dipesh Dhakal, Amit Kumar Chaudhary, and Jae Kyung Sohng. 2018. 'Improved Production of 1-Deoxynojirymicin in Escherichia Coli through Metabolic Engineering'. *World Journal of Microbiology and Biotechnology* 34 (6): 77.

Repp, R., Teruko Tamura, C Bruce Boschek, H. Wege, Ralph T Schwarz, and H. Niemann. 1985. 'The Effects of Processing Inhibitors of N-Linked Oligosaccharides on the Intracellular Migration of Glycoprotein E2 of Mouse Hepatitis Virus and the Maturation of Coronavirus Particles.' *The Journal of Biological Chemistry* 260 (29): 15873–79.

Roekel, H. van, K. L. Bullis, O. S. Flint, and IVI. K. Clarke. 1941. 'Poultry Disease Control Service'.

Rose, David R. 2012. 'Structure, Mechanism and Inhibition of Golgi α-Mannosidase II.' *Current Opinion in Structural Biology* 22 (5): 558–62.

Rotilio, Domenico, Anna Della Corte, Marco D'Imperio, Walter Coletta, Simone Marcone, Cristian Silvestri, Lucia Giordano, Michela Di Michele, and Maria Benedetta Donati. 2012. 'Proteomics: Bases for Protein Complexity Understanding'. *Thrombosis Research* 129 (3): 257–62.

Ruch, Travis R, and Carolyn E Machamer. 2011. 'The Hydrophobic Domain of Infectious Bronchitis Virus E Protein Alters the Host Secretory Pathway and Is Important for Release of Infectious Virus.' *Journal of Virology* 85 (2): 675–85.

Ruch, Travis R, and Carolyn E Machamer. 2012a. 'The Coronavirus E Protein: Assembly and Beyond.' *Viruses* 4 (3): 363–82.

Ruch, Travis R, and Carolyn E Machamer. 2012b. 'A Single Polar Residue and Distinct Membrane Topologies Impact the Function of the Infectious

Bronchitis Coronavirus E Protein.' *PLoS Pathogens* 8 (5): e1002674.

Ruddock, L. W., and M. Molinari. 2006. 'N-Glycan Processing in ER Quality Control'. *Journal of Cell Science* 119 (21): 4373–80.

Sambrook, J, and David William Russell. 2001. *Molecular Cloning - Sambrook & Russel - Vol. 1, 2, 3*. *CSH Press*.

Sasaki, Kanae, and Hiderou Yoshida. 2015. 'Organelle Autoregulation--Stress Responses in the ER, Golgi, Mitochondria and Lysosome'. *Journal of Biochemistry* 157 (4): 185–95.

Sawicki, Stanley G., Dorothea L Sawicki, and Stuart G Siddell. 2007. 'A Contemporary View of Coronavirus Transcription'. *Journal of Virology* 81 (1): 20–29.

Schalk, A. F., and M. C. Hawn. 1931. 'An Apparently New Respiratory Disease of Baby Chicks.' *J. Am. Vet. Med. Assoc* 78 (19): 186.

Schrag, Joseph D., John J.M. Bergeron, Yunge Li, Svetlana Borisova, Michael Hahn, David Y. Thomas, and Miroslaw Cygler. 2001. 'The Structure of Calnexin, an ER Chaperone Involved in Quality Control of Protein Folding'. *Molecular Cell* 8 (3): 633–44.

Shang, Jian, Yuan Zheng, Yang Yang, Chang Liu, Qibin Geng, Chuming Luo, Wei Zhang, and Fang Li. 2018. 'Cryo-EM Structure of Infectious Bronchitis Coronavirus Spike Protein Reveals Structural and Functional Evolution of Coronavirus Spike Proteins.' *PLoS Pathogens* 14 (4): e1007009.

Shao, Wenhan, Xinxin Li, Mohsan Goraya, Song Wang, and Ji-Long Chen. 2017. 'Evolution of Influenza A Virus by Mutation and Re-Assortment'. *International Journal of Molecular Sciences* 18 (8): 1650.

Sheets, R. 2000. 'History and Characterization of the Vero Cell Line.' *Vaccines and Related Products Advisory Committee*, 1–12.

Shen, S., Y. C. Law, and D. X. Liu. 2004. 'A Single Amino Acid Mutation in the Spike Protein of Coronavirus Infectious Bronchitis Virus Hampers Its Maturation and Incorporation into Virions at the Nonpermissive Temperature'. *Virology* 326 (2): 288–98.

Spaan, W, D Cavanagh, and M Horzinek. 1988. 'Coronaviruses: Structure and Genome Expression'. *J. Gen. Virol* 69: 2939–52.

Spencer, Kelly-Anne, Michael Dee, Paul Britton, and Julian A Hiscox. 2008. 'Role of Phosphorylation Clusters in the Biology of the Coronavirus Infectious Bronchitis Virus Nucleocapsid Protein.' *Virology* 370 (2): 373–81.

Spencer, Kelly-Anne, and Julian A. Hiscox. 2006. 'Characterisation of the RNA Binding Properties of the Coronavirus Infectious Bronchitis Virus Nucleocapsid Protein Amino-Terminal Region'. *FEBS Letters* 580 (25): 5993–98.

Stanley, Pamela. 2011. 'Golgi Glycosylation'. *Cold Spring Harbor Perspectives in Biology* 3 (4): a005199–a005199.

Stanley, Pamela, Naoyuki Taniguchi, and Markus Aebi. 2015. 'N-Glycans'. *Essentials of Glycobiology*, 1–14.

Stern, D F, and B M Sefton. 1982. 'Coronavirus Proteins - Structure and Function of the Oligosaccharides of the Avian Infectious-Bronchitis Virus Glycoproteins'. *Journal of Virology* 44 (3): 804–12.

Takasu, Soo, Isabella Supardi Parida, Shinji Onose, Junya Ito, Ryoichi Ikeda, Kenji Yamagishi, Oki Higuchi, *et al*. 2018. 'Evaluation of the Anti-Hyperglycemic Effect and Safety of Microorganism 1-Deoxynojirimycin'.

Edited by Tatsuo Shimosawa. *PLOS ONE* 13 (6): e0199057.

Tatu, U, and A Helenius. 1997. 'Interactions between Newly Synthesized Glycoproteins, Calnexin and a Network of Resident Chaperones in the Endoplasmic Reticulum.' *The Journal of Cell Biology* 136 (3): 555–65.

To, Janet, Wahyu Surya, To Sing Fung, Yan Li, Carmina Verdià-Bàguena, Maria Queralt-Martin, Vicente M Aguilella, Ding Xiang Liu, and Jaume Torres. 2017. 'Channel-Inactivating Mutations and Their Revertant Mutants in the Envelope Protein of Infectious Bronchitis Virus'. Edited by Stanley Perlman. *Journal of Virology* 91 (5): e02158-16.

Trevor, Bagust . J. 2013. 'Poultry Health and Disease Control in Developing Countries'. https://doi.org/10.1016/B978-0-444-59397-9.00010-4.

Trinkle-Mulcahy, Laura. 2012. 'Resolving Protein Interactions and Complexes by Affinity Purification Followed by Label-Based Quantitative Mass Spectrometry'. *Proteomics* 12 (10): 1623–38.

Tyrrell, Beatrice Ellen, Andrew Cameron Sayce, Kelly Lyn Warfield, Joanna Louise Miller, and Nicole Zitzmann. 2017. 'Iminosugars: Promising Therapeutics for Influenza Infection.' *Critical Reviews in Microbiology* 43 (5): 521–45.

Ujike, Makoto, and Fumihiro Taguchi. 2015. 'Incorporation of Spike and Membrane Glycoproteins into Coronavirus Virions'. *Viruses* 7 (4): 1700–1725.

Ulferts, Rachel, and John Ziebuhr. 2011. 'Nidovirus Ribonucleases: Structures and Functions in Viral Replication'. *RNA Biology* 8 (2): 295–304.

USDA/ FAS. 2018. 'Livestock and Poultry: World Markets and Trade'.

USDA/ NASS. 2018. ‘Poultry-Production and Value 2017 Summary’.

Välikangas, Tommi, Tomi Suomi, and Laura L. Elo. 2017. ‘A Comprehensive Evaluation of Popular Proteomics Software Workflows for Label-Free Proteome Quantification and Imputation’. *Briefings in Bioinformatics*, no. March: 1–12.

Venkatagopalan, Pavithra, Sasha M. Daskalova, Lisa A. Lopez, Kelly A. Dolezal, and Brenda G. Hogue. 2015. ‘Coronavirus Envelope (E) Protein Remains at the Site of Assembly.’ *Virology* 478 (April): 75–85.

Vigerust, David J., and Virginia L. Shepherd. 2007. ‘Virus Glycosylation: Role in Virulence and Immune Interactions’. *Trends in Microbiology* 15 (5): 211–18.

Vogels, Mijke W., Bas W M Van Balkom, Dora V. Kaloyanova, Joseph J. Batenburg, Albert J. Heck, J. Bernd Helms, Peter J M Rottier, and Cornelis A M De Haan. 2011. ‘Identification of Host Factors Involved in Coronavirus Replication by Quantitative Proteomics Analysis’. *Proteomics* 11 (1): 64–80.

Wang, Dandan, Jing Liang, Yu Zhang, Bin Gui, Feng Wang, Xia Yi, Luyang Sun, Zhi Yao, and Yongfeng Shang. 2012. ‘Steroid Receptor Coactivator-Interacting Protein (SIP) Inhibits Caspase-Independent Apoptosis by Preventing Apoptosis-Inducing Factor (AIF) from Being Released from Mitochondria.’ *The Journal of Biological Chemistry* 287 (16): 12612–21.

Wang, Huan, Yingjie Sun, Xiang Mao, Chunchun Meng, Lei Tan, Cuiping Song, Xusheng Qiu, Ding , Chan, and Ying Liao. 2018. ‘Infectious Bronchitis Virus Attaches to Lipid Rafts and Enters Cells via Clathrin Mediated Endocytosis’. *BioRxiv*, June, 352898.

Wang, Jibin, Shouguo Fang, Han Xiao, Bo Chen, James P. Tam, and Ding Xiang Liu. 2009. 'Interaction of the Coronavirus Infectious Bronchitis Virus Membrane Protein with β-Actin and Its Implication in Virion Assembly and Budding'. Edited by Dong-Yan Jin. *PLoS ONE* 4 (3): e4908.

Wang, Weixun, Christopher H Becker, Haihong Zhou, Hua Lin, Sushmita Roy, Thomas A Shaler, Lander R Hill, Scott Norton, Praveen Kumar, and Markus Anderle. 2003. 'Quantification of Proteins and Metabolites by Mass Spectrometry without Isotopic Labeling or Spiked Standards'. *Analytical Chemistry* 75 (18): 4818–26.

Werr, Margaret, and Reinhild Prange. 1998. 'Role for Calnexin and N-Linked Glycosylation in the Assembly and Secretion of Hepatitis B Virus Middle Envelope Protein Particles.' *Journal of Virology* 72 (1): 778–82.

Westerbeck, Jason W., and Carolyn E. Machamer. 2015. 'A Coronavirus E Protein Is Present in Two Distinct Pools with Different Effects on Assembly and the Secretory Pathway.' *Journal of Virology* 89 (18): 9313–23.

Wickramasinghe, I N Ambepitiya, R P de Vries, a Gröne, C a M de Haan, and M H Verheije. 2011. 'Binding of Avian Coronavirus Spike Proteins to Host Factors Reflects Virus Tropism and Pathogenicity.' *Journal of Virology* 85 (17): 8903–12.

Wickramasinghe, Iresha N Ambepitiya, Robert P de Vries, Amber M Eggert, Nantaporn Wandee, Cornelis A M de Haan, Andrea Gröne, and Monique H Verheije. 2015. 'Host Tissue and Glycan Binding Specificities of Avian Viral Attachment Proteins Using Novel Avian Tissue Microarrays.' *PloS One* 10 (6): e0128893.

Wickramasinghe, Iresha N, S. J. van Beurden, E A W S Weerts, and M. H. Verheije. 2014. 'The Avian Coronavirus Spike Protein.' *Virus Research*

194 (December): 37–48.

Winter, Christine, Christel Schwegmann-Weßels, Dave Cavanagh, Ulrich Neumann, and Georg Herrler. 2006. 'Sialic Acid Is a Receptor Determinant for Infection of Cells by Avian Infectious Bronchitis Virus'. *Journal of General Virology* 87 (5): 1209–16.

Winter, Christine, Christel Schwegmann-Wessels, Ulrich Neumann, and Georg Herrler. 2008. 'The Spike Protein of Infectious Bronchitis Virus Is Retained Intracellularly by a Tyrosine Motif.' *Journal of Virology* 82 (6): 2765–71.

Wit, J. J. de, Jane K. A. Cook, and Harold M. J. F. van der Heijden. 2011. 'Infectious Bronchitis Virus Variants: A Review of the History, Current Situation and Control Measures'. *Avian Pathology* 40 (3): 223–35.

Wong, Jason W. H., and Gerard Cagney. 2010. 'An Overview of Label-Free Quantitation Methods in Proteomics by Mass Spectrometry'. In , 273–83. Humana Press.

Wu, Weining, Kim C Tran, Michael N Teng, Kate J Heesom, David A Matthews, John N Barr, and Julian A Hiscox. 2012. 'The Interactome of the Human Respiratory Syncytial Virus NS1 Protein Highlights Multiple Effects on Host Cell Biology.' *Journal of Virology* 86 (15): 7777–89.

Wurm, T, H Chen, T Hodgson, P Britton, G Brooks, and J A Hiscox. 2001. 'Localization to the Nucleolus Is a Common Feature of Coronavirus Nucleoproteins, and the Protein May Disrupt Host Cell Division'. *Journal of Virology* 75 (19): 9345–56.

Xie, Qingmei, Jun Ji, Jingwei Xie, Feng Chen, Manshan Cai, Baoli Sun, Chunyi Xue, Jingyun Ma, and Yingzuo Bi. 2011. 'Epidemiology and Immunoprotection of Nephropathogenic Avian Infectious Bronchitis Virus in Southern China'. *Virology Journal* 8 (1): 484.

Xue, Yu, Qingmei Xie, Zhuanqiang Yan, Jun Ji, Feng Chen, Jianping Qin, Baoli Sun, Jingyun Ma, and Yingzuo Bi. 2012. 'Complete Genome Sequence of a Recombinant Nephropathogenic Infectious Bronchitis Virus Strain in China.' *Journal of Virology* 86 (24): 13812–13.

Yang, Zhiwei, Nan Wu, Yuangang Zu, and Yujie Fu. 2011. 'Comparative Anti-Infectious Bronchitis Virus (IBV) Activity of (-)-Pinene: Effect on Nucleocapsid (N) Protein.' *Molecules (Basel, Switzerland)* 16 (2): 1044–54.

Youn, Soonjeon, Ellen W Collisson, and Carolyn E Machamer. 2005. 'Contribution of Trafficking Signals in the Cytoplasmic Tail of the Infectious Bronchitis Virus Spike Protein to Virus Infection.' *Journal of Virology* 79 (21): 13209–17.

Yu, F., F. Qiu, and J. Meza. 2016. 'Design and Statistical Analysis of Mass-Spectrometry-Based Quantitative Proteomics Data'. In *Proteomic Profiling and Analytical Chemistry: The Crossroads: Second Edition*, 211–37. Elsevier.

Zhang, Ming, Brian Gaschen, Wendy Blay, Brian Foley, Nancy Haigwood, Carla Kuiken, and Bette Korber. 2004. 'Tracking Global Patterns of N-Linked Glycosylation Site Variation in Highly Variable Viral Glycoproteins: HIV, SIV, and HCV Envelopes and Influenza Hemagglutinin'. *Glycobiology*.

Zhao, Xuesen, Fang Guo, Mary Ann Comunale, Anand Mehta, Mohit Sehgal, Pooja Jain, Andrea Cuconati, *et al*. 2015. 'Inhibition of Endoplasmic Reticulum-Resident Glucosidases Impairs Severe Acute Respiratory Syndrome Coronavirus and Human Coronavirus NL63 Spike Protein-Mediated Entry by Altering the Glycan Processing of Angiotensin I-Converting Enzyme 2'. *Antimicrobial Agents and Chemotherapy* 59 (1): 206–16.

Zheng, Jie, Yoshiyuki Yamada, To Sing Fung, Mei Huang, Raymond Chia, and Ding Xiang Liu. 2018. 'Identification of N-Linked Glycosylation Sites in the Spike Protein and Their Functional Impact on the Replication and Infectivity of Coronavirus Infectious Bronchitis Virus in Cell Culture'. *Virology* 513 (January): 65–74.

Zhong, Yanxin, Yong Wah Tan, and Ding Xiang Liu. 2016. 'Recent Progress in Studies of Arterivirus- and Coronavirus-Host Interactions'. *Viruses*.

Zhu, Lu, Apostolos Malatras, Matthew Thorley, Idonnya Aghoghogbe, Arvind Mer, Stéphanie Duguez, Gillian Butler-Browne, Thomas Voit, and William Duddy. 2015. 'CellWhere: Graphical Display of Interaction Networks Organized on Subcellular Localizations'. *Nucleic Acids Research*.

Zhu, Z., Y. Xu, J. Zhao, Q. Liu, W. Feng, J. Fan, and P. Wang. 2015. 'MiR-367 Promotes Epithelial-to-Mesenchymal Transition and Invasion of Pancreatic Ductal Adenocarcinoma Cells by Targeting the Smad7-TGF-β Signalling Pathway'. *British Journal of Cancer*.

Ziebuhr, John, Eric J. Snijder, and Alexander E. Gorbalenya. 2000. 'Virus-Encoded Proteinases and Proteolytic Processing in the Nidovirales'. *Journal of General Virology* 81 (4): 853–79.

Chapter 8

Appendix

Appendix 1

Image Report: dnj-s pb_3+dnj-s pb_4

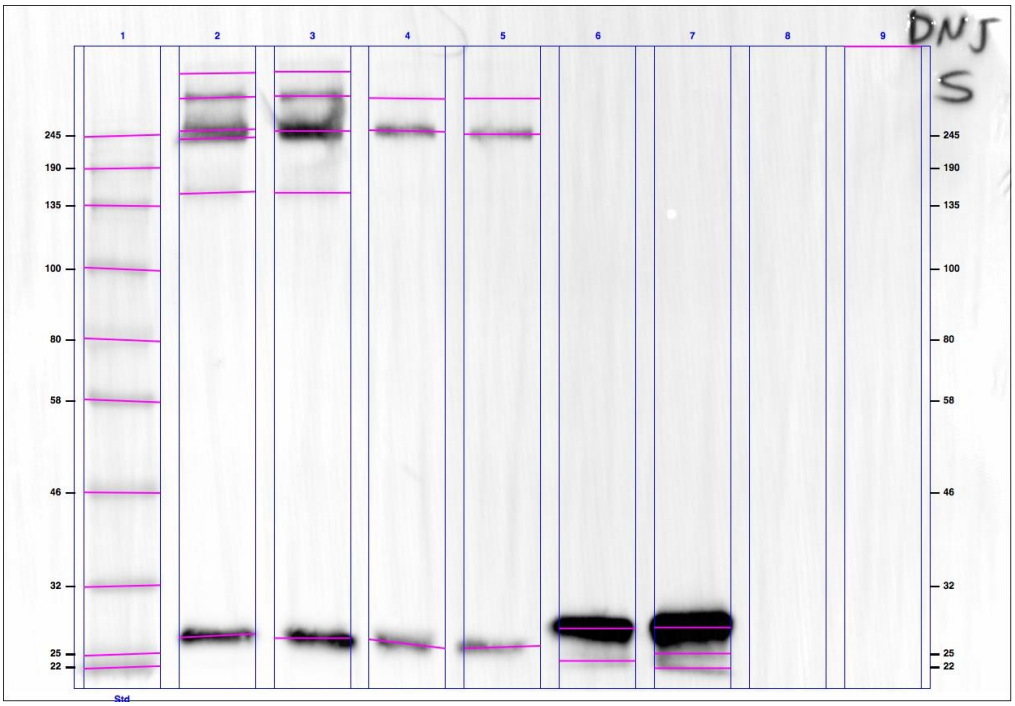

/Users/zana/Google Drive/PhD Liverpool/Year 4/My Thesis/Chapter 5/Drug WB 293T Figures/dnj-s pb_3+dnj-s pb_4.scn

Acquisition Information

Imager	Merged Image

Image Information

Acquisition Date	05/10/2018 3:35 pm
User Name	Zana
Image Area (mm)	X: 85.4 Y: 58.1
Pixel Size (um)	X: 68.9 Y: 68.9
Data Range (Int)	117 - 35309

Notes

Merged images:
Image 1: dnj-s pb_3
Image 2: dnj-s pb_4

Analysis Settings

Detection	Lane detection: Manually created lanes Band detection:

	Automatically detected bands with custom sensitivity: 100 Lane Background Subtraction: Lane background subtracted with disk size: 10 Lane width: 6.48 mm
Mol. Weight Analysis	Standard: NEB P7712 Standard lanes: first Regression method: Point to Point (semi-log)

Lane And Band Analysis

Lane 1 - NEB P7712

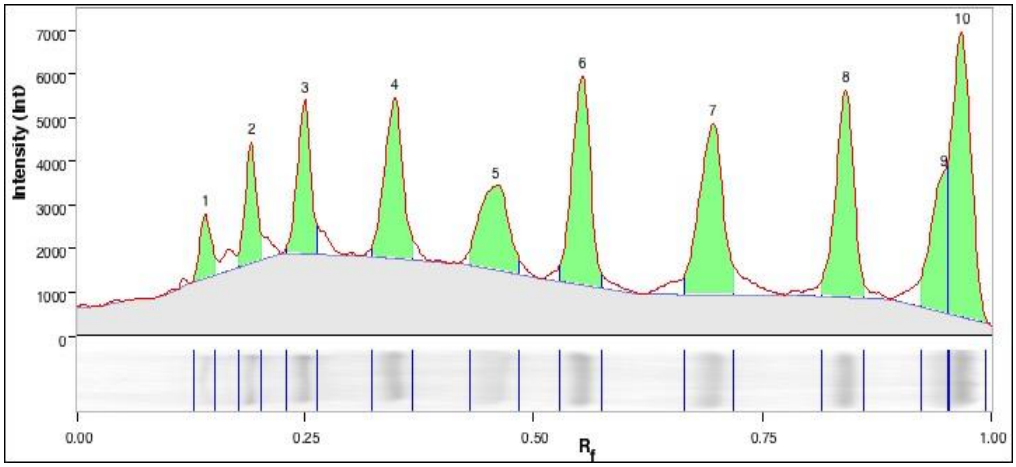

Band No.	Band Label	Mol. Wt. (KDa)	Relative Front	Volume (Int)	Abs. Quant.	Rel. Quant.	Band %	Lane %
1		245.0	0.140	1,776,412	N/A	N/A	2.5	2.3
2		190.0	0.191	3,368,866	N/A	N/A	4.7	4.3
3		135.0	0.249	5,072,240	N/A	N/A	7.1	6.5
4		100.0	0.348	7,221,738	N/A	N/A	10.2	9.3
5		80.0	0.458	5,974,546	N/A	N/A	8.4	7.7
6		58.0	0.552	9,438,916	N/A	N/A	13.3	12.1
7		46.0	0.695	9,921,512	N/A	N/A	14.0	12.7
8		32.0	0.841	9,325,176	N/A	N/A	13.1	12.0
9		25.0	0.947	5,639,718	N/A	N/A	7.9	7.2
10		22.0	0.967	13,209,350	N/A	N/A	18.6	16.9

Band Detection	Automatically detected bands with custom sensitivity: 100
Lane Background	Lane background subtracted with disk size: 10
Lane Width	6.48 mm
Regression Equation	A single equation is not available for this method

Lane 2

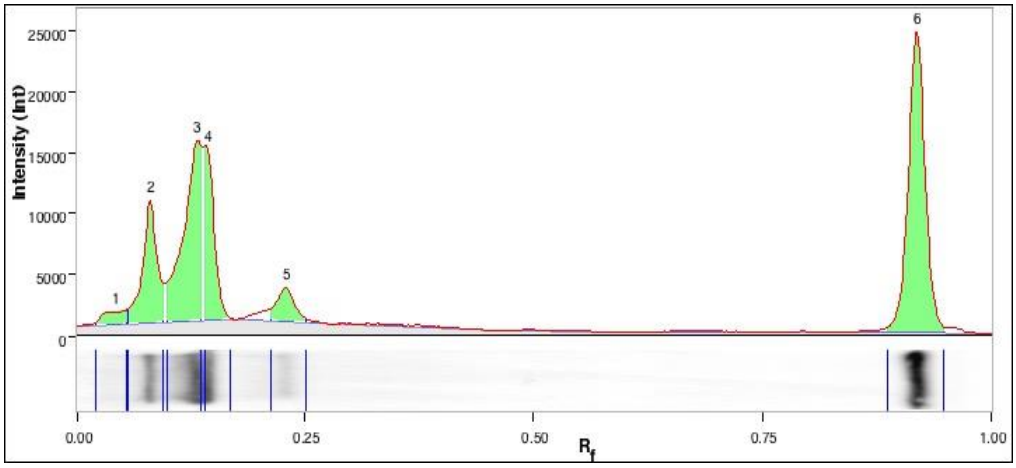

Band No.	Band Label	Mol. Wt. (KDa)	Relative Front	Volume (Int)	Abs. Quant.	Rel. Quant.	Band %	Lane %
1		245.0	0.043	2,749,782	N/A	N/A	2.5	2.3
2		245.0	0.081	15,678,824	N/A	N/A	14.2	13.0
3		245.0	0.131	27,678,770	N/A	N/A	25.0	23.0
4		240.4	0.144	14,596,226	N/A	N/A	13.2	12.1
5		152.0	0.229	5,297,558	N/A	N/A	4.8	4.4
6		26.7	0.918	44,496,686	N/A	N/A	40.3	37.0

Band Detection	Automatically detected bands with custom sensitivity: 100
Lane Background	Lane background subtracted with disk size: 10
Lane Width	6.48 mm
Regression Equation	A single equation is not available for this method

Lane 3

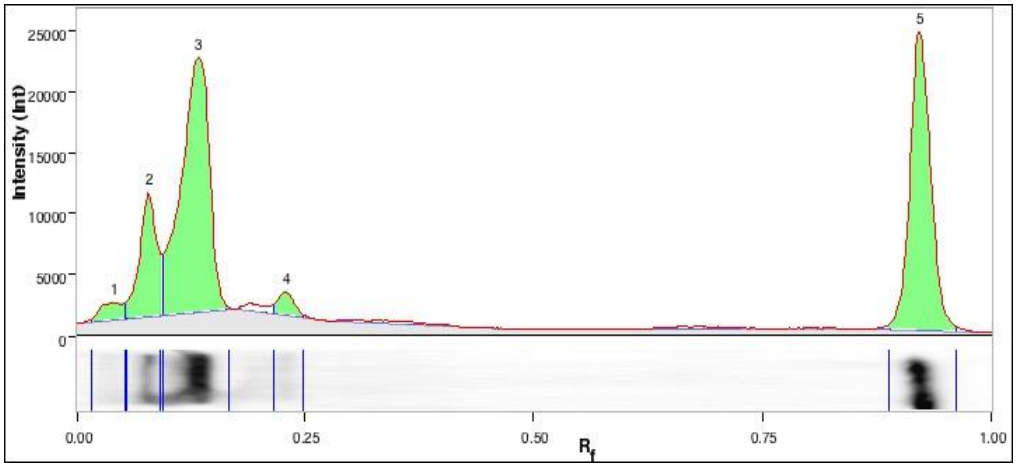

Band No.	Band Label	Mol. Wt. (KDa)	Relative Front	Volume (Int)	Abs. Quant.	Rel. Quant.	Band %	Lane %
1		245.0	0.040	3,405,338	N/A	N/A	2.5	2.4
2		245.0	0.078	17,533,444	N/A	N/A	13.0	12.4
3		245.0	0.133	59,780,052	N/A	N/A	44.3	42.2

4		152.0	0.229	3,149,282	N/A	N/A	2.3	2.2
5		26.5	0.922	50,967,552	N/A	N/A	37.8	36.0

Band Detection	Automatically detected bands with custom sensitivity: 100
Lane Background	Lane background subtracted with disk size: 10
Lane Width	6.48 mm
Regression Equation	A single equation is not available for this method

Lane 4

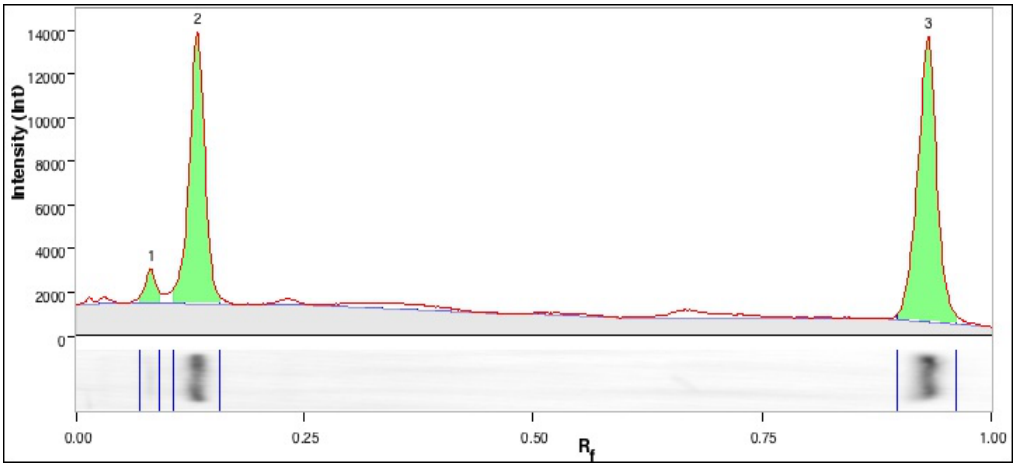

Band No.	Band Label	Mol. Wt. (KDa)	Relative Front	Volume (Int)	Abs. Quant.	Rel. Quant.	Band %	Lane %
1		245.0	0.082	1,719,730	N/A	N/A	3.8	3.2
2		245.0	0.133	19,183,520	N/A	N/A	42.1	36.0
3		26.0	0.930	24,610,234	N/A	N/A	54.1	46.2

Band Detection	Automatically detected bands with custom sensitivity: 100
Lane Background	Lane background subtracted with disk size: 10
Lane Width	6.48 mm
Regression Equation	A single equation is not available for this method

Lane 5

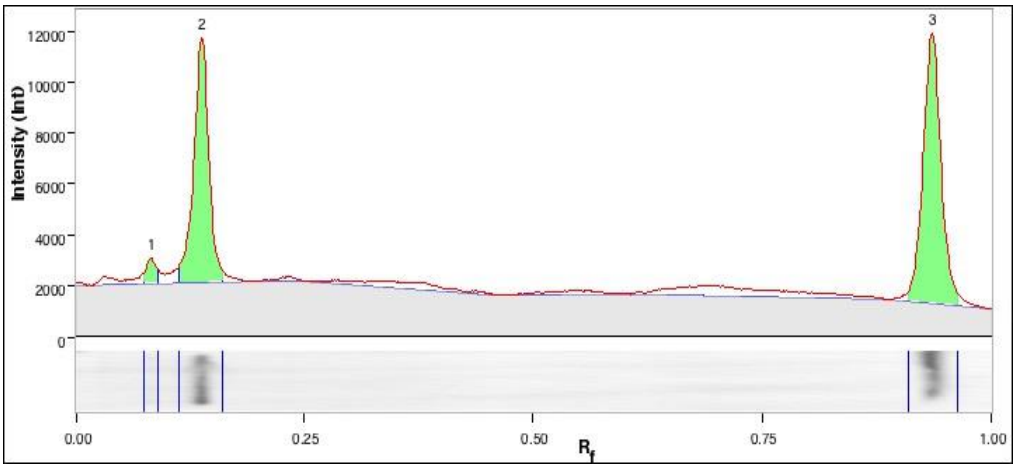

Band No.	Band Label	Mol. Wt. (KDa)	Relative Front	Volume (Int)	Abs. Quant.	Rel. Quant.	Band %	Lane %
1		245.0	0.082	954,288	N/A	N/A	2.9	2.2
2		245.0	0.138	13,916,136	N/A	N/A	42.1	31.6
3		25.7	0.936	18,191,256	N/A	N/A	55.0	41.3

Band Detection	Automatically detected bands with custom sensitivity: 100
Lane Background	Lane background subtracted with disk size: 10
Lane Width	6.48 mm
Regression Equation	A single equation is not available for this method

Lane 6

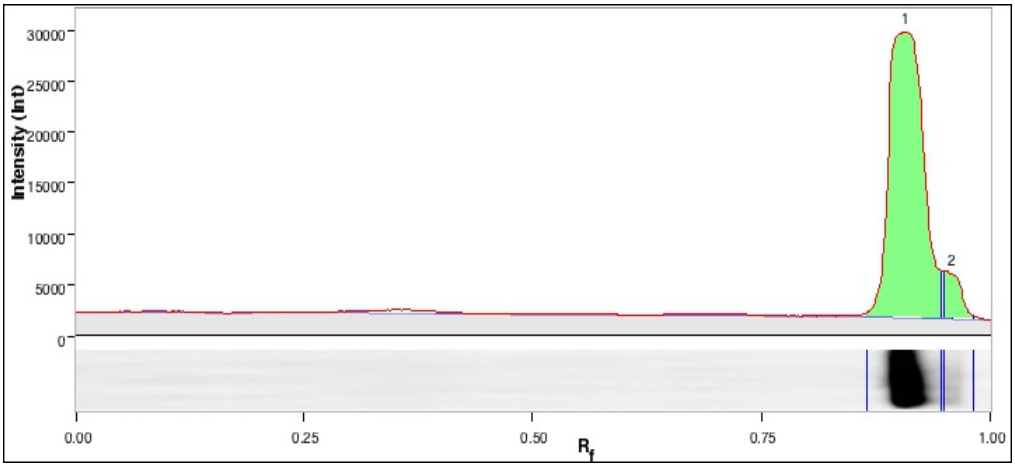

Band No.	Band Label	Mol. Wt. (KDa)	Relative Front	Volume (Int)	Abs. Quant.	Rel. Quant.	Band %	Lane %
1		27.5	0.906	104,903,060	N/A	N/A	92.7	85.9
2		23.5	0.957	8,275,572	N/A	N/A	7.3	6.8

Band Detection	Automatically detected bands with custom sensitivity: 100
Lane Background	Lane background subtracted with disk size: 10
Lane Width	6.48 mm
Regression Equation	A single equation is not available for this method

Lane 7

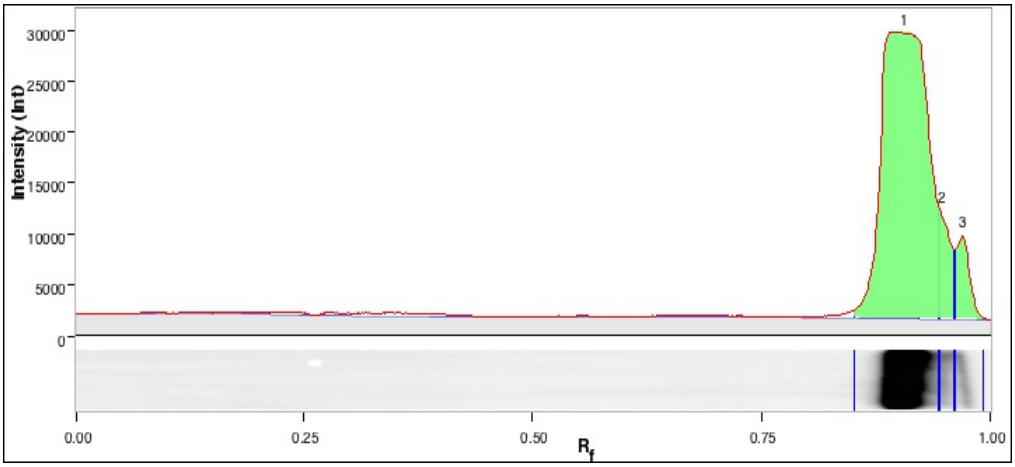

Band No.	Band Label	Mol. Wt. (KDa)	Relative Front	Volume (Int)	Abs. Quant.	Rel. Quant.	Band %	Lane %
1		27.5	0.905	144,327,130	N/A	N/A	85.6	80.4
2		25.1	0.946	12,549,188	N/A	N/A	7.4	7.0
3		22.0	0.968	11,813,074	N/A	N/A	7.0	6.6

Band Detection	Automatically detected bands with custom sensitivity: 100
Lane Background	Lane background subtracted with disk size: 10
Lane Width	6.48 mm
Regression Equation	A single equation is not available for this method

Lane 8

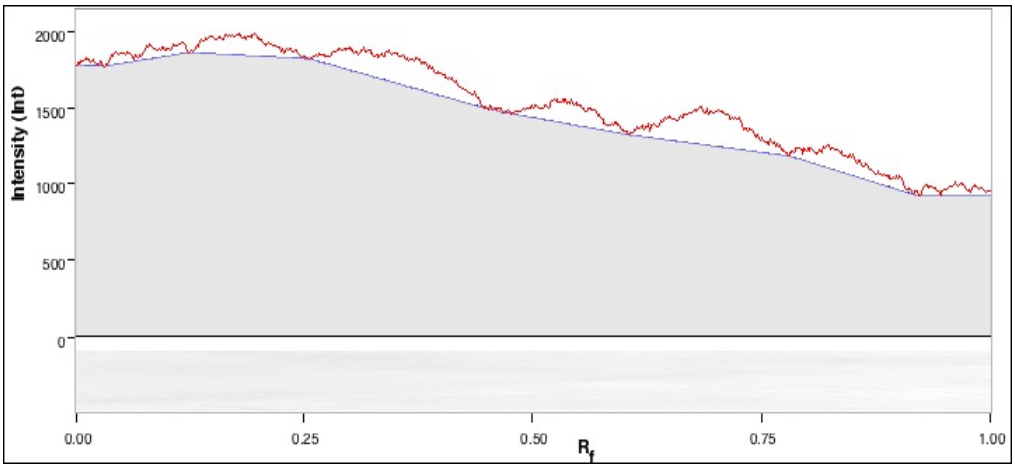

Band No.	Band Label	Mol. Wt. (KDa)	Relative Front	Volume (Int)	Abs. Quant.	Rel. Quant.	Band %	Lane %

Band Detection	Automatically detected bands with custom sensitivity: 100
Lane Background	Lane background subtracted with disk size: 10
Lane Width	6.48 mm
Regression Equation	A single equation is not available for this method

Lane 9

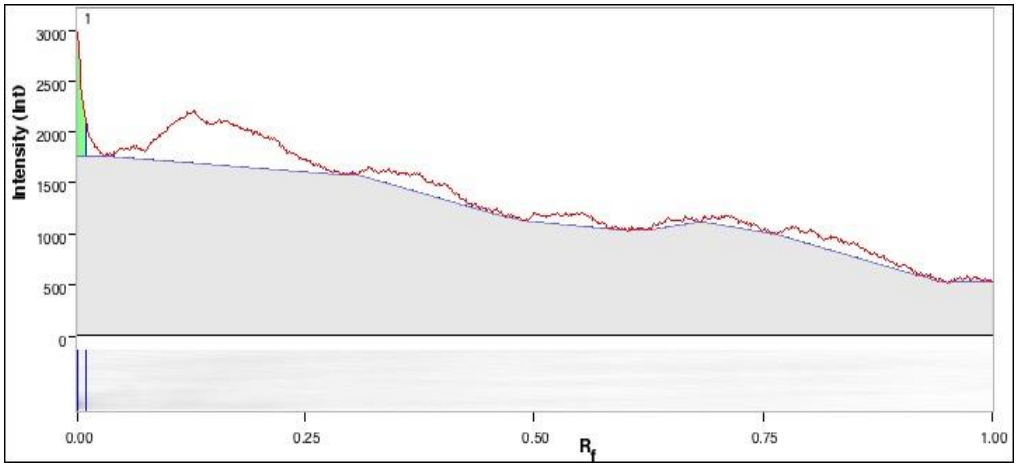

Band No.	Band Label	Mol. Wt. (KDa)	Relative Front	Volume (Int)	Abs. Quant.	Rel. Quant.	Band %	Lane %
1		245.0	0.001	609,590	N/A	N/A	100.0	6.0

Band Detection	Automatically detected bands with custom sensitivity: 100
Lane Background	Lane background subtracted with disk size: 10
Lane Width	6.48 mm
Regression Equation	A single equation is not available for this method

Appendix 2

Image Report: dmj-s pd_3+dmj-s pd_4

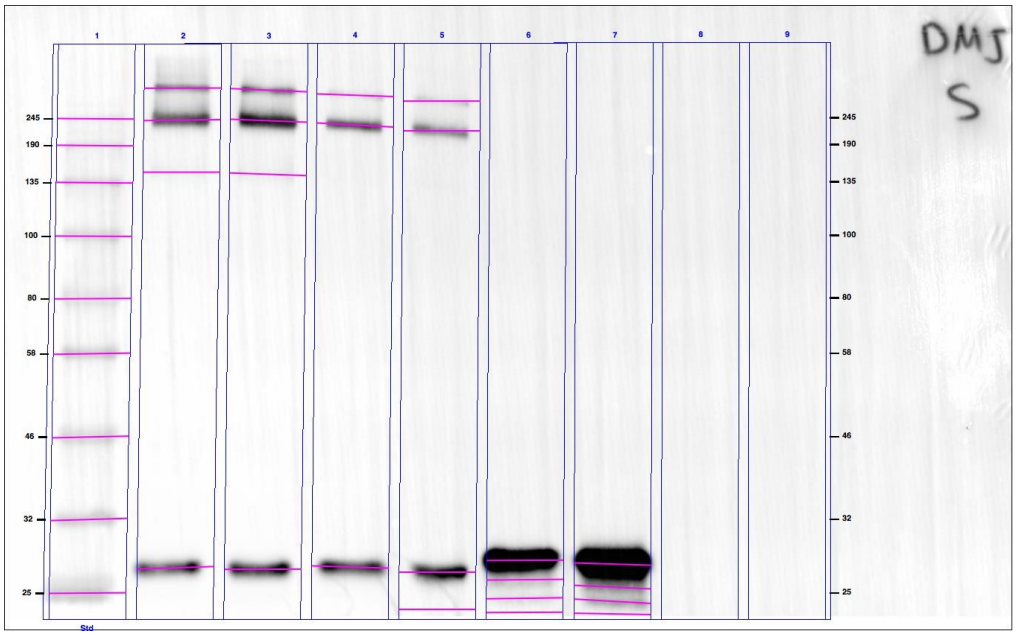

/Users/zana/Google Drive/PhD Liverpool/Year 4/My Thesis/Chapter 5/Drug WB 293T Figures/dmj-s pd_3+dmj-s pd_4.scn

Acquisition Information

Imager	Merged Image

Image Information

Acquisition Date	05/10/2018 3:38 pm
User Name	Zana
Image Area (mm)	X: 93.2 Y: 56.6
Pixel Size (um)	X: 68.9 Y: 68.9
Data Range (Int)	111 - 34578

Notes

Merged images:
Image 1: dmj-s pd_3
Image 2: dmj-s pd_4

Analysis Settings

Detection	Lane detection: Manually created lanes Band detection: Automatically detected bands with custom sensitivity: 100 Manually adjusted bands

	Lane Background Subtraction: Lane background subtracted with disk size: 10 Lane width: 7.10 mm
Mol. Weight Analysis	Standard: NEB P7712 Standard lanes: first Regression method: Point to Point (semi-log)

Lane And Band Analysis

Lane 1 - NEB P7712

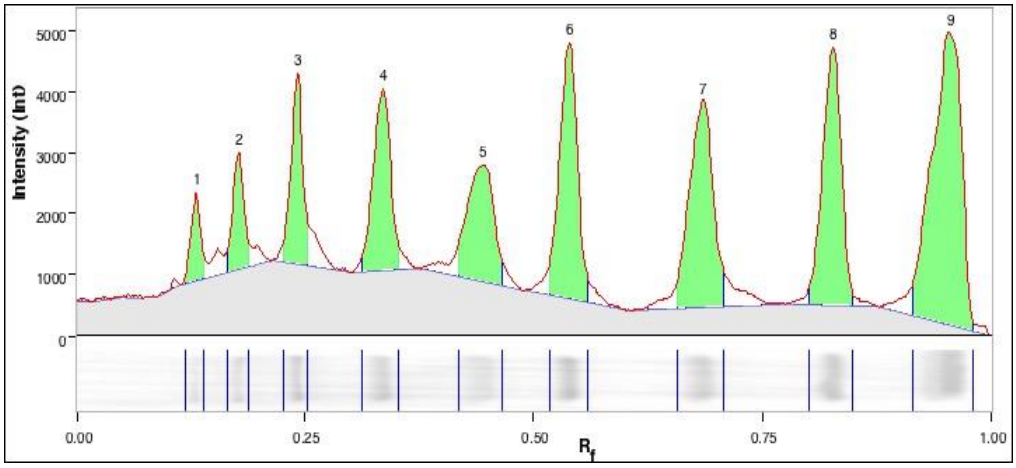

Band No.	Band Label	Mol. Wt. (KDa)	Relative Front	Volume (Int)	Abs. Quant.	Rel. Quant.	Band %	Lane %
1		245.0	0.130	1,446,429	N/A	N/A	2.5	2.3
2		190.0	0.177	2,275,785	N/A	N/A	4.0	3.5
3		135.0	0.242	3,830,158	N/A	N/A	6.6	6.0
4		100.0	0.335	5,431,190	N/A	N/A	9.4	8.4
5		80.0	0.443	5,309,753	N/A	N/A	9.2	8.3
6		58.0	0.539	7,839,124	N/A	N/A	13.6	12.2
7		46.0	0.683	8,356,390	N/A	N/A	14.5	13.0
8		32.0	0.827	8,335,275	N/A	N/A	14.5	13.0
9		25.0	0.955	14,777,204	N/A	N/A	25.7	23.0

Band Detection	Automatically detected bands with custom sensitivity: 100
Lane Background	Lane background subtracted with disk size: 10
Lane Width	7.10 mm
Regression Equation	A single equation is not available for this method

Lane 2

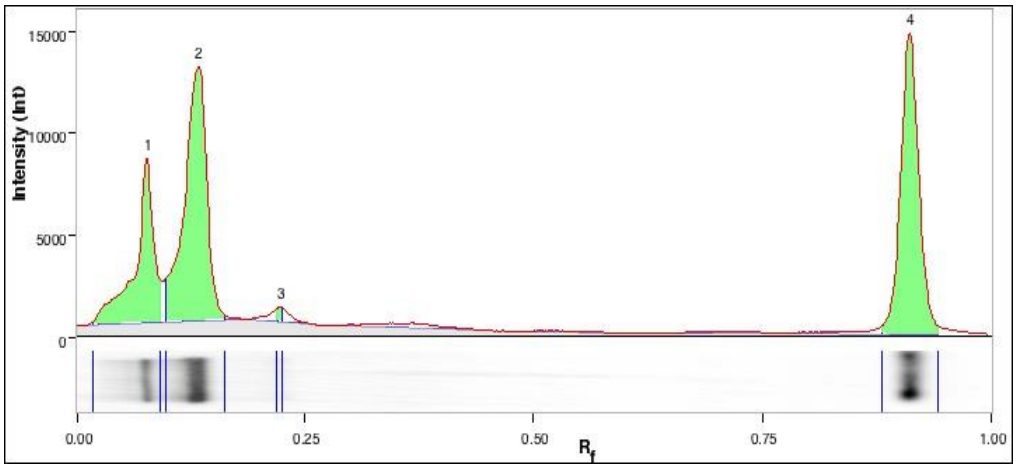

Band No.	Band Label	Mol. Wt. (KDa)	Relative Front	Volume (Int)	Abs. Quant.	Rel. Quant.	Band %	Lane %
1		245.0	0.078	19,560,215	N/A	N/A	21.2	19.5
2		241.6	0.133	36,836,405	N/A	N/A	39.8	36.6
3		148.6	0.224	557,745	N/A	N/A	0.6	0.6
4		27.2	0.911	35,502,761	N/A	N/A	38.4	35.3

Band Detection	Automatically detected bands with custom sensitivity: 100
Lane Background	Lane background subtracted with disk size: 10
Lane Width	7.10 mm
Regression Equation	A single equation is not available for this method

Lane 3

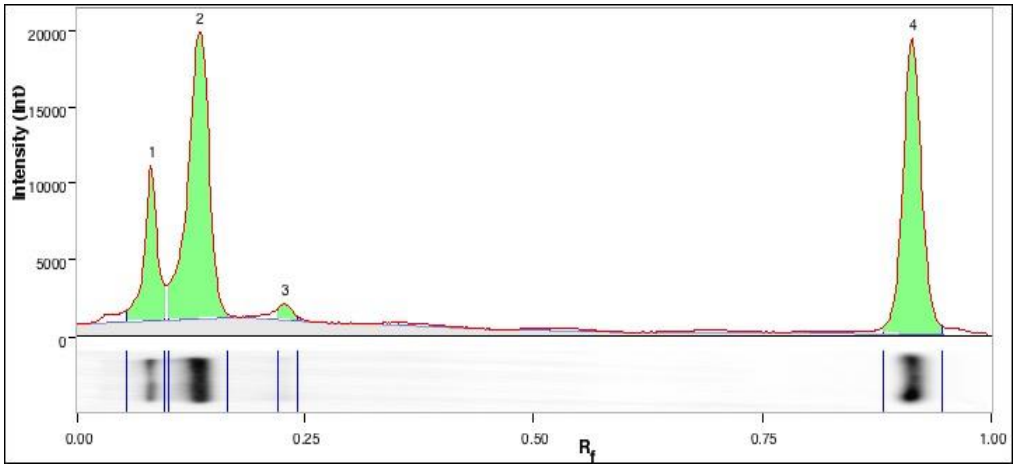

Band No.	Band Label	Mol. Wt. (KDa)	Relative Front	Volume (Int)	Abs. Quant.	Rel. Quant.	Band %	Lane %
1		245.0	0.081	15,868,283	N/A	N/A	14.7	13.5
2		239.9	0.134	47,586,206	N/A	N/A	44.1	40.6
3		145.5	0.227	1,638,421	N/A	N/A	1.5	1.4
4		27.1	0.913	42,696,178	N/A	N/A	39.6	36.4

Band Detection	Automatically detected bands with custom sensitivity: 100
Lane Background	Lane background subtracted with disk size: 10
Lane Width	7.10 mm
Regression Equation	A single equation is not available for this method

Lane 4

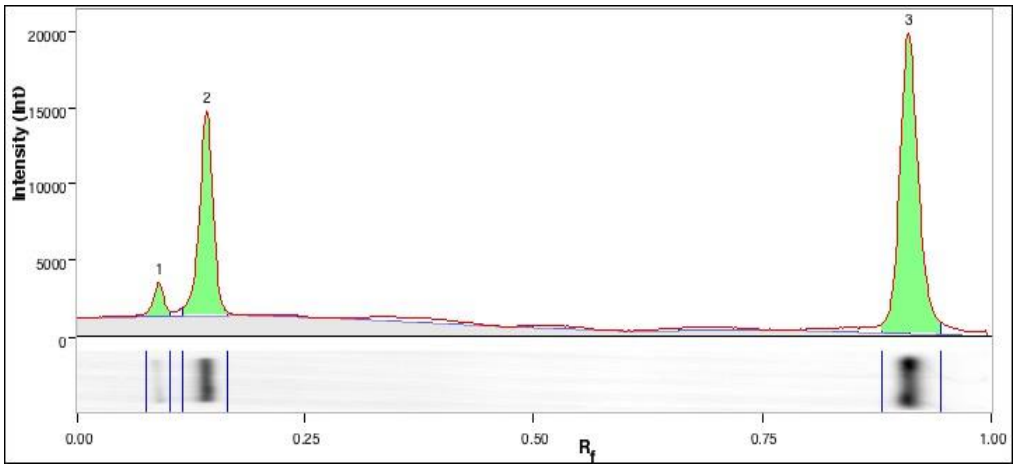

Band No.	Band Label	Mol. Wt. (KDa)	Relative Front	Volume (Int)	Abs. Quant.	Rel. Quant.	Band %	Lane %
1		245.0	0.090	2,791,094	N/A	N/A	4.1	3.5
2		229.9	0.142	21,866,694	N/A	N/A	32.2	27.4
3		27.3	0.910	43,342,812	N/A	N/A	63.7	54.3

Band Detection	Automatically detected bands with custom sensitivity: 100
Lane Background	Lane background subtracted with disk size: 10
Lane Width	7.10 mm
Regression Equation	A single equation is not available for this method

Lane 5

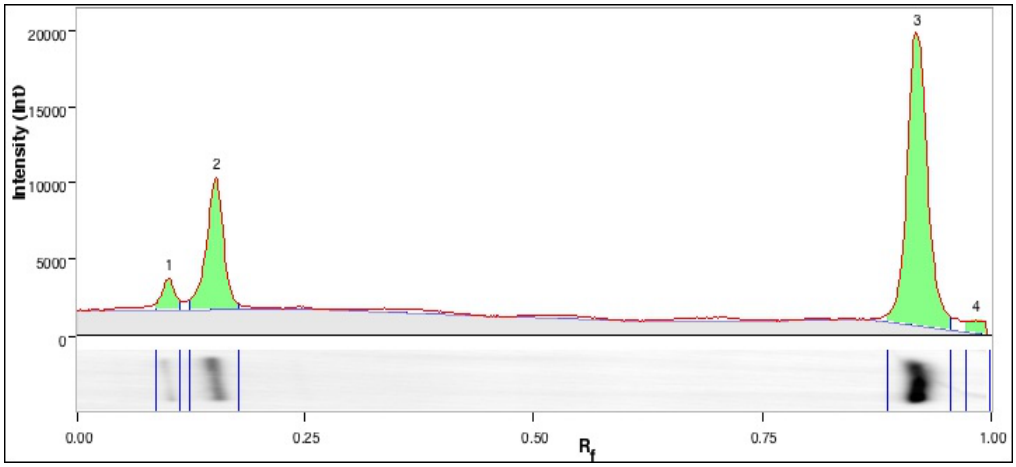

Band No.	Band Label	Mol. Wt. (KDa)	Relative Front	Volume (Int)	Abs. Quant.	Rel. Quant.	Band %	Lane %
1		245.0	0.101	3,108,643	N/A	N/A	4.6	4.0
2		217.3	0.152	17,151,560	N/A	N/A	25.4	22.1
3		26.8	0.919	45,490,465	N/A	N/A	67.4	58.7
4		25.0	0.983	1,694,762	N/A	N/A	2.5	2.2

Band Detection	Automatically detected bands with custom sensitivity: 100
Lane Background	Lane background subtracted with disk size: 10
Lane Width	7.10 mm
Regression Equation	A single equation is not available for this method

Lane 6

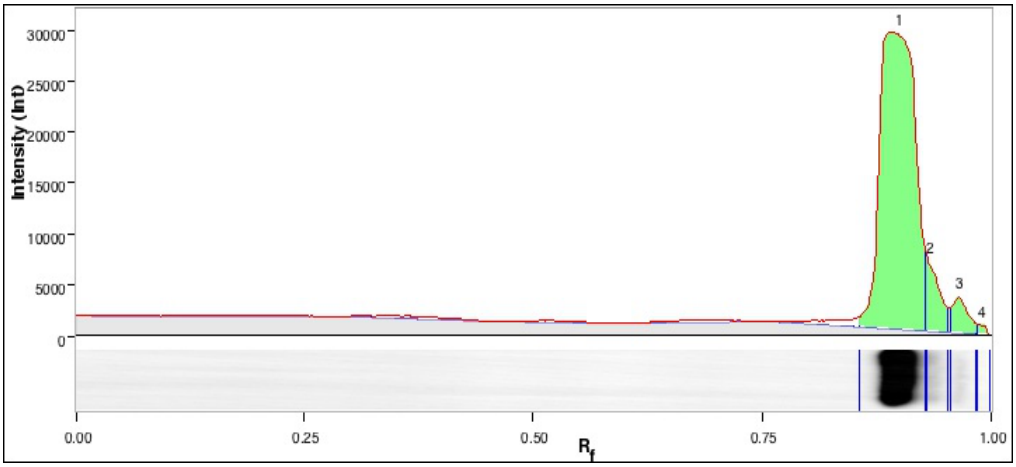

Band No.	Band Label	Mol. Wt. (KDa)	Relative Front	Volume (Int)	Abs. Quant.	Rel. Quant.	Band %	Lane %
1		27.9	0.898	114,537,545	N/A	N/A	86.9	80.1
2		26.1	0.932	10,278,576	N/A	N/A	7.8	7.2
3		25.0	0.964	6,033,946	N/A	N/A	4.6	4.2
4		25.0	0.988	896,512	N/A	N/A	0.7	0.6

Band Detection	Automatically detected bands with custom sensitivity: 100
Lane Background	Lane background subtracted with disk size: 10
Lane Width	7.10 mm
Regression Equation	A single equation is not available for this method

Lane 7

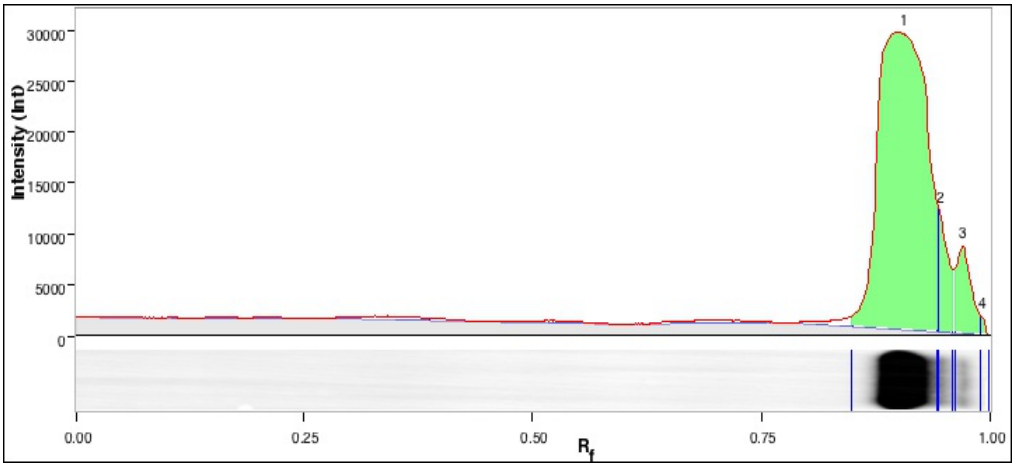

Band No.	Band Label	Mol. Wt. (KDa)	Relative Front	Volume (Int)	Abs. Quant.	Rel. Quant.	Band %	Lane %
1		27.5	0.905	162,595,388	N/A	N/A	85.0	79.8
2		25.5	0.945	13,429,758	N/A	N/A	7.0	6.6
3		25.0	0.969	14,498,383	N/A	N/A	7.6	7.1
4		25.0	0.991	844,188	N/A	N/A	0.4	0.4

Band Detection	Automatically detected bands with custom sensitivity: 100
Lane Background	Lane background subtracted with disk size: 10
Lane Width	7.10 mm
Regression Equation	A single equation is not available for this method

Lane 8

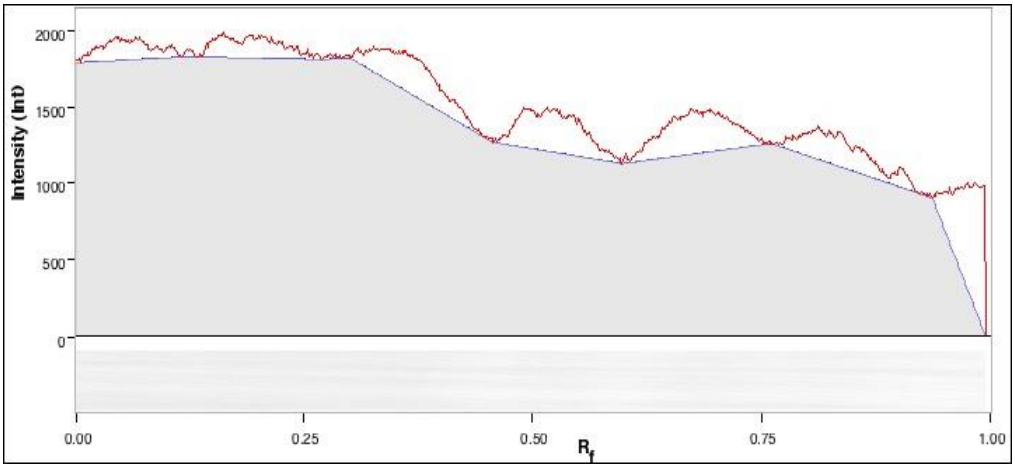

Band No.	Band Label	Mol. Wt. (KDa)	Relative Front	Volume (Int)	Abs. Quant.	Rel. Quant.	Band %	Lane %

Band Detection	Automatically detected bands with custom sensitivity: 100
Lane Background	Lane background subtracted with disk size: 10
Lane Width	7.10 mm

Regression Equation	A single equation is not available for this method

Lane 9

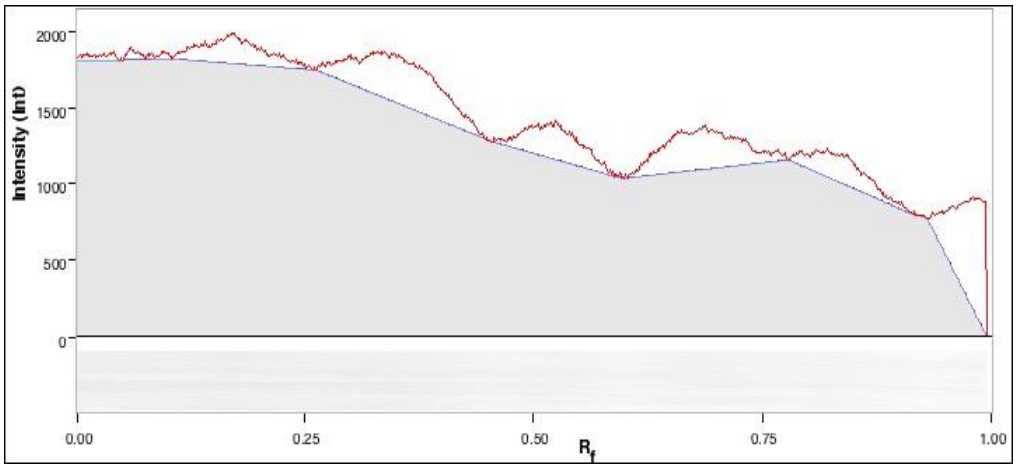

Band No.	Band Label	Mol. Wt. (KDa)	Relative Front	Volume (Int)	Abs. Quant.	Rel. Quant.	Band %	Lane %

Band Detection	Automatically detected bands with custom sensitivity: 100
Lane Background	Lane background subtracted with disk size: 10
Lane Width	7.10 mm
Regression Equation	A single equation is not available for this method